UNIVERSITY OF SOUTHAMPTON

CYCLONIC DEWATERING OF OIL

by

Ian C. Smyth

DEPARTMENT OF MECHANICAL ENGINEERING

Thesis submitted for the degree of
Doctor of Philosophy

November 1988

PREFACE

The work described in this thesis – the development and testing of a hydrocyclone for dewatering oil – relates to research carried out by the author between December 1979 and February 1983 as a postgraduate student and from February 1984 to May 1987 as a contract researcher in the Dept. of Mechanical Engineering at the University of Southampton. The studentship was jointly sponsored by the S.E.R.C. and BP as a C.A.S.E. award, which, whilst providing first–hand background information on the engineering requirements through the industrial sponsor, put an emphasis on hardware solutions. This practical angle was reinforced during the contract research period by the addition of an equipment builder, BWN Vortoil (U.K.), to the sponsoring group (with monies from SERC now being channelled through the Marine Technology Directorate) and latterly Shell Expro.

The research is still continuing.

I.C.Smyth

November 1988.

CONTENTS

UNIVERSITY OF SOUTHAMPTON

ABSTRACT

FACULTY OF ENGINEERING AND APPLIED SCIENCE
DEPARTMENT OF MECHANICAL ENGINEERING

Doctor of Philosophy

CYCLONIC DEWATERING OF OIL

by Ian Charles Smyth

The development and operation of hydrocyclone designs for removing water dispersed in oil is investigated with the primary objective being to produce an effective and compact formation water–crude oil separator for use on offshore production platforms. A variety of water–distillate oil systems, most extensively water–kerosine, have been used in laboratory tests at ambient temperatures to model the conditions near the well–head. Aspects of feed characterisation and test rig development, including dynamic drop sizing and on–line water content analysis, are addressed. The range of feed conditions for which useful separation might be achieved is generally found to be restricted to oil viscosities $< 1 \times 10^{-5} m^2 s^{-1}$ and drop sizes $> 10\mu$.

Feed water concentrations (K_i) up to phase inversion have been tested and best dewatering and recovery of oil is obtained by operating just above a critical split ratio, $(1-F)_{crit}$. This parameter depends most strongly on K_i and oil type, $(1-F)_{crit}/K_i$ being a constant ($\triangleq 1.3$) for water–kerosine dispersions. Understanding of these effects is reinforced by consideration of coalescence processes and LDA measurements of radial profiles for axial velocity with changing split (10–50%). A critical flowrate at which separation is a maximum is also identified. This has been primarily linked to turbulent shear induced drop break up and is roughly determined by a droplet Weber number for a given hydrocyclone or inlet velocity for a given water–oil system.

A solid–liquid analogue has been used to aid preliminary geometry development and provide a reference dispersion with stable particles.

Constant inlet velocity scaling of hydrocyclone size to maintain performance appears to have some validity, although prediction of separation using equivalence relationships has only been partly successful. Correlations between pressure coefficient and Reynolds number incorporating split and water content are demonstrated.

It is estimated that the best of the geometries developed can match the water removal efficiency of Forties production separators, with a 60–70% space and weight saving on the system as a whole.

ACKNOWLEDGEMENTS

The author would like to thank his supervisor, Mr. M.T. Thew, for his encouragement and guidance throughout the period of this work. I am also grateful to University colleagues Dr. K. Nezhati, Mr. J.H. Hargreaves, Mr. O. Baran, and in the past Dr. D.A. Colman and Dr. B.C. Millington, for their advice and suggestions. Thanks is due to Mr. M.A. Batey and the technical support staff of the Mechanical Engineering Department, and in particular Mr. S.I. Roberts, for their invaluable assistance with the construction of rigs and test hydrocyclones, and also to Mrs. H.S. Paul for typing this thesis.

At BP Research Sunbury, I wish to acknowledge the foresight of Mr. E.E. Davies in setting up the C.A.S.E. study and the help of my industrial supervisor Mr. B.J. Oswald and his successor Dr. G. Morgan.

The research was made possible by the financial backing of the SERC and BP and latterly BWN Vortoil and Shell Expro, for which I am grateful.

Finally, I should like to thank my long suffering wife and family for their continual support.

NOMENCLATURE

a	radial acceleration = v_θ^2/r
A	hydrocylone body area = $\frac{1}{4}\pi D^2$, with subscript refers to the indicated port
b	width of rectangular inlet (see Appendix D)
C	capacitance (pF)
C_{Pxy}	pressure drop coefficient = $\Delta P_{xy}/\frac{1}{2}\rho v_i^2$
$\bar{C}_{Pxy}$	applied to 2−component flow, substitute $\bar{\rho}$ for ρ in above
C'_{Pxy}	accounting for the effect of split, see equation 4.12
d	particle diameter (μ)
d_S	Stokesian diameter
d_f	free fall diameter (= d for spherical rigid particles, = d_S for $Re_p < 1$)
$d_{(n)}$	n^{th} percentile of cumulative volume undersize distribution
$(n1)^d(n2)$	size range between percentiles n1 and n2
$\bar{d}$	volumetric mean particle diameter = $d_{(50)}$
d'_{50}	particle size for which MP'(d) = 0.5
D	hydrocyclone body diameter (mm), with suffix/subscript see Appendix D

E	overall efficiency $= F\left[\frac{(K_i - K_u)}{K_i(1-K_i)}\right]$
E_{or}	oil recovery index $= F\,\frac{(1-K_u)}{(1-K_i)}$
f	frequency (see Appendix C for range of sub/superscripts)
$1-F$	split ratio % by volume ($F = Q_u/Q_i$)
$(1-F)_{crit}$	critical split ratio, when E is a maximum (see Fig.9.7)
h	distance from hydrocyclone end wall to base of inlet (see Appendix D)
Hy	hydrocyclone number $= \frac{Q_i \Delta\rho d_S^2}{D^3 \mu}$ — note — particle diameters are for feed dispersions
$Hy(\bar{d})$, etc.,	$\bar{d}$ replaces d_S in above
K	concentration of dispersed phase, % or ppm by volume for fluid systems, mg/ℓ for solid–liquid systems (oil industry units for salt in crude = ptb, pounds per thousand barrels; 1ptb ≙ 3mg/ℓ); for water/oil test systems represents concentration of water
ℓ	length of vortex finder
ℓ_K	Kolmogorov microscale $= (\nu^3/\bar{\epsilon})^{\frac{1}{4}}$
L	overall hydrocyclone length, with suffix/subscript see Appendix D
m_{xy}	mean gradient of ΔP_{xy} vs. split relationship
M_{xy}	$= m_{xy}$ at $Q_i = 50$ ℓ/min.
$MP(d)$	particle migration probability to downstream $= \frac{p_d(d)K_dQ_d}{p_i(d)K_iQ_i}$

$MP'(d)$ reduced migration probability = $\frac{MP(d)-(1-F)}{F}$

n refractive index (see Appendix C); generally used exponent

N mixing (masher) pump speed (rpm)

$p(d)$ dispersion % differential volumetric particle size distribution

P pressure (barg)

ΔP_{xy} pressure drop between ports x and y = $P_x - P_y$ (bar), where xy = iu, id or du

$\overline{\Delta P}_{xy}$ mean pressure drop from inlet to outlet = $\frac{\Delta P_{iu}Q_u+\Delta P_{id}Q_d}{Q_i}$

Q volumetric flowrate (ℓ/min, oil industry units = bpd, barrel per day; 110 ℓ/min = 1000 bpd).

r radial position

R hydrocyclone radius = D/2

Re Reynolds number

Re_p applied to the dispersion = $\frac{u\rho d_f}{\mu}$

Re_D applied to the flowfield = $\frac{v_i\rho D}{\mu}$

Re'_D applied to the flowfield = $\frac{v_i\bar{\rho}D}{\mu_a}$

S swirl number = $\frac{\pi DX_i}{2A_i}$

$\bar{t}$ mean residence time = V/Q_i

T	temperature (°C)
u	relative velocity of particle to surrounding fluid
v	time averaged flow velocity (m/s)
$\bar{v}_z$	mean axial velocity = $\frac{4Q_i}{\pi D^2}$
v_{cell}	velocity through annulus of Aquasyst cell or optical cell for drop sizing
$\overline{v^2}$	average of the square of the velocity differences over a distance = d, see equation 8.2
V	volume (ℓ, oil industry units = bbℓ, barrel; 1 bbℓ = 159ℓ)
W	water build up rate in capacitance cell, % (as measured by Aquasyst)/min.
We_c	critical droplet Weber number = $\frac{\overline{v^2}\rho d_{max}}{\sigma}$ (see also equation 8.6)
X_i	distance of the tangential component of the inlet centre line from the hydrocyclone axis
z	axial position (measured from hydrocyclone end wall)
α	hydrocyclone cone (or taper section) included angle; angle of light scattering in LDA (°)
γ	interfacial tension (N/m)
$\bar{\varepsilon}$	mean power dissipated (input)/unit mass (W/kg)
θ	hydrocyclone contraction included angle, see Appendix D. (°)
λ	wavelength

μ	dynamic viscosity (cP, $\equiv$ Pa.s. $\times 10^{-3}$)	refer to contin-
μ_a	apparent viscosity, see equation 4.11	uous (oil) phase
ν	kinematic viscosity (cSt, $\equiv m^2s^{-1} \times 10^{-6}$)	unless subscript
ρ	density (kg/m^3)	indicates otherwise

$\Delta\rho$ density difference = $|\rho - \rho_p|$

$\bar{\rho}$ weighted mean density = $\rho(1-K_i) + \rho_p K_i$

σ_g geometric standard deviation

SUBSCRIPTS

d	downstream outlet
D	hydrocyclone body diameter; flowfield
i	inlet
max	maximum
min	minimum
o	oil
p	particle; dispersed phase
r	radial
u	upstream outlet
w	water
z	axial
θ	tangential

TERMINOLOGY

Terms of reference frequently used in the text are defined below:

conventional hydrocyclone:	refers to Rietema–type geometries commonly used for solid–liquid separation e.g. Fig.D.6.
deoiling:	opposite of dewatering (see below)
dewatering:	operating a separator to produce a water free oil stream, implication that water is dispersed in the feed.
discharge streams:	the upstream discharging flow for a dewatering hydrocyclone may also be referred to as the *process* or *oil stream*, the downstream flow as the *reject* or *water stream*. (Note – for deoiling hydrocyclones the reject stream becomes the upstream and the process stream the downstream).
LDA:	laser Doppler anemometry
MOL pumps:	main oil line pumps
particle:	any dispersed element.
water and oil systems:	*water–oil* means water dispersed in oil, *water/oil* (oil/water) indicates either phase could be dispersed and is also used when referring to interfacial conditions. Water/oil systems are commonly referred to by the oil type only.

LIST OF TABLES

LIST OF FIGURES

LIST OF PLATES

CHAPTER 1

INTRODUCTION

1.1 The Hydrocyclone and its Operation.

The hydrocyclone is a mechanical device which converts the energy of a flowing liquid into rotational motion. This promotes a centrifugal action such that any dispersion within the flow is subjected to a segregating force which operates by virtue of the density difference between the dispersed and continuous components. The rotational motion, which roughly takes the form of a free vortex with a forced vortex at its core, is usually produced by tangential injection of the flow into a cylindrical unit. If, as is commonly the case, the dispersion is more dense than the carrying liquid, the centrifugal acceleration induced by the spinning flow causes an outward radial movement of the dispersion (with respect to the continuous phase). The geometry of the hydrocyclone, where it is usual for the body of the unit to become conical away from the inlet, dictates that flow is moving towards the cone apex near the wall with flow reversal occurring around the axis of the separator. Hence, the bulk of the lighter component

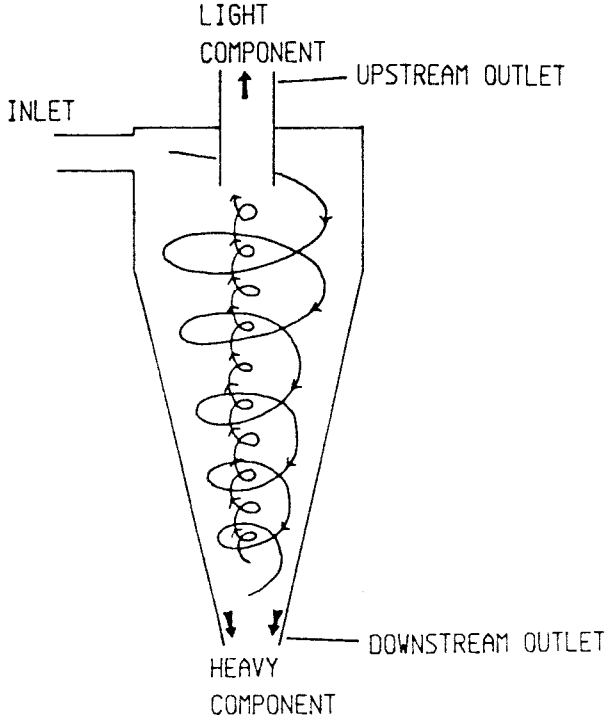

discharges centrally 'above' the inlet at the upstream outlet (through a projecting pipe termed the vortex finder), whilst most of the heavier component moves 'down' the walls of the hydrocyclone to be removed at the downstream outlet.

Some of the factors that control the degree of separation achieved in a hydrocyclone can be found by considering how the radial forces on a particle interact. Essentially, for Stokesian particle movement, the drag force is opposed by the centrifugal force such that at equilibrium

$$3\pi\mu u_r d_S = \frac{\pi d_S^3}{6} \Delta\rho \; a$$

$$u_r = \frac{d_S^2 \Delta\rho \; a}{18\mu} \qquad (1.1)$$

where d_S is the Stokesian particle diameter, a the centrifugal acceleration ($= v_\theta^2/r$; v_θ – tangential velocity, r – radial distance from axis), μ the dynamic viscosity, $\Delta\rho$ the density difference between the dispersion and continuous component and u_r the terminal velocity of the particle in the radial direction. The magnitude of u_r determines the particle's chance of removal in the discharge flow appropriate to its density characteristic when considered in terms of the relative motion of the carrying liquid. This in turn will be a function of hydrocyclone geometry and operating conditions. Models predicting separation performance are extensively reviewed in the two principle texts (in English) on hydrocyclones by Bradley and Svarovsky [1,2], the variety of approaches reflecting the complexity of the internal flowfield.

1.2 The Hydrocyclone as a Liquid–Liquid Separator.

Although hydrocyclones can function as classifiers (splitting the dispersion on the basis of either size or density differences) or contactors, they are also commonly used for maximising the removal of a solid dispersion from a liquid. Separating immiscible liquids relies on the same mechanisms as for solid–liquid systems but tends to be more difficult as the density difference between the components is generally much lower and droplets are susceptible to break up in the high shear conditions associated with hydrocyclones, especially on entry. A

conflict therefore exists in that increasing swirl to compensate for low $\Delta\rho$ also tends to promote the forces which cause drop disintegration.

Coalescence may also have a significant influence on the effective separation of immiscible liquids, in view of the droplet concentrating action of the hydrocyclone, with phase inversion of the dispersion being the ultimate product of this process. Practically, however, hydrocyclones are only able to produce one relatively pure phase in a single pass and which this is depends on the relative magnitude of the discharge flows. For example, if the lighter of the two liquids was required to be cleaned up, this would involve restricting the flow at the upstream outlet to below that of the feed flow rate of the light component, rejecting a mixture of the liquids at the downstream. Generally, higher purity will be attainable for the phase which is continuous at the feed. The balance or split between the flows leaving the separator at atmospheric pressures, common to many solid–liquid applications, is a function of the geometry of the hydrocyclone (especially outlet size). However, in the pressurised systems most usually associated with liquid–liquid separation, more flexible control is achieved by back pressure adjustment using external valves. This mode of operation also suits the variability of feed dispersion concentrations often found with liquid–liquid applications and eliminates the entrained air core phenomenon resulting from direct discharge to atmosphere.

Regarding water/oil separation, deoiling a water continuous system is an easier prospect than dewatering an oil continuous system. This reflects the higher viscosity of a continuous oil phase, increasing drag on the drops (so lowering settling velocities) and also reducing their tendency to coalesce (as a result of longer film drainage times between drops in collision). In addition, viscous resistance to shear is lower for water droplets and their settling out is a counter– rather than a co–current process.

1.3 Stimulus for Research

The main commercial stimulus for this research comes from the oil industry's search for compact devices for separating water/crude oil emulsions close to the well–head. This is part of an effort to reduce the size and cost of offshore

production facilities to allow the exploitation of marginal fields. Hydrocyclones have the required high throughput/size characteristic but had generally lacked good liquid–liquid separation capability.

Work on liquid–liquid separation with hydrocyclones has been in progress (intermittently) for almost 20 years in the Mechanical Engineering Department at Southampton University. Early emphasis had been on oily water treatment, and by 1979 an effective deoiling geometry had been developed (later to be successfully commercialised) which, taken together with promising results from a bench–top undergraduate study of cyclonic water–kerosine separation [3], indicated progress might also be made with dewatering hydrocyclones.

1.4 Objectives and Scope of Research Programme

In the very broadest sense, the aim of the work is to develop an efficient hydrocyclone geometry for liquid–liquid separation where the dense phase is dispersed, gaining knowledge of operational characteristics in the process. More specifically, the primary concern of the industrial sponsors is for removing formation water (brine) from crude oil at well–head conditions. In this context, and using BP's Forties field as a reference point, two areas where crude dewatering is needed have been identified, providing a quantitative framework to which research objectives can be related.

(i) production separators – this is a fairly general application as feed conditions vary widely and are often not well defined. Free gas usually constitutes a significant fraction of produced fluids but it is assumed that this would be largely removed in a preliminary separation stage. Nevertheless, a hot emulsion with a range of characteristics (notably variable oil type) needs to be treated, the aqueous component being finely dispersed and comprising anything from a few percent to complete inversion (K_i up to 50%+). Target discharge water levels between 0.5 and 1.0% would appear realistic (matching existing Forties production separator operation), with minimum loss of oil in the reject flow and a low pressure drop to limit dissolved gas release being important associated objectives.

ii) pump seal flush flow dewaterer – this was a need specific to the main oil line (MOL) pumps on Forties platforms. As the feed in this instance is taken from the oil line beyond the production separators, K_i will be lower and drop size also smaller than for (i). The sole operational requirement (apart from effective solids removal) is to minimise water content (to nominally $<$ 1.0%) in an oil flush stream of 20–25 ℓ/min. A limitation on hydrocyclone length was also considered desirable (to $<$0.5m) to avoid major redesign of the recently modified harness holding the existing solids removing hydrocyclones and associated flowmeters, although this was a minor consideration.

Further background to these applications is given in Section 3.1 but it is clear from the wide ranging nature of the possible feed conditions already outlined that more than one optimal geometry and operating mode for the hydrocyclone would be required to cover this ground. In particular, a wide range of split ratios needs to be accommodated, a significant difference from conventional mineral processing or typical water deoiling applications.

The practical and financial constraints imposed in trying to reproduce field conditions in the laboratory necessitated working with oil phases which were stable at near ambient temperatures and pressures and could be easily reused. In particular, a water–kerosine model provided a good match in terms of bulk characteristics to the Forties well–head emulsion (see Tables 3.2 and 7.2). However, to effectively test and progressively develop a dewatering hydrocyclone geometry, the research programme needed to include the following:

(i) the development of test rigs, instrumentation and experimental techniques not only for liquid separation but also for more fundamental studies of flow structure and solid–liquid analogue systems.

(ii) the evaluation and use of appropriate performance criteria and scaling techniques.

(iii) close consideration of the properties of water–oil systems and how they respond to passage through a hydrocyclone, particularly in terms of coalescence and break up processes.

Accordingly, the thesis structure takes the following form. After a review of previous workers attempts at liquid–liquid separation in hydrocyclones (with the emphasis on dense dispersions) in Chapter 2, potential industrial applications (principally relating to dewatering crude oil) are discussed in Chapter 3. Chapter 4 looks at performance presentation and scaling techniques, whilst Chapter 5 covers the use of a solid–liquid analogue for the water–kerosine test system as an aid to preliminary geometry development for low K_i conditions, and includes a comparison between the behaviour of drops and solid particles. Chapter 6 considers the nature of the hydrocyclone's internal flowfield and some of the implications for liquid–liquid separation. Also within this chapter, LDA (laser Doppler anemometer) measurements showing how axial velocity profiles change with valve controlled split are discussed, a key aspect of hydrocyclone operation in the context of the wide range of K_i under consideration. The water–oil separation test programme representing the core of the work is introduced in Chapter 7, which looks at the test rigs, their operation, the nature of the water–oil systems used and instrumentation development. Droplet stability through the hydrocyclone is analysed in Chapter 8, which completes the scene setting for Chapter 9 where the separation tests proper are presented. Here the influence of feed and operating parameters, oil type and separator geometry are assessed. Chapter 10 investigates to what extent the laboratory results relate to oil–field conditions and considers some of the practicalities of using hydrocyclones for dewatering crude on production platforms. Discussion of future work and concluding comments are found in Chapters 11 and 12 respectively.

CHAPTER 2

REVIEW OF PREVIOUS WORK

An appraisal of published papers and reports dealing with liquid–liquid separation in hydrocyclones (particularly where the dispersed phase is densest) is presented, illustrating some of the operational characteristics and limitations to be expected and attempts to optimise geometry. Experimental and interpretative techniques are also closely considered.

To help clarify the review, work has been arranged alphabetically by authors and headed with keywords to indicate content. An explanation of performance criteria used in this section is provided in Chapter 4.

Bohnet, 1959 [4]; WATER/OIL, OPERATING PARAMETERS, SHEAR EFFECTS. Working with a $\mu = 3$ cP, $\rho = 860$ kg/m^3 lubricating oil and water at 60°C in a 50mm diameter conventional hydrocyclone, Bohnet expressed the general importance of split (adjusted using valves) to achieving phase separation. Critical inlet velocities (v_i) were identified for optimum discharge stream clarity, which varied, depending on whether clean oil or clean water was required, within the range 3.0 – 6.5 m/s. Optimum inlet velocity also appeared to be an inverse function of feed water concentration (K_i = 10 and 36%), and this was interpreted in terms of a "separation surface" concept, when a link with changing drop size might have been more realistic. Whilst theoretical consideration was given to some of the shear forces acting on droplets, ideas were not pursued in the experimental work where drop size was neither controlled nor measured and generally the presentation of results lacked clarity.

Regarding geometry, Bohnet recommended "axial flow cyclones" of cylindrical form with both outlets at the downstream end (the oil taken off axially, water at the wall) [see also Regehr], although no experimental evidence for this preference was presented.

Burrill and Woods, 1970, [5]; CARBON TET.– WATER, RANKING OPERATING PARAMS., DROP SIZE, COALESCENCE. Attempted a statistical analysis of some of the primary operational parameters involved in separating a $CC\ell_4$ dispersion (ρ = 1630 k/m^3) from water using a 51mm diameter hydrocyclone operating without an air core. The use of regression techniques showed overall efficiency (E) to be most sensitive to volume split (1– F), followed by feed concentration of the dispersion (K_i) and feed drop size distribution. However, 1– F and K_i were both only varied in the range 10– 20%, whilst variation in feed drop size (by adjustment of a mixing valve) produced Sauter means of 150– 300μ, well above the estimated d'_{50} (flowrate was kept constant). Hence, efficiency for most tests was controlled by hindered discharge mechanisms and the value of the ranking exercise is therefore limited. Nevertheless, E values up to 0.95 were achieved.

Feed drop size distributions (determined by photographic methods) were found to be log normal, narrowing as mixing increased and independent of K_i.

An interesting concept proposed was that the concentration of the light phase in the downstream outlet could be interpreted in terms of a droplet packing density, to give an indication of the extent to which coalescence occurred in the hydrocyclone. Working from inlet drop size data, a minimum of ~15% interstitial space was predicted for the densest possible packing before some coalescence must be assumed. As K_d ‹ 85% in the tests, it was concluded that coalescence was minimal. However, this model takes no account of radial concentration gradients and assumes drop surfaces are highly stable (as in a surfactant stabilised emulsion) which is unrealistic for this system.

Colman and Thew (and co– workers), 1980– 84, [6, 7, 8]; LIGHT DISPERSION, OIL– WATER, GEOMETRY, INTERNAL FLOWS, SCALING. These papers highlight an extensive development programme, culminating in a deoiling hydrocyclone design which has been widely patented and achieved considerable commercial success. Features of general application to liquid– liquid separation include a high aspect ratio (L/D), maximising droplet residence time, and comparatively large inlet(s) and entry diameter (2D), reducing pressure losses and turbulent shear levels and hence also droplet breakage tendencies. In the general absence of drop coalescence (oil concentrations typically <1%) and break

up, solid– liquid analogues proved an effective tool for early design development. Also, with the measurement of feed and outlet drop sizes, grade efficiency curves were constructed and correlations derived.

The ability to closely control and monitor test conditions and the attention given to determining the flow structure within the hydrocyclone (flow visualisation, residence time measurements and LDA studies were undertaken) are considered to be critical to the success of this work.

Hitchon, 1959, [9]; AQUEOUS PHASE/KEROSINE, INLET:TWIN/SIZE, MASS TRANSFER, SERIES OPERATION. Tried to separate essentially water/kerosine (ρ = 783 kg/m^3, μ = 1.8 cP) mixtures in a 10mm diameter cyclone at flows of ~1 ℓ/min as well as monitoring mass transfer efficiencies of an uranium compound from the aqueous phase. No attempt was made to condition or monitor the drop size of the feed flow. Most testing was undertaken with a single 2mm diameter inlet (A_i/A = 0.04) and separating efficiency was found to fall off as flows increased from comparatively low levels – presumably due to droplet break up. That stability was maintained over a wider range of flowrates when the bulk of the flow left via the upstream outlet, probably reflects a more favourable internal flow/shear structure at low split ratios (split adjustment by changing outlet diameters). Halving inlet size (raising v_i 4– fold to levels >12 m/s) resulted in the loss of virtually all separating power, whilst increasing the inlet diameter to 3mm marginally improved separation and also lowered the pressure requirement of the hydrocyclone.

Two other aspects of the experimentation are of interest. Firstly the use of twin inlet passages at diametrically opposite sides of the cyclone feed region such that the two phases could be injected separately (equal flowrates for each). This gave similar separation and mass transfer results to the area equivalent single inlet geometry, where the water and kerosine were joined in a tee prior to the inlet, showing that the majority of mixing occurred within the cyclone rather than the feed pipework. The contacting characteristic of the cyclone is illustrated by mass transfer efficiencies* of up to 0.57 being observed for residence

---

* In terms of the concentration of uranium in the aqueous phase,

$$\text{mass transfer efficiency} = \frac{\text{initial} - \text{final}}{\text{initial} - \text{equilibrium}}$$

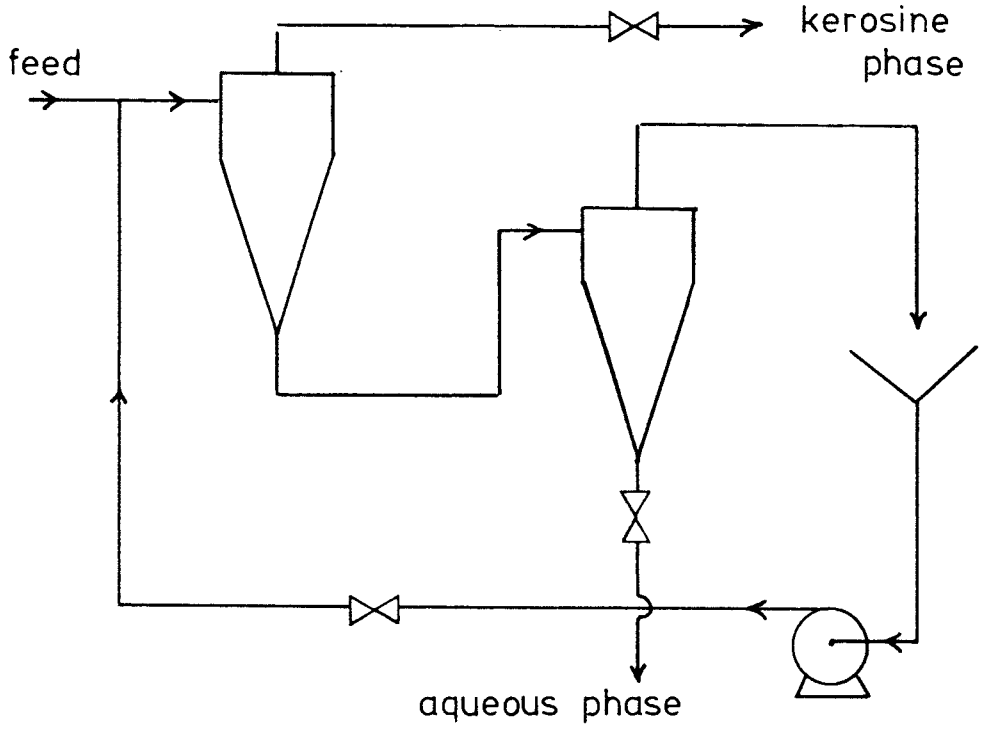

times of ~ 0.5s, although separation efficiency was lower for good transfer conditions. The second aspect of the tests which is worthy of comment involved the operation of two hydrocyclones working in series to try and obtain two "pure" discharge streams. Although better than 95% purity of both aqueous and kerosine phase was achieved, this was not as good as predicted from the single cyclone runs and was attributed to emulsification effects from the centrifugal pump initially used to recycle the unwanted overflow from the second cyclone. Similar work by Bradley [10] preceded Hitchon's studies.

Johnson et al., 1976, [11]; FREON– ICE & BRINE OR WATER, DROPLET BREAK UP, 3 PHASE, PERFORMANCE PREDICTION. Examined the ability of two cyclones (D = 50 and 25 mm) to separate Freon (ρ = 1500 kg/m^3) from water and from an ice– brine slurry. As Freon concentrations were low (< 8%) coalescence was neglected and theoretical efficiencies, based on Bradley and Pullings' formula for d'_{50} derived for solid– liquid separation [12] and adapted for drops, were found to "match" measured efficiencies for the larger unit (although only to within ± 20% and then using 'best fit' rather than measured

flowfield parameters). However, with the smaller hydrocyclone (and v_i in a higher velocity range of 5–12 m/s), experimental efficiencies fell well below predicted performance levels and droplet break up was assumed to be the cause. Certainly photomicrographic analysis of inlet and upstream flows for $1-F = 0$ showed a fall in mean drop size ($\bar{d}$) from 24 to 20μ through the hydrocyclone, although internal shear conditions may have differed somewhat at the operational splits of 10–30%.

The presence of ice crystals (up to 10% by volume, $\rho = 920$ kg/m^3) in some of the tests did not appear to impair liquid–liquid separation, even though the relative movement of the two dispersed components for this system was in opposite directions.

Listewnik, 1984, [13]; OIL–WATER, INTERNAL FLOW, TURBULENCE. Theoretically considered the influence of local flow–field characteristics on the movement of drops through the hydrocyclone. He suggested that the Magnus effect could have considerable influence on droplet 'settling' under certain circumstances and that drop break up was determined by turbulent shear and could be characterised by a critical droplet Weber number. Experimental work included LDA analysis of the flow and considerable radial anisotropy of the fluctuating v_z component was revealed.

The hydrocyclone tested in this work was akin to that of Regehr's (see later) although in a more recent paper [14] a geometry closer to that of Colman and Thew in concept has been used.

Lynn, 1973, [15]; WATER–FUEL OILS, EMULSIFICATION. In considering the problem of cleaning up ship propulsion fuels of water and solid contaminants, he reported on water–oil separation tests using a hydrocyclone, undertaken at Mississippi and Oklahoma State Universities. For K_i between 1 and 50%, up to 60% water removal was achieved ($d_i \simeq 50\mu$) from fuels such as JP–3 kerosine and diesel, although this modest performance fell rapidly for smaller drop sizes. Also trials with Naval Distillate ($\nu = 6$ cSt, $\rho = 888$ kg/m^3) were abandoned because the hydrocyclone tended to further emulsify the dispersed water. It was concluded that hydrocyclones would not be effective at separating drops $< 10\mu$ or stabilised emulsions.

Two U.S. patents for hydrocyclones to separate an immiscible dense liquid from a lighter one [16,17], seem to be a product of these studies. Both geometries described, whilst retaining the classical reverse flow format, favour annular take off of the dense liquid at a high level in the hydrocyclone body. In the author's view, this is undesirable as only a comparatively short time is allowed for droplet migration to the wall.

Regehr, 1962, [18], LIGHT DISPERSION, GEOMETRY, PRESSURE DROP. Primarily concerned with the separation of oil dispersed in water, but testing also included the use of light solids giving data free from drop break up. Wide ranging consideration was given to the geometrical form of the hydrocyclone and its interaction with internal flows. It was concluded that separation was strongly influenced by the velocity loss ratio, α (= v_θ/v_i at entry of feed), and residence time (represented by L/D). A best hydrocyclone design was proposed with outlets

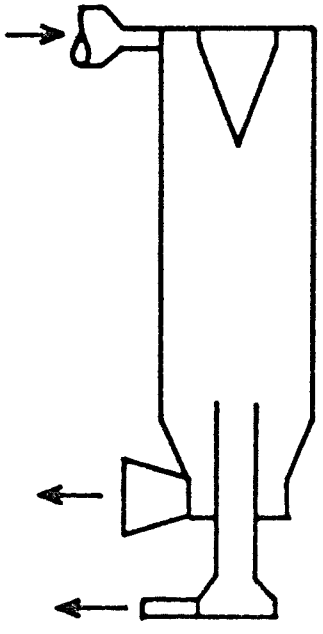

and inlets at opposite ends of the separation chamber. This gave better separation for the same pressure drop (note $\Delta P \propto Q_i^{1.86}$) than an equivalent conventional reverse flow geometry. However, this advantage might not extend to higher flowrates (maximum test $Q_i \simeq 35$ ℓ/min in D = 44mm units).

Sheng et al., 1974, [19]; WATER/PARAFFIN, SOLID–WETTING, EMULSIFICATION. Emphasized the importance of the solid wetting characteristics of the process liquids (in this case water and paraffin) to the hydrocyclone's liquid separation performance. They claimed that the addition of polyethylene particles ($\leq$ 4% by volume), which are wetted preferentially by oil, helped to inhibit emulsification tendencies. In addition, much improved separating efficiencies were reported for hydrocyclones with vortex finders made of a material interfacially favourable to the lighter oil phase i.e. with lower drop contact angles than for water. Although this design philosophy may act to discourage water movement in the short circuit flow through the boundary layer to the upstream outlet, it is difficult to see such a wall effect being quite as significant as suggested.

The experiments also showed the importance of the balance between phase ratio and split and that the use of a relative efficiency parameter (which ratioed the achieved E over the ideal or maximum possible E at that split) could provide a valuable assessment tool (as E can only = 1 when $1-F = K_i$, see Fig.4.1).

Intense "emulsification effects" were noted at high flowrates for K_i = 50% (1:1 phase ratio) with a substantial loss in separating power. Tepe and Woods [20] report similar problems at this kind of phase ratio for the hydrocyclonic separation of isobutyl alcohol/water systems. It is presumed this is linked with phase inversion effects, when the dispersed and continuous phases are not clearly defined.

Simkin and Olney, 1956 [21]; LIGHT OILS/WATER, OPERATING PARAMETERS, GEOMETRY, MASS TRANSFER. Tested a 95 mm cyclone using water mixed with either kerosine (ρ = 800 kg/m^3, μ = 1.4 cP) or "white oil" (ρ = 840 kg/m^3, μ = 8.9 cP) over a range of flowrates between 20 and 95 ℓ/min and water concentrations between 10 and 75% by volume. Best separation (in terms of E) was found at low Q_i when the split (in this case defined as Q_d/Q_u) matched the phase ratio at the inlet (Q_w/Q_o). At higher Q_i, optimum E fell and moved towards Q_d/Q_u = 1, which was principally explained by remixing effects within the hydrocyclone. The inlet drop size of the dispersion in these tests seems to have been fairly coarse, the mixing valve in the

feed pipework being fully open for most runs. Sizing (by photographic techniques) was only undertaken at one operating condition (10% water in white oil, Q_i = 45 ℓ/min) giving a Sauter mean diameter of 1.56 mm for the open valve; throttling to halve this diameter was seen to reduce separation considerably (at Q_d/Q_u = 1/3.4, E fell from 0.71 → 0.10). However, feed drop sizes would also have been affected by flowrate, phase ratio and oil type and yet no attempt was made to quantify such changes, making the interpretation of results problematical.

Geometry was fairly comprehensively varied (within conventional bounds) without "strongly influencing" the separation, although an optimum for inlet/outlet diameters at ~0.28D was recognised. It was concluded, therefore, that separation efficiency was primarily a function of operational factors with effective performance only achieved for feed drop sizes > 1mm.

Mass transfer effects were also considered (for an amine solute) and an inverse proportionality found between mass transfer and separation efficiencies.

Ternovskii and Kutepov, 1979, [22]; BRINE OR WATER–CRUDE OIL, FINE DROP SIZE, OPERATING PARAMETERS, GEOMETRY. Tests were carried out using 20 and 30mm hydrocyclones for dewatering two types of crude oil with similar bulk characteristics ($\rho \simeq 830$ kg/m^3 and $\mu \simeq 3.2$ cP) in a closed recirculation rig without phase separation. Substantial quantities of free air were found to be entrained in the emulsion and although not quantified the level of gas was kept constant. Whilst drop sizing of both inlet and outlet streams was undertaken by sampling/sedimentation methods (suitable only for stable drops), results were not reported in any detail. However, $\bar{d}_i$ is believed to have been fine, ~ 10–15μ. Best separation achieved of a 3–fold reduction in K_i, and then only with poor oil recovery, should be viewed in this context.

Close analysis of the test data showed that the effect on separation of changing K_i over the range 3–14% depended on flowrate. For increasing K_i, K_u/K_i fell at low flows but rose at high flows. A doubling of density differences by the introduction of an aqueous NaCℓ phase in place of the water was found to have no effect on separation. This may have reflected an emulsion stabilising effect caused by the addition of the salt. An optimum inlet diameter

($D_i/D = 0.32$) and a preference for small cone angles ($< 10°$) was also identified.

A major weakness of the experimentation was the progressive diminution of the dispersion on its recirculation (using a gear pump) through the test hydrocyclone. Although this phenomenon was recognised by the authors, there is no indication what allowance (if any) had been made for this temporal drift in $\bar{d}_i$ in the assessment of operating and geometry vairables. However, the paper concludes that in industrial tests higher degrees of separation were achieved than in the experiments for the first passage of the emulsion through the hydrocyclone feed.

Russian studies seem to have been the closest to the specific problem of hydrocyclonic dewatering of crude oil (see also [23]). However, interpretation of material is often difficult as there is a tendency for work to be incompletely reported.

Van Rossum, 1961, [24]; WATER–OIL, VISCOSITY. Tested a number of refined oils with a range of viscosities, but similar densities, in a $D = 125$mm conventional cyclone for a dispersed water phase with a $\bar{d}_i$ between $50-100\mu$ (centrifugal pump mixing). Running at $K_i = 8\%$ and one particular flowrate ($v_i = 8$ m/s), he concluded that separation progressively fell as oil viscosity rose, being poor over the 10–30 cSt range ($E < 0.5$) and virtually zero above 30 cSt. This probably reflected both an increase in viscous drag slowing droplet migration to the wall and higher shear forces promoting the splitting of drops. Certainly for the 11 cSt oil tested, doubling inlet velocity showed no improvement in separation.

Little change in separation performance was discovered for operation with an air core (majority of testing without an air core) or for an increase in the length of the cylindrical body, although some reduction in pressure requirements was noted.

Summary

Some aspects of the operation and testing of liquid–liquid hydrocyclones were seen to recur. Increasing flowrate caused separation fall off at some stage in virtually every paper (optimum v_i $\rangle$ 8 m/s), with shear induced drop break up effects overcoming the increasing centrifugal action. Sensitivity to this phenomenon inevitably increased with drop size, as did the peak separation achieved. The importance of other operating variables, especially split and its relationship to the relative concentration of the liquid components, was also emphasized. However, in many cases failure to control and/or measure inlet drop sizes whilst evaluating the influence of other operating parameters on performance, limits the value of observations and the basis for comparison with other research. The deoiling work reported by Colman and Thew is exceptional in that not only was feed drop size controlled, but both inlet and outlet dispersions were measured to give droplet separation or grade efficiency curves. However, such a depth of analysis is restricted to systems where dispersions remain stable through the hydrocyclone.

Regarding geometry, a preference for large inlets and a small cone angle was evident, resulting in modest swirl (swirl number, S $\langle$ 11) and pressure drop characteristics.

Consideration of how internal flows change with geometry and operating conditions and the effect of this on drop movement and stability within the hydrocyclone has received little attention.

The degree of separation achieved was very much system dependent ranging from virtually zero, when stable emulsification of the liquids occurred (either before or within the hydrocylone) or for $\nu > 30$ cSt, to "complete" cleanliness of one of the discharge streams for more tractable dispersions, although typically with the loss of a considerable fraction of the process liquid in the reject stream. Separation was seen to be most effective when the density difference between the liquids was large, continuous phase viscosity low and coalscence of the dispersed phase readily occurred.

CHAPTER 3

SCOPE FOR INDUSTRIAL APPLICATIONS

This chapter is primarily devoted to providing a background to the process problem of greatest interest to the industrial sponsor BP, that of separating a water phase from a crude oil emulsion. Particular emphasis has been given to offshore production sites where the potential for utilising the compact nature of dewatering hydrocyclones is probably greatest. The Forties oil–field and associated treatment facilities are used as a case study, as research objectives have been related to this system (see Section 1.4). Dehydration of fuel oil and other possible applications where a need exists for separating a dense from a lighter immiscible liquid, are considered more briefly.

Any assessments as to the appropriateness of hydrocyclones to a particular application are made in the light of the research described later in this thesis and other relevant sources which are referenced.

3.1 Dewatering Crude Oil at the Production Site

3.1.1 Sources of water in crude

Crude oil deposits typically comprise a layer of free gas above an oil layer above a large body of ground or formation water (which is generally saline), the reservoir as a whole being capped by an impervious rock stratum. The oil zone actually contains some water at all levels, as most geological materials are preferentially wetted by water and also water will displace oil by capillary action. Although the majority of this water remains locked in the formation as irreducible connate water, a small portion will emerge with the first crude produced. The greater mobility of water in response to local pressure reductions at the base of oil wells also means that break through of formation water to the production stream may well occur at an early stage in the field's life, and the proportion of brine in the well outflow will increase with time until it becomes

uneconomic to continue. This limiting condition will be largely dependent on the cost effectiveness of water removal at the surface.

Another potential source of water in the flow from a well comes from a regularly used technique of artificially pressurising the reservoir to improve oil recovery. Natural driving pressures, like gas cap expansion, tend to result in variable production rates and low oil recovery (< 20% of deposit), but controlled injection of water (or gas) allows reservoir pressures to be optimised making both production and recovery more efficient. The water used for re-injection may be in part separated produced water, but because of the high injection rates required (5,500-27,500 ℓ/min [50,000-250,000 bpd] [25]) another source is also needed and for offshore operations sea-water can be used. Pre-injection treatment is required to ensure chemical and biological inactivity in the reservoir and removal of solids. Without this treatment, undesirable by-products of the interaction between sea-water and formation brine may cause choking of the reservoir e.g. for the Forties oil-field, where this kind of secondary recovery mechanism has been used from the start, barium sulphate could be precipitated (see Table 3.1 for details of dissolved solids in the two systems).

Increasingly, tertiary techniques are being applied, which act directly to increase oil mobility in the reservoir, in an attempt to recover at least part of the remaining 70% (on average) oil left underground. One such technique is microemulsion flooding [28], where an oil/water emulsion with a sub-micron drop size is used as the flushing medium whose mobility and interaction with the reservoir oil can be closely controlled by surfactant addition. This type of operation contributes to the water cut in the crude and probably also the stability of the produced emulsion.

Hence, there will always be an aqueous phase associated with produced oil varying from a few percent initially to as much as 70% or more in the later stages of a well's working life e.g. many of the Louisiana near-shore production platforms [29]. Brine characteristics will not be static though, and will change depending on which sources are contributing to the aqueous component of the discharge stream.

	Forties Formation Water		N.Sea Seawater
	Type 1 [26]	Type 3 [27]	(Forties) [27]
Sodium	31,000	17,100	11,000
Potassium	890	740	346
Calcium	4,100	1,200	403
Magnesium	560	290	1,320
Iron	0.9	0.2	0.25
Barium	350	90	Nil
Strontium	548	137	-
Zinc	0.7	0.09	-
Lead	1.4	0.8	-
Chloride	57,620	29,430	19,800
Sulphate	-	Nil	2,480
Carbonate	-	Nil	Nil
Bicarbonate	-	990	134
Total dissolved solids	95,531	49,840	35,500
pH at 25°C	6.8	7.4	7.7
Suspended solids	15 - 50		<1

Units: mg/ℓ

Table 3.1 ANALYSES OF DISSOLVED SOLIDS IN FORTIES FORMATION WATER AND SEA-WATER.

3.1.2 Characteristics of well-head emulsions.

The mixing action of flow through piping and flow control devices (especially the well-head choke) together with the agitation caused by gas release as pressures drop between reservoir and the water-oil separator, causes the brine-crude system to become finely emulsified i.e. form a mixture with stabilised interfaces and small drop sizes (a few tens of microns). The stabilising agent, termed an emulsifier or surfactant of which there are many sources in or associated with crude oil [30], is preferentially attracted to the water/oil interface,

most commonly generating water dispersed in oil emulsions. However, at very high water cuts, reverse (oil– in– water) emulsions are likely so long as water soluble emulsifiers are present, whilst multiple (oil– in– water– in– oil) emulsions are sometimes encountered for produced fluids with a complex history. If well– head emulsions can be typified, it is by their diversity. The crude itself represents a complex mixture of hydrocarbons (which may take solid, liquid or gaseous form depending on the prevailing pressure/temperature environment) plus minor amounts of organo– metallic, sulphur and nitrogen compounds. The chemistry of the produced water can also be very varied (as indicated in the previous section). In addition the emulsion may also contain a suspension of sediment (up to silt/fine sand size [31] but usually only in small quantities, 100– 300 mg/ℓ by mass is typical for North Sea operations [32]). Physical characteristics of brine/crude systems in general and Forties in particular are given in Table 3.2.

Regarding the density of the liquids, it is evident that Forties crude is comparatively light on a global basis but would be about average for the N. Sea province (see Table 3.3). The possible brines coming up with Forties crude are not especially salty, but many of the central N. Sea fields operated by Shell, for example, have extremely saline produced water close to saturation limits [33]. The resulting density differences between brine and oil, therefore, may be quite variable but will always be greater at the typically elevated well– head temperatures (80°C for Forties) compared with ambient conditions, as oil expands more rapidly than water over this temperature range [30] (refer also to Table 3.2). In addition, as oil densities quoted are for degassed crudes, the presence of dissolved gas in the oil closer to the well– head will pull down effective oil densities, further raising the potential for production separator applications.

Forties data for viscosity of crude again appears typical of N. Sea oil– fields with significant viscosity reductions occurring as temperatures increase (see Tables 3.2 and 3.3). Further but less marked, reductions can be expected when the more volatile hydrocarbons are present in the oil prior to stabilisation (the degassed form of the oil when stored prior to refining or shipment and the most likely point at which samples for analysis would be taken). The increase in effective viscosity of the emulsion as a whole with water cut is considered in Section 4.2.1.

	ρ (kg/m^3)	$\Delta\rho$ (kg/m^3)	ν (cSt)	γ(N/m)
General:				
formation brine	1000-1200[1] (970-1160)	0-420		0.01-04[7]
crude	780-1000[2]		3-50,000[3]	
Forties:				
brine-type 1	1063[4](1037)			
type 2	1033[5](1007)	188-225		
N.Sea	1026[5](998)	(198-237)		0.025[8]
crude	838[6](800)[5]		6.9[6] (1.6)[6]	

T = 20°C (80°C)

High temperature brine densities estimated from Perry and Chilton [136].

Indices 1→7 indicate data sourced from respectively [30, 36, 33, 26, 27, 37, 32, 38].

TABLE 3.2 OIL–FIELD (FORTIES) BRINE/CRUDE OIL CHARACTERISTICS.

	ρ(kg/m^3)	ν(cSt)	
	at 15°C	20°C	80°C
Auk (UK)	834	7.8	2.2
Brent blend (UK)	832	6.8	1.5
Dan (Denmark)	873	14.5	3.7
Dunlin (UK)	848	9.0	2.2
Ekofisk (Norway)	804	3.3	1.2
Statfjord (Norway)	832	6.0	1.7
Thistle (UK)	832	5.5	1.9

Sourced from [39]

TABLE 3.3 DENSITY AND VISCOSITY CHARACTERISTICS OF A SELECTION OF NORTH SEA CRUDES

The interfacial characteristics of the Forties system have been summarised in Table 3.2 using γ, the interfacial tension, and it is generally taken that the lower this value the more stable the dispersion. However, surfactants play a fundamental role in the formation and stabilisation of brine–crude emulsions [34] and the interfacial films which result are not easily characterised. For example, at the neutral pH conditions associated with Forties production, interfacial viscosities are only 0.1 cP compared with ~40 cP (at the same pH) for the Ninian oil–field [35]. As interfacial viscosity exerts considerable control on the rate at which drops approach each other during the final stages of flocculation, the precursor to coalescence, greater resolution problems are encountered for Ninian emulsions and yet γ = 0.030 N/m, 20% higher than for Forties. Qualitatively, Forties as a moderate wax, low asphaltene, very low sulphur content crude should be less susceptible than most crudes to forming stable emulsions. The nature of the water/oil interface is discussed further in Section 7.2.2.

It is noteworthy that even though Forties is recognised as a low GOR (gas: oil ratio) field, free gas accounts for between 50 and 75% of the volume of produced hydrocarbons at well–head pressures [27, 40].

3.1.3 Emulsion resolution and separation.

Separation of oil (and gas) from the valueless brine at the production site reflects the desire to make the most efficient use of field to refinery transmission facilities. This is particularly important for remote oil–fields, like those offshore, where the cost of providing and operating such facilities is high.

The emulsion emerging from the well generally requires treatment to encourage drops to flocculate and coalesce in the production separator(s). This is commonly achieved by injecting chemical demulsifiers, which function by displacing the natural emulsifiers from the oil/water interface, replacing the tough skin by an elastic thin film. Typical reagent dosages are of the order of 10–30 ppm prior to conventional separators [26] although with effective mixing and early injection lower concentrations may be viable [41].

The type of separation mechanisms commonly used are as follows:–

i) normal gravity effect – exploiting the buoyancy forces resulting from the density difference between the phases. This tends to require large settling vessels to allow sufficient residence time to give acceptable separation.

ii) high acceleration field – created by spinning up the flow. In addition to increasing separating forces, this can also help to 'break' emulsions as droplet collision velocities are higher than for gravity settling. Vessels can therefore be made more compact .

iii) coalescence enhancement – this may take the form of parallel plate stacks, reducing drop settling distances, or cartridges/packings of hydrophilic strands acting like selective filters. In both cases coalescence of the water drops occurs on the intercepting surfaces with gravity drainage of the now much larger drops, reducing required system residence times.

iv) electric field effects – in most cases, this involves the application of a uniform a.c. field to the emulsion which causes water droplets to become increasingly mutually attracted due to the induced dipole effect. This also acts to distort drops weakening their surface film [34], encouraging coalescence into larger drops which rapidly settle out.

3.1.4. The need for production separator miniaturisation

As most potential offshore oil–fields are in deeper waters or of smaller size than existing developments, bringing them into production in the near future must increasingly rely on more cost effective means of exploitation, especially in view of the anticipated stability in crude prices at their current low levels into the 1990's [42]. Reduction of platform topside weight has been identified as being critical to achieving these savings [43] and integral with this, the increased use of floating or tethered production systems [43]. Every tonne of equipment on a fixed platform requires typically 3 tonnes of super and sub–structure to support it, and process equipment and associated steel work accounts for ~20% of topside weight [45]. Hence, any reduction of separator size could be of considerable benefit.

In addition, if innovative designs can reduce manpower needs in terms of operating and maintenance duties, progress towards very much cheaper unmanned facilities can be made.

Similar arguments apply for subsea production systems if preliminary separation is to be achieved in a dry environment within them, although space rather than weight saving would be the more critical aspect of compactness.

3.1.5 Comparison between hydrocyclones and other separators.

Treatment of well-head fluids usually involves removal of gas and water from the oil in an integrated, multistage process, with secondary clean-up systems to purify the gas and water phases. Hence, whilst the primary concern in this section is to evaluate oil dewatering separators which might be used in an offshore environment, it should be appreciated that multi-phase separation may occur in some units.

For example, the first vessel in many separation trains is termed a free water knock-out (FWKO), essentially a gravity settling tank for removing free water (i.e. that which will readily coalesce and drop out of the oil) but which also commonly vents off gas as well, to act as a 3-phase separator (see Fig.3.1 and Section 3.1.6). This is particularly the case when the FWKO is not preceded by degassing units. A variety of vessel orientations, flow induction formats, baffles and screens are found in gravity separators to aid their operation.

A second conventional dewatering device is the electric dehydrator (Fig.3.2). Operating at a nominal electrode voltage of 16,500 V, the power requirement increases with oil conductivity and is usually in the range 0.5-1.5 kW per thousand bpd [34]. This type of electrostatic treater is often used for deep dehydration of crudes (i.e. to refinery specifications, see Section 3.2.1).

Regarding miniaturised separators, the high efficiency achievable by cartridge coalescers for immiscible liquid separation prompted BP to develop a dewatering/deoiling system based on this technique in the early 1980's. The prototype design is shown in Fig.3.3, with the necessary protection of the

cartridge elements from solids (d > 2μ) undertaken by an automatic backflushing pre-filter [34, 48]. Gas carryover of up to 5-10% by volume can be accommodated [40].

The use of a hydrocyclone based system for dewatering, where the high capacity is derived from the large 'g' forces generated by the swirling flow within the separator, is anticipated for oil-field conditions in Section 10.4. Direct testing has not been carried out in this environment, but performance can be roughly estimated using lab results (Section 10.3). This then provides a basis for comparing hydrocyclones with the other separator types discussed in this section in terms of the critical criteria of space requirement, weight and separation efficiency, as shown in Table 3.4. The systems described include water clean up facilities, as this was the form of comparison used in a key source reference [41]. However, these facilities are comparable in the context of flowrate/size with the dewatering units, so the calculated throughput factor still gives a good indication of the compactness of the dewatering plant.

Whilst the predicted separating efficiency for the dewatering hydrocyclone can be seen to be comparatively modest, the levels of water in the discharged crude would be within most pipeline specifications (typically 1-3% in N. Sea, 5% for Brent [46]). Perhaps more significantly the hydrocyclone system is by far the most compact and, in addition, as hydrocyclones operate in multiple parallel units, modules can be arranged to fit into 'difficult' spaces with incremental alterations to the system size easily achieved. Such characteristics also provide operational flexibility, with banks of separators being switched in or out of use as required or interconnected in series to increase separation potential.

Other advantages in using hydrocyclones include their low maintenance requirements, not being prone to scaling or silting up and an estimated 5 year life for internals provided solids levels are not excessive [32]. Settling vessels require periodic digging or flushing out of accumulated sediments, whilst coalescer elements need to be replaced at regular intervals, typically every 6 weeks for the oily water treatment unit highlighted [47]. The small diameter and cylindrical form of hydrocyclones allows enclosure in standard pipe with safe operation at high pressures and in making use of reservoir pressure energy to generate separating action, dewatering hydrocyclones could also reduce emulsification

SEPARATING SYSTEM (990 $m^3/hr^{(3)}$ oil containing 20% water)	DECK AREA (m^2) / OPERATING WEIGHT (tonne)	THROUGHPUT PER UNIT DECK AREA PER UNIT WEIGHT (m/hr. tonne $\times 10^{-3}$)	PRINCIPAL DEWATERING UNIT	
			NOMINAL RESIDENCE TIME (s)	EXPECTED WATER CONTENT OF OIL DISCHARGE (%)
Electrical dehydrator (Petrolite) + gas floatation water clean up [41]	400 / 514	48	1800	~0.1
Forties 3-phase gravity separator + effluent control system[1] (see Section 3.1.6)	90 / 200	55	400	0.5-1.0
BP cartridge coalescer system[2] [41]	90 / 105	105	180	~0.05
2-stage hydrocyclone system (see Fig.10.3, and Section 10.4)	37 / 80	335	1-2	0.4-0.6

Notes 1. an allowance for gas removal has been made (20% reduction in space/weight figures)

2. published data has been reduced by 25% as a result of improved throughput in field trials

3. 150,000 bpd or 16,500 ℓ/min.

Water discharge to within North Sea spec. of < 40 ppm oil

Table 3.4 SIZE, WEIGHT, EFFICIENCY COMPARISON FOR OFFSHORE WATER/OIL SEPARATING SYSTEMS

enhancing pressure drops through the well-head chokes. Electric dehydrators by comparison require a high voltage power supply and it would cost ~$500 a day to treat the throughputs envisaged in Table 3.4 [34], whilst the large volume of typical gravity settling vessels necessitates a particularly massive construction if high pressures are to be safely withstood. Insensitivity to motion (or orientation) is a very advantageous feature of hydrocyclones in the context of floating platforms, where major upsets in performance are encountered with settling tanks in bad weather. Compared to the more conventional separators, the requirement for chemicals may also be lower for hydrocyclones [32] possibly reflecting their better contacting characteristics. Similar claims are made for the coalescer system [48].

The negative aspects of hydrocyclones include a possible need to pump the flow to the unit if reservoir pressures drop too low, but it should be recognised that effective separation can still be achieved at ~1/4 the designed for pressure drops (see Table 9.1). In addition, the very low residence times of hydrocyclones means that whilst they can respond rapidly to input transients, they will be quickly swamped by even short duration single phase slugs [49]. Finally, the reject flow from the dewatering hydrocyclone is likely to contain a relatively large proportion of oil (at least 10%) compared to the other separators considered and a good deal of uncertainty exists as to the precise nature and required size of this stream under field conditions. These operational aspects, including the possible effect of gas on performance, are discussed further in Chapter 10, and have been allowed for in the comparison in Table 3.4.

3.1.6 Offshore dewatering case study – Forties Alpha

This is one of four production platforms covering the Forties oil-field and is linked to the mainland via a crude oil pipeline. A simplified view of the oil production process is presented in Fig.3.4* with emphasis on dewatering, the two key areas being the primary production separator and the flush flow to the main oil line (MOL) pump seals.

---

* Information, including size/weight figures given in Table 3.4, obtained in a visit to the platform by the author in 1981, and updated by contact with BP personnel.

The bulk of water is removed from the produced fluids leaving the wells in a pair of 3– phase separators operating in parallel (a smaller test separator option is not shown in the figure). These are essentially gravity settling devices but incorporate a vortex inducing inlet geometry and demisting screens to enhance separation, with weirs and flow straighteners to optimise vessel hydraulics. This kind of coarse single stage treatment of the oil is generally confined to the earlier North Sea platforms with pipelines that have further onshore treatment plant (see Section 3.2.3). More recent production platforms tend to have a 2 or 3 stage separator train for oil clean up, allowing more efficient compression of the evolved gas and also, when required, a lower water (salt) content to the discharged crude. The water taken out from the oil on Forties rigs is treated with an effluent control system comprising a flash tank and Wemco floatation cell.

The flush flow to the mechanical seals of the MOL pumps is taken from the production stream. Cyclonic removal of sediment is practised to protect the seal faces from grit, but a high incidence of seal failure occurred in the late 1970's due to vaporisation damage which appeared to be closely related to increasing amounts of formation water breaking through from the 3– phase separator (1%+). The existing separators were not effective in removing this water and whilst developments in seal face material have since mitigated the problem [50], it is still desirable to minimise the water content of the flush stream.

The potential damage to seals has further been reduced by the manner in which the platform has been operated, where one of the priorities has been to minimise the risk of high water levels in the crude going to the pipeline. In 1981, with production around 17,600 ℓ/min (160,000 bpd) and planned to rise to a peak of 19,250 ℓ/min (175,000 bpd) (ex wells), water cuts were averaging ~13% and rising steadily i.e. the effluent control system was approaching its limiting operational capacity, beyond which water would be pushed back into the main oil stream. The need for an additional dehydrating stage (plus water clean up system) was anticipated. However, space was limited and an alternative strategy of extensive well re– lining was carried out instead to reduce water entrainment from the reservoir. The resulting operating conditions in July 1987 (Fig. 3.4) show water levels have only increased modestly, but with a now falling total production (oil and water) profile the existing separating system may remain effective.

3.2 Desalting Crude Oil

3.2.1 The need for desalting

At some point in the transfer of crude from the field to the refinery, the salt content of the flow needs to be at a level which is acceptable for refining. This is usually below the 'coarse' standards of near well-head treatment and hence further removal of brine (and possibly salt crystals as well if temperature changes have allowed them to form) is required. If this 'desalting' is not carried out clogging and corrosion problems will result in the refinery, particularly in the distillation plant. Acceptable salt tolerances of 10 ptb (pounds per thousand barrels) are applicable to BP refineries, equivalent to ~30 mg/ℓ salt or 0.05 – 0.1% of Forties formation water, although Shell will accept 25 ptb from their own oil-fields [46].

3.2.2 Separation techniques

Such deep dehydration could be carried out at the production site with separating conditions as described in Section 3.1. However, with offshore oil-fields, additional treatment is likely to be onshore, possibly at the end of a pipeline. This differs from the well-head conditions in that the aqueous phase that has stayed in suspension will probably have a finer drop size spectrum and be more stably entrained than before. Also temperatures are lower, being close to the environmental temperature of transportation, and reheating is essential before further dewatering can be attempted. Heat aids treatment by:–

(i) reducing the viscosity of the oil
(ii) weakening or rupturing the interfacial film by expanding the water drops
(iii) increasing the density difference between the fluids
(iv) raising chemical activity – encouraging demulsifier action.

Limitations include the problem of controlling the vaporisation of the commercially valuable light ends in the crude and also that it is more than twice as expensive to heat up the same volume of water as crude. The costs of unnecessary heating are high [51]. Commonly the heating unit is fully

integrated into a single separating vessel and is termed a heater–treater. The use of such separators is widespread and is not restricted to desalting alone but can often be found at a much earlier stage in the production process in land based operations when produced fluid temperatures are low.

Greatorex [52] describes the kind of procedure that might be expected during desalting:

(i) addition of fresh water (~4% is the critical minimum volume, below which stable emulsions tend to be produced) to wash out salt particles and destabilise the finely dispersed brine

(ii) a simple mixing system to maximise contact between the fresh water and the emulsion

(iii) demulsifier addition

(iv) for a basic pressure settling vessel, heating to temperatures sufficient to reduce crude viscosities to < 2 cSt should result in $>$ 90% salt removal. This means temperatures may well be in excess of 100°C [36].

The applicability of the hydrocyclone in this situation would also be largely dependent on the degree of oil viscosity reduction and drop size increase achieved by such pre–separation treatment methods, but there are other factors which make its use less attractive than in the offshore environment. Dewatering down to a few thousands of ppm contamination or less would probably require two stage operation and the space/weight savings that should still exist over most conventional separators are not so critical to land–based operations. Also artificial pressurising of the flow would be needed to drive the emulsion through the hydrocyclone system. Nevertheless, the use of hydrocyclones for this type of separation problem deserves consideration, if only as a preliminary clean up/contacting device.

3.2.3 Onshore desalting case study (Forties)

The Forties pipeline comes ashore at Cruden Bay and links with the Grangemouth refinery via a 130 mile landline. Immediately prior to the refinery

is the Kinneil processing plant where crude stabilisation is achieved before transfer to storage for shipping or directly to the refinery. The operating levels shown in Fig.3.5 are those prevailing in April 1981 (during a visit by the author) and whilst some streamlining has occurred since, the conditions described are believed to be typical of this kind of facility. The primary objective of the plant is degassing but desalting is also attempted with the aid of limited wash–water addition. A sufficient concentration of demulsifier was considered to be already present in the crude so no further addition was made. Unfortunately the true residence time for much of the oil through the flow tank was a matter of minutes rather than hours due to very poor hydraulic behaviour [53]. This resulted in inefficient operation, so another desalting stage was required in the refinery.

Refinery separation involves either electrostatic or gravity separators at operating temperatures of 130°C (achieved in heat exchange units). Wash water addition (at ~4%) precedes both treatment techniques, the gravity unit also requiring demulsifier injection (at ~15ppm). Final salt concentrations in the crude of 2 ptb were typical.

3.3 Dewatering Distillate Fuels on Ships

Ship propulsion fuels are subject to aqueous contamination, between initial acquisition from a supplier and final shipboard use through seepage, condensation and, in some cases, sea water ballasting (solid detritus may also be present in the fuel).

The widespread use of high performance turbine engines in ships, particularly naval vessels, involves the need for cleaner fuel (to prevent blade corrosion/erosion) than could be used by diesel engines and boilers. As the distillate fuels used in these cases tend to be lighter, kerosine–type fractions this makes the application of a hydrocyclone for contaminant control a more feasible prospect.

3.3.1 Nature of contaminant

A study of contaminants in Naval Distillate gas turbine fuel used on a U.S. destroyer [54] found water in concentrations $<1\%$ (volume) as small droplets with an average diameter of 15μ. However after ballasting, mean water drop sizes of 50μ were found in some samples, with the water phase comprising up to half the volume of the emulsion. Solid particle contamination, largely iron oxides, was typically between 200 and 400 mg/ℓ. These solids were considered important in stabilising the post-ballasting emulsions by acting as surfactant material.

The level of contamination that can be tolerated depends on the type of power unit being operated. Generally, for gas turbines about 10 ppm free water and 2 mg/ℓ solids) would be the upper limits, with diesel engines <100 ppm sea water might be an appropriate target, whilst boilers can tolerate BS & W (base sediment and water) levels up to 0.1% [55].

3.3.2 Conventional separation equipment on ships and the potential for hydrocyclones

Turbine fuel clean up is usually achieved in two stages:-

(i) coarse separation using an in-line centrifuge, bringing water contents down to perhaps 200 ppm or less (98% water removal for 15μ drops) and taking out the majority of the solids [55]
(ii) fine separation using a coalescing filter, to get down to the acceptable values quoted.

Engine room temperatures can approach 40°C, which puts the viscosity of a typical turbine fuel between 1.8 and 4.5 cSt. Such viscosities may be low enough to allow viable operation of a hydrocyclone, but only as a preliminary separation stage. Tests comparing a pumped hydrocyclone and centrifuge showed considerably inferior water and solids separation for the former [15] (see Lynn, Chapter 2). However, noted assets of the hydrocyclone system included savings estimated at 98.5% on space and 98.1% on power, lower capital and maintenance costs, quietness of operation and its light and robust construction.

3.4 Other Applications

There appear to be few broadly based commercial situations where there is a need for the removal of a denser dispersed liquid from a lighter continuous one, apart from dewatering oil. Applications tend to be fairly specific and a hydrocyclone's requirement of a density difference exceeding ~100 kg/m^3 and lowish continuous phase viscosities to work effectively, further narrows the field. However, two particular areas can be cited where hydrocyclones have been tried:–

(i) in the field of refrigeration, the removal of contaminant oil from a liquid ammonia cooling system [56]

(ii) in the nuclear power industry, solvent extrication of fissile material from irradiated fertile material and fission products in an aqueous phase, where both the contacting and separating action of hydrocyclones was made use of [9] (see Hitchon, Chapter 2).

One field where a potential application has been identified is in the dewatering of edible oils. Storage of palm oil in 500 tonne tanks results in the settling out of a few tons of condensate water (steam cleaning residue). The oil is required to be 'dry' before it can be used, so this water residue is drained off manually (with the loss of several hundred kilos of oil) to a level which ensures that the dehydrator downstream of the storage tank receives no more than its operational limit of 0.5% inlet water concentration. Employing a hydrocyclone as a coarse clean up device between tank and dehydrator to be used during this first stage of emptying has been considered a viable proposition in cutting down oil wastage [57].

A further possible application involves mineral processing where dense liquids like TBE (ρ = 2900 kg/m^3) need to be removed from water continuous systems [58].

CHAPTER 4

PERFORMANCE PRESENTATION AND SCALE UP

4.0 Introduction

Although the field systems ultimately being modelled may be multi-phase, the form of analysis presented in this chapter relates to the experimental programme's restriction to 2-component incompressible systems, in particular where the denser component is dispersed and more especially water-oil, for hydrocyclones with two outlets.

For a given hydrocyclone geometry and mixture, performance is evaluated by comparing the characteristics of the inlet and two outlet streams in the context of the prevailing operating conditions. The parameters measured in practice to assess performance (together with an indication of which were under the control of the operator) are shown in Table 4.1 and it can be recognised that only two of the streams need be analysed to gain knowledge of the make-up of the third stream from volume balance considerations (for Q, K and, assuming particles remain discrete, p(d)). It should also be noted that the absence of outlet stream dispersion sizing data for the water-oil tests (as dictated by experimental practicalities) limits their description to bulk concentration based separation efficiencies rather than the more useful particulate parameters. [Section 4.1]

Broader analysis, allowing meaningful comparisons between test results for different hydrocyclones and mixtures as well as performance prediction to be achieved, requires that the vital components of hydrocyclone operation can be encapsulated in dimensionless form. This in turn implies an understanding of flow and separation processes within the hydrocyclone. Accordingly the following factors should be considered, although knowledge may be imperfect in some areas:-

	WATER-OIL (see Chapter 7)		NYLON-WATER (see Chapter 5)	
	UNDER OPERATOR CONTROL	MEASURED	UNDER OPERATOR CONTROL	MEASURED
Q_i	✓	✓	✓	
K_i	✓	✓	✓	
P_i	✓	✓	✓	✓
$p_i(d)$	✓	✓		
Q_i	✓		✓	✓
Q_u	✓	✓	✓	✓
K_u		✓		✓
K_d				✓
P_u		✓		✓
P_d		✓		✓
$p_u(d)$				✓
$p_d(d)$				✓

Table 4.1 CONTROL AND MEASUREMENT OF PERFORMANCE DEFINING PARAMETERS

	WATER-OIL	NYLON-WATER
ρ	✓	✓
ρ_p	✓	✓
μ	✓	✓
μ_p	✓	n/a
γ	✓	n/a

Table 4.2 MEASURED 2-COMPONENT SYSTEM DEFINING PARAMETERS

- the properties of mixtures to be separated (Table 4.2)

- the dimensions of hydrocyclone geometries

- the resulting internal flow structure for a given set of operating conditions. [Section 4.2]

4.1 Performance Characterisation.

At the simplest level, the priority is to attain a minimum content of the denser dispersion (water) in the upstream discharge (clean oil stream) which can be monitored in terms of a volumetric percentage as K_u. This gives no indication of the degree of separation achieved in the hydrocyclone, but reference to the inlet concentration to generate K_u/K_i provides an easily interpretted efficiency parameter which will be used extensively. Similarly, the condition of the downstream (water reject) can be viewed in terms of K_d and K_d/K_i. Note that K_u/K_i goes from $0 \rightarrow 1$ and K_d/K_i from $1/K_i \rightarrow 1$ as respective stream separation efficiencies, $1-(K_u/K_i)$ and $1-((1-K_d)/(1-K_i))$, go from $1 \rightarrow 0$. The minimum in K_u/K_i with increasing flowrate will be termed $(K_u/K_i)_{min}$.

So far no account has been taken of the split ratio ($1-F = Q_d/Q_i$), a very significant operational parameter with the substantial range in K_i under investigation. It helps determine the yield of a system, which it is commonly desirable to maximise (i.e. minimise loss of light component to the downstream for dewatering). Accordingly, an important performance measure in the context of commercial water–oil separation is the oil recovery index – the fraction of influent oil retained in the process stream

$$E_{or} = \frac{(1-K_u)}{(1-K_i)} \cdot F \qquad (4.1)$$

The problem of reflecting both product quality and yield in a single parameter is more generally interpreted by the overall or reduced efficiency.

$$E = F\left[\frac{(K_i - K_u)}{K_i(1-K_i)}\right] \qquad (4.2)$$

which represents the sum of the flowrates of the pure discharged components expressed as a fraction of the feed flowrate, and is extensively discussed by Tengbergen and Rietema [59].

These two efficiences, together with the concentration ratios outlined earlier, are plotted against split for best possible separation (i.e. either $K_u \to 0$ or $K_d \to 1$) in Fig. 4.1. The inter-related form of the curves comes out from the volume balance equation

$$K_i = FK_u + (1-F)K_d \qquad (4.3)$$

It can be seen that at the K_i illustrated (< 0.5, typical of the water-oil tests), there is a greater sensitivity in E to 'overloading' the downstream outlet i.e. when Q_d is insufficient to remove all separated water and some is pushed back upstream, than to 'underloading' i.e. when Q_d is more than sufficient to remove the water. However, as this asymmetry emphasizes a clean oil stream over a clean water stream it is compatible with the general aims of the programme.

It is also evident from the plot how important the balance between K_i and $1-F$ is in maximising performance. A significant gradient change occurs in all plotted parameters at a critical split, defined as $(1-F)_{crit}$, which has been characterised by the ratio

$$\frac{(1-F)_{crit}}{K_i} \qquad (4.4)$$

This is unity for the ideal circumstances under consideration, but practically it will be >1 (see Fig.9.7) and the more the deviation the lower the potential maximum in both E and E_{or} and the poorer the degree of coalescence and capacity for phase inversion of the dispersed component (water) in the hydrocyclone. However, practically it may be important for the operator to be able to deal with a range of K_i without having to adjust split.

Particulate separation efficiency data was only obtained from solid–liquid testing, where the particle migration probability is defined as the chance of a specific particle size being separated to the downstream outlet

$$MP(d) = \frac{p_d(d)K_dQ_d}{p_i(d)K_iQ_i} \qquad (4.5)$$

where p(d) represents the percentage by volume particle size distribution. The reduced form of the migration probability is more generally used as it removes the effect of the 'dead flux' due to the split ratio to become

$$MP'(d) = \frac{MP(d)-(1-F)}{F} \qquad (4.6)$$

It should be emphasized that this is a more significant exercise for the comparatively high split levels used in dewatering applications than for typical deoiling or mineral processing applications, where reject flows are small.

Flowrate, Q_i, and pressure drop, ΔP, are important interdependent capacity defining parameters which are also functionally related to the separation. Turn–down ratio, the maximum flowrate divided by the minimum flowrate at which a certain level of efficiency is attained, defines the working flow range of the hydrocyclone (TDR = Q_{max}/Q_{min}). This can be combined with $(K_u/K_i)_{min}$ as $TDR/(K_u/K_i)_{min}$ to provide a more general guide to performance capabilities, which it is desirable to maximise. Turn–down can also be looked at in terms of allowable pressure drop range.

4.2 Scaling and Dimensionless Analysis.

Generalisation of results, to provide the basis for scaling and comparative work, requires the operation and performance of the hydrocyclone to be characterised by appropriate dimensionless parameters.

4.2.1 Flowfield level.

(i) low dispersion concentrations – in this case, the flow can be assumed to behave as if it were only the continuous liquid phase, and as gravity effects are relatively insignificant in the hydrocyclone, the system can largely be typified by the force ratios:–

$$C_P = \frac{\Delta P}{\frac{1}{2}\rho v_i^2} \tag{4.7}$$

$$Re_D = \frac{\rho v_i D}{\mu} \tag{4.8}$$

where C_P is a pressure coefficient or Euler number and Re_D is a flowfield Reynolds number. The value of these numbers is a function of how representative of the system are the variables that comprise them. The velocity and diameter terms used were chosen because of how v_i directly represents entry conditions and closely links with v_θ, and also how D (defining the widest point of the main conical section) has a common identity over a wide range of geometry types.

(ii) high dispersion concentrations – with increasing K_i, a point is reached when some account should be taken of the 2–component nature of the flow ($K_i \triangleq 10\%$, see later this section). Both density and viscosity terms will be affected, although local variations in dispersion concentration through the hydrocyclone (including phase inversion) provide a difficult target for a single representative value to be applied. The characteristics of the feed are more readily defined and a weighted mean density can be readily determined, $\bar{\rho} = K_i\rho_w + (1-K_i)\rho_o$. This differs little from the continuous or oil component density (e.g. for $K_i = 40\%$, $\bar{\rho}$ is only 10% greater than ρ) but provides slightly more rigor to the dynamic head term in the pressure coefficient, whence $\bar{C}_P$ incoporates $\bar{\rho}$ instead of ρ.

Reynolds number contains both density and viscosity parameters and its seems inappropriate to increase density without also considering the viscosity effect, i.e. $\bar{Re}_D$ will not be defined. Hence an apparent viscosity needs to be evaluated as well, for a system which is almost certainly non–Newtonian. This is

problematical as no measurements in the test programme were specifically directed towards obtaining such viscosity data and even if the feed flow had been sampled and analysed*, there would still be no accounting for the effect of concentration and also shear gradients within the hydrocyclone. However, it is clear that viscosity changes introduced by increasing K_i are much more significant than the effect on density, and this is shown in Fig 4.2 where $\bar{C}_{Piu}$ is plotted against K_i for a constant value of Re_D in geometry 36NS5(S). If the changes in $\bar{C}_{Piu}$ are looked at in the context of a $\bar{C}_{Piu}$ vs. Re_D plot for K_i = 5% (close to no water) and at the same split ratio (Fig. 9.22), an apparent viscosity (μ_a) *characteristic of the system between inlet and upstream outlet pressure tappings* can be determined on the basis of a $\bar{C}_{Piu}$ vs. Re'_D plot being independent of K_i, where

$$Re'_D = \frac{v_i D\bar{\rho}}{\mu_a} \qquad (4.9)$$

For example, from Fig.4.2 for kero(SG) as K_i goes from 0 → 40%, $\bar{C}_{Piu}$ falls from 11 to 7, this represents a 4.5− fold drop in Re_D in Fig.9.22 which would mean a 5− fold increase in viscosity had occurred (allowing for the 10% rise in mean density).

This degree of variation is not predicted by simple theoretical models for the apparent viscosity of two pure immiscible liquids [60, 61], but Graifer et al [62] considering water− crude emulsions suggest a more vigorous relationship of the form

$$\log_e\left[\frac{\mu_a}{\mu}\right] = B\,K_i \qquad (4.10)$$

where B (= 2−6) is an empirically derived coefficient dependent on the level of dispersion of the water. This has been adapted by the author, based on the experimental results shown in Fig.4.2, to give

$$\begin{aligned} K_i &< 0.1 && \mu_a = \mu \\ 0.4 &> K_i > 0.1 && \mu_a = \mu.\exp(B(K_i-0.1)) \end{aligned} \qquad (4.11)$$

---

* Dealy [63] comments that to make reliable measurements of the viscosity of non− Newtonian fluids, the shear rate within the viscometer should be approximately uniform, which is only the case for small gap rotational viscometers.

where B ≙ 5.5, and implies that continuous component based parameters are reasonably representative up to dispersion concentrations of 10%. In addition, as the value for B is fairly narrowly defined for both distillates tested over a considerable drop size range ($\bar{d}_i \simeq 25 \rightarrow 150\mu$) an independence of viscosity from the level of dispersion is indicated, in agreement with the conclusion of Thompson et al., regarding simulated formation water–crude emulsions above a critical $\bar{d}$ (15–30μ) [64].

Fig.4.3 shows that the concentration effect is comparable, although less severe, for the inlet to downstream pressure coefficient, with B in equation 4.11 coming out at ~3, by analagous reasoning to the upstream analysis (exponent for $\bar{C}_{Pid} \propto Re_D^q$ relationship obtained from Table 9.1, q = n–2).

As a postscript to this discussion, for solid particles Medronho reports a decrease in hydrocyclone pressure coefficient with increasing dispersed phase concentration to a minimum ~ 10% (by volume), rising thereafter [121]. This underlines some of the complexity of concentration effects on hydrocyclone operation.

(iii) split ratio – the effect of this parameter can be incorporated into the pressure coefficient by using a 'reduced' pressure drop representing ΔP at 50% split, ΔP_{50}, such that

$$C_P' = \frac{\Delta P_{50}}{\frac{1}{2}\bar{\rho} v_i^2} \qquad (4.12)$$

Considering Fig.9.6, where pressure drop changes with split at Q_i = 50 ℓ/min are shown, m = dΔP/d(1–F) appears to be roughly constant regardless of oil type and also as $\Delta P \propto Q_i^n$, so $|m| \propto Q_i^n$. Hence for 36NS5(S), averaging gradients in Fig.9.6 and exponents from Section 9.1 and Fig.9.22, the reduced pressure drop can be evaluated using

$$\Delta P_{50} = \Delta P + \left[M \left[\frac{Q_i}{50} \right]^n (F-0.5) \right] \text{ bar} \qquad (4.13)$$

where $M = m$ at $Q_i = 50$ ℓ/min and for ΔP_{iu} $M_{iu} = -0.42$ bar and $n = 2.2$, whilst for ΔP_{id} $M_{id} = 1.03$ bar and $n = 2.35$, and Q_i is in ℓ/min.

Similar gradients are anticipated for 35NS7(V), as evidenced by Fig.9.16.

4.2.2. Particle level

Movement of particles within the hydrocyclone can be fairly realistically viewed using a local field concept, as discussed by Bedeaux with regard to viscosity [65]. This means a particle Reynolds number can be defined with continuous component rather than medium based parameters as

$$Re_p = \frac{u d_f \rho}{\mu} \qquad (4.14)$$

where u is the particle velocity relative to the surrounding liquid and d_f the 'free fall' particle size (see Section 5.2.4).

Local dimensionless groups illustrative of drop stability, notably break up characterisation using a Weber number, are discussed in Chapter 8.

4.2.3. Separation

(i) Hydrocyclone number

The simplest basis for comparing the separation efficiency of two hydrocyclones operating with different 2–component mixtures is to require that the hydrocyclones have similar geometries so that equal Re_D will reflect similar flow structures, given that split ratios are also the same. This implies that at equivalent points in the hydrocyclones the various components of the flow velocity relate in the same manner. Hence, particle trajectories and therefore migration probabilities can also be linked, and adopting Stokesian settling principles for the radial movement of the particles the dimensionless parameter

$$Hy = \frac{Q_i \Delta\rho d_S^{\,2}}{D^3 \mu} \qquad (4.15)$$

can be derived to make the comparison, where d_S is the Stokes diameter of the particle. This was termed the hydrocyclone number by Colman and is fully derived in his thesis [67]. However, effectively the same dimensionless group has been widely recognised by other workers and is often referred to as the Stokes number (= 0.698 Hy) [2].

The conditions for using this technique, apart from geometrical similarity and equality of Re_D, must also include the assumptions implicit in Stokes Law, namely

(i) particles behave like independent solid spheres

(ii) flow around the particles is laminar ($Re_p < 1$)

The application of Hy, together with a wider discussion of the assumptions involved in its use for both solid particles and droplets, is demonstrated for low K_i systems in Section 5.2.4. This includes a modification to the hydrocyclone number in an attempt to characterise dispersions (by using $\bar{d}_i$ as the drop diameter term) so that bulk efficiencies can be assessed and also investigation of the limits to its use set by drop break up.

A more direct parameter, advocated by Abrahamson and Allen working with cyclones, is the ratio $|u_r/v_r|$ at $r = D_u/2$ [66]. Whilst being comparatively independent of geometry, the knowledge needed of internal velocity structures makes it difficult to define.

(ii) Normalised efficiency (after Colman [67])

Comparisons between two different geometries for solid–liquid tests has been approached by trying to compare efficiencies for the same mixture using Hy and C_P, in an attempt to resolve the problem of whether at a given flowrate better separation at the cost of a higher pressure drop, which might result from a design change, actually represents a more effective hydrocyclone.

The way the normalisation process works requires that for one of the hydrocyclones the variation of an efficiency parameter, E say, with through–flow, Q, is known. Denoting specific parameters relating to this geometry with subscript 1, this hydrocyclone has a diameter D_1 and operates at a condition $Q_1, \Delta P_1$ to give E1. Using C_P it is required to find the effective diameter D_1' which represents the flow/pressure conditions Q_2, ΔP_2 of the other hydrocyclone (geometry 2). Using Hy, the flowrate equivalent of D_1' in the D_1 hydrocyclone can be predicted, Q_1', and the normalised efficiency E_1' read off from the Q vs. E plot for geometry 1 and compared directly with E_1.

To operate this technique effectively Re_D should be similar for the two hydrocyclones being compared, which implies that they are of the same nominal size if the simplifying case of using common mixtures is taken. Hence, ΔP_2 and Q_2 can be chosen to be near typical ΔP_1 and Q_1 conditions so that D_1' will not significantly differ from D_1 nor Q_1' from Q_1 which means that $Re_{D_1} \simeq Re_{D_1'}$ and thus it also follows that Re_p equality will prevail, both conditions for validity of Hy.

With flow Reynolds numbers being similar, C_P, interpreted as $\Delta P / \frac{1}{2}\rho(Q/\frac{1}{4}\pi D^2)^2$ can also be taken as being equal giving

$$\frac{\Delta P_1}{(Q_1^2/D_1^4)} = \frac{\Delta P_2}{(Q_2^2/D_1'^4)} \qquad \rho \text{ constant}$$

$$D_1' = \left[\frac{Q_2^2}{\Delta P_2} \cdot \frac{\Delta P_1}{Q_1^2}\right]^{\frac{1}{4}} D_1 \qquad (4.16)$$

Now Hy will relate particles of similar separation potential and as the mixture is the same d, $\Delta\rho$ and μ can be eliminated from the relation which becomes

$$\frac{Q_1'}{D_1'^3} = \frac{Q_1}{D_1^3} \qquad (4.17)$$

for equal separation efficiency.

The use of the normalisation process for liquid–liquid systems, is not really practical as the peaking then fall off in efficiency with increasing flowrate due to drop disintegration cannot be readily predicted or scaled. Hence, projections of flowrate:efficiency plots are not very meaningful.

4.2.4 Geometry

Geometry definition in terms of simple length and diameter ratios is covered in Appendix D. However, some of these parameters can be combined to provide a measure of the 'swirl' injected by synthesizing a v_θ/v_z ratio which represents the relative degree of spin of the flow as it enters the conical section (at diameter D) for a loss free system. This is termed the swirl number, S, and is derived (refer to Appendix D for terminology) by combining

$$v_i A_i = \frac{\pi}{4} D^2 \bar{v}_z$$

with

$$\frac{D}{2} v_\theta = \frac{x_i}{2} v_i$$

(assumptions: $v_\theta r$ = const., angular momentum conserved, $\partial v_\theta/\partial z = 0$)

such that

$$S = \frac{v_\theta}{\bar{v}_z} = \frac{\pi X_i D}{4 A_i} \qquad (4.18)$$

The higher the value of S the greater the separation potential of the hydrocyclone but also the greater the likelihood of higher pressure drops, flow instabilities and droplet break up.

CHAPTER 5

USE OF SOLID PARTICLES IN PRELIMINARY GEOMETRY DEVELOPMENT

5.1 The Need for a Solid–Liquid Analogue

The starting point for the research programme was a hydrocyclone design, developed from some limited experimental studies of geometry by Debenham [3], which gave best separation performance for a water–kerosine system. Initial trials were carried out using Debenham's test rig (L1, Fig.7.1) to repeat and extend results for this 'optimal' geometry (Fig.D.1). The detail of rig operation is covered in Section 7.1 and typical test results are considered later in this chapter (Section 5.3) and also in [2]. However, the efficacy of the set–up was restricted by a number of factors, in particular:

- inlet drop size was coarse and largely unknown, and with pumping and mixing being achieved in a single pump the ability to vary feed drop size was limited

- the oil feedstock volume was restricted and as the rig operated on a 'single pass' basis this allowed only short run times with substantial intervals between tests to allow water to settle out from the oil before re–use.

The subsequent development of the water–oil test rig and associated instrumentation (especially for drop sizing) to overcome these problems is documented in Chapter 7. However, as an interim measure it was considered that a solid–liquid analogue might provide a useful model for the water–kerosine system, at least for low dispersion concentrations. A similar approach to the analysis of oil–water systems in hydrocyclones had been pioneered by Regehr [18], and Colman later developed the concept as a major technique in establishing a viable deoiling hydrocyclone design [67]. Certainly the use of solids facilitates a recirculation format for the rig, speeding experimentation. In addition, if water is used as the continuous phase, sizing of feed (and discharge) dispersions can be rapidly undertaken using a Coulter Counter (available in the department) to allow a more definitive measure of separation performance.

A solid– liquid test system was set up on this basis and primarily used in two ways:–

(i) as a means of geometry development, where hydrocyclone design modifications were made that were perceived to be advantageous to liquid– liquid separation, and which were judged successful if pressure drop compensated normalised efficiencies (see Section 4.2.3) with the analogue were not adversely affected.

(ii) for the hydrocyclone which was a product of process (i), to attempt a prediction of water– kerosine separation based on the hydrocyclone number, Hy, (see Section 4.2.3) and by comparison with later test data for the liquid– liquid system, gain knowledge of the extent of drop break up and coalescence effects.

5.2 Solid– Liquid Analogue Separation Tests

5.2.1. Choice of Solids

The choice of solid– liquid system needed to broadly reflect the character of the water– kerosine system whilst also being sufficiently difficult to separate that even small changes in hydrocyclone geometry would produce clear changes in efficiency (i.e. $\bar{d}_i \triangleq d'_{50}$). From Hy, which relates particles of equal separation potential, the properties of the mixture are characterised by $\Delta\rho d^2/\mu$ and for water– kerosine $\Delta\rho = 218$ kg/m^3 and $\mu = 1.40$ cP (20°C), although drop size was still an unknown quantity at this stage. Given the convenience of using water as the continuous phase for the analogue, some kind of plastic powder seemed an appropriate material for the dispersion, being homogeneous, relatively inert and of the right kind of density. After investigation of a number of powders, a nylon was chosen with $\rho = 1140$ kg/m^3, hence $\Delta\rho = 142$ kg/m^3, and $\mu = 1.00$ cP (20°C). This provided a good match in terms of $\Delta\rho/\mu$ to water– kerosine. The nylon particles were shown to have a slightly rounded, ellipsoidal form under the electron– microscope (Plate I) with a roughly normal size distribution (by volume) about $\bar{d} = 31\,\mu$ (for more detail see Section 5.2.4.)

5.2.2. Test rig

The test rig used is shown in Fig.A.1 and whilst only an outline of the experimental procedure is given here operational details can be found in Appendix A.

About 700 mg/ℓ of nylon powder (a convenient working concentration) is set up in a mixing tank together with a wetting agent to prevent particle flocculation. The suspension is pumped around the flow circuit, through the test hydrocyclone and back to the mixing tank where the suspension is maintained by the stirring effect of the discharge flows. Stream samples give mass concentrations of nylon by filtration and weighing, with selected samples being sized by Coulter Counter.

5.2.3 Geometry development

Debenham's hydrocyclone design, geometry code 30PD(T) (see Appendix D), had shown promising levels of separation for water–kerosine (Section 5.3) although only for coarse dispersions (subsequently sized at $\bar{d}_i = 200-250\mu$ for $K_i = 12.5\%$) and flows up to 12 ℓ/min, above which performance fell away, presumably as a result of the onset of significant drop break up. As this process is believed to be a function of shear levels in the hydrocyclone (see Chapter 8) geometry changes were planned that were considered would smooth the passage of the flow through the hydrocyclone, minimising unnecessary shear and also promoting vortex stability. Translated into the reference frame of the nylon–water analogue, the target became to try and at least maintain good solids separation for the lowest pressure requirement with the assumption that on reverting to a liquid dispersion, performance would be superior.

More specifically, 30PD(T) (Fig.D.1) is constructed from Perspex modules and takes the form of a D= 30mm hydrocyclone with twin, diametrically opposed, circular inlets whilst the main body of the separator comprises a series of cylindrical units connected by contraction sections. The inlet area ($A_i/A = 0.0625$) is at the larger end of the range found for conventional solids separating hydrocyclones and the aspect ratio (at L/D = 16) is considerably longer than is typical [2].

Two principal areas were perceived to be in need of change:

(i) inlet section – energy lost by the flow on entry to the hydrocyclone is believed to be a major source of turbulent shear [1, 13]. Increasing inlet size lowers the pressure loss here and if the accompanying reduction in inlet velocity can be compensated by feed entry at a greater radius ($v_i r$ = const.), the injected angular momentum characteristics of the unit can be maintained but with the dangers of drop break up reduced. On contracting this large diameter swirl generating chamber back to the original hydrocyclone body size, D, high angular velocities are produced (by conservation of angular momentum) comparable with the original unit. Colman shows an approximate doubling of the maximum stable drop size which can be handled by a hydrocyclone when using a swirl chamber (compare [6] and [67]).

(ii) conical section – smoothing of the stepped pseudo–cone should help stabilise the vortex in this area.

The 'New Series' geometries (NS1→ 3) explore these kind of changes using available Perspex components (Figs.D2→ 4) and performance is assessed based on plots of K_u/K_i vs. Q_i (Fig.5.1) and ΔP vs. Q_i (Fig.5.2) relative to Debenham's original geometry for a working split ratio of 12.5%.

30NSl(T) represents a stream lining of the conical section of 30PD(T) which improves separation without increasing the pressure requirement. The effect of introducing a swirl chamber is shown in general terms by comparing 30NS2(T) with 30NS3(T). Whilst a slightly lower normalised efficiency is evident for 30NS3(T) (with double the inlet area and a swirl chamber), this should be viewed in the context of Dl only being wide enough to generate 80% of the swirl achieved in 30NS2(T), although this deficit may be partly offset by a change to rectangular inlets which introduce more of the flow close to the wall. On balance it seems the introduction of the swirl chamber is of little, if any, detriment to hydrocyclone performance with solids.

Working from these results and with the M.O.L. pump seals flush application in mind (Section 1.4), geometry 36NS4P(T) was constructed (see Fig.D.5) as essentially a larger scale refinement of the NS3 design, but with

smaller inlets to generate a swirl characteristic comparable with PD and NS1 (S= 13). Looking to run at a feed flowrate of 45 ℓ/min, Q_i/D^3 scaling was applied (from Hy) to find the hydrocyclone diameter to match the separation achieved at 27 ℓ/min in a D = 30mm unit (considered to be a flow at which the rate of improvement in K_u/K_i with increasing Q_i was slowing down considerably). Refinements include the synthesis of the 4° and 10° contraction sections to a single α = 6° cone with approximately the same overall length and the shortening of the swirl chamber (largely by eliminating the space 'above' the inlets which is believed to contribute to short circuit flow [1]) with a corresponding reduction in vortex finder length. The removal of the cylindrical downstream section was considered to take little away from the performance and was primarily undertaken to limit the length of the hydrocyclone, a requirement relating to the possible fitting of such a unit into an existing harness in the M.O.L. pumps application. Reversion to circular inlets facilitated lathe based workshop manufacture, whilst the similarly sized outlets appropriate to an even discharge from upstream and downstream (oil stream of ~23ℓ/min required, 50% split) were retained.

Results of tests with nylon– water for 36NS4P(T) are also shown on Figs. 5.1 and 5.2 and it is seen from normalised data that this, presumed low shear, geometry out–performs the earlier designs* with the expectation of an equivalent if not better advantage in liquid–liquid applications (see Section 5.3).

5.2.4. Prediction of water–kerosine separation

Use of the nylon–water test data to predict the separation of other dispersions, and especially water–kerosine, requires an effective correlation to be established between the systems. One such technique, based around using the

---

* It should be pointed out that the limited similarity between geometries, as evidenced by a degree of variation in the log ΔP: log Q_i gradients in Fig 5.2, and narrow range of flowrates tested, both act to limit the reliability of the normalisation process. Hence, the normalised efficiencies quoted should only be treated as a general guide to the potential of a particular geometry.

hydrocyclone number (Hy) to non-dimensionalise particle migration probabilities is attempted and the limits to its application explored by comparison with experimental results from the up-graded water-oil test facility (Rig L2, Fig.7.2) incorporating the newly developed dynamic drop sizing system for characterising the feed (Section 7.3.2.).

Whilst primarily concerned with the 36NS4P(T) geometry, this exercise was also carried out for a conventional hydrocyclone essentially designed to remove solids (32MANF.A, Fig.D.6), but also recommended by the manufacturer as an oil dewaterer. In this respect, it had been the best commercial geometry tried for the M.O.L. pump seals flush application. To facilitate the comparison between the prediction from the analogue and experimental data for the water-kerosine system, the solid-liquid and liquid-liquid tests were run at the same split ratio (50%), comparatively low dispersion concentrations (700 mg/ℓ nylon, 5% water) and similar flowfield Reynolds numbers (10^5). However, the finest feed dispersion which could effectively be achieved in the water kerosine tests turned out to be a somewhat larger size range with a higher mean ($\bar{d} = 43\mu$, $(20)^d(80) = 34\mu$) than the nylon particle size distribution ($\bar{d} = 31\mu$, $(20)^d(80) = 16\mu$), see Fig.5.3, and as will be shown, closer overlap would have been desirable.

Separation of dispersions can be characterised for dynamically similar hydrocyclones based on the assumption that particles of similar migration probability, MP, are related by equal Hy, although the primary concern here is with establishing links between differing dispersions in the same hydrocyclone. The migration probability of a (heavy) particle has been calculated based on outlet flow analysis of the nylon-water work as:

$$MP(d) = \frac{p_d(d)K_dQ_d}{p_d(d)K_dQ_d+p_u(d)K_uQ_u} \qquad (5.1)$$

Both Hy and MP are introduced in greater depth in Section 4.2.3. For this analysis, the reduced form of the migration probability (MP') will be used (equation 4.6) to isolate the true separation from the split effect, whilst the particle size term in Hy will be replaced by a more widely applicable settling related term, the free fall diameter, d_f, which represents the size of a sphere with the same terminal velocity in a fluid as the particle ($d_f = d_S$ for laminar

flow conditions). Although some of the rigor of the correlation may be lost for particle Reynolds numbers (Re_p) > 1, similarity will always be maintained for equal Re_p [67]. Corrections need to be applied for the shape of the nylon particles, as the Coulter based sizing responds to the particle volume and then assumes sphericity, whilst it can be seen from Plate I that the particles are roughly ellipsoids with major diameters in the ratio 2.1: 1.5 : 1 on average and will therefore have a relatively higher drag than spheres of the same volume. Heywood [69] provides a method for making this correction based on empirical data which caters for settling conditions extending to Re_p above the Stokesian regime. Working from estimated (see Section 6.3) acceleration fields at D/4 from the axis in 36NS4P(T) and mid-size range particles, $d_f = 0.87 \rightarrow 0.89$ d for flowfield Reynolds numbers, $Re_D = (1.2 \rightarrow 2) \times 10^5$. These will also be the nominal conditions used for calculating Re_p.

Particle terminal velocities, u_r, and hence Re_p can also be determined using Heywoods paper, and for the majority of particles $Re_p < 1$ in the test hydrocyclones. The assumption that near-terminal particle velocities are achieved during separation appears wholly valid, as calculations show that the time taken to accelerate particles to 99% u_r is typically 3 orders of magnitude smaller than hydrocyclone residence times. Hindered settling effects (particle interaction) can certainly be ruled out for the very low concentrations of nylon-in-water being used and independence of separation performance from K_i has been shown experimentally up to 10,000 mg/ℓ for this system [70].

Hence, the nylon-water system looks to conform well to the requirements for sound applicability of Hy and the correlation between $Hy(d_f)$ and $MP'(d_f)$ it provides is plotted in Figs.5.4 and 5.5 for 36NS4P(T) and 32MANF.A respectively.

The 'S' shaped form of the relationship is clear from Fig 5.4 (note log scale for $Hy(d_f)$) and good superimposition of data is obtained from quite a broad based test flow range for 50% split i.e. a very weak dependence on Re_D is indicated, at least in this range. Operation of 36NS4P(T) at a lower split of 12.5% (comparable with the geometry development test condition) can be seen to be considerably less efficient and implies a deterioration (with regard to separation) has occurred in the hydrocyclone flowfield structure.

The form of the curve for the commercial hydrocyclone (Fig.5.5) mainly differs from 36NS4P(T) at $1-F = 50\%$ in having a deficiency in separation at high $Hy(d_f)$ or more specifically for large nylon particles. This indicates re-entrainment of this material is occurring in the reversed flow to the upstream outlet. For 12.5% split, classification is sharper, although the same bulk separation (K_u/K_i) is achieved as for 50% split at the same flowrate.

In extending the correlation to the water-kerosine system, the general evidence which might indicate the degree to which drops behave like particles will be considered first, before looking more specifically at how the available test data can be related to the migration probability curves.

The assumption is made for the water drops that $d = d_f$ and this implies that the drops behave as rigid spheres. The drops certainly look spherical before entering the hydrocyclone (Plate VIII) and settlement enhancing internal circulation effects are considered to be negligible for water/kerosine viscosity ratios at the low Re_p conditions encountered in the hydrocyclone's acceleration field. The assumption of a surface 'skin' is probably also justified as the liquids are not pure and even small amounts of surfactant can resist the 'driving' hydrodynamic stresses [71]. Even with $K_i = 5\%$, it is thought that droplet agglomeration and hindered settling effects can be neglected [72], whilst the dispersion is still too dilute to cause much macroscopic change to the flow-field [11]. Also, as large reject flows are being used the condition of $(1-F) >> K_i$, necessary for good separation is the same for both water-kerosine and nylon-water.

To achieve flowfield similarity, the nylon-water tests were run at lower Q_i to compensate for the higher kinematic viscosity of kerosine compared to water, even though Re_D is not a dominant group. However, Re_p for equal sized particles comes out slightly higher for the water-kerosine tests (typically $1.5 \rightarrow 3 \times$ greater) with an increased prevalence but still minority of conditions where $Re_p > 1$ for the dispersion as a whole.

The most significant problem, however, is that the differences between the size distributions of the water and nylon dispersions are magnified by the d_f^2

term in $Hy(d_f)$. Hence, for 36NS4P(T) tests with nylon–water, $Hy(d_f) = 2 \times 10^{-5} \rightarrow 7 \times 10^{-3}$ whilst with water–kerosine $Hy(d_f) = 8 \times 10^{-5} \rightarrow 5 \times 10^{-2}$. As gross water–kerosine separation performance is strongly dependent on the migration probability of the largest drops, the process of extrapolating the correlation beyond the measured nylon–water data points in Figs.5.4 and 5.5 is rather critical. Statistically the uncertainty is raised by the low numerical frequency of the larger nylon particles.

As only inlet size spectra and not migration probability data are available for the water–kerosine tests comparisons between the liquid–liquid system and its solid–liquid analogue cannot be made directly using the $MP'(d_f)$ vs. $Hy(d_f)$ curve. Instead the integrated effect of this correlation can be used to predict water–kerosine separation efficiency (in terms of K_u/K_i) based on known inlet conditions. Svarovsky [2] has shown that:

$$\frac{K_d Q_d}{K_i Q_i} = \int_0^1 MP(d_f)\ dp_i(d_f) \qquad (5.2)$$

now

$$\frac{K_d}{K_i}(1-F) = 1 - \frac{K_u F}{K_i}$$

and by substitution from equation 4.5 ($d \rightarrow d_{(f)}$), it can be shown that

$$1 - \frac{K_u}{K_i} = \int_0^1 MP'(d_f)\ dp_i(d_f) \qquad (5.3)$$

where $MP'(d_f)$ is obtained from $Hy(d_f)$.

A comparison with water–kerosine data could now be made but only in the region of $Hy(d_f)$ overlap, so to broaden the scope of the correlation a characteristic diameter was sought which could be used in Hy such that it typified the dispersion and fell within a well defined portion of the curve. Predictions from equation 5.3 for water–kerosine tests at low flowrates can be closely matched (to within about 5% of K_u/K_i values regardless of hydrocyclone geometry) by using $\bar{d}_f$ as this characteristic diameter, where $Hy(\bar{d}_f)$ is used to obtain a single $MP'(\bar{d}_f)$ parameter from Figs.5.4 and 5.5 which can be converted directly to K_u/K_i by the reduction of equation 5.3 for monosized particles to give

$$\frac{K_u}{K_i} = 1 - MP'(\bar{d}_f) \qquad (5.4)$$

Hence, a prediction of water–kerosine volumetric separation performance can be simply made based on the observed nylon–water migration probability spectra and the curves so generated are shown plotted against $Hy(\bar{d}_f)$ in Fig.5.6 together with experimental data.

The upturn in the experimental water–kerosine K_u/K_i, equivalent to a fall off in separation performance, is probably related to the onset of significant droplet break up in the hydrocyclone with increasing flowrate and the correlation, with its assumption of drop rigidity will not be valid under these conditions. Therefore, in evaluating the correlation consideration will only be given to operation below the K_u/K_i minima.

For both 36NS4P(T) and 32MANF.A, accepting the limited number of experimental points, the prediction of water–kerosine separation appears to be reasonable with a slight overestimate of K_u/K_i. This implies that a separation enhancing effect is occurring and there is some through–wall photographic evidence to suggest that this may be linked with droplet coalescence (see Section 8.1).

Also in this figure, the operating curve for hydrocyclone 26NS4P(T) (Fig.D.7) with the same water–kerosine dispersion has been plotted and whilst showing a close affinity to the separation predicted by its larger counterpart with the nylon–water analogue, experimental K_u/K_i values seem a little higher for the smaller unit at the same $Hy(\bar{d}_f)$, indicating the presence of a size effect. This is investigated further in Section 9.5.4.

The lack of agreement between the predictions for 36NS4P(T) and 32MANF.A. illustrates the substantial differences that must exist between their respective flow–fields, and strictly, comparisons between them should not be made with this plot. Similarly, the need for care in using this format to forecast how other mixtures might separate is shown by the poor match between nylon–water bulk efficiency data in Fig.5.6 and the generalised prediction based on its own

particulate separation data. Clearly $\bar{d}_f$ is inadequate in characterising the comparatively narrow, normal size distribution of nylon and reversion to the integration method of equation 5.3 would be necessary.

Establishing the point at which the model breaks down due to shear related droplet disruption in the liquid–liquid system with increasing flowrate is clearly important in delineating its range of application. This complex problem of characterising the hydrodynamic splitting of drops in a hydrocyclone is considered in greater depth in Sections 8.2 and 9.1, from which a working guide of keeping feed velocities below 5.5 m/s for this dispersion is indicated.

To summarise, the technique described has shown that a reasonable prediction of the bulk separation of water–kerosine can be obtained based on comparatively quick and easy testing with a nylon–water analogue in the same hydrocyclone (but see also Section 9.4). Restrictions to low dispersion concentrations apply such that particle interactions are negligible – for nylon, mass concentrations up to 1% were found to be workable, whilst for the water dispersion, as signs of drop coalescence were evident at K_i = 5% (by volume), this probably represents a rough limit above which the quality of the prediction will worsen. In addition, application for $v_i > 5.5$ m/s with water–kerosine ($d_{max} \triangleq 100\mu$) is not advised due to droplet break up effects, whilst split ratios are required to be fairly similar between the two systems.

At a more general level, if a solid–liquid analogue is to be used to predict separation in a liquid–liquid system it is desirable that the $Hy(d_f)$ range for the analogue tests is wide enough to encompass that of the system being modelled. Also the solid particles should ideally be spherical or at least of the same geometrical form and similar relative dimensions so that corrections for shape are facilitated. Regarding the dispersion concentration limits imposed by coalescence, water–kerosine is a comparatively unstable mixture and water–oil systems with more stable interfaces should be predictable to higher K_i, possibly 10% although droplet agglomeration and hindered settling effects may begin to need consideration then. The extent to which $\bar{d}_f$ can be used to characterise the bulk separation of liquid dispersions is also not broadly established, but it looks useful for distributions comparable with water–kerosine (i.e. log normal,

$\sigma_g \triangleq 1.5$). The requirements of dynamic similarity in terms of flowfield and particle Reynolds number should be adhered to although it is clear from solids work that Re_D can differ by up to a factor of 2 without significant change in the flowfield.

5.3 Assessment of Geometry Development using Solid Particles with a Water– Kerosine System.

To conclude this chapter, a comparison of performance with water– kerosine is presented between the original 30PD(T) geometry and, the product of this stage of the development process, 36NS4P(T). Results for the conventional hydrocyclone, 32MANF.A, are also included to put the data into perspective. A simple plotting format has been adopted, Q_i vs. K_u/K_i and ΔP_{iu} ($\equiv \Delta P_{max}$), shown in Figs.5.7 and 5.8 respectively, as the paucity of data and lack of similarity between hydrocyclones (although of comparable diameter,D) removes the basis for more sophisticated comparisons.

For the ΔP at which 30PD(T) has its minima in K_u/K_i, separation looks to be comparable in 36NS4P(T). However, the very much smaller $\bar{d}_i$ in the tests for 36NS4P(T) and ultimately lower attainable K_u/K_i values are clearly indicative of a superior geometry. 32MANF.A also lags well behind 36NS4P(T), with a much higher pressure requirement producing only indifferent separation. Hence, the design philosophy for dense dispersion liquid– liquid hydrocyclones outlined in 5.2.3 is reinforced.

CHAPTER 6

INTERNAL FLOWFIELD AND ITS MEASUREMENT

6.0 Introduction

The broad characteristics of the flowfield within a (reversed flow) hydrocyclone are well established, namely a Rankine vortex with flow spiralling downstream near the walls and back upstream near the centre (see also Section 1.1). Detailed knowledge of flow structure, however, can contribute significantly to understanding the influence of geometry and operating conditions on hydrocyclone performance. This is particularly important for the small differential density associated with liquid–liquid flows. Accordingly, velocity measurements have been made using the powerful laser Doppler anemometry (LDA) technique, but due to restrictions on rig availability and lack of suitably constructed hydrocyclones, analysis was only possible for time averaged axial velocities (v_z) in geometry 36NS4P(T). Nevertheless, the wide variation in externally adjusted split ratio investigated represents an original area of study and results are interpreted with reference to complementary flow visualisation and residence time distribution (RTD) data.

The possible values of other velocity components are considered and estimates made of mean shear gradients within the hydrocyclone. For conditions where dispersion levels are significant, the effect of concentration gradients and phase inversion is also speculated upon.

6.1 Velocity Measurements Using LDA

Whilst practically the flow of interest in this research programme is 2–component, such systems are not transparent and internal probe based measuring techniques that might be used, see Cheremisinoff [73], cause disturbances which would propagate throughout the hydrocyclone due to the strong radial pressure gradients [74]. In addition, resolution of dispersed and continuous component motions would be complex.

More reliable velocity measurements can, therefore, be obtained for single component and externally based measurement. As these methods tend to rely on light, there is a need for the flow and hydrocyclone walls to be transparent, with tracer material fine enough to follow closely the motion of the carrying medium. The resulting velocity profiles can be considered to represent that of the continuous phase for low dispersion concentrations. The LDA technique pioneered by Yeh and Cummins in 1964 [75], has the advantage over tracer "tracking" methods [76, 77] in that both time averaged and fluctuating velocity components can be rapidly evaluated with a high degree of spatial and temporal resolution.

LDA uses the principle that the frequency of light scattered by a moving object is changed, relative to that of the incident light, by an amount proportional to the object's velocity. This effect, first described by Doppler (for sound) has been practically exploited in these experiments by splitting a laser beam (an intense, coherent light source) into a weak reference beam, which is aligned directly through the hydrocyclone to a photo–detector, and a strong main beam, which is angled to intersect with the reference beam to define the scattering or measuring volume. Any fine particles in the flow passing through this region will scatter some radiation from the main beam (changing its frequency) in a direction parallel to the reference light. This mixes with the reference beam to generate a beat frequency which can be monitored by the detector and in this case is output as a voltage that is proportional to the magnitude of the particle velocity. The velocity component being measured is that which bisects the angle between the reference and main beam and lies in their plane. To avoid confusion with regard to the sign of this component a frequency shift is commonly applied to the reference beam.

Fuller details of the LDA rig, theory and its application (including accounting for refraction through the hydrocyclone walls) is given in Appendix C.

It is noteworthy that laser anenometry could be used for very dilute water–in–oil dispersions to give drop sizing and concentration data as well as drop velocities [78, 79], although more sophisticated analysis of the Doppler 'bursts' would be required than is possible with the system used here.

6.2 Analysis of Axial Velocity Profiles

Time averaged axial velocity profiles were measured parallel to the inlets at three planes normal to the hydrocyclone axis in 36NS4P(T) for three split ratios set by external values and with the gas core suppressed (see Fig. 6.1). Inlet flowrate was set using water to give $Re_D = 1.0 \times 10^5$, in the middle of the typical operating range for kerosine ($Re_D = 0.6 - 1.4 \times 10^5$) over which no significant changes in flow structure were anticipated [67, 74]. Axial velocity, v_z, has been non-dimensionalised by $\bar{v}_z$ ($= Q_i/\pi R^2$), radial position from the centre line, r, by R ($= D/2$) and axial distance from the end wall, z, by D. Axial fluxes within the hydrocyclone have been evaluated by integration of the velocity profile assuming bilateral symmetry as

$$\pi \int v_{z1}\, r\, dr + \pi \int v_{z2}\, r\, dr \qquad (6.1)$$

where v_{z1} and v_{z2} represent the left and right hand sides of the traverse as viewed in Fig.6.1. These fluxes are are presented in Tables 6.1 and 6.2.

The tables also show the upstream and downstream flows for the various splits tested and this provides a basis to estimate the accuracy of the LDA measurements. Table 6.1 reveals that the flux balance for the lower cone ($z/D = 7.9$) is 6–17% down on what it should be to match Q_d. Also from Table 6.2, the reversed flux in the centre of the swirl chamber ($z/D = 1.4$) can be seen to be between 13–15% less than Q_u. In this latter case short circuit flow across the hydrocyclone end wall might be invoked to explain the discrepancy but even then, the magnitude indicated for this bypass flow is much greater than would be expected. For example, Parfitt's RTD work on the same geometry, using a salt solution tracer to detect the spread of time taken for simultaneously injected feed flow to reach the outlets, gives estimates of 5% Q_u (3.5% Q_i) for short circuiting at $1-F = 30\%$ [80]. Adjusting the LDA generated fluxes to comply with the RTD data (and assuming there is no radial outflow from the core above $z/D = 1.4$) could be accommodated by increasing $|v_z|$ by just under 10%, This would bring short circuit flows to 4 – 5% Q_u for all tested splits and flux balances for the lower cone to vary much more closely around Q_d and, hence, probably represents a realistic overall error. Consideration is given to sources of error in Appendix C.5.

This apart, all the traverses (plotted with uncorrected data) show good repeatability and symmetry with the characteristic region of reversed flux around the hydrocyclone axis and net downstream (positive) movement outside this. It is convenient to analyse these two zones separately:

1-F =	10%	30%	50%
Flux balance at z/D = 7.9:			
Upstream moving flux	-5	-3	-1.5
Downstream moving flux	7	9.5	11
Net axial flux	2	6.5	9.5
Q_d	2.3	6.9	11.5

Table 6.1 FLUX BALANCE NEAR DOWNSTREAM OUTLET (ℓ/min)

1-F =	10%	30%	50%
Upstream moving flux in core, location (z/D):			
Lower cone (7.9)	- 5	- 3	- 1.5
Upper cone (3.9)	-18.5	-14	-10
Swirl chamber (1.4)	-17.5	-14	-10
Q_u	-20.7	-16.1	-11.5

Table 6.2 CENTRAL REVERSED FLUX THROUGH HYDROCYCLONE (ℓ/min)

6.2.1 Central reversed flow

This takes the form of a fast moving annulus ($v_z/\bar{v}_z$ up to -20) with a slower moving core. As the radial extent of the region remains roughly constant in the upper portion of the hydrocyclone at $r = 0.45 - 0.5R$, with increasing split (and falling axial pressure gradient), reversal velocities fall whilst the central velocity defect becomes more pronounced.

Loader [86] describes a very similar central re-reversal tendency of the v_z profile for swirling flow in a vortex tube (comparable to a cylindrical hydrocyclone without an upstream outlet) at high $Re_D(\sim 10^5)$, but in this instance it would appear that it is the presence of (and flow through) the upstream outlet that is promoting the phenomenon. Certainly the profiles in the upper part of the hydrocyclone ($z/D = 1.4$ and 3.9) are influenced more than those at $z/D = 7.9$. When the swirling reversed flux enters and travels up the vortex finder, frictional losses cause the spin to slow, the radial pressure gradient to fall and, hence, the axial pressure to rise, creating a tendency to drive flow on the axis back up the outlet pipe. This secondary hydrocyclonic action acts to oppose the primary reversal pattern but its effect only becomes significant as the strength of the return flow diminishes and the mean upstream discharge velocity falls with increasing split. Although, for the most part, the resulting velocity defect may not be particularly critical to the separating efficiency of the hydrocyclone, if re-reversal occurs and persists into the downstream outlet undesirable loss of 'product' (oil in the water-oil situation) might result and a narrower vortex finder would be recommended to increase mean v_u. Dabir and Petty [81] stress the importance of vortex finder diameter and form to the characteristics of the central flow structure. In LDA analyses at $1-F = 20\%$ on a conventional hydrocyclone, they found a reversing annulus within which were counter current flows which they related to contractions in the upstream outlet. The 36NS4P(T) geometry, and generally all those used in this work, expand from their outlet diameters to 19mm pipe at a distance $\pm D$ of the defined hydrocyclone margins. Dye injection tests have also shown that flow reversal in the downstream outlet does not extend beyond this expansion point [80].

One further aspect to consider is that as v_z values are time averaged, any oscillation of the flowfield would not be directly picked up. Now precession of the vortex core is a common characteristic of high Reynolds number, swirling flows and more specifically has been observed by Colman and Smith [67, 74] in hydrocyclones of high L/D ratio, decreasing in intensity downstream. Hence, if it is assumed that the (− ve) axial velocity increases to a single maximum at the centre of the vortex system which is precessing about the geometric centre of the hydrocyclone (but never passing through it), then the time averaged velocity measurements would show this as an apparently double peaked profile. Also, if precession is present in the test hydrocyclone the scale of the effect may well be expected to increase with split as core stabilising radial inflow falls. However, the degree of change is unlikely to be sufficient to cause the substantial development of the central defect seen between $1-F = 10\%$ and 50%, only to enhance it.

Radial movement of material can be inferred to some extent by comparison of the central negative fluxes at the traversing levels (Table 6.2). The close similarity of the reversed flows between $z = 1.4$ and 3.9, regardless of split, indicates the probable absence of radial flow into or from this zone.* This is confirmed by dye injection tests, where dye persists in a roughly cylindrical form down to about the level of the upper cone traverse, coincident with the locus of zero axial velocity around the core. This surface has been widely recognised in cyclones and can be considered as the primary mantle. Bradley's dimensions of 0.43D for its diameter and axial termination where the cone narrows to 0.7D (from dye injection experiments with a variety of hydrocyclone designs and operating conditions [11]), is in general agreement with what can be inferred for the NS4P(T) geometry (see Fig.6.2).

Negative fluxes have fallen substantially by $z/D = 7.9$ indicating, by continuity, that the majority of inward radial movement is occuring in the mid− cone region. However, split appears to have a considerable influence on the extent to which flow travels downstream before reversing back up to the core.

---

* It is noteworthy that the steep contraction between swirl chamber and cone lies between these levels.

Whilst Parfitt's RTD analysis reveals earlier arrival of the first flow at the upstream for higher splits (excluding short circuit flows), the mean residence time of the upstream discharging flow has increased [80], and it is evident from Table 6.2 that a smaller fraction of the throughflow has moved inwards to the reversal region between z = 3.9 and 7.9 at 50% split compared to 10% (~40% Q_i against ~65% Q_i). The net effect of this behaviour on separation processes can be seen to be a small reduction in upstream water levels for kero(SG) with increasing split ($>(1-F)_{crit}$, K_i = 5%; see Fig.9.10). However, looking at the same figure, it seems that for more viscous oils this trend is reversed (kero(63) at $\bar{d}_i = 25\mu$). This might relate to differences in the radial concentration of the dispersions at the level in the hydrocyclone where the premature radial inflow is occurring as split increases. Hence, if feed drop size for the kero(63) system were sufficiently larger, with segregation to the wall occurring more rapidly, the performance curve might more closely resemble that of the kero(SG) test, as indicated for the projection of the $\bar{d}_i = 60\mu$ data, also shown in Fig.9.10. This explanation assumes the flow structure in 36NS5(S) is similar to that for 36NS4P(T). Measurements of pressure drop for changing split with different oils in Section 9.2.3 indicate there may also be a Reynolds number effect, particularly at low splits.

Generally, it is clear that the radial extent of the central reversal region at all levels in the hydrocyclone is unaffected by externally adjusted split. Assuming re-entrainment of dense material travelling down the cone wall is a function of the spatial extent of the reversal flux, a constancy in this process is implied for this mode of operation. However, Dabir and Petty [82] have shown an association between the diameter of this zone in the cone and vortex finder diameter. Hence, if split were upstream outlet size controlled, a variable entrainment effect might be surmised, being most detrimental to separation at low splits for a geometry like that used in the tests. Downstream outlet diameter and cone angle are thought to have little influence on the locus of zero vertical velocity [83].

6.2.2 Flow outside the central reversal

The characteristics of this part of the profiles are very similar for all tested splits. In the swirl chamber, flow velocities in the outer regions are small ($v_z/\bar{v}_z < 1.5$ or $|-0.5|$) being positive (downstream mobile) near the wall, falling to become negative in the region $r = 1.0 - 1.4$ R and recovering to positive velocities again before the main reversal zone. Therefore, although the majority of the flow is downward moving a small fraction is being slowly recirculated. As data is only available fron one traversing position, assessing where radial flow is occurring, is largely conjectural. However, it seems likely that the upward moving flux is essentially fed by the partial deflection of the downward moving flow at the steep contraction leading to the main cone, creating a double recirculating cell structure and secondary mantles (see Fig. 6.2). Dye persistence 5–6 times mean residence time is reported for this region by Parfitt [80]. Similar secondary mantles have been observed by the author and also Bhattacharyya in deoiling geometries [83], although the counter–current 'shells' of flow occur within a much narrower zone ($<$R) around the axis. Complex recirculation patterns are also reported by Exall [84] for axial flow cylindrical hydrocyclones.

The velocities of downward moving flow increase substantially through the contraction to the cone (v_z near wall has more than doubled by $z/D = 3.9$) and the slow moving reversal zone is eliminated. Travelling down the cone towards its apex, positive velocities tend to increase further as the annular area carrying this flow reduces faster than flux is transferred to the central return flow. This tendency is marginally enhanced at higher splits.

The extent of the boundary layer at the hydrocyclone wall is largely obscured because the strength of the signal obtained when the measuring volume incorporates the Perspex/water interface swamps that due to the particulate matter carried in the adjacent flow, so no clear reduction in v_z is evident as the wall is approached. However, as the length (radially) of the measuring volume can be calculated to be 0.85mm, this puts an upper limit on boundary layer thickness.

6.3 Other Flowfield Characteristics

Having considered axial and implied radial flows, knowledge of tangential velocities, v_θ, in the dewatering hydrocyclone is lacking. However, other workers – notably Colman and Dabir & Petty using LDA [67, 81, 82] and Knowles using cine film [77] – have produced fairly comprehensive analyses of v_θ in hydrocyclones operating without an air core, and their results can perhaps be used as a general guide.

All the researchers identified the outer free vortex type system, approximating $v_\theta r^n$ = constant. However, whilst Knowles obtains values of $n = 0.2 - 0.4$ with a conventional geometry (Rietema's optimum design), Dabir and Petty using the same design evaluate n at between 0.6 and 0.7. Colman's data puts n even higher (0.8 – 1.0), and closest to the free vortex condition, for a hydrocyclone with a swirl chamber and gently tapering conical section i.e. a similar design concept to NS4P, and also notes only a 10% loss in flow velocity on entry (comparing v_i with v_θ at entry radius). The inevitable transition to solid body rotation is put at $r \leqslant 0.15R$ by all workers, which would mean that for NS4P the annulus of fastest moving reversed flow is largely outside the forced vortex. Hence, any dispersed phase would still be subject to significant separating forces ($\propto v_\theta^2/r$) which will peak at the inner edge of the free vortex.

Although flow through the contraction between swirl chamber and cone should spin up the flow near the wall increasing the acceleration field, visual observations of the helical movement of droplet 'streaks' down the hydrocyclone wall indicate conservation of angular momentum through the contraction may be poor. Swirl angle ($= \tan^{-1}[v_\theta/v_z]$) can be seen to change from ~80° in the swirl chamber to ~65° in the upper cone, and given that v_z near to the wall has roughly doubled (from LDA) between traverses $z/D = 1.4$ and 3.9, this implies v_θ is about the same (or slightly lower) at this much reduced radius. For the approximate halving of diameter through the contraction and assuming conservation of angular momentum ($v_\theta r$ = const.) and axial flow ($v_z A$ = const.), v_θ should have doubled and v_z quadrupled in a loss free system, which would have meant a reduction in swirl angle to only 70°. However, with flow being recycled in the swirl chamber it is difficult to establish flow continuity between the two traversing positions. Further measurements would be required to clarify the situation.

The most significant time averaged velocity gradients in the hydrocyclone are radial and these have been plotted in Fig. 6.3, based on the experimental data for $\partial v_z/\partial r$ and estimated velocities for $\partial v_\theta/\partial r$ [67], for the upper cone at 30% split. These shear rates can be seen to be relatively low for the downward moving flux, except in the boundary layer at the hydrocyclone wall, peaking around the system axis in the reversed flux at $\sim 10^4 s^{-1}$ for gradients due to v_θ, which tend to dominate. Such high levels of shear will be an advantage when operating with non–Newtonian shear thinning media (e.g. water–crude oil emulsions [64]), but may also be a cause of some droplet break up. However, as the hydrocyclone flow is turbulent and shear stresses due to turbulent fluctuations are considered to be more significant in this respect than due to viscous effects, droplet stability in the hydrocyclone will probably be more closely related to turbulence intensities. This is discussed in more detail in Section 8.2. Turbulence will also have a significant effect on the movement of drops in the separator, particularly with regard to entrainment of 'separated' particles close to the cone wall into the reverse flow to the upstream outlet [85]. Experimental workers report a generally anisotropic character to the turbulence where intensities are greatest, most notably on entry, but also close to the wall and near the axis of hydrocyclones and similar confined swirling flow systems [13, 86, 87]. Blackmore, working with vortex tubes, further identifies wall geometry discontinuities as a source of turbulence (like the contraction section) as well as showing a strong dependence of r.m.s. axial and tangential turbulent fluctuations on v_i [88].

The introduction of 2–component liquid systems (water–oil) with substantial dispersion concentrations into the hydrocyclone will increase the apparent viscosity of the flow and is likely to dampen down turbulence, flatten tangential velocity profiles and cause spin rates to fall more rapidly as flow moves down the hydrocyclone. This in turn, will reduce flow reversal flux.
However, the setting up of radial density gradients with increased segregation of the water towards the wall (and also progressively towards the hydrocyclone vertex) will steepen radial pressure gradients and tend to axially extend flow reversal effects i.e. opposing the action of increased viscosity.

CHAPTER 7

WATER–OIL SEPARATION TESTS: PROCEDURE AND MEASUREMENT

A major objective of the programme was to develop an effective experimental rig to test the separating capabilities of a hydrocyclone on a dispersed water–in–oil system. This required that both feed and operating parameters could be varied over a significant range in a controlled and independent manner, and that accurate, or at least repeatable, measurements could be made of all factors relating to performance (see Tables 4.1 and 4.2). In addition, 'effective' implies that a certain level of productivity could be achieved regarding number of test runs in a given time period.

After consideration of rig development and an overview of operational procedure, the test oils used and practical aspects of water/oil interfacial stability are discussed, followed by a section on the difficult instrumentation areas of water–in–oil concentration measurement and drop sizing. Much of the detail of procedures and analysis has been put into Appendix B, including assessment of errors.

7.1 Test Rig Development and Operation

Three main stages in the progression of the dewatering test rig can be identified (and their capabilities are summarised in Table 7.1):–

Rig L1 (Fig. 7.1) – represents the first basic facility, a once through system where feed flow generation and mixing were achieved in a single pump, with oil and water sourced and metered separately to provide a controlled K_i. Drop sizes produced were coarse (d_{max} visible to naked eye 500–750μ) and although they could be kept constant with changing Q_i by use of the bypass, variation in $\bar{d}_i$ could not be achieved. Generally, only a very limited range of operating conditions could be tested and running time was restricted.

Rig L2 (Fig. 7.2) – was designed so that the pumping and mixing processes could be separated. This was attempted by introducing a variable speed, high shear turbine pump in–line to provide a controllable mixing effect on the already pressurised and metered oil and water flows after they had been tee–ed together. (A similar concept had been used successfully by Colman in deoiling experiments [6]). The degree of drop size control achieved and the microphotographic sizing technique developed during this period are assessed in Section 7.3.2. Partial metering of the Q_u range reduced the need for manual timed sampling to determine split, improving both control and the speed of setting up a test condition. The higher pressure rating and flow capacity of the rig approached laboratory safety limits, the most restricting being a maximum of 300ℓ oil inventory for the rig. Practically this meant only 2 operating conditions (at most) could be tested per day, to allow time for gravity settling out of the dispersed water phase in the dump tank before re–using the oil.

Rig L3 (Fig 7.3, Plate II) – incorporated an integral oil recycling and clean up system so that much longer test periods could be achieved (limits now set by water supply and disposal).* The higher level of funding now available for the project also allowed a greater degree of on–line instrumentation to be used, with interactive data logging and correction by computer further improving both control and speed of experimentation. The feed conditioning system of rig L2 was retained but with drop sizing being obtained over a more extensive range of operating conditions using a macrophotographic based technique (Section 7.3.2).

As the productivity of this test rig greatly exceeded that of the earlier once–through facilities, it provides the greater proportion of experimental results presented in this thesis. Accordingly the detailed description of operating procedure and performance measurement in Appendix B primarily relates to rig L3, although much of it also applies to rig L2.

---

* A rig format where all discharged flows would be continuously recirculated via a mixing tank to the feed was rejected at an early stage because of concern regarding the stability of K_i and $\bar{d}_i$ [22].

TEST RIG AND PERIOD OF USE	Q_{imax} (ℓ/min)	P_{imax} (barg)	K_i (%) [at Q_{imax}]	1-F(%) [based on Rotameters at Q_{imax}]	LIMITING RUN TIME (min) [at Q_{imax}, K_{imax}]	d_i
L1 (3/80-10/80)	18	0.5	1.5-17	manual	7	constant; not controlled or measured
L2 (7/81-11/83)	50	6.0	0.4-40	40-94	5	controlled variation; measurement limited to K_i < 10%, N < 1750rpm, P_i < 2 bar, Q_i < 40ℓ/min
L3 (12/84-1/87)	70[1]	5.5	0.3-43	10-85	11[2]	controlled variation; only limit to measurement K_i < 30%

1. Lower limits imposed by recycle/ clean up problems for the more viscous test oils and smaller drop sizes.
2. Running could continue the same day.

Table 7.1 WATER–OIL TEST RIG CAPABILITIES

In brief, the main areas tested with the different rigs were as follows:–

L1 – single, pre–development geometry; limited range of operating conditions with kerosine (see Chapter 5, Fig.5.7 and reference [68]).

L2 – range of geometries including swirl chamber format, 6° and 3° cones, single and twin tangential inlets, changes in scale and conventional (solid–liquid separation) style; range of operating conditions, especially split and water concentration, with kerosine.

L3 – range of geometries including involute feed, D = 15mm size, variable outlets and deoiler style; wide range of operating conditions, including different mixing levels and high water concentrations but most particularly with a variety of oils and interfacial conditions.

It should be stated that the direction and pattern of testing was significantly influenced by commercial interests, which was not always compatible with a progressive programme of development.

7.2 Water–Oil System Characteristics

Two important requirements for the water–oil systems to be used were that they should be well defined and stable so that good characterisation and repeatability of separation tests could be achieved. Tap water and refined distillates at laboratory temperatures proved to be appropriate in this respect, whilst also matching many brine–crude systems at well–head temperatures in terms of bulk characteristics, if not detailed chemistry (see Section 3.1.2).

7.2.1 Oil phase

The principal oil used in the experimentation was a well refined kerosine (BP Premium Grade [Solvent 350]; by weight only 6% aromatics, the rest an even split between paraffinic and napthenic hydrocarbons [106]), which when

combined with tap water produced a tractable mixture with bulk characteristics at laboratory temperatures closely comparable with Forties brine–crude at well–head temperatures (see Table 3.2). The kerosine was defined in terms of its density, viscosity and interfacial tension against a water phase (γ), as shown in Table 7.2. The ranges on these parameters reflect batch differences (rig inventory renewed once a year on average) and system drift in between times (e.g. due to evaporation, but see also microbial problems in Section 7.2.2). This degree of variation is comparable with the effects of rig operating temperatures, where for kerosine, rising through the extremes of recorded test temperatures (17 → 26° C), μ_o would fall by 14%, γ by up to 9% and ρ_o by 0.8% ($\Delta\rho$ increases by ~3%). In terms of sepation test repeatability, K_u/K_i varied between 0.019 and 0.026 for regular check runs of 36NS4P(T) with kerosine (K_i = 5%, Q_i = 45 ℓ/min, 1–F = 50%, N = 2000 rpm). This was reflected a high K_i by correspondingly greater fluctutations in performance (see Fig.7.4). For the most part, however, a more closely defined system would be expected over short time scales (one or two months). See also comments in the following section and Section 9.0.

Testing of higher oil viscosities was considered vital to establishing the limits of viable operation for the dewatering hydrocyclone in view of the number of potential 'low' temperature applications with Forties crude and thicker oils generally (see Chapter 3). This was achieved by blending the kerosine (1.9 cSt) with a BP Heavy Gas Oil (refined ex Forties) of ~18 cSt to generate two intermediate distillates, kero(63) and HGO(07), with ν = 3.8 and 14.5 cSt respectively. However, increasing the viscosity by this method also resulted in higher oil ρ and lower γ, with even more substantial variation in water/oil interfacial conditions occuring due to the necessary addition of biocide in some systems to control microbial growth (see Section 7.2.2). Independent variation of viscosity was, therefore, not attained but in an attempt to isolate interfacial changes from viscosity/density effects, a second kerosine was tried (kero(SG) [BP Solvent 300]; similar to Premium Grade but with a higher aromatics content, 17% by weight [106]) with an artificially lowered γ. Details of all water–oil systems used are given in Table 7.2.

OIL PHASE	kerosine [kero]	kerosine (standard grade) = kero(SG)	63% kero 37% HGO = kero(63)[1]	93% HGO 7% kero = HGO(07)[1]
μ (cP)	1.35 - 1.50	1.58	3.06	12.5
ρ (kg/m^3)	775 - 781	792	817	863
$\Delta\rho$	223 - 217	206	181	135
ν (cSt)	1.74 - 1.92	2.00	3.75	14.5
γ(N/m$\times 10^{-3}$)[2]	31 - 28	19 - 23	23	a. 24 none
BIOCIDE CONC. IN WATER PHASE (= TAP WATER)	none	200 ppm Panabath	100 ppm Phylatol	b. 13 1000 ppm Panabath c. 17 ? 50 ppm[3] Panabath
TEST PERIOD	6/80-1/86	12/86	6-7/86	3-4/86

All data measured at or corrected to 20°C.

Units: cP $\equiv$ Pa.s $\times 10^{-3}$

cSt $\equiv$ $m^2s^{-1} \times 10^{-6}$

1. bracketed figure shows % by mass of kerosine in the blend, prefixed by the dominant fraction (HGO = Heavy Gas Oil)

2. measured using ex rig oils against distilled water (+ biocide if appropriate) for an interface age of 5 minutes, to nearest unit

3. following partial flushing of the 1000 ppm Panabath aqueous phase.

Table 7.2 WATER–OIL TEST SYSTEMS

As a rider to this section, it should be appreciated that drop size also changes with system characteristics (for a given mixing input) and this needs to be accounted for in the interpretation of separation test results as well (see Section 7.3.2).

7.2.2. Water/oil interfacial characteristics

Whilst the bulk phase characteristics, for given mixing inputs and dispersion concentrations, will help determine the environment in which a dispersion exists, its response to those conditions will be strongly dependent on the nature of the interface. This will be a function of the oil type, aqueous phase chemistry and, especially, the extent to which surfactants are present in the system. These materials are preferentially absorbed to the water/oil interface and act to stabilise it, creating an emulsion. They comprise either polar molecules or groups of molecules, usually derived from the oil, e.g. organic acids (from the oxygenation of the aromatics), waxes or fine particulates (microbes, rust, etc.).

System interfacial tension provides a convenient static parameter for characterising the interface. Generally, the lower γ, the easier interfaces can be created for a given energy input and, hence, the smaller drop sizes might be expected to be (see HGO(07) data in Fig.7.10). The presence of surfactants will depress γ, but the rheology of the resulting visco–elastic skins formed around drops must also be considered if the dynamic response of the interface is to be understood [35]. Certainly as interfacial area increases, the interfacial viscosity contributes more to the bulk apparent viscosity of the emulsion [64]. Measurements of interfacial dilational and shear characteristics, however, are still a specialised field. One particular aspect of the surfactant films is that they inhibit droplet coalescence, hence, their influence will be greatest at high dispersion volumes when droplet interaction is more significant.

An overriding consideration in determining the effect of surfactants on a system is the age of the interfaces, as surfactants take a finite time to migrate there. Accordingly the older an interface the more stable it becomes. In the context of the test rig, with water and oil mixed only a few seconds before entry

to the hydrocyclone, interfaces will be no older than this and possibly younger (depending on the flow regime and flowrate [89]). The separation process is only affected, therefore, by the more mobile surfactants or those present in higher concentrations.

Interfacial stability over longer time scales, important for test reproducibility, is also of concern. Following rig cleaning and/or oil renewal, a progressive drift in the stability of the water–kerosine system was usually apparent over a period of months. Symptoms included the onset of phase inversion occurring at lower and lower water contents ($K_{imax} = 50 \rightarrow 35\%$) with erratic separation results above $K_i \triangleq 30\%$ (see Fig.7.4), the development of quasi–stable hazes of the finest water droplets (est. $1-2\mu$), increased foaming effects where the discharge streams from the hydrocyclone enter the dump tank and lower values of γ. This implied a build up in surfactant levels was occurring which seemed to mirror an increasing presence of organic material in the rig, most clearly evident at the water/oil interface in the dump tank. Such microbial contamination is not uncommon in water/oil systems, with the microbes typically living in the water phase and feeding off the oil, and whilst this results in some degradation of the oil, more significantly the microbes themselves and the by–products of their growth can be highly surface active. Colony development is encouraged by the action of running the rig, as finely dispersing the water in the oil provides large interfacial areas ideally suited for microbial growth, which is further enhanced by oxygenation effects resulting from discharging the flow above the free surface of the dump tank. The introduction of more viscous oil blends, with an order of magnitude increases in drop settling time, resulted in a microbial population explosion with their physical presence rapidly bringing effective rig operation to a halt.

At this stage biocide was introduced into the steel water feed cylinders, whose decaying bitumenous anti–corrosion linings appeared to be harbouring the source of the contamination, in an effort to kill the microbes (see Table 7.2). The treated water was retained within the rig, being pumped back to the feed cylinders from the dump tank (after settling) via a secondary holding tank. However, biocides tend to incorporate dispersants to improve their efficacy and also their concentration is likely to fall with time due to evaporation and by

degradation in destroying microbes. This means dosing a system typically has a detrimental effect on interfacial characteristics, in terms of the resolution of the water–oil dispersion, and may itself contribute to the temporal drift problem.

More quantitative and detailed consideration of interfacial conditions is presented in Appendix B.2, with particular reference to interfacial tension measurements and the microbial contamination problem for the specific test water/oil systems used.

In summary, the kerosine represents a well refined and comparatively surfactant–free distillate which when agitated with clean water produces an unstable mixture. Prolonged usage in the test rig leads to a certain degree of interfacial degradation, mainly caused by microbial growth, which shifts the system towards an emulsion with surfactant stabilised interfaces. This reflects the system state for the majority of separation tests undertaken with water–kerosine. For the kerosine/HGO blends, interfacial films against the water phase are evident before significant rig use, implying that the heavier distillate itself contains substantially more surfactant material than kerosine and the resulting comparatively stable emulsions are possibly interfacially nearer to typical field conditions. The addition of biocides to the water–distillate systems also tends to act to stabilise interfaces and lower γ, both detrimental to separation processes.

7.3 Instrumentation Development

Considerable effort was devoted to the development of techniques for measuring upstream water concentration and dispersion drop size, where progress towards on–line, real time analysis was sought in order to achieve greater test productivity and representativeness, whilst also being a significant step towards 'instantaneous' assessment of hydrocyclone performance.

7.3.1. Water–in–oil concentration

Assessment of hydrocyclone separation particularly relies on an effective measurement of K_u. This needs to be accurate in the range $K_u = 0.1 - 0.3\%$ (where the bulk of data for kerosine tests lie) but also able to reflect K_u up to ~50% (for flow conditions below critical splits). In addition, variations in Q_u (15–60 ℓ/min), d_u and oil type should not affect the measurement.

The most direct method for evaluating K_u is to take a full stream sample of this discharge stream at the dump tank (~4ℓ), allow it to settle out overnight and then by decanting into measuring cylinders assess the relative volume of water in the oil. The advantages of this technique are its accuracy, simplicity, low cost, freedom from sampling errors and ability to cover a wide range of water levels by selective use of different sized measuring cylinders (from 10mℓ to 2ℓ). Against this, the requirement for complete settling out of the two components means the process is time consuming and only really suited to light oils, where adequate segregation can be achieved in around a day or less. (Kerosines and kero(63) samples needed typically 8–30 hours settling).

The Karl–Fischer test (IP356/82) gives a total water concentration (by mass) based on titrating a pre–calibrated reagent against a sub–sample of the 'liquor' (~1 mℓ). The method is primarily intended for crude oil with water contents up to 5%, and was assessed for distillates using samples taken with HGO(07) in the test rig (see Appendix B.4). Apart from the limited range for K, the main problem with this technique appeared to be in obtaining a representative sub–sample to work with.

For on–line measurement, capacitance techniques seemed most appropriate given the very much greater dielectric constant for water ($D_k = 80$) compared with oil ($D_k \triangleq 2.5$) [90] and the importance of sensitivity at low K_u. The instrument chosen for evaluation was the Endress and Hauser Aquasyst, comprising a 'standard' sensing cell (Plate III) and controlling analyser with a continuous water concentration display (see Plate II, top RH corner of main instrumentation board). Designed for the custody transfer of crude oil, it was claimed water contents up to 45% could to be measured up to within ±0.05% in the range 0–2% (v/v). It was considered by the manufacturers that for the well defined conditions in the hydrocyclone test rig even better accuracy could be attained.

Initial tests with kerosine, however, showed that at the kind of required operational flowrates, stable water concentration readings could not be achieved due to water build up effects on the internal surfaces of the cell [91]. The manufacturer accordingly recommended an increase in flow velocity through the cell (minimum v_{cell} of 2 m/s) and more pre-cell mixing. Cell modifications carried out by the author, principally to reduce the annular gap between electrodes so that v_{cell} would be raised for a given flowrate, are shown in Fig.7.5. The ultimate 'Southampton' design also incorporates a scalloped PTFE flow deflector to maximise turbulence on entry and a hydrophobic Teflon coating for the inner electrode (see Plate III). Effective changes in mixing were expected to be covered by the range of operating conditions under evaluation.

Tests with the three cell geometries on Rotameter-set water concentrations over the range 1-4% reveal a progressive reduction in the water build up rate in absolute terms (W) with increasing v_{cell} (Fig.7.6). This implies that the progressive modifications to the cell were a significant positive step. However, for typical discharge flows from a hydrocyclone, the Aquasyst reading still shows a build up effect (at a little over 0.01%/min) which appears to be independent of cell velocity (Fig.7.7).

The explanation for this would seem to lie with the dispersion drop size, which in turn is strongly a function of water concentration and degree of mixing. Although information is incomplete, and allowing for some inconsistancies, it is postulated that as drop size increases, the rate of water build up is higher and the ultimate equilibrium condition*, when $W \rightarrow 0$ (see Fig.7.8, post 17 min for clean system), occurs more rapidly. At low cell velocities (typical of the standard cell) this dependency is unaffected, but at higher cell velocities (typical of the Southampton cell) wall shear stress levels are now sufficient to disrupt the build up process for larger droplets. This might account for the similar build up rates shown by cells for small drop sizes in Fig.7.7, diverging for the larger drop sizes in Fig.7.6 (at approximately equivalent flowrates).

---

*This equilibrium was rarely achieved in $<$15min (hence basis for averaging period in Fig.7.6)

Complicating this picture is that in increasing annular velocity 3– fold between the standard and Southampton cell, the electrode gap has been reduced by a factor of 2.5. In addition, because of the change in relative diameters of the electrodes, the active capacitance of the cell will also have increased. Hence, for the same thickness of water film on the electrode, the response of the Southampton cell will be ~4x that of the standard unit. Flow Reynolds number (with the annular gap, L_a, as the length parameter), however, has only increased by ~20% and both cells will be operating around transitional flow conditions (Re averages ~3000 for typical Q_u). Hence, although it is unclear whether wall shear stresses relate to laminar ($\propto v_{cell}/La$) or turbulent ($\propto \sim v_{cell}^2$) flow conditions [92, 93], they can be expected to increase by 7–9 fold in the Southampton cell (same Q).

Referring again to Fig.7.7, it is evident that initial Aquasyst readings (for a flushed water free cell) agree very closely with data from sampling/settling analysis. Values taken quickly after setting up a test condition may, therefore, allow a fairly accurate assessment of the true water level to be made.

One aspect of the water–oil system which had a clear influence on the Aquasyst operation was the stability of the interface. Fig.7.8 shows that following the accidental contamination of the kerosine with a surfactant–rich cutting oil (γ down by ~10%), a very significant reduction in the water build up rate occurred. It seems that the film created by surfactants around the water droplets reduces their ability to wet/settle on the electrode surfaces, an advantage for operation with crude oils.

Greater emulsion stability is probably a key factor in accounting for the absence of water build up found for subsequent testing of the Aquasyst (Southampton cell) with HGO(07). However, achieving a stable calibration for the cell was problematical, although this had not been the case for kerosine. This and other aspects of Aquasyst operation are considered in Appendix B.3.1.

In conclusion, the Aquasyst was found to be a very sensitive instrument, but of limited use with distillates at the flow and mixing conditions encountered in the testing, especially as a continuously acting monitor. For kerosine, cell modifications significantly improved reading drift due to internal water build up at higher water contents (>1%), but continued poor reading stability at lower, more typical K_u values meant measurement quality fell short of that achieved by the sampling/settling technique. For HGO(07), although the Aquasyst was effectivley less accurate than with kerosine, the impracticalities of the other measurement methods tried and much poorer hydrocyclone performances (Fig.9.19) made its use acceptable. Details of measurement accuracies generally can be found in Appendix B.4.

Hence, the measurement of K_u was undertaken using the sampling/settling technique for the kerosines and kero(63), and the Aquasyst (with the Southampton cell) for HGO(07)

7.3.2. Water–in–oil drop size

As separation is particularly dependent on drop size (see equation 1.1), the most important point to measure the dispersion is at the hydrocyclone inlet, so that the feed can be characterised. This represents a considerable range of drop sizes (roughly 5–500μ) and water concentrations (up to ~50%) or drop densities. Sizing techniques applied for stable water–oil systems – sedimentation (as used in [22]), electronmicrographs of small frozen emulsion samples [94], photographs of samples on microscope slides (as used in [24]) – are not appropriate for the less stable water–distillate mixtures used in these tests, where the drop size distribution represents a dynamic equilibrium dependent on the turbulent mixing in the feed pipework. In–line drop sizing is therefore required, and this can only be achieved practically over this range of K_i using short duration flash/exposure photography (with magnification if required) though transparent wall sections or optical cells (as used in [5, 21]).

Preliminary investigation indicated a magnified image was required and that back–lighting provided the best means of establishing contrast between drop and background. The main problems associated with this approach were the 'freezing' of the dispersion motion and having sufficient illumination at the film plane (especially difficult at high droplet densities and for the less transparent oils). These were largely overcome by using a very high speed, intense light source shining through a 'thinned–down' flow section with optical windows. However, some 'static' shots, where the flow motion was suddenly arrested, were also taken for reference.

The development and operation of the technique, together with details of how the photographs were analysed to obtain drop size measurements are considered in Appendix B.3.2.

Before considering how the dispersion is affected by the operating conditions, it is important to clarify that the drop size distributions being examined represent the product of the passage of the water–oil system through the variable speed turbine mixing pump and then 3.6m of 3/4" feed pipework (transit time 1–2s depending on Q_i), both of which may effect the nature of the dispersion entering the hydrocyclone.

The shape of the drop size distributions seems to approximate to log normality and typical examples are shown in Fig.7.9. A tendency for a slight bi–modal character and truncation at larger drop sizes is evident, whilst the spread of the distributions is within σ_g = 1.2–1.9 of the geometric mean, $\bar{d}_i (= d_{(50)})$. The scale of analysis was too small to be able to relate particular aspects of the drop size distribution form to changes in oil type or mixing/flow conditions, except that σ_g appears to be smaller for kero(63) than kerosine (Fig. 7.11).

Generally, dispersions have been characterised by $\bar{d}_i$ and the effect of mixing pump speed, N, is shown in Figs.7.10 and 7.11 for low feed water levels. Good agreement is evident between the currently used macrophotographic technique (11/85 onwards) and the earlier microphotographic method (7/82 and 3/83; see also Appendix B.3.2). From the figures, and by analogy with kerosine–in–water data for a similar mixing system [95], the general form of the relationship at low K_i ($\lesssim$10%) for N in rpm is

$$\bar{d}_i \propto e^{-8.2\times10^{-4}N} \qquad (7.1)$$

although $\bar{d}_i$ appears to be approaching a minimum for high N.

The smaller mean drop sizes for the kero(63) system compared with kerosine at equivalent conditions might well be expected considering the slightly lower interfacial tension and higher density (more easily generated interface and increased flowfield shears). However, for HGO(07) (+ surfactant rich biocide), where even greater susceptibility to break up might be anticipated, drop sizes exceed those for both kero(63) and kerosine (at the 750 rpm mixing condition for which data is available). This may be explained by an increased interfacial elasticity and a dispersed:continuous phase ratio away from unity, both of which favour deformation rather than break up for a given shear rate [96]. Further, substantially lower levels of turbulent shear will be associated with the flow of HGO(07), indeed Re becomes laminar in the sample line to the sizing cell.

Drop sizing for the kero(SG) system indicated dispersions were very coarse ($\bar{d}_i > 90\mu$ for a range of conditions comparable with data in Figs.7.10 and 7.11 [97]). These measurements, taken prior to the separation tests, are believed to be spurious (see Appendix B.2.2) and truly representative drop sizes are probably very close to those for kerosine (possibly 5–10% smaller).

The effect of water content on drop size can be of comparable importance to mixing pump speed and the interaction of these parameters is particularly significant, see Fig.7.12. This shows that a relationship of the form

$$\bar{d}_i \propto K_i^{\,n} \qquad (7.2)$$

has a general application over a wide concentration range, but whereas at comparatively high mixing speeds $n \simeq 0.58$ and 0.55 for kerosine (2000 rpm) and kero(63) (1500 rpm) respectively, at 1000 rpm drop size is a much weaker function of K_i.* Hence, it appears that as water levels increase, mixing pump speed has a reduced influence on $\bar{d}_i$ which becomes virtually independent of N above $K_i \triangleq 25\%$.

---

* Shiloh et al [71] working with stirred tanks for an aqueous liquor in kerosine gives n at 0.4 – 0.5 for $K_i < 5\%$.

One intention of the rig design – utilising an in–line turbine pump for mixing – was to be able to vary pump speed, and hence drop size, independently of flowrate. The extent to which this is possible is shown in Fig.7.13. Whilst the finer dispersions and higher mixing levels show this desired stability, at 1000 rpm there is a tendency for both kerosine and kero(63) to show a peak in $\bar{d}_i$ around 40–45 ℓ/min. This trait can be interpreted with the help of Fig.7.14, which shows that at these conditions the turbine pump is operating at just a sufficient speed to overcome the head loss caused by its presence in the feed flow i.e. the pressure rise through the pump is zero. Hence, in this region the energy input into the flow (/unit vol.) will be a minimum, as at higher flowrates the pump will act partly as a static mixer, whilst at lower flowrates the increased residence time in the high shear environment within the pump allows for greater mixing.

Measurements of drop size can also be obtained using these micro/ macrophotographic techniques both within (near–wall) and in the outlet flows from the hydrocyclone, notably in the upstream discharge. Such data has not been collected generally because of the time consuming nature of the analysis, but some measurements have been taken to illustrate droplet coalescence and break up effects through the hydrocyclone (see Section 8.1).

It was considered that on–line sizing using a laser scattering method might be viable for d_u measurement with the low K_u values typically encountered (0.1–0.3%) and as the oils being used were transparent. Such techniques have the potential to provide on–line, real time determinations of both particle size and concentration simultaneously by monitoring the (usually forward) scattered light intensity profiles from a low powered C.W. laser [73, 98]. The principal limitation to their use, however, is the restriction to very low dispersion concentrations ($\lesssim$0.1% by volume for $\bar{d}_u \triangleq 10\mu$ and 2.5mm path length), tightening as particle sizes get smaller [99]. This makes such instrumentation of only peripheral use to the experimental programme. This was confirmed when brief tests with a Malvern (2600D) system and variable path length optical flow cell were carried out by the author [97], although recent progress towards more sophisticated analysis of multiple scattering effects is pushing concentration limits higher [100].

CHAPTER 8

DROP STABILITY THROUGH THE HYDROCYCLONE

8.1 Evidence of Drop Instability

Although considerable circumstantial evidence for drop break up and coalescence in test hydrocyclones can be inferred from the experimental results described later in Chapter 9, some more direct measurements have been made to illustrate the instability of the water–oil dispersion through the hydrocyclone under certain conditions.

Photographs of near–wall drops in the upper cone were attempted with a kerosine oil phase in geometry 36NS4P(T). The technique adopted was based on the early feed drop sizing method of using a high speed flash and camera mounted on a microscope (see Appendix B.3.2). The experimental set up is shown in Fig.8.1, the operating principle being that light from the two shutter synchronised flash sources is condensed to intersect at the small area where the camera is focused (0–2 mm from the wall), providing back illumination and possible haloing of the water droplets to enhance their contrast against the background. However, the conflicting requirements of a short enough flash duration to 'freeze' the droplet movement and directing adequate light on the subject to provide sufficient contrast, in what is a low contrast system, made clear imaging difficult. As a result, the photomicrographs obtained are of poor quality, (Plate IV), although it should be appreciated that some loss of definition has occurred in the reproduction from the original prints. Maximum drop sizes can at least be obtained, and are compared with inlet dispersions in Table 8.1. This shows clear evidence of coalescence having occurred and that whilst feed dispersions are quite similar at the low mixing and flowrates for K_i = 5 and 10%, considerably larger drops are present at the wall for the higher K_i condition, reflecting greater droplet densities. Presuming the dispersion being photographed contains a substantial fraction of drops which have undergone separation from the main body of the flow, evidence from the solid analogue model (Fig.5.6) indicates that the coalescence that is occurring at

K_i[1] (%)	FEED DISPERSION		NEAR CONE WALL DISPERSION[2]
	$\bar{d}_i$ (μ)	d_{max} (μ)	d_{max} (μ)
10	70-75	105-115	280-300
5	65	103	145-160

1. N = 1000 rpm; Q_i = 20 ℓ/min; 1−F = 50%; T = 20°C; 36NS4P(T).
2. refer to Fig.8.1 for axial position.

Table 8.1 COMPARISON OF FEED AND NEAR CONE WALL DROP SIZES WITH KEROSINE

d (μ)	% DIFFERENTIAL VOL.		MP'(d) (equations 4.5, 4.6)
	INLET ($p_i(d)$)	UPSTREAM ($p_u(d)$)	
>10<20	1.5	2.0	-0.27
20-30	1.9	5.3	-1.66
30-40	5.2	12.1	-1.22
40-50	3.6	10.9	-1.89
50-60	3.6	8.1	-1.15
60-70	5.8	15.4	-1.54
70-80	5.6	6.3	-0.07
80-90	4.4	16.6	-2.95
90-100	9.8	9.8	0.05
100-120	14.1	4.3	0.71
120-140	19.1	9.1	0.55
140-160	25.6	0	1.00
	100.0	100.0	

$\bar{d}_i$ = 108.3μ $\bar{d}_u$ = 67.8μ

Q_i = 40 ℓ/min Q_u = 20 ℓ/min

K_i = 5% K_u = 4.78%

N = 750 rpm HGO(07), γ = 0.013 N/m

T = 20°C 35NS7(V)

Table 8.2 INLET AND UPSTREAM DROP SIZE SPECTRA COMPARED FOR HGO(07)

K_i = 5% has only a small effect on the separation and must therefore be happening very close to the wall. At K_i = 10%, however, it appears concentrations are high enough for coalescence to occur in areas further out from the wall, where a more positive impact on separation can be made (see Fig.9.17).

Generally, it can be expected that as the (segregated) water dispersion moves down the wall towards the hydrocyclone apex, finer drops will join it and also the continued centrifugal forces will cause inter-droplet films to thin, bringing drops together such that phase inversion may eventually occur, building from the wall inwards. At the low K_i conditions under test here, this inverted (continuous) water phase (perhaps containing some oil) may not have had the chance to develop. Even if it had, this might not have been obvious from downstream sizing as the water layer is likely to get re-entrained in what is predominantly an oil stream for the 50% operating split ratio (K_d < 20%). As split rises fluid will increasingly be drawn from further up and possibly nearer the centre of the hydrocyclone, raising oil levels in the reject. The inversion phenomenon is most easily demonstrated for high K_i values, as illustrated in Plate V, where a clear water phase can be seen developing in the mid-cone region around an oil rich core from an opaque water-in-kerosine feed (K_i = 50%). With the occurrence of inversion, local viscosities can be expected to fall and any dispersed elements (i.e. oil drops) will be subject to separating action, allowing further clarification of the water phase with the potential for K_d to approach 100%. If inversion does not occur, some oil will always be trapped interstially, no matter how closely packed the water droplets, setting a base level for oil contamination in the reject which will be reflected in $(1-F)_{crit}$.

Evidence of drop break up occurring in the hydrocyclone can be seen by comparison of the feed and upstream drop size distributions for a test run using 35NS7(V) with the viscous distillate blend HGO(07) and surfactant rich water phase (γ = 0.013 N/m), see Table 8.2. The poor separation achieved for this test run (K_u/K_i = 0.955) means drop sizes at outlet and inlet would be almost the same if the dispersion remained intact through the separator. However, $\bar{d}_u$ can be seen to be only 60% of $\bar{d}_i$ and practically all size bands up to 90μ show upstream differential volumes more than twice their equivalent inlet values.

As $1-F = 50\%$, this implies that a greater number of drops of these sizes are leaving the hydrocyclone *from the upstream outlet alone* than are entering the feed. Similarly, reduced migration probabilities based on this data are almost without exception negative and yet a positive, if small, amount of (bulk) separation has been achieved.

8.2 Drop break up

In order to understand and possibly predict the occurrence of droplet disintegration in the hydrocyclone, the possible mechanisms for break up need to be addressed. These can be identified as:–

(1) viscous shear due to time–averaged velocity gradients
(2) transient shears and local pressure fluctuations imposed by turbulence.

Other workers using hydrocyclones for liquid–liquid separation have postulated that inertial forces dominate [11,, 13], even though high steady state shears exist (up to 10^4-10^5 s^{-1}, [17] and Fig.6.3). Davies has also shown that for valve homogenisers, where these shear rates are nearer 10^6 s^{-1}, drop sizes can be predicted from turbulence theory [101]. Certainly by assuming the structure of turbulence in the hydrocyclone is homogeneous and isotropic, the Kolmogoroff microscale [102], ℓ_K, commonly taken to mark the boundary between viscous and inertially determined processes, can be calculated* as no more than a few tens of microns for the test conditions compared with the largest drops in the dispersions of around 100μ i.e. $d_{max} >> \ell_K$. Accordingly, with μ_p being low enough that internal viscous forces can be neglected, Kolmogoroff concludes that the beginning of disintegration in a dispersion is dependent only on the external inertial shear and the resisting surface force, which can be characterised by a critical droplet Weber number

---

* $$\ell_K = (\nu^3/\bar{\varepsilon})^{0.25} \qquad (8.1)$$

where $\bar{\varepsilon}$ is the average power dissipated per unit mass through the hydrocyclone, determined from equation 8.4.

$$We_c = \frac{\overline{v^2}\ \rho\ d_{max}}{\gamma} \qquad (8.2)$$

where d_{max} is the largest stable drop size and $\overline{v^2}$ is the mean of the square of the velocity fluctuations over a distance equal to d_{max} (see also Hinze [103]). Continuing with the simplest case of isotropic homogeneous turbulence, $\overline{v^2}$ can be approximated for non-coalescing systems by

$$\overline{v^2} = 2(\bar{\varepsilon}\ d_{max})^{2/3} \qquad [40,\ 108] \qquad (8.3)$$

Practical evaluation of We_c requires $\bar{\varepsilon}$ and d_{max} to be determined for hydrocyclone operating conditions at which the dispersion starts to break up. It is assumed that the minimum in the K_u/K_i against Q_i performance curve is fairly representative of this condition, although strictly first departure from the curve representing the behaviour of the drops without break up or coalescence, i.e. acting like solid particles, would be at lower flows (see Fig.5.6). d_{max} can be taken from the feed drop size analysis (although $d_{(95)}$ will be used as it is statistically easier to define), whilst $\bar{\varepsilon}$ can be calculated based on measurements of flow and pressure drop at this minimum as

$$\bar{\varepsilon} = \frac{Q_i\ \overline{\Delta P}}{V\ \rho} \qquad (8.4)$$

where $\overline{\Delta P} = (\Delta P_{iu} Q_u + \Delta P_{id} Q_d)\ /Q_i$ and V is the hydrocyclone volume.

Interestingly, Levich's interpretation of Kolmogoroff's work [104] incorporates a macroscopic length scale and mean stream velocity term which infers a relationship for hydrocyclones of the form

$$\bar{\varepsilon} \propto \left[\frac{v_i^3}{D_i}\right]^{3/5} \qquad (8.5)$$

compared with $\bar{\varepsilon} \propto v_i / D_i$ which comes out from equation 8.4 (single circular inlet assumed). However, quantification of $\bar{\varepsilon}$ working from Levich appears problematical so equation 8.4 has been used here. Hence, substituting from equations 8.3 and 8.4 the critical Weber number can be re-written as

$$We_c = 2\left[\frac{Q_i \overline{\Delta P}}{V}\right]^{2/3} \frac{d_{(95)}^{5/3}\ \rho^{1/3}}{\gamma} \qquad (8.6)$$

Modifications to this parameter to account for conditions when ρ_p differs substantially from ρ or μ_p is considerably more viscous than for water, are summarised by Hesketh et al. [105].

Table 8.3 shows how We_c is obtained for different water–oil systems in hydrocyclone 36NS5(S) at a low K_i (5%) for which coalescence is considered effectively absent. The approximate 2:1 range in We_c (0.45–0.8), although not of much use for predictive purposes, is encouraging in view of the assumptions made and degree of uncertainty involved in pinpointing $d_{(95)}$ and critical Q_i. Further reinforcement of this range comes from very recent unpublished results by the author for a heavy distillate blend ($\nu \triangleq 8.5$ cSt, $\rho = 844$ kg/m^3, with $d_{(95)} = 135\mu$) which shows $We_c = 0.65$, whilst Hesketh et al. [105] report that the band 0.6 – 1.7 covers a wide variety of liquid–liquid mixers and energy inputs.

WATER-OIL SYSTEM [N(rpm); 1-F(%)]	γ (N/m)	ρ (kg/m^3)	Q_i (ℓ/min)	$\overline{\Delta P}$ (bar)	$d_{(95)}$ (μ)	ℓ_K* (μ)	$\bar{\varepsilon}$* (W/kg)	We_c*
kerosine [2000; 10]	0.028	781	62.5	3.1	87	9	804	0.82
kero(SG) [2000; 15]	0.023	792	55	2.2	?87	9	495	0.78
kero(63) [1000; 25]	0.023	817	45	1.3	85	22	232	0.45

* see equations 8.1, 8.4 and 8.6.

Conditions for $(K_u/K_i)_{min}$ at K_i = 5% through 36NS5(S) (V = 0.515ℓ). T = 20°C

Table 8.3 CRITICAL DROPLET WEBER NUMBER FOR VARIOUS OILS

Table 8.4 extends the analysis to compare different hydrocyclones with the same water–kerosine dispersion and reveals a much greater variation in We_c, both between geometries and for different sizes of the same unit.

GEOMETRY	V (ℓ)	1-F (%)	Q_i (ℓ/min)	$\overline{\Delta P}$ (bar)	$\bar{t}$ (s)	$\bar{\varepsilon}$* (W/kg)	We_c*
36NS4P(T)	0.404	50	46	2	0.53	480	0.59
26NS4P(T)	0.145	50	32	3.6	0.27	1580	1.30
15NS4P(T)	0.0302	50	8.5	2(est.)	0.21	1200	1.08
35NS7(V)	0.336	15	62.5	3.5	0.32	1390	1.19
30D01(T)	0.783	50	52	0.9	0.90	128	0.24
30D02(T)	0.783	50	75	1.6	0.63	328	0.45

* see equations 8.4 and 8.6

Conditions for $(K_u/K_i)_{min}$ with kerosine : K_i = 5%, N = 2000 rpm $d_{(95)}$ = 87μ, ℓ_K = 8–15μ, T ≙ 20°C.

Table 8.4 CRITICAL DROPLET WEBER NUMBER FOR VARIOUS GEOMETRIES.

A principal reason for the discrepancies, especially regarding geometry changes, is thought to be the weakness of the isotropic, homogeneous turbulence assumption for the hydrocyclone as a whole (see evidence presented in Section 6.3 and especially references [86] and [88]). In particular, greater turbulence intensities are anticipated where the feed enters the hydrocyclone (Johnson et al. suggest up to ten times greater than average levels [11]) and perhaps most significantly all the dispersion passes through this region prior to separation. Also, with the steep velocity gradients which occur in hydrocyclones, it is likely that the structure of the turbulence will be anisotropic [107] and van der Linden reports that drop break up under such circumstances will be governed by turbulent eddies that have the largest velocity component in the direction of flow [108], effectively the tangential component here. Hence, the importance of v_i to the disintegration process is indicated, a factor illustrated in the experimental work (Section 9.1). Johnson [11] emphasizes the need to consider the velocity loss

ratio (v_θ/v_i at entry) in establishing turbulence levels associated with the feed, although this ratio is believed to be close to unity for the large inlet/swirl chamber formats used for Southampton based liquid–liquid hydrocyclone designs (see Section 6.3). Measurements of the turbulent flowfield within the test hydrocyclones would clearly be helpful. It should also be stated that the effects of the steady state shear field may not be negligible.

It is of note that the breakage time for the largest drops in the dispersions studied is of the order of 10^{-4}s ($d_{(95)}/(\overline{v^2})^{\frac{1}{2}}$ [109]), comparatively short with regard to hydrocyclone residence times, $\bar{t} = Q_i/V$ (Table 8.4), but considerably greater than the viscous response times for these drops ($\mu_p/\rho_p \overline{v^2}$ [101]) at $10^{-6} - 10^{-5}$s i.e the system is prone to disintegration.

The mode of droplet break up may have a bearing on its visibility in the context of gross efficiency parameters (like K_u/K_i). For example, as the greater part of the feed dispersion is generally considerably larger than d'_{50} ($\bar{d}_i > 2 \times d'_{50}$ for the tests with kerosines), if the largest drops split in half on break up, the resulting daughter droplets will still have a very good chance of being separated. If, however, they disintegrate into a large number of much smaller drops, the effect on upstream water concentrations will be more noticeable. Evidence from viscous shear studies [96] indicates that systems with the viscosity ratio, μ_p/μ, = 0.2 → 1 (water–kerosine = 0.7) are particularly prone to break up rather than extended deformation with increasing strain rates. Although it is difficult to generalise such effects to turbulent conditions, Collins and Knudsen photographing oil–water mixtures in turbulent pipe flow indicate that for viscosity ratios around unity a typical break up event leads to two similarly sized daughter drops with a few much smaller satellite drops [111] i.e. necking (the presumed source of the smaller drops in this instance) is limited. Ogawa comments that for dispersion processes in general the more We exceeds We_c the more complex the rupture mechanisms and chaotic the disintegration process becomes [110].

Finally, as dispersion concentrations increase, some account needs to be taken of the damping of turbulence by the drops, even for non-coalescing systems. This has been allowed for by increasing We_c by a factor $(1+AK)^{5/3}$, where A is a constant [109], but see also equation 8.8. The interaction of concentrated suspensions of particles with turbulence in hydrocyclones is considered in greater detail by Neese et al. [112].

8.3 Drop Coalescence

As feed water levels increase, drop coalescence can play an increasingly important part in determining the distribution of the phases within the hydrocyclone, and hence its performance capabilities.

Moving downstream from the inlet it is postulated that with the radial segregation of the dispersion imposed by centrifugal action, a layering effect will develop analagous to gravity settlers. For a coarse dispersion which will readily coalesce, this is illustrated schematically below.

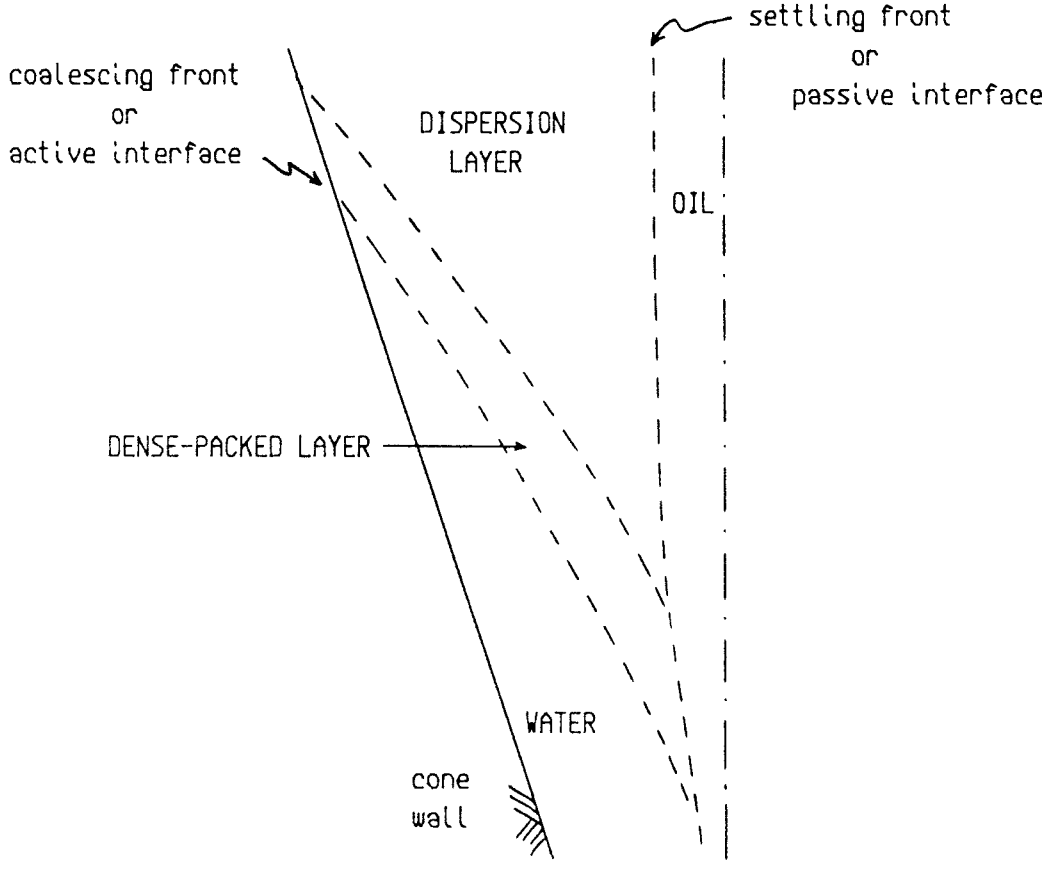

Travelling from the centre outwards, the clear oil zone is followed by the dispersed water layer in which drop sizes and local water concentrations increase until the dense–packed layer is reached, where the drops touch on all sides to form a 'bed' and finally coalescing completely to generate the clear water phase. Whilst turbulence will undoubtedly blur these divisions, for smaller feed drop sizes and surfactant stabilised interfaces, insufficient residence time may cause the loss of the 'pure' oil and water layers. However, even unstabilised drops with adequate time to separate can generate secondary sub–micron hazes during the process of coalescence according to Smith and Davies [113]. Further subdivisions of the dispersion band may also occur due to droplet sorting effects during hindered settling [61]. The nature and relative thicknesses of the layers present will be a complex function of the characteristics of the water–oil system being separated, the hydrocyclone's internal flowfield and operating conditions, and the axial position in the separator.

Generalising, what happens in the dispersion band will be most significant with regard to water droplet removal from the oil stream (K_u/K_i), whilst processes in the dense–packed layer (and nearer the wall) will be more relevant in determining critical split ratios. In both cases, coalescence can play a primary role which can be better understood by considering the mechanisms which control it.

Coalescence of drops within the hydrocyclone will occur by interaction with neighbouring drops, a non–spherical fluid interface (coalescence front) or a solid surface (hydrocyclone wall). For liquid–liquid interactions the process can be subdivided into three stages:–

(i) collisions between drops, this only applies in the dispersion layer and would occur as either head–on impacts linked with turbulence or overtaking collisions relating to the variation in settling velocities of different drop sizes (note also $\partial v_z/\partial r$ and $\partial v_\theta/\partial r \neq 0$)

(ii) drainage of the continuous phase film between drops to a critical thickness, the rate of which would be principally controlled by its viscosity

(iii) rupture of the film, which usually occurs more rapidly than stage (ii) and is believed to be in part dependent on the strength of inter– molecular attraction within the dispersed phase [114], although in general the process is poorly understood [108].

Complicating this picture there are likely to be repelling forces acting to keep interfaces apart. These may result from flow induced surface charges or more generally the ionic double layer around the water drops. Such effects are not negligible for low conductivity continuous phases like crude oil and more particularly distillates [61, 116]. In addition, surfactant materials at the water/oil interface, will also tend to cause repulsion of similar surfaces (over short distances) and the rupture process in particular is likely to be significantly affected by their nature and concentration. In some circumstances, however, surface chemistry and charge may be such as to actively encourage flocculation.

In the dispersion band, not all drops that collide due to local turbulence will combine and the efficiency of this process primarily relates to the balance between interdrop film drainage times and the duration of the eddies bringing the drops together. This collision efficiency is likely to be higher for overtaking collisions where more extended droplet contacts can be envisaged. The product of the collision efficiency and collision rate (principally dependent on droplet density) can be viewed as the coalescence rate.

In the dense– packed layer, where droplets are already in contact and relative radial velocities are negligible, the driving force behind film drainage is the 'weight' of drops in the bed 'above' a particular level. However, the situation is liable to be confused by slippage caused by the tangential and axial velocity gradients across the bed. Certainly film drainage times are likely to be longer than in the dispersion zone because of the constricted nature of the drainage paths. Observations of this kind of layer in transparent models of gravity settlers by Barnea and Mizrahi [61] indicate that drops increase in mean diameter towards the coalescing front accompanied by considerable distortion from sphericity.

Coalescence rates at the coalescing front appear to be very difficult to assess and there are numerous contradictions in experimental studies as to the importance of controlling parameters [61]. A great deal of this uncertainty probably relates to the progressive concentration of contaminants as coalescence proceeds and interfacial area falls towards the coalescing front. Small satellite drops of continuous phase (oil) also tend to be generated as the dispersion (water) inverts, often associated with irregular cyclic variation in the dense–packed bed depth [113].

Selker and Sleicher studying phase inversion in stirred tanks with water/oil systems [116] showed a considerable and roughly symmetrical range of concentrations (by volume) over which either water or oil could be dispersed, termed the range of ambivalence. They found this range to be widest for kerosine:water–like kinematic viscosity ratios, at 22 to 71% water, with the higher concentration being achieved by starting the test with water dispersed. They also noted that as the viscosity of a phase increased, its tendency to disperse also increased. Ward suggests that for relatively pure water/oil systems, water is more likely to constitute the continuous phase because of the greater mutual attraction of water molecules above oil molecules [114]. However, crude oil emulsions may have dispersed water concentrations >90% according to Monson [30].

The build up of water at the hydrocyclone wall and phase inversion close to it may well be influenced by the wettabilitiy of the wall material involved. Significant changes in water/organics separation performance have been reported for both hydrocyclones [19] and gravity settling cells [113] depending on the relative wettability of vessel surfaces. There may, therefore, be an advantage in using preferentially water wetting material to line the hydrocyclone cone (e.g. certain ceramics), although it is presumed that the effect is dulled by contaminants in the system, e.g. use of crudes in contrast to distillates, and there is evidence to suggest the effect decreases with increasing vessel size [117].

Putting the coalescence phenomena into some kind of quantitative framework is clearly problematical. Most analysis in this area relates to agitated vessels and gravity settlers and works from basic models assuming binary drop–drop coalescence and isotropic (random) turbulence at the coalescing front. Derived relationships for coalescence rates, w, tend to rely heavily on empirical data but some general dependencies have been found as follows. At the coalescence front $w \propto \mu^{-1} d^{-1.5}$ [61] with an added dependency on the dense–packed bed depth [118] and acceleration field acting. In the dispersion band, $w \propto K$ is a widely quoted relationship, as is an inverse dependency on d [61, 114]. However, Shiloh et al. conclude that for viscous flow regimes (which are likely to prevail for the movement of many of the smaller drops in the test dispersions within the hydrocyclone) w is independent of d [71].

Hartland and Jeelani suggest a range of models for predicting the thickness of the settling layers, the choice of which can be gauged from the results of simple batch sedimentation and coalescence tests with the system to be evaluated [118]. One simplifying assumption which might be appropriate for a system like water–kerosine (which readily coalesces) is to assume every drop collision results in coalescence, thereby eliminating the dense settling layer from the problem.

In the absence of any systematic measurement of outlet drop sizes or of the internal distribution and degree of dispersion of phases for the test hydrocyclones, little progress can be made towards quantifying coalescence effects. Some estimates of the extent of drop coalescence (as it effects the separation of the dispersion) can be made, however, by indirect means.

For example, Fig.9.18 shows that K_u/K_i (above the critical split) is unchanged for a given feed drop size when increasing K_i from 5 to 10% with kero(63). Assuming the system was sufficiently dilute for Stokesian settling laws to apply, this test result would indicate that the drops were behaving like solids i.e. no coalescence was occurring. Using the corrected form of the law to account for hindered settling effects (according to Neese et al. [112])

$$u = \frac{d^2 \Delta\rho\, a}{18\mu} (1-K)^{4.65} \qquad (8.7)$$

shows that migration velocities will be slowed as dispersion concentrations rise and hence that drop sizes must increase if efficiency is unchanged i.e

$$d^2 \propto (1-K)^{-4.65} \qquad (8.8)$$

Using K_i to represent K, an effective 13% increase in drop diameter can be anticipated for K_i = 10% over 5% in the zone of separation.

Similarly, a rough estimate of inversion timescales can be obtained for the water–kerosine system used in Plate V, based on single phase v_z profiles (Fig.6.1) and residence time analyses [80] for a comparable 6° cone geometry. At the 50% feed water concentration in use here, drops will be almost continually in contact i.e. approaching the dense–packed layer structure. A drop travelling close to the wall can be seen to have become continuous phase by about half way down the cone in an estimated time of $\bar{t}/4$. This can be considered an upper time limit, therefore, for a water phase to coalesce out from a dense–packed layer and hence, if a drop near the wall is within this time period of leaving the hydrocyclone and is not yet part of the dense–packed bed, inversion of the dispersed phase will not occur.

Finally, some indication of the dispersion levels at which coalescence processes become significant to hydrocyclone performance would be useful. From the evidence discussed in Section 8.1, for kerosine, any K_i > 5% seems to be affected (effectively the whole experimental range). Blends containing the heavy gas oil appear more stable, compare Figs.9.17 and 9.18, but coalescence processes near the hydrocyclone wall are clearly of importance even at low water levels, as indicated by the sensitivity of $(1-F)_{crit}$ to K_i at these concentrations for kero(63) (Fig.9.12). Van der Linden et al. working with a water–in–turbine oil system (typical ρ = 860 kg/m^3, ν = 40 cSt, γ = 0.024 N/m) in agitated tanks [108] states that drop–drop coalescence only becomes significant in determining the dispersion characteristics above 6% (vol.) water during mixing. That this limit rises to 15% for characterising "demixing" or settling tests reflects the lower droplet interaction rates when turbulence is absent from the system.

8.4 Unified Approach to Drop Stability in the Hydrocyclone

Whilst it is helpful to consider break up and coalescence separately in identifying the role these processes play in the operation of liquid– liquid hydrocyclones, a unified approach to drop stability is desirable.

A commonly used method for amalgamating the two effects is by introducing a correction term to account for volume fraction into the break up characterising correlation equation, whence

$$d_{max} = \frac{We_c \gamma}{\overline{v^2}\rho} (1+BK) \qquad (8.9)$$

where B is a constant which has been reported to vary between 2.5 and 9 by van der Linden et al. [108] reviewing other workers experimentation in agitated vessels. This variability reaffirms the significant effect of small amounts of contaminants.

A simplified but instructive approach adopted by Shinnar [89] assumes that $\bar{\epsilon}$ is the key determinant of the stability of a dispersion. He showed that there is a maximum drop size, d_{max}, below which break up is effectively zero which, for locally isotropic turbulence in the inertial range, depends on $\bar{\epsilon}^{-2/5}$ (from equation 8.6) and similarly a minimum drop size, d_{min}, above which coalescence is effectively zero, that depends on $\bar{\epsilon}^{-\frac{1}{4}}$. Since these two functions must cross, as shown in Fig.8.2, four regions are formed. Above both lines most drops break up and few coalesce, the condition being reversed below both lines. In the region where $d_{min} > d_{max}$, drops readily break and coalesce and a finite rate of dispersed phase mixing is estab lished. In the region where $d_{min} < d_{max}$ little breakage or coalescence can occur yielding a "turbulence stabilised" dispersion. On the basis of the widely reported mass transfer capabilities of liquid– liquid hydrocyclones [9], it seems reasonable to assume that normal operating conditions might in part overlap with the zone of dispersed phase mixing, with the implication that interfacial renewal may be a significant process which would reduce the influence of surfactants. It should be pointed out that there are a number of weaknesses in the application of this model, however,

notably the uncertainty of the inverse dependency of coalescence on drop size and the similarity of ℓ_K to the smaller drop sizes for typical test dispersions. Also one must be aware of the changing dispersed phase concentrations and non– uniformity of energy losses through the hydrocyclone.

Seymour [118] suggests a third rate process needs to be considered in continuous flow sytems (like hydrocyclones), that of departure. For example, large drops entering a vessel may be unstable and disintegrate to sizes at which coalescence can occur, but might then have a higher probability of leaving the system than actually coalescing.

In the author's view a way forward towards an integrated coverage of events in the dispersion band is to adopt a population balance approach to provide a statistical description of the passage of the dispersion through a hydrocyclone, as has been developed in the field of stirred reactors by Tavlarides and co– workers [119, 120]. Such an approach complements the probabilistic nature of turbulence, but requires substantial knowledge of process frequencies and the internal flow structure of the hydrocyclone to be effective.

CHAPTER 9
WATER–OIL SEPARATION TESTS: DISCUSSION OF RESULTS

9.0 Introduction

This chapter is primarily concerned with investigating and improving the understanding of the operation and design of dewatering hydrocyclones for various water–oil systems and feed conditions, in the context of the objectives and applications outlined in Section 1.4. Briefly, the priority in terms of performance is for effective water removal from oil over a wide range of water concentrations and flowrates, with minimisation of reject flows and pressure drops important but generally secondary requirements. The work described here, although not treated chronologically, follows on from the preliminary studies outlined in Chapter 5. Test procedures and explanations of performance criteria have been described in Chapters 7 and 4 respectively.

Behavioural aspects of hydrocyclone operation relating to flowrate, the balance between split and water concentration, and water–oil system characteristics (including degree of dispersion) are discussed in the first three sections of the chapter. The use of dimensionless groups to try and establish patterns in the performance of a particular hydrocyclone type is considered in Section 9.4, including changes in size, whilst the effect of geometry is looked at in Section 9.5. An inevitable degree of overlap occurs between sections and parameters like pressure drop are considered throughout.

Practical constraints and the applications oriented nature of the research has meant that the full range of test conditions has not been investigated with a single geometry but with a range of dewatering designs (see Section 9.5 and Appendix D for dimensional details) which can be considered as 'good' separators and show a similar form of response to a given stimulus. This broad based approach in combination with uncertainty regarding long term water–oil system stability has meant that comparisons are sometimes difficult to make and only limited regression or optimisation analysis has been attempted. Nevertheless,

where performance data for different geometries are shown on the same plot it can be taken that closely comparable system states existed during testing (which would usually be contemporaneous). Test periods are dated where uncertainty exists.

The effect on the dewatering operation of the hydrocyclone of the presence of solids, gas and transients in water/oil flow, which might be expected in a production environment close to the well-head, are assessed in Chapter 10. Small excursions from the experimentally defined conditions towards these more complex regimes would not be expected to invalidate the findings in this chapter.

9.1 Effect of Flowrate

Fig.9.1 shows the typical characteristics of a flowrate vs. efficiency plot for water-oil separation in a hydrocyclone. At low flows separation is poor due to low spin rates and as Q_i and spin increases, separation improves until a minimum in K_u/K_i occurs beyond which separation falls away. This has been attributed to droplet break up effects caused by rising shear levels counteracting the influence of a strengthening radial acceleration field. For the water distillate systems being tested, this performance peak is found at modest flows (see below) compared with deoiling hydrocyclone operation (~80-110 ℓ/min, using geometries of comparable D and S, separating similar $\bar{d}_i$ for Forties in water dispersions [95]). Characterisation of this condition is clearly critical in establishing the limits of operation.

The nature of the feed is significant. Fig.9.1 shows that the lower interfacial tension of the kero(SG) system, relative to kerosine, depresses the flowrate at which $(K_u/K_i)_{min}$ occurs and in combination with a doubling of viscosity, as for kero(63) in Fig.9.2, the difference is even more substantial. The effect of drop size can be seen for 36NS5(S) by altering mixing in Fig.9.2 for kero(63), $\bar{d}_i$ increases by a factor $\simeq 2$ as N changes from 1500 → 1000 rpm, and water content in Fig.9.1 for kerosine, $\bar{d}_i$ increases by a factor of almost 3 as K_i goes from 5 → 30%. Whilst the tendency is for the coarser dispersion to have a slightly lower optimal flowrate, the difference is small for what are relatively

large changes in $\bar{d}_i$. Split is thought not to influence the phenomenon over the typical working range here (10 – 50%), although Bohnet suggests different optimal flows may be required depending on whether the hydrocyclone is being operated to give clean oil or clean water [4]. Finally, as evidenced by Fig.9.3, drop break up is seen to be a function of hydrocyclone geometry.

Drawing these aspects together to try and characterise droplet stability in a dimensionless form has already been attempted in Chapter 8. However, accounting for the non–uniform nature of shear within the hydrocyclone seems impossible without specific knowledge of internal velocity fields. The best general guide for predicting the optimal flowrate for a given water–oil dispersion seems to be the inlet velocity. For kerosine with K_i = 5% and N = 2000 rpm ($d_{max} \simeq 100\mu$), $(K_u/K_i)_{min}$ occurs when v_i (Q_i/A_i) is between 5.5 and 8 m/s (based on results from a wide range of dewatering geometries, Table 9.1), D = 15 → 36 mm (Fig.9.5), and also using conventional solid–liquid hydrocyclones [70]). This implies a substantial element of break up is associated with turbulence on entry of the feed and endorses the swirl chamber design concept for liquid–liquid hydrocyclones.

In practical terms, the hydrocyclone may be viable at flows considerably higher than the optimal condition if the form of the Q_i vs. K_u/K_i plot is a fairly shallow curve. Limits on Q_i (and ΔP) might therefore best be established on the basis of an acceptable level of separation. This has been interpreted in the context of Fig.9.3, where the extremes of potential operation have not been fully investigated, by defining the flowrate turn–down ratio (TDR) in relation to $(K_u/K_i)_{min}$ for that particular geometry and using $TDR/(K_u/K_i)_{min}$ as a guide to viability. Hence, as shown in Table 9.1, whilst 30DO1(T) has the highest TDR of the geometries tested in this comparison, this is offset by its relatively poor $(K_u/K_i)_{min}$. Note also that the feed conditions for the DQ geometries may have been slightly more tractable than for the other geometries based on the evidence of Fig.7.4. Choice of optimal geometries, considered in Section 9.5.5, must take account of capacity determining aspects as well (Q_{max} and ΔP) and these are also shown in the table. The experimental data from which the pressure drop parameters are derived comes from Fig.9.4, although for clarity, only ΔP_{iu} has been plotted as it reflects the greater of the pressure drops to

	$(K_u/K_i)_{min}$	TURN-DOWN, for separation within 0.005 of $(K_u/K_i)_{min}$			TDR/ $(K_u/K_i)_{min}$	ΔP_{iu} at Q_{max} (bar)	From ΔP_{iu} or $(\Delta P_{id}) \propto Q_i^n$ => n		v_i at $(K_u/K_i)_{min}$ (m/s)
		Q_{max} (ℓ/min)	Q_{min} (ℓ/min)	TDR					
36NS4P(T)[1]	0.038	59 (57)[2]	30	2.0	53	4.5	2.25	(2.3)	6
36NS5(S)	0.021	80 (77)[2]	45	1.8	86	5.3	2.3	(2.5)	8
35NS7(V)	0.022	77	47	1.6	73	5.6	2.25	(2.4)	8
30DO1(T)[1]	0.038	69 (94)[2]	35	2.0	53	2.5	2.10	(2.2)	5.5
30DO2(T)[1]	0.048	87 (118)[2]	57	1.5	31	3.0	2.35	(2.3)	7.5

1. data estimated by analogy with curves for $1-F = 50\%$
2. Q_{max} for D = 35mm unit calculated from constant v_i scaling (TDR, ΔP and $(K_u/K_i)_{min}$ unchanged, see Section 9.5.4.)

Table 9.1 SUMMARY OF PERFORMANCE FOR VARIOUS HYDROCYCLONE GEOMETRIES BASED ON FIGS.9.3 AND 9.4 (KEROSINE, $K_i = 5\%$, $1-F = 10\%$)

the outlet streams (for these geometries and splits) and changes less with split than ΔP_{id} (see Fig.9.6). The principal feature of the pressure/flowrate relationship is the constancy of exponent 'n' in the proportionality $\Delta P \propto Q_i^n$ for this range of Re_D ($0.7 \rightarrow 2 \times 10^5$). The variation with geometry in 'n', between 2.1 – 2.35 for ΔP_{iu} and 2.2 – 2.5 for ΔP_{id}, may in part be related to split differences. Table 9.2 indicates system type is significant as well (Re_D down to 0.3×10^5) and K_i may also effect the exponent, although data is not available to confirm this. It should be pointed out that the error in evaluating 'n' could be as much as ± 0.1 when only 4 experimental points are used in its determination.

Dimensionless representations of pressure requirements (C_P vs. Re_D) and separation potential (K_u/K_i vs. $H_y(\bar{d})$) are discussed in Section 9.4.

Whilst split has been controlled by valves to be constant during these tests, it has a tendency to fall slightly with increasing flowrate if the valves are left unadjusted. The extent of this effect has not been fully investigated, but by way of illustration, in doubling Q_i through 36NS5(S) with kero(63), 1−F reduces from 50 to 46%.

	kero(SG) [see Fig.9.1]		kero(63) [see Fig.9.2, N = 1000rpm]	
	ΔP_{iu}	ΔP_{id}	ΔP_{iu}	ΔP_{id}
36NS5(S)	2.1	2.35	2.3	2.5
35NS7(V)	2.1	2.25	2.3	2.4

Table 9.2 EXPONENT 'n' FROM $\Delta P \propto Q_i^n$ FOR VARIOUS WATER–OIL SYSTEMS (K_i = 5%)

9.2 Effect of the Balance between Split and Feed Water Concentration

These two parameters are treated together because of the very substantial changes in separation performance which result from their interaction. In the field it is envisaged that the former will be controlled to follow variations in the latter.

9.2.1 Split ratio variation

This is illustrated in Fig.9.7 for a 5% water dispersion in kero(63), using K_u/K_i, K_d/K_i and E to monitor hydrocyclone performance as split changes (see Section 4.1 for background, including idealised form of this type of plot, Fig. 4.1). At a certain critical split ratio overall efficiency is seen to peak, with operation above this condition favouring minimisation of upstream water content and operation below it favouring maximisation of reject stream water levels. This split represents the point of break through of significant volumes of water to the upstream as the downstream outlet becomes overloaded (with falling split). As K_u/K_i is most relevant to dewatering objectives and $(1-F)_{crit}$ can be recognised from the 'knee point' in its curve, this is the favoured form of separation presentation.

Curves for K_u/K_i against split are shown in Figs.9.8, 9.9, 9.10 and 9.11 covering a range of K_i, Re_D, water–oil systems and hydrocyclone geometries. Some characteristics are general, like the greater sensitivity to sub–critical splits at lower K_i, but the shape of the curves above $(1-F)_{crit}$ tends to fall into two groups. For the kerosines, K_u/K_i appears to continue dropping slightly as split increases although there are signs of a levelling off and perhaps rise in K_u/K_i at very high splits (60%+). This latter effect may be related to increased mixing as flow patterns unfavourable to the geometry are imposed by the external valves. For the distillate blend kero(63), $(1-F)_{crit}$ appears to mark a minima in K_u/K_i regardless of split. The reason for this dichotomy is speculated on in Section 6.2.1, making use of internal flow measurements.

Identifying $(1-F)_{crit}$, however, is clearly the most important consideration in choosing the best split ratio at which to operate, and results from early separation tests with kerosine indicated that constancy of the ratio $(1-F)_{crit}/K_i$ might be an effective guide [68]. This data is plotted against K_i in Fig.9.12, together with subsequent measurements from a variety of test programmes. For kerosine generally, $(1-F)_{crit}/K_i$ ranges between 1.03 and 1.55, although for any given test period it remains roughly constant (to within ± 10%) as K_i changes between 5 and 40% and this also implies an independence of drop size. Minor differences due to geometry are evident for the same test period and K_i values (compare 36NS5(S) and 35NS7(V) or 26NS4P(S) and 26NS5(S)), but the bulk of

variation appears to be linked with fluctuating system stability. Stability in this context must principally reflect the ability of the dispersion to coalesce and invert (or possibly deform) and does not seem to be associated with the separating action of the hydrocyclone ($\bar{d}_i >> d'_{50}$ for water–kerosine systems even at low K_i). Higher values of $(1-F)_{crit}/K_i$ are reflected in reduced K_d/K_i and oil recovery but K_u/K_i remains approximately the same (for a given K_i at $(1-F)_{crit}$). A reference point for the magnitude of $(1-F)_{crit}/K_i$ is provided by considering that the uniform dense packing of a log normally distributed set of rigid spheres requires an interstitial volume of 20% [5], although the radial grading of such particles in the hydrocyclone downstream outlet means this would be a conservative figure in practical terms. Hence, the water–kerosine system featured in Fig.9.8 (for which $(1-F)_{crit}/K_i$ averages 1.05) is likely to have been in a particularly pristine and unstable state, with phase inversion in the downstream and K_d averaging 92% at $(1-F)_{crit}$.

For kero(63), critical split ratios are relatively higher than for kerosine, as might be expected for a more viscous oil with more stable interfaces against water (i.e. increased film drainage time between interacting drops). However, an inverse relationship between $(1-F)_{crit}/K_i$ and K_i is apparent. This may be a product of the small $\bar{d}_i$ at low K_i ($\bar{d}_i$ approaching d'_{50}), causing reduced droplet densities near the wall and lower coalescence rates (see Section 8.3) compared with higher K_i. The link with d_i further implies that the separation achieved and $(1-F)_{crit}/K_i$ may be correlated within certain limits, although the similarity between K_u/K_i for 5 and 30% K_i in 36NS5(S) at $(1-F)_{crit}$ (Figs. 9.10 and 9.11) and yet substantial differences in $(1-F)_{crit}/K_i$ (Fig.9.12), indicates these limits may be quite narrow (see next section for discussion of concentration effects). In addition, it seems evident, although not entirely clear from experimental data, that the angularity of the 'knee point' in the K_u/K_i:split curve will also reflect the quality of phase separation within the hydrocyclone, becoming more rounded for kero(63) compared with kerosine.

Practically, $(1-F)_{crit}$ would need to be established by testing at the anticipated extremes of water concentration and an operating split chosen above $(1-F)_{crit}$ by a margin dependent on the short term stability of K_i and the penalties of either pulses of higher water contamination in the process stream or excessive amounts of reject flow.

9.2.2. Water content variation

Fig.9.13 shows the effect of changing K_i for operation in the near supra-critical split region. The 'U' shaped form of the curves against K_u/K_i reflects the improved separation achieved as drop size and probably coalescence rates within the hydrocyclone increase with K_i (see Fig.7.12 and also Section 9.3.1) until a point is reached (at 20-25% for the systems illustrated here) when these positive effects become swamped by the negative influence of other system changes linked with higher K_i. These include an increasing apparent viscosity of 2-component systems with rising K_i (see Section 4.2.1), reducing spin and therefore the radial acceleration field within the hydrocyclone as well as raising the drag on migrating droplets, and the onset of phase inversion in the feed when the clear division between dispersed and continuous phases becomes clouded as dual or multiple emulsions e.g. water-in-oil-in-water develop. Hindered settling effects will also increase with dispersion concentration (equation 8.6) but it is felt droplet agglomeration will not be of significance in the high shear conditions within the hydrocyclone. These aspects together with consideration of internal concentration gradients have been discussed in Chapter 8.

The information in Fig.9.13 has been replotted in Fig.9.14 for 36NS5(S) to show directly how K_u varies with K_i, and it is evident that for systems which readily coalesce, like water-kerosine, low water levels in the oil stream can be sustained over considerable ranges of feed water cut (in this case down to $<0.3\%$ for $K_i \lesssim 30\%$). The dashed lines at higher K_i indicate areas of experimental uncertainty and appear to be linked with poor system stability at these water levels. Longer term instabilities are underlined by test results for some D = 15mm geometries shown in Fig.9.15. The lowest K_u/K_i values in this plot are for K_i as high as 45%, where a remarkable 99.97% of water is being removed in 15NS4P(T) leaving only 300 ppm in the upstream discharge. Performance beyond this K_i drops away dramatically such that by 55% water cut only half of the water is being removed from the oil. In comparison with Fig.9.13, this implies water remains as a clearly dispersed phase to much higher water levels and inversion, when it occurs, affects a more narrowly defined region. Apart from the differences in hydrocyclone scale and geometry, which

are not considered significant in this context, the kerosine used for the tests shown in Fig. 9.15 was a new batch put into the rig after a thorough cleaning and flushing exercise, June 1985 (γ estimated up to 0.035 N/m), whilst the data in Fig.9.13 was obtained with kerosine which had been in the rig many months and was therefore comparatively contaminated, Dec. 1985 (γ = 0.028 N/m), see Section 7.2.2. These stability differences are illustrated in Fig.7.4 with reference to a maximum K_i value for which a certain degree of separation can be achieved.

Operation for K_i beyond the region of a simply defined water–oil system is shown in Fig.9.9, for K_i = 45% over a wide range of splits (March 1985 test date). Good dewatering with reasonable oil recovery is clearly difficult to achieve and characterisation of these curves also looks problematical. Evidence of very poor hydrocyclone performance for liquid–liquid separation with around 50:50 feed compositions is widespread (isobutyl alcohol–water [20]; water–crude oil at 10°C [122]).

9.2.3 Pressure drop changes linked with 1–F and K_i

Pressure drop changes across the hydrocyclone associated with varying split are shown in Fig.9.6 for the principal test oils. The geometry used to illustrate the relationship, 36NS5(S), was probably the most generally effective of the dewatering designs (see Section 9.5.5). It is evident that $\Delta P_{iu} > \Delta P_{id}$ over most of the useful operational range i.e. the reject is typically at a higher pressure than the process stream. The point where $\Delta P_{iu} = \Delta P_{id}$ ($\Delta P_{du} = 0$) can be considered as the 'natural' split of the hydrocyclone. The effect of geometry on this reference point is considered in Section 9.5.3 and summarised in Table 9.5. Whilst ΔP_{du} can be viewed as a gross axial pressure gradient, its use as a diagnostic tool regarding flow reversal characterisation is limited by the remoteness of the pressure tappings (see Appendix B.1) and the potential complexity of axial velocity profiles near the hydrocyclone axis (see 6.2.1).

As split changes, the increased flow to an outlet is a function of the lower pressure at the outlet. However, the change is much greater for ΔP_{id} than ΔP_{iu}, which must reflect differences in the pattern of energy losses in the flow paths taken by the flow streams which emerge at either end of the separator. The rate of change of ΔP with the split seems roughly linear, with a gradient which appears to be relatively independent of oil type but must change with flowrate as $\Delta P \propto Q_i^n$ (see Section 4.2.1 (iii)). For the more viscous distillates, the lower pressure drops to the outlets reflect the fall in Re_D for these systems (Q_i constant). Other trends include a small movement of $\Delta P_{du} = 0$ to higher $1-F$ values causing a corresponding increase in ΔP_{du} at splits below this level. These effects in combination mean that $\Delta P_{du}/\Delta P_{iu}$ rises substantially as the oil type becomes more viscous and dense. One further effect associated with this change in oil type appears to be the comparatively high ΔP_{iu} required to operate at the lowest splits.

One means of contributing to the evaluation of the optimum split operating range for a particular geometry (and oil) might be by using the power consumption/unit mass calculated as

$$\Delta P_{id} Q_d + \Delta P_{iu} Q_u \qquad (9.1)$$

where higher values might be interpreted as being associated with increased mixing effects. This parameter has been calculated for the kero(63) data in Fig.9.6 and shows a fairly stable minimum level between 30 and 70% split at ~115 W/kg increasing by about 20% as the split varies beyond this range to 5 and 95%. Separation performance has not been monitored in sufficient detail or extensively enough to assess the value of this technique.

The introduction of the water dispersion into the feed (see Fig.9.16 for water–kero(SG) at $K_i = 30\%$) complicates the smooth relationship between split and pressure drop shown in Fig.9.6. In particular, a step in the profiles is evident corresponding to the critical split ratio. This represents a drop in required pressure as water breaks through into the oil stream with falling split (Fig.9.11) and because of the likelihood of this water being coarsely dispersed, having been subject to the separating action of the hydrocyclone, the phenomenon is interpreted as being a product of water rapidly concentrating along the inside

surface of upstream outlet and reducing wall friction. Although data is incomplete, similar patterns of behaviour can be found for kero(63) and at low K_i. The importance of this effect to the operator lies in its potential use in identifying the critical split ratio from pressure measurements alone, without the need to take flow samples to gauge water concentrations. The gradient of the ΔP vs. $1-F$ relationship with water in the system appears to differ slightly from the oil only condition for upstream pressure drops, but not enough data is available to generalise the effect. Compare Fig.9.16 for 36NS5(S), $M_{iu} = -0.20$ and $M_{id} = 0.99$, with Fig.9.6, $M_{iu} = -0.42$ and $M_{id} = 1.03$.

In absolute terms, the pressure losses across the hydrocyclone fall with increasing K_i and this is explained in terms of higher apparent system viscosities (μ_a) reducing effective Reynolds numbers. This is illustrated in Fig.4.2 and further discussed in Section 4.2.1 where a basis for predicting μ_a is suggested. The balance of pressure drops to the outlets also tends to change with rising water cut and this is reflected by a shift in $\Delta P_{du} = 0$ to lower splits. Whilst this may be only a few percent change for a geometry like 36NS5(S) (compare Figs. 9.6 and 9.16, $K_i = 0$ and 30% respectively for kero(SG)), with 30DO2(T), for which ΔP_{id} and ΔP_{iu} are closer and less variable against split, $\Delta P_{du} = 0$ falls from $1-F = 55\%$ to 38% as K_i goes from 5 to 40% (kerosine) [123]. This direction of change is opposite to that found earlier for reduction in Re_D by changing oil viscosity and density, and indicates the complexity of the concentration effect on hydrocyclone pressure characteristics.

A correlation between pressure coefficient and Reynolds number incorporating the effect of K_i and $1-F$ is presented in Section 9.4.

9.3 Effect of Water–Oil System Characteristics

9.3.1 Drop Size (see Section 7.3.2 for measurement details)

The effect on K_u/K_i of changing drop size by varying mixing pump speed (only) is shown in Figs. 9.17 and 9.18 for kerosine and kero(63) respectively. Whilst an expected improvement in separation with increasing $\bar{d}_i$ can be

observed, both systems show a tendency for a minimum in K_u/K_i developing which may well reflect the larger drops in the feed dispersion approaching a drop size stability limit for the test hydrocyclones (assuming this is lower than for the feed pipework). At the operating conditions given in the figures, this is very roughly estimated at 250μ, for the kerosine system and 180μ for the narrower distribution of the water–kero(63) dispersion. This is very much larger than the kind of maximum drop sizes found at $(K_u/K_i)_{min}$ in the variable flowrate tests (see Table 8.3), and further work would be needed to reconcile these aspects.

Coalescence effects are evident for the kerosine data, where substantially better separation is found for $K_i = 10\%$ over 5% for the same feed drop size. This indicates the higher droplet densities at $K_i = 10\%$ are resulting in coalescence within the separation zone of the hydrocyclone. In contrast, the superposition of data points for 5 and 10% K_i for kero(63) (with one exception), implies there is a lower but not insignificant rate of coalescence for this system. This has been explained and quantified in Section 8.3.

9.3.2 Physical properties

Testing with different distillate blends and a range of biocides in the water phase has provided variation, although not generally independently, in γ, μ and ρ (see Section 7.2 and Table 7.2 for details of changes). This makes the assessment of the individual influence of these parameters on performance difficult, especially in view of the likely changes in unmeasured interfacial properties (like elasticity), and the differences in drop size between systems. Nevertheless, trends can be identified and some worthwhile generalisations made.

Regarding interfacial tension, the HGO(07) oil was tested for three values of γ, adjusted by addition of biocide. Fig.9.19 shows a steady improvement in separation as γ increases from 0.013 → 0.024 N/m (the highest value representing a biocide–free system) for $K_i = 5\%$ and $Q_i = 40$ ℓ/min. The major part of this change can probably be attributed to the larger feed drop sizes which were generated for higher γ conditions (see Fig.7.10). However, the much higher mixing rate for the biocide–free system (1500 rpm cf. 750 rpm for

the lower γ tests) might well be expected to more than compensate for this effect (although no formal sizing was undertaken for this particular system) and yet lower K_u/K_i values are still found. Similar results are evident for the two kerosine systems, water– kerosine (γ = 0.028 N/m) and water + biocide (200 ppm Panabath) – kerosine(SG) (γ = 0.023 N/m), as shown in Fig.9.1. Whilst differences between the bulk properties of the oils are minor, some uncertainty exists regarding drop sizes for the kerosine(SG) system (believed to be similar to those for kerosine, see Section 7.3.2) and its interfacial stability over the test period (see Appendix B.2.2).

Viscosity is relatively the most variable physical property of oils and accordingly has been changed in the tests by a factor of 8 to try and establish the limits to useful hydrocyclonic dewatering. A generalised plot has been drawn, Fig.9.20, showing expected performance bands for 36NS5(S) at K_i = 5 and 20% as viscosity changes, based on the experimental results for the various water– distillate systems tested. Broadly, the solid curves represents the best separation expected for a comparatively 'clean' water– oil system with drops readily coalescing within the hydrocyclone and the feed dispersion tending to be towards the larger end of the indicated size range, like water– kerosine. The dashed curves represent a more surfactant– rich system with lower γ, a more stable interface and is associated with the smaller feed drop sizes, like the biocide modified test emulsions. Some equivalence can be implied between the former and a well conditioned oil-field brine– crude system, probably containing demulsifying chemicals, and the latter, and a moderately conditioned field system.

Hence, a rough estimate can be made of limiting viscosities for a given targeted water content in the discharged oil stream, see Table 9.3, providing a guide for possible applications. It should be appreciated that the results quoted are for the NS5(S) geometry which represents a design developed using kerosine. Higher viscosity oils may have a different optimal geometry and this is speculated on in Section 9.5.5. The possible effects of other complicating aspects of oil– field brine– crude separation, like the presence of gas, are discussed in Chapter 10.

The trend, as the distillate viscosity increased, was for $\Delta\rho$ and γ to drop, factors which should be allowed for when considering Fig.9.20, as all such changes appear to be detrimental to separation. Whilst variation in μ and γ was clear cut enough to see this experimentally, the effect of $\Delta\rho$ was obscured and can only be inferred from theory. Predicting the combined effect of system characteristics on hydrocyclone performance is attempted using dimensionless analysis in the next section.

		LIMITING VISCOSITY, ν(cSt)	
K_i (%)	TARGET K_u (%)	well conditioned system	moderately conditioned system
5	1	10	5.5
	0.5	7	3.5
20	1	5.5	3
	0.5	4	2.5

Table 9.3 VISCOSITY LIMITS FOR CYCLONIC DEWATERING OF OIL ESTIMATED FROM FIG.9.20

To summarise the effects of changing oil type on overall performance, working from the experimentation reported in terms of K_u/K_i in Figs.9.10 and 9.11 and operating at splits just above $(1-F)_{crit}$ as K_i goes from 5 → 30%, results for kero(63) are found in the following ranges cf. kerosine. K_u is higher, at 0.7 → 4.0% (cf. 0.1 → 0.3%), but K_d lower, at 20 → 50% (cf. 50 → 67%) with oil recovery correspondingly reduced, E_{or} = 0.82 → 0.62 (cf. 0.95 → 0.80), as is overall efficiency, E = 0.72 → 0.56 (cf. 0.94 → 0.78). (Note, flowrates are probably sub-optimal for kerosine).

9.4 Use of Dimensionless Groups

Plotting separation data for splits just above the critical condition for a range of water–oil systems (from Figs. 9.1, 9.2, 9.12) using $Hy(\bar{d})$ (= $\Delta\rho\ \bar{d}_i^2 Q_i/D^3\mu$, see Section 4.2.3. for derivation and further discussion in Section 5.2.4) allows some of the problems in accounting for different water–oil systems with a simple dimensionless parameter to be illustrated (see Fig.9.21). Hydrocylone diameter has not been varied in this instance to help reduce the complexity of interpretation, although scaling on that basis is considered later in this section. A low value of K_i has been used (= 5%) so that coalescence and two component flow effects can be largely disregarded. However, droplet break up (indicated by a trend towards negative gradients for a set of data) clearly affects some results, especially at higher oil viscosities, and this is incompatible with the droplet integrity assumed in the derivation of Hy. Other aspects of uncertainty include whether the flowfield structure has changed substantially with the order of magnitude variation in Re_D resulting from the range of oils tested (Fig.9.22), the representativeness of $\bar{d}_i$ with respect to both dispersion size distributions and test conditions (sizing data being sparse in some areas) and the influence of a variable split. On the positive side, the requirement of Stokesian settling of drops ($Re_p < 1$) is generally fulfilled.

A tentative common curve has been drawn through the data for both the geometries tested in Fig.9.21, which represents the separation expected at optimal splits for operating conditions when K_i is low and feed drop sizes are believed to remain stable through the separating zone of the hydrocyclone. However, without a means of readily identifying when drop break is occurring, this type of plot is of very limited use in predicting the potential performance of the hydrocyclone on an untested water–oil system.

Similar problems are evident in dealing with changes in hydrocyclone size as shown in Fig.9.23, again using $Hy(\bar{d})$ but with nominally the same dispersion so scaling is effectively based on Q_i/D^3 i.e. constant residence time. The implications of the apparent inability to improve separation efficiency as D is reduced and a more practical dimensional basis for scaling geometry size are considered in Section 9.5.4.

The relationship between flowrate and pressure drop is encapsulated in dimensionless form using Reynolds number and pressure drop coefficient (see Section 4.2.1) and is plotted in Fig.9.22, for ΔP_{iu} (the principal pressure let down across the hydrocyclone). A small steady increase in $\bar{C}_{Piu}$ with Re_D is evident for $Re_D > 10^4$, although data for individual oils tends to show slightly steeper curves than the overall trend, especially at low flowrates. A minimum in the plot at $Re_D \triangleq 10^4$ is just discernible and reflects the point below which frictional losses come to dominate over the contribution from centrifugal head to $\bar{C}_{Piu}$ and the hydrocyclone vortex is not fully developed [124]. The curve for 36NS5(S) has been drawn based on a couple of experimental points and by analogy with 35NS7(V) data (exponents for $\Delta P \propto Q^n$ are similar).

Differences in split can be clearly seen to affect $\bar{C}_{Piu}$ in Fig.9.22 through ΔP_{iu} (see Fig.9.6), but this can be largely eliminated by introducing a 'reduced' pressure drop into the coefficient, reflecting ΔP_{iu} at $1-F = 50\%$. Further, if water content is varied to any degree, even greater changes in $\bar{C}_{Piu}$ result (see Fig.4.2). This can be accounted for by using a compensatory apparent viscosity term in the Reynolds number. These manipulations are discussed more fully in Section 4.2.1 and the resulting modified parameters C'_{Piu} and Re'_D defined (equations 4.12 & 4.13 and 4.9 & 4.11 respectively). They are plotted together in Fig.9.24 for a wide ranging set of system and operating variables (with splits generally supra-critical). A similar plot can be made based on ΔP_{id}, although the effect of K_i is smaller (Fig.4.3) and the influence of changing split much greater (Fig.9.6 and Section 4.2.1), see Fig.9.25. Log regression generates the following characterising equations

$$C'_{Piu} = 1.27\ Re'^{0.193}_D \qquad (9.2)$$

$$C'_{Pid} = 0.67\ Re'^{0.233}_D \qquad (9.3)$$

with correlation coefficients $\triangleq 0.95$ and maximum errors of $\lesssim 15\%$ for the indicated operating range, by ignoring points below $Re'_D = 10^4$, where the upturn is imminent, and two points for kerosine with high K_i at $Re'_D = 4.5 \times 10^4$ (implying the μ_a formula, equation 4.11, is only appropriate for characterising less stable interfaces). The curves generated by these equations

have been plotted in the figures. Fig.9.26 gives experimental confirmation that variation in hydrocyclone size can also be effectively accommodated with this type of plot, making it a powerful predictive tool once the curve for a given geometry is established.

It should be noticed that whilst the dimensionless plots of Figs.9.24 and 9.25 are for 35NS7(V), the adjustments for split and concentration have been made largely based on results for 36NS5(S). This reflects a more limited data set for 35NS7(V) regarding K_i and $1-F$ variation and an absence of performance data for 36NS5(S) with HGO(07) (i.e. only a narrow range of Re_D). However, that the two geometries behave similarly is evidenced by the effectiveness of the C_P': Re_D' correlation and is probably primarily a function of their identical outlet sizes and comparable overall length. Nevertheless, the available data set for 35NS7(V) (25 points) has been used to obtain the following relationships

$$\bar{C}_{Piu} = 1.27\ Re_D^{0.20}\ (1-F)^{-0.011}\ \exp(-1.11\ K_i) \qquad (9.4)$$

$$\bar{C}_{Pid} = 0.41\ Re_D^{0.29}\ (1-F)^{0.19}\ \exp(-0.43\ K_i) \qquad (9.5)$$

by excluding the same experimental data points as for the $C_P':Re_D'$ regression. Correlation coefficients of 0.94 and 0.96 with maximum errors of 12% and 20% were found for equations (9.4) and (9.5) respectively.

9.5 Effects of Geometry

Working from the basic cyclone form developed during the preliminary experimentation (Chapter 5) incorporating a swirl chamber (NS4P(T)), further developments of the geometry, coded 'NS' have been tested (Figs.D.7 – D.13) together with a pair of deoiling hydrocyclones, coded 'DO', based on Colman's design [7] but with larger upstream outlets (Figs.D.14 and D.15). Terminology and further background can be found in Appendix D. The majority of tests have been undertaken with water–kerosine dispersions, although geometries 36NS5(S) and 35NS7(V) have also been tried with other water–oil systems. From these results, the influence of changing specific design parameters is speculated on and optimum geometries suggested.

9.5.1 Angular momentum generation

The aspects of design investigated here relate to the size and form of the inlet(s), the diameter and length of the swirl chamber and nature of the contraction into the main conical section.

The swirl number, S, provides a means of condensing some of these geometrical parameters ($S = (2X_i/D).(A/A_i)$) to synthesize a v_θ/v_z ratio representative of the relative degree of spin of the fluid as it enters the cone (at diameter D), as discussed in Section 4.2.4. Whilst the value of a swirl chamber has been demonstrated in Chapter 5, it is not clear to what extent the hydraulic diameter of the hydrocyclone at the level of the inlet(s) can keep being increased and yet be compensated for by a larger inlet area, without detriment to the separation. The limit will probably be set by increased frictional losses between inlet and cone and possibly also the development of unfavourable recirculating flows in the swirl chamber encouraging re-mixing. Experimentally, the only direct comparison between geometries of equal swirl number displaying this kind of variability is shown in Fig.9.27 for 15NS4P(T) ($2X_i/D = 1.68$, $A_i/A = 0.128$; Fig.D.8) and 15NS8(V) ($2X_i/D = 2.15$, $A_i/A = 0.170$; Fig.D.13) where $S \triangleq 13$. Unfortunately, the influence of these differences on separation is probably subordinate to the effect of swirl chamber length (see later). Generally, it is assumed, over this fairly narrow range of $2X_i/D$ and A_i/A, that a similar level of swirl can be achieved in the cone and so the larger inlet at greater radial distance is favoured because of the lower inlet pressure requirement and reduced potential for drop break up. The topic of swirl number optimisation will be treated later in the discussion of optimum geometry in Section 9.5.5.

Regarding the form of the inlets, Fig. 9.28 shows the general improvement in separation for diametrically opposed, circular, tangential, twin inlets over an equivalent area single, tangential inlet with geometry NS4P (Figs.D.5 and D.7)*. This may be a product of an anticipated improvement in vortex symmetry and, indeed, Colman [67] observed a more stable core for twin inlet operation in the

---

* The more extreme advantage shown by 36NS4P(T) over 36NS4P(S) is believed to be in part due to a change in system stability between tests.

development of deoiling geometries whilst Thew et al. [125], in analysing flow residence time for similar hydrocyclones, suggest turbulence levels are generally lessened. However, in going from single to twin inlets, flow is being injected closer to the hydrocyclone wall at the same velocity, increasing S by almost 7%. An improved hydraulic coupling between feed and driven body of liquid in the swirl chamber might also be expected. Consequently shear levels and separation forces at any given position within the hydrocyclone are likely to be higher for the twin inlet version. This may explain its better performance at low flowrates but steeper upturn in K_u/K_i at higher Q_i when separation becomes very close to that for the single inlet form. An approximately 4% higher pressure drop is also required to operate the twin feed geometry.

A single inlet format for the feed is preferred for commercial applications because of the simplicity of manifolding. A number of workers suggest that there is a measurable advantage for an (in)volute, rectangular inlet over the tangential circular type [1, 2, 67, 126]. Dewatering tests with a 360° involute (side ratio D_i:b = 3.3:1) and much shortened swirl chamber geometry (L1 = D_i), 15NS8(V), reveal marginally poorer efficiency than for the twin circular inlets of 15NS4P(T) (L1/D = 1.92), see Fig. 9.27. However, work with deoiler geometries for oily water clean up has found no significant differences in terms of separation or pressure requirement between volute feeds (D_i:b = 3:1) with truncated swirl chambers (analagous to NS8(V)) and the more conventional designs with twin inlets (comparable with DO1(T) and analagous to NS4P(T)), Fig.D.14).

The conclusions to be drawn from this appear to be that well designed volute and twin circular inlets have virtually identical performance characteristics and, hence, that volute injection would be the preferred choice for a single inlet unit. Whilst part of this advantage may be due to the more oblique and gradual entry of the flow into the hydrocyclone through an involute with possibly lower levels of associate turbulence, the rectangular inlet shape, keeping injected flow close to the wall, is also considered significant especially for large inlet areas (Colman [67] suggests D_i:b = 3:1 is a good optimal ratio). The better separation shown by 15NS4P(T) compared with 15NS8(V), for equal vortex finder lengths, is therefore postulated to be largely a product of the reduced swirl chamber length of the latter having a much greater impact on overall hydrocyclone length, L, (or more strictly vortex length, $L-\ell$) and residence time

for the dewatering geometries (L/D goes from 9.4 → 8.1), than for the much greater aspect ratio deoilers (L/D goes from typically 40 → 38 in truncating the swirl chamber).

The contraction linking the swirl chamber to the main cone must also be brought into this discussion. Its primary function is to spin up the flow passing down into the cone with a minimum loss of angular momentum and least flow disturbance. The form of this transition has typically been a frustoconical section with an included angle (θ) of either 90° (NS4P, NS5, NS6) or 20° (DO1, DO2). Whereas the venturi–like lower value may seem preferable from a fluid mechanical view point, Colman's developmental work for light dispersion hydrocyclones [67] showed that separation was marginally better for a 90° construction, even though associated with greater core precession. The amount and nature of recirculation in the swirl chamber fed from the contraction zone seems to be similar, however, based on LDA v_z profiles (compare Fig.6.1 θ = 90°, with Fig.6 from reference [7] θ = 20°). Possibly the most important factor is not the angle but the total length of the contraction/swirl chamber composite – too short and the hydrocyclone capacity falls together with the effective length of the separation zone, too long and angular momentum decay will reduce the potency of the acceleration field in the cone. For an S = 12, 3° cone geometry type with kerosine, a good optimum for this composite length, L_S/D, would appear to be 2 – 3, where L_S = L1 + ((D1 – D)/(2 tan½θ)). Additionally, radiusing of the margins of the contraction (as in NS7(V)) or use of a continuous curve to connect feed and cone (as in NS8(V)) are considered advantageous in reducing the risk of flow separation from the hydrocyclone wall.

9.5.2 Vortex finder and upstream outlet

The diameter of the upstream outlet was not varied for most of the tested geometries from $D_u \triangleq 0.28D$, a value typical of conventional heavy dispersion hydrocyclones [1, 2]. However, with the adaption of the deoiler geometries two larger outlets were tried, D_u = 0.33D and, testing the boundaries of conventional wisdom, 0.50D in, respectively, 30DO1(T) and 30DO2(T) (Figs.D.14 and D.15).

The pressure drop benefits of DO2 over DO1 are evident from Fig.9.4 and yet whilst DO2 shows distinctly poorer separation at K_i = 5% and 1−F = 10%, the margin has diminished when 1−F = 50% (Fig.9.3), and becomes negligible at high K_i and 1−F (Fig.9.29), even though the flowrate in these latter tests is probably unfavourably low for DO2. Indeed $(K_u/K_i)_{min}$ is achieved at considerably higher Q_i in DO2 than DO1, although in combination with a lower turn down ratio, maximum capacity is probably only improved by 25% (based on Table 9.1).

The comparative effectiveness of the 0.50D oil stream outlet supports Bhattacharyya's view [83] that the diameter of the inner or primary mantle (locus of zero vertical velocity) is wider than and increases with D_u and is not, as suggested by Bradley and Pulling [12], a constant ≙ 0.43D representing an upper limit on useful vortex finder diameter.

Recent unpublished work by the author based on a geometry equivalent to 35NS7(V) (i.e. D_u/D = 0.28) except with a larger inlet such that S = 12, has shown only inferior water−oil separation for larger outlets (D_u/D = 0.33 and 0.43). This was evident at splits of both 10% (K_i = 5%) and, to a lesser extent, 50% (K_i = 30%). Testing was only carried out at one flowrate, however, 60 ℓ/min.

The need to protect the upstream discharge from the loss of coarse elements of the dispersion in short circuit flow across the hydrocyclone end wall is demonstrated in Fig.9.30, where a variable projection vortex finder has been tested for the two deoiler based geometries. A limit to the useful length of the projection (ℓ) is indicated by a gradual fall off in performance beyond a critical point, as the effective length of the vortex is reduced so increasing the chances of fine drops being lost with the oil. However, it is evident that separation is more sensitive to undersizing rather than oversizing ℓ. Optimum vortex finder lengths for these and two other dewatering geometries are logged in Table 9.4 based on experimentation at low splits when radial pressure gradients across the end wall are steepest. The table also demonstrates that best characterisation of this optimum length appears to be in relation to the axial extent of the inlet(s) into the hydrocyclone, which the vortex finder should exceed by 0−0.2D. This

allows any space between the inlets and end wall (as in the 'DO' designs) to be accounted for. Flush fitting of inlets against the end wall would in fact be recommended, to avoid erosion problems caused by solids which tend to get entrained in this space [27].

	optimum ℓ (mm)	$\frac{\ell}{h}$	$\frac{\ell-h}{D}$	$\frac{\ell+D_i-h}{D}$	$\ell/L1$
36NS5(S)	20	1.54	0.20	0.56	0.29
35NS7(V)	18	1.13	0.05	0.51	0.51
30DO1(T)	25	1.0	0	0.33	0.24
30DO2(T)	30	1.2	0.17	0.5	0.29

Tested with kerosine, K_i = 5%, 1−F = 10%;
h = D_i for inlets flush with end wall

Table 9.4 CHARACTERISATION OF OPTIMUM VORTEX FINDER LENGTH.

9.5.3 Cone and Downstream Outlet

The NS4P geometry was designed with $D_d \triangleq D_u$ to allow the hydrocyclone to be operated up to quite high splits (50−60%) without unduly constraining the outflow, allowing a flexible response to water levels initially up to 30%. As applications for higher K_i (up to inversion) also became important, larger downstream outlets and smaller cone angles were tried to reduce the tendency for flow reversal, which was believed would facilitate operation at the higher splits. However, assessment of the impact of these modifications at all levels of K_i needs to be considered.

Tests with kerosine were carried out for three D = 25.8mm, single, circular inlet geometries, identical except that NS4P has a 6° cone and D_d/D = 0.27, NS5 has a 3° cone and D_d/D = 0.27, whilst NS6 has a 3° cone and D_d/D = 0.50 plus a cylindrical extension pipe beyond at this same diameter to match the overall length of NS5 (Figs.D.7, D.10 and D.11 respectively). These

changes to the NS4P geometry can be seen to have increased the natural split ($\Delta P_{du} = 0$) of the hydrocyclone from Table 9.5. The effect on hydrocyclone performance is shown in Figs. 9.31 and 9.32. Considering the influence of cone angle first (NS4P and NS5 compared), at lower K_i, and therefore smaller $\bar{d}_i$, the extra length of the 3° cone significantly improves separation efficiency and whilst this margin narrows as K_i and $\bar{d}_i$ increase, the roughly one third lower pressure requirement of NS5 makes this a generally more effective separator regardless of split, although a slightly reduced turn down ratio can be expected (see Table 9.1). Use of the larger downstream outlet diameter (NS6 compared with NS5) only becomes advantageous at higher K_i (> 35%) and split (> 50%) and then principally due to the lower pressure drop.

	$\alpha(°)$	D_d/D	D_d/D_u	1-F (%) at $\Delta P_{du}=0$[1]	Q_i (ℓ/min)
26NS4P(S)	6	0.27	0.96	54	30
26NS5(S)	3	0.27	0.94	57	30
26NS6(S)	3	0.5	1.77	95	30
30DO1(T)	$1\frac{1}{3}$	0.53	1.61	70	45
30DO2(T)	$1\frac{1}{3}$	0.53	1.06	38[2]	45

1 kerosine or kero(SG) with K_i = 30–45%

2 sub–critical split ratio

Table 9.5 EFFECT OF OUTLET SIZE AND CONE ANGLE ON THE 'NATURAL' SPLIT ($\Delta P_{du} = 0$)

Based on recent unpublished work by the author, the contribution of the downstream extension tube only appears significant in bringing overall hydrocyclone length (L) up to 15–16D for this type of geometry (S = 12, 3° cone). This means that if the cone is truncated to create an outlet larger than the standard 0.27D of NS5, as with NS6, there is still sufficient residual swirl in the system to achieve a useful improvement in separation for an extension pipe up to this critical hydrocyclone length, beyond which no further

benefit is evident. Strictly, as all geometries tested had a short section of brass tube (D in length, diameter D_d) linking them to the discharge hose*, the effective overall length of the hydrocyclones should be D longer than quoted values of L used in the text and figures.

Further lengthening of the hydrocyclone by reduction of the cone angle to even more acute levels, as with geometries 30DO1(T) and 30DO2(T) ($\alpha = 1\ ^1/_3°$), does not appear particularly productive for low K_i needs (Fig. 9.3), although swirl numbers are also lower for these designs. However, with their large downstream outlets (D_d = 0.53D), these deoiler based units appear closer to matching the separation achieved by the later 'NS' series geometries for high K_i applications (compare Figs.9.29 and 9.31, but be aware of stability differences Fig.7.4), with a lower pressure requirement.

Curiously, the favoured $1\ ^1/_3°$ cone 'DO' design for these extreme conditions, where the flow split to the downstream exceeds that to the upstream is DO2 (see previous Section 9.5.2), whereas for the 3° cone 'NS' designs, NS6 is the preferred geometry, and yet in terms of D_d/D_u and natural split these two hydrocyclones look very different (see Table 9.5). This implies that the complexities of flow reversal are not easily characterised by simple geometrical ratios or discharge pressures, especially for large outlets and high K_i (see Section 9.2.3).

9.5.4 Hydrocyclone diameter

Three diameters of NS4P(T) were tested, D = 15, 25.8 and 35.6mm, and the separation achieved is shown in Fig.9.5. Plotting against v_i provides reasonable agreement between the curves for the different sized units and some kind of basis for scaling with a given geometry and water–oil system (compare with Fig.9.23). The theoretical expectation of more efficient separation for a particular v_i as D falls is not fulfilled, the assumption being that this has been balanced by increased droplet break up effects reducing the dispersion size.

---

* The point of flow expansion into the discharge hose was considered to be functionally the end of the hydrocyclone (see Section 6.2.1).

This may reflect a stronger influence of viscous shear and wall effects on droplet stability for these smaller hydrocyclones. Even though test dates were not contemporaneous, note system conditions were probably most favourable for separation with D = 15mm (see Fig.7.4), $(K_u/K_i)_{min}$ does not differ significantly between sizes and turn down ratio appears to drop with D (see summary Table 9.6). In addition, if this dependence of separation limits on v_i could be more formally established from further experimentation, it would mean there would be very little pressure advantage in using a smaller unit (relating only to the change in C_p' as Re_D' falls with D), although this is not particularly clear from the table.

	$(K_i/K_i)_{min}$	TURN DOWN, for separation within 0.005 of $(K_u/K_i)_{min}$			$\frac{TDR}{(K_u/K_i)_{min}}$	ΔP_{iu} at Q_{max} (bar)
		Q_{max} (ℓ/min)	Q_{min} (ℓ/min)	TDR		
15NS4P(T)	0.021	10	6.5	1.5	70	3(est.)
26NS4P(T)	0.022	38	24	1.6	70	5.5
36NS4P(T)	0.026	59	30	2.0	76	4

Separation data based on Fig. 9.5

Table 9.6 SUMMARY OF PERFORMANCE FOR VARIOUS SIZES OF GEOMETRY NS4P(T) (KEROSINE, K_i = 5%, 1−F = 50%)

9.5.5 Optimum hydrocyclone geometry

To conclude this section on geometry an overview is presented of what might constitute optimal designs for oil dewatering within the bounds of the test conditions reported on. The criteria by which judgement has been made are primarily maximisation of water removal from the oil but with maintenance of a reasonable operating capacity. Minimisation of reject flows was also an objective layed down at the start of the research, but this only appears to be a very weak function of hydrocyclone design.

For kerosine–like oils, two designs are recommended to cover the range of water levels up to 50% and their dimensions, in terms of the hydrocyclone defining parameters, are presented in Table 9.7.

At low to medium water cuts (K_i < 30%) and related splits ($1-F$ up to 50%) a geometry similar to NS5 is suggested for best separation with supporting evidence in particular coming from Table 9.1, where test results are shown for the greatest variety of hydrocyclones of comparable size using closely similar dispersions. A larger inlet area than used with NS5 has been recommended because of the apparent link between v_i and limiting flowrates plus the benefits of increased capacity, with the swirl number maintained at S = 12 by raising the feed entry radius.

At higher water cuts (K_i = 30–50%) and splits ($1-F \gtrsim 50\%$), performance comparisons between different geometries were made more difficult because of the problems in obtaining reproducible experimental conditions for such K_i values. Nevertheless available test results (see Figs.9.15, 9.29, 9.31) would seem to indicate a hybrid of NS6 and DO2 might be appropriate. Compared with the lower K_i applications, drops will be larger and therefore more easily separable but also more prone to break up. In addition less flow needs to be encouraged to return upstream. Accordingly, spin enhancing features can be toned down from the NS5 type geometry i.e. swirl and cone angle reduced, whilst the downstream outlet is enlarged. A general increase in outlet size is also encapsulated in the recommended design to reduce overall pressure requirements, a modification which does not seem to compromise performance for this less demanding separation task, with split control being effectively achieved by the external valves.

Whilst these two dewatering hydrocyclones have been recommended for different water content ranges, inevitably a degree of overlap occurs in which effective operation can be achieved by the nominally 'out of range' geometry. Such a broad band approach has been adopted for patenting (see Chapter 12) to encompass geometries that will provide an acceptable degree of water from oil removal.

	A_i/A [3]	$2X_i/D$	S	$\frac{\ell - h}{D}$	D_u/D	D_d/D	θ (°)	L1/D	L_S/D	α (°)	L_d/D	L/D
TESTED	0.13→	1.54→	7.2→	-1.7→	0.27→	0.26→	20→	0.7→	1.1→	$1\frac{1}{3}$→	0→	8.1→
RANGE	0.22	2.15	15.0	3.0	0.50	0.53	90	3.4	6.0	6	22	48
Optimum (Low→ Medium K_i)[1]	0.18	2.15	12	0→ 0.2	0.28→ 0.30	0.26			2→3	3		16→17
Optimum (High K_i)[2]	0.18→ 0.21	1.8→ 2.15	9→10	0→ 0.2	0.33→ 0.38	0.45→ 0.50			1→2	2→3		17→20

Blank boxes denote no particular dimensional preference, however, should be compatible with more general parameter to the right.

1. $K_i < 30\%$, $\bar{d}_i < 120\mu$ 2. $K_i = 30-50\%$, $\bar{d}_i \geq 120\mu$

3. favoured inlet type : 360° volute, D_i:b = 2 → 3:1

Table 9.7 OPTIMUM HYDROCYCLONE GEOMETRIES EOR WATER-KEROSINE SEPARATION

For water–oil systems considerably more viscous than kerosine (or with lower γ), little variation in geometry has been tried. However, it does seem that they do not benefit from geometries with high swirl numbers, as indicated by the increasing margin between 36NS5(S) (S = 12) and 35NS7(V) (S = 15) as oils become less tractable (Figs.9.1 and 9.2). Shear levels may be a dominant factor here and perhaps a low swirl number (S = 7–8) but comparatively steep cone angle (α = 4–6°), to compensate for higher rates of swirl decay, could be an appropriate combination.

CHAPTER 10

APPLICATION OF RESULTS FROM LABORATORY STUDY

10.1 Introduction

One of the uncertainties of the research is how representative the laboratory results with water–distillate systems are of the targeted application of hydrocyclone operation with oil–field produced fluids. Whilst it is considered the bulk characteristics of the water and oil components have been effectively modelled, the additional complexity of real oil–field emulsions (e.g. their interfacial chemistry and the presence of non–liquid phases) together with the problem of clearly defining such systems (e.g. water drop size and the nature/frequency of any flow instabilities), makes it difficult to predict hydrocyclone performance in practice. Only field trials can provide unambiguous answers and these are imminent. In the interim, a judgement as to the aptness of the oil dewatering laboratory data is presented, making use of experimental results with gaseous and solid dispersions at the University and tests undertaken at BP Research, Sunbury, with a close simulation of Forties production conditions using live crude.

This chapter also considers the practicalities of how dewatering hydrocyclones might be deployed as production separators.

10.2 Influence of Gas and Solids

It is evident that crude oil at the well–head always contains some gas, either in solution or as a vapour, with its evolution and expansion progressing as pressures fall through the stages of production. In terms of cyclonic separation of the water and oil components, it was therefore apparent that gas might be an important 'contaminant' of the dewatering process, especially as gas bubbles would move inwards and water droplets outwards under the action of the centrifugal field within the hydrocyclone. Accordingly, some experiments injecting free gas

into the feed during dewatering tests have been carried out and although incomplete, provisional results are as follows.

Working with a lower swirl number version of the geometry 35NS7(V) (S = 12 rather than 15, by adjustment of inlet size), at near optimal split and flowrates, the addition of a uniformly dispersed free gas phase (nitrogen) at volumes up to 20% in the feed left the water–kerosine separation virtually unchanged for K_i = 5% whilst for K_i = 30%, K_u/K_i rose steadily from 0.01 to 0.04. Typically the bubbles separated out very rapidly (within the length of the swirl chamber) to create a gas core, before being swept out of the upstream outlet by the axial pressure gradient ($P_d > P_u$) with substantial slip against the liquid phase (mean axial velocity for the gas core is estimated at 5x that of the liquid it displaces). The resulting choking effect pushes flow back downstream, increasing the liquid split ratio. However, tests with larger upstream outlets produced only lower dewatering efficiencies, the difference being more pronounced with gas than without. Even for gas volumes at inlet of 40% (50%–65% in the upstream) the effect on the separation of the water phase was still comparatively small (E_{or} down to 0.87 from 0.94 with no gas), whilst slugging flow with slug frequencies of several hertz, was generally found to be less disruptive than dispersed gas for the same time averaged voidage.

Dissolved gas can be expected to be liberated where the most significant pressure drops occur in the hydrocyclone, namely on entry and close to the core. However, the rate and nature of dissolution are unknown and gas may not even have time to evolve within the hydrocyclone if residence times are short enough.

To summarise, at the simplest level the very presence of gas reduces the throughput of liquid phases, lowering the effective capacity of the separator. However, it seems that so long as gas movement through and evolution within the hydrocyclone are restricted to near the inlet and core, interactions with water drops will be low and good dewatering can still be maintained with virtually 100% of the free gas exiting in the oil stream. The degree of overlap between these two separation zones with regard to the gas phase will be a function of its bubble size and voidage and the tests indicate that, in broad terms, bubbles $\geqslant$ 0.2mm

diameter and volumetric feed gas:oil ratios (GOR) $\lesssim$ 2/3 (or more strictly $\lesssim$2 for the upstream) can be accommodated without undue loss of performance when separating a range of water dispersions and concentrations from oil, most especially at low Ki and 1−F. However, it seems that even for oil−fields designated as having a low GOR, more free gas than liquid is typically present at well−head pressures (see Section 3.1.2). Also if surface chemistry dictates that bubbles collecting at the core remain as a foam rather than collapsing to a free gas phase as in the laboratory tests, it is probable that increased drag effects will reduce axial velocities near the core [128] and thus lower the gas handling capacity of the hydrocyclone. In addition, whilst high frequency slugging appears not to be a problem, longer duration pulses of gas may well destabilise the liquid separation process.

Ideally then, it is desirable to operate the dewatering hydrocyclone with as little gas present as possible. To this end geometries with low pressure drops operating at high feed pressures would be favoured, as dissolved gas break−out and free gas expansion* are comparatively small under such conditions.

Solids constitute a very small fraction of material coming up from the well (see Section 3.1.2), but may act to stabilise water/oil interfaces if particles are sufficiently fine [30]. The dewatering hydrocyclone is certainly capable of efficient solids removal from a single liquid phase, as illustrated for nylon−water in Chapter 5. Using the scaling principles employed there to project water−kerosine separation, removal of the fine quartz sand ($\bar{d}$ = 52μ) found in the Forties oil−line prior to the M.O.L. pumps [129] can be estimated. For 36NS4P(T) running at 45 ℓ/min throughput and 50% split, this gives $\gtrsim$99.2% removal of solids (by mass) to the reject stream, equivalent to a d_{75} of 3.8μ [130]. It is of note that a considerable fraction of solids can get carried through conventional gravity production separators in the oil stream rather than dropping out with the water phase due to oil wetting of the particles. Such 'bonding' is more likely to be overcome in the turbulent conditions and high acceleration field of a hydrocyclone.

---

* A 10 bar pressure drop for a feed pressure of 30 bar would result in a 50% increase in gas volume, but for a feed pressure of 15 bar this increase would be 270% (based on an ideal gas).

Erosion problems will be reduced compared with conventional hydrocyclones as inlet velocities are lower. Nevertheless, use of wear resistant materials for the feed manifold and swirl chamber are recommended to maximise hydrocyclone life (see Section 3.1.5).

10.3 Dewatering Prediction

The problem of M.O.L. pump seal failure on Forties platforms, outlined in Section 3.1.6, prompted BP to build a test facility at their Sunbury Research Centre to enable the mechanical seals to be tested in an environment closely simulating present and possible future operating conditions using mixtures of live Forties crude oil, formation water and sand. The rig is shown in Fig.10.1 and details of its operation can be found in reference [50]. Hydrocyclones can be seen to be integral to the rig, being used to remove impurities from the flush flow to the seals and part of the test programme included the evaluation of one of the author's hydrocyclone geometries (26NS4P(S)). It has therefore been possible to make a comparison between separation achieved from this detailed reconstruction of Forties production conditions and the water–kerosine model of these conditions in the laboratory at Southampton.

Fig.10.2 shows the two sets of results with K_i = 20% plotted for variable flowrate and split. The Sunbury data [130] relates to feed pressures of 20 barg whilst the Southampton work [129] has discharge pressures close to atmospheric. The order of magnitude difference shown in upstream water content between the two systems is probably largely a function of widely differing drop size distributions. The water–kerosine $\bar{d}_i$ of 100μ reflects the finest dispersion which could be generated at this K_i in the laboratory test rig (N = 2000 rpm). Measurements of drop size on the Sunbury simulation showed a range of only 1–5μ, but this degree of dispersiveness may be mostly a product of gas evolution from samples as they were depressurised from rig to atmospheric conditions for analysis. Rough estimates of feed drop size based on performance (K_u/K_i) matched against dimensionless projections of nylon–water separation data for 36NS4P(T) (see Section 5.2.4) indicate $\bar{d}_i$ = 15μ might be more realistic. The smaller drop size, and probably also more stable interfaces, of the Sunbury system allows considerably higher flows to be achieved before separation starts to deteriorate, but pushes up $(1-F)_{crit}/K_i$ to 1.8 compared with 1.3 for kerosine.

The form of the variable split plot for the Forties simulation actually appears closer to that for the kero(63) laboratory system (see Fig.9.11 for 36NS5(S) at K_i = 30%), although the improved separation stability with flowrate characteristic does not appear to apply to the distillate blend (see comments in Section 9.1). However, hydrocyclone pressure drops in the seals rig were accurately reflected in the water–kerosine tests, with due allowance for flow and split differences only, indicating close hydrodynamic similarity between the systems.

So how realistic is the Sunbury simulation? The main doubt concerning its authenticity with regard to separator operation lies in the way the aqueous dispersion was set up. The experimental technique involved adding the appropriate volume of brine to the crude in the closed circuit rig and recirculating the mixture for several hours before taking any measurements. The emulsion so generated is likely to be stable and finely divided. An emulsion entering a production separator, however, will probably have had the bulk of its interfacial area generated only a few seconds (or tens of seconds) earlier at the well–head choke and in combination with the addition of demulsifier chemicals, greater levels of coalescence can be anticipated. Whether dispersion drop sizes will also be larger depends very much on the conditions upstream of the separator, especially the degree of mixing the flow is subject to. Whilst no measurements are available, for the higher operating pressure envisaged for hydrocyclones acting as production separators (and therefore lower choke pressure drops) and with a pre–separator conditioning vessel, (see next section), it is considered drop sizes will be intermediate between the seals rig simulation and the water–kerosine system (N = 2000rpm).

Hence, it seems reasonable to suggest that, assuming gas levels are not significant, the amount of dewatering achieved in a test hydrocyclone with kerosine using the highest mixing pump speed (2000 rpm) should be decreased by 2–3 fold to give a realistic figure for field operation as a Forties production separator (i.e. for a geometry like NS5(S), typical K_u = 0.4 – 1.0% for K_i up to ~30%) with a slightly higher reject flow required than for the distillate model (i.e. ~1.5 – 1.6 K_i). In addition, an increased capacity can be anticipated in terms of flows achieved before substantial drop break up occurs (est. 30% higher) and probably also an improved turn–down ratio.

Regarding the M.O.L. pump seal flush clean up application, presuming the dispersion has already undergone a preliminary separation stage, drop sizes may well be closer to the Sunbury data and separation correspondingly worse (see also comments at the end of the next section).

The characteristics of well–head emulsions have been discussed in broader terms in Section 3.1.2.

10.4 Envisaged Production Separator System Incorporating Hydrocyclones

A possible scenario for the inclusion of dewatering hydrocyclones in a production separator train is shown in Fig.10.3 for a comparatively low gas content field, typical North Sea well–head pressures and a Forties–type emulsion with a 20% water cut.

The system is operated such that wells are only choked to match the one with the lowest discharge pressure, and after manifolding together and addition of chemicals, the flow goes to a small high pressure separator which allows free gas to be removed. This vessel also enables phase instability to be absorbed and a degree of droplet coalescence to occur, conditioning the feed flow to the dewatering hydrocyclones without significant pressure loss. Effective clean up of the process stream is anticipated in a single pass through the parallel operated hydrocyclone units with split control achieved by valves beyond the outlets. For the oil discharged upstream, pressures can now be dropped without any concern for possible mixing effects and the evolved gas is taken out in a low pressure separator. For the reject stream (~30% of the feed flow), with similar volumes of oil and water, uncertainty exists as to whether or not the flow comprises distinct dispersed and continuous liquid phases. Hence, treatment with a 3–phase separator is envisaged, primarily to provide a water stream that suits the operation of deoiling hydrocyclones i.e. $\leq$ 2000 ppm oil. The oil discharged from this medium pressure stage can have several percent water content, as on rejoining the main process stream it constitutes only a small fraction of the flow. A similar argument applies to the upstream flow from the deoiling hydrocyclones.

The staged take–off of gas facilitates its efficient recompression and maximises the yield of oil. However, if the production system links with an oil–line, the final LP separator may not be needed and the comparatively high water/oil separator discharge pressures can be used to reduce the amount of pumping required to bring the oil up to pipeline feed pressures. (In this instance, a small degassing pot for free gas removal may be needed for the upstream discharge from the dewatering hydrocyclones, depending on the gas handling capabilities of the pumps).

In essence then, the use of hydrocyclones as production separators offers a condensed treatment facility which can operate at high pressures so that pre–cyclone sources of shear resulting in drop break up, which mostly occurs at control valves, can be minimised. Whilst it seems necessary to retain some longer residence time tankage in the train, the size of such separating vessels is also small. In its totality, therefore, the oil/water separating equipment is highly compact with estimated space (footprint)/weight requirements of the operational units broken down as indicated in the table below.

	m^2	tonne	
HP separator	8	13	
MP separator	13	24	refer to Fig.10.3
Dewatering hydrocyclones	20	38	
Deoiling hydrocyclones	5	12	

Table 10.1 OPERATIONAL SPACE/WEIGHT REQUIREMENTS FOR OIL/WATER PRODUCTION SEPARATOR TRAIN INCORPORATING HYDROCYCLONES

The size/performance of the separating vessels (HP and MP) have been estimated by analogy with Forties production equipment. The data for the deoiling hydrocyclones reflects the operation of standard BWN Vortoil modules

(4–in–1 *, D = 60mm) which have been widely tested in the field [131, 132]. The size of the dewatering hydrocyclone plant has been based on that of the Vortoil separators with a conservative 30% reduction in space and weight allowed for the shorter length of dewaterers (typically 1/3rd that of deoilers). However, with such large flows to be treated, it would seem more practical to use bigger modules (20–in–1 plus) which would be even more compact. Hydrocyclone performance for crude dewatering has been based on the water–kerosine separation achieved by 36NS5(S) with allowances for field conditions, as quantified at the end of Section 10.3, and size using v_i scaling to maintain separation efficiency, as suggested by results described in Section 9.5.4. Hence, in going from laboratory to field, $K_u \simeq 0.2\%$ (Fig.9.14) becomes 0.4–0.6% and the reject flow rises from ~27% (Fig.9.12) to ~30% of the feed flowrate, which itself is pushed up from 80 (Table 9.1) to 105 ℓ/min for D = 35.6mm, therefore becoming 300 ℓ/min for D = 60mm. Field pressure drops can be estimated, using a non–dimensionalised version of Fig.9.32 at 11 bar for ΔP_{iu} and 8 bar for ΔP_{id} in 60NS5(S). It is noteworthy that the pressure saving in adopting smaller diameter units is marginal using Q_i/D^2 scaling as $\Delta P D^{-0.2}$ = constant, although if the wider swirl chamber/larger inlet area version of NS5 suggested in Section 9.5.5 were adopted, a much reduced pressure requirement would be anticipated.

Whilst water cuts below 20% should be easily handled with the system shown in Fig.10.3, higher water levels may need some additional separator units. Assuming the water phase is still dispersed and increasing drop size compensates for any higher apparent viscosity effects, the dewatering hydrocyclones should still be able to function with a suitable split adjustment (although replacement of internals with a more appropriate geometry may be worthwhile, see Section 9.5.5). However, much higher rejected water flows will probably increase the required size of the 3–phase separator to maintain a low enough oil concentration feed to the deoiling hydrocyclones, which themselves will need extra units to cope with the higher throughput.

---

* This represents the number of hydrocyclone units (internals) which share a common pressure vessel, feed and discharge manifolds.

Staged or series use of hydrocyclones, where the process stream provides the feed for a second unit to enhance dispersion removal, might be an alternative solution to these deoiling problems rather than increasing the size of the 3-phase separator, given that adequate pressure was available. Certainly the control of such a system can be easily automated to continuously optimise performance, as demonstrated by Marsden et al. [133]. However, if required water specifications for the oil product were lower than could be achieved in a single pass through a dewatering hydrocyclone, staged operation for this production separator application would not be practical because of the comparatively large size of the reject streams and importance of oil recovery. The M.O.L. pump seal flush application would be a more appropriate candidate for the sequential use of dewatering hydrocyclones, as abundant feed pressure is available from the pump (typically 50 bar) and reject flows are unimportant.

Comparisons between hydrocyclones and other more conventional water/oil separators have been made in Section 3.1.5, in the context of an offshore production environment.

CHAPTER 11

FUTURE WORK

This is discussed primarily in the context of what can be achieved in a University environment in pursuit of an effective crude oil dewatering hydrocyclone for well-head conditions encompassing a wide range of water cuts. As using large volumes of hot crude in the laboratory is impractical, a close synthesis of such field conditions is an unrealistic target. However, the ambient temperature water-distillate model has proved a useful tool in covering a range of system characteristics and whilst some consolidation of this work is required, further research in two areas can be anticipated. Firstly, an applied approach where the more complex features of true production emulsions, like gas phases and varied water/oil interfacial chemistry, can be introduced and the effects on dewatering performance monitored externally, with particular emphasis on establishing operational limits. Secondly, a more fundamental level of study (which may involve returning to simpler fluid systems) concerned with local internal measurements, to help identify and provide understanding of the processes which control the water-oil separation and how they interact with geometry.

Theoretical concepts can be integrated with this work, which might ultimately provide a numerical model which could predict the performance of a dewatering hydrocyclone. Initially, however, progress is sought in improving the identification of good and bad features of hydrocyclone design in relation to feed characteristics and clarifying similarity criteria and scaling procedures so that laboratory data can be projected to field conditions with a greater degree of confidence. An important priority in this respect is for some field tests with prototype designs, where the production conditions can be closely specified. This would allow the modelling process to be assessed and refined.

More specifically, areas where the research could be developed are as follows:

(i) Characterisation of the feed – measurement and control of water/oil interfacial conditions needs to be improved as surface chemistry has a significant influence on drop stability. Whilst interfacial tension has been periodically measured, this does not provide a complete guide to interfacial behaviour, especially for the impure systems being used. More sophisticated analysis of interface rheology is possible but requires complex instrumentation. An indirect but more practically useful means of indicating interfacial stability, and generally the ease with which an emulsion can be resolved, could be obtained from simple settling tests (analogous to IP methods 19/76, 289/74, 290/73). Part of the uncertainty regarding test repeatability, that due to poor system stability with time, may be overcome by using more refined and tightly specified oils with controlled addition of known amounts of stable surfactants to vary interfacial conditions. Some attempt to mimic oil–field emulsifying agents and the chemicals added to counter their effects might be envisaged.

(ii) Further externally monitored variable feed/operating condition tests – primarily to provide a broader and more detailed set of results from which dimensionless groups for characterising the performance of a particular geometry can be clarified and if necessary modified in the light of (i) and (iv). In particular, work should be undertaken for at least two more oil viscosities to 'fill–in' between previous systems (say 3 an 8 cSt) and generally a more extensive range of flowrates should be tested for a greater variety of dispersion sizes and concentrations.

(iii) Addition of other phases – both solids and gas are present in produced fluids and it is envisaged that they would be introduced separately into the laboratory system to readily identify the effect each might have on the dewatering performance of the hydrocyclone, the separation of the added phases themselves being of secondary importance. Gas is the more significant contaminant because of its ubiquity in either (or both) free or dissolved form and the fact that bubbles will migrate inwards in the hydrocyclone, counter–current to water droplet movement. Work with free gas has already been initiated and should include consideration of slugging flow and use of

photographs to determine how gas moves through the hydrocyclone. Dissolution effects also need characterising.

The critical aspect for solids is probably the extent to which water/oil interfaces are stabilised by their presence. This will be determined by particle size and mineralogy and the effect on dewatering operation should be looked at most carefully where coalescence processes are important i.e. high water concentrations and critical split conditions.

(iv) Internal measurements – greater knowledge of the key processes of drop coalescence and break up in the hydrocyclone are crucial to improving the understanding of its operation and in developing behavioural models. To this end, local non–invasive measurements of flow structure, drop size and concentration gradients would be important.

Using transparent walled test hydrocyclones, LDA can provide high quality time averaged and fluctuating velocities for single phase conditions, with more extensive measurements being allowed by using refractive index matching techniques to eliminate refraction effects where wall geometry is complex. Such data would allow validation of numerical models (similar to those being developed for deoiling hydrocyclones [134]) and provide a basis for assessing the relative importance of steady state and small–scale turbulent shear to drop break up. Certainly inertial effects would be better characterised than by the unsatisfactory assumption of homogeneous isotropic turbulence used in the droplet Weber number parameter. Understanding would be further strengthened if local drop size measurements could be made, to establish local breakage rates. Such sizing is probably only feasible for very diffuse dispersions, and laser diffraction methods would be favoured. When higher dispersion levels are introduced, concentration effects (incorporating coalescence) might be examined experimentally by mapping out areas of phase inversion using conductivity methods, where electrodes are fitted flush with the hydrocyclone wall. In addition, closely spaced pressure tappings along the cone wall could be instructive in identifying axial density gradients. In spite of the interference with the flowfield, some form of invasive measurement using fine optical or conductivity probes may also be helpful.

(v) Geometry – for a given dewatering application, it is considered further developments would only incrementally improve performance of the optimum designs suggested in Section 9.5.5 and that (iv) might be the most instructive aspect of the future work proposed in this regard. However, separation results obtained with a more systematic variation of geometry than has been undertaken so far may be instructive in generating empirical correlations incorporating geometry parameters which can be related to hydrocyclone operation, including changes in oil type. One particular area which may repay investigation is the limit to which the inlet can be pushed out radially (with a compensatory increase in inlet area) and a pressure advantage still be gained for a given throughflow without loss of separation performance. It is envisaged this would include consideration of the nature of the contraction into the main cone as well.

(vi) Engineering of hydrocyclone systems – even though prediction of field operation may be uncertain, staged tests in the laboratory, where either discharge stream is treated by further hydrocyclones, could be usefully carried out to give an indication of the scale of improved separation which might be achieved and an insight into aspects of control. Alternatively, the combination of hydrocyclones with other complimentary separators might be investigated.

CHAPTER 12

CONCLUDING COMMENTS

The complex fluid mechanics of two component liquids moving through a swirling flowfield, in combination with a need to provide hardware solutions to a broadly defined water– oil separation problem, has directed the research into the development of oil dewatering hydrocyclones towards a wide ranging, essentially empirical programme. Hence, whilst theoretical understanding of some of the phenomena encountered is limited, significant practical advances have been made during the course of this work which can be summarised as follows:

(i) The development of experimental methods and instrumentation to allow repeatable, controllable and measurable testing of separators with water– distillate oil mixtures. Notable amongst these is the dynamic drop sizing technique for characterising a dispersion in the feed (or exit) pipework to the separator, catering for stream velocities up to 4m/s, $K \lesssim 30\%$ and $\bar{d} \gtrsim 20\mu$ ($d > 5\mu$). This technique was also extended to provide through– wall images of drops in the hydrocyclone itself, the first known measurements of their kind. The adaption of the Aquasyst on– line water– in– crude content meter for operation at low flows with distillate oils is considered a partial success.

(ii) Use of particle migration data from a solid– liquid analogue to provide reasonable predictions of bulk water– kerosine separation in the same hydrocyclone geometry at low K_i and Q_i using a dimensionless group, $Hy(\bar{d})$.

(iii) A greater understanding of the operation of liquid– liquid hydrocyclone separators where the dense dispersion concentrations vary substantially (5– 40%) and drops are unstable. Integral to this has been the insight gained into the behaviour of 2– phase liquid systems in passing through the hydrocyclone, including apparent viscosity effects and droplet coalescence and break up processes.

Distinctive operational features include the need to run the hydrocyclone close to a critical split ratio for effective dewatering of the oil stream and minimum reject flow, and that this critical split is found to be a simple function of the water content for kerosine $((1-F)_{crit}/K_i \simeq 1.3)$. LDA analyses of axial velocity profiles within the hydrocyclone also show that the external valve control of split used in the tests has little effect on the relative spatial distribution of upward and downward moving regions of flow, acting more to change flux intensities (at least for $1-F = 10-50\%$).

Some progress has been made in relating the peak in dewatering efficiency with increasing flowrate, caused by drop break up, to a critical Weber number for a given hydrocyclone and inlet velocity for a given water–oil system. Certainly, inertial shear effects appear to be the dominant influence.

Feed to outlet pressure drops have been accounted for using modified pressure coefficient: Reynolds number plots which, whilst allowing for changes in oil type, flowrate and hydrocyclone size in the conventional manner, also incorporate factors to include the effect of split and high water concentrations. Useful operational aspects demonstrated are that an approximately constant gradient exists for split against ΔP_{iu} or ΔP_{id} regardless of oil type for a given flowrate ($K_i = 0$) and that a discontinuity occurs in ΔP_{iu} and ΔP_{id} on moving through the critical split condition.

(iv) Hydrocyclone designs have been developed which can provide highly efficient dewatering of light distillate oils at ambient temperatures over a wide range of feed conditions for modest pressure drops. However, with increasing oil viscosity and decreasing drop size (the feed characteristics varied the most during tests) the separation achieved deteriorates, typically reaching $K_u/K_i = 0.5$ at $\nu \simeq 10$ cSt ($\bar{d}_i = 40-80\mu$) or $\bar{d}_i = 10\mu$ ($\nu = 2$ cSt).

Nevertheless, it has been estimated that for oil–field use, such hydrocyclones could match the dewatering performance of Forties production separators but with a 60–70% saving in space and weight on the water/oil treatment facility as a whole.

Improved separation is also evident with these geometries for solid as well as liquid dispersion removal from a liquid compared with commercial hydrocyclone designs used for this purpose on the brine and sand contaminated oil flush flow to the M.O.L. pump seals on Forties platforms.

Finally, the author is pleased to report that stemming directly from this work, patent applications have been filed internationally by BP and BWN Vortoil for oil dewatering cyclone geometries (European PA . No. 0 259 104, U.S. PA. No. 4749490, both 1988) and field tests with engineered versions of these geometries are imminent.

APPENDIX A

NYLON– WATER EXPERIMENTATION

A.1 Test Rig

The basic rig layout, shown in Fig.A.1, disguises a number of stages of rig modification primarily aimed at increasing hydrocyclone test flowrates. The recirculation pump unit was originally a Jabsco 1" (flexible impeller, 0.4 kW drive; maximum $Q_i \simeq 30$ ℓ/min), later changed to a multistage centrifugal Grundfos CP3–100K (2kW drive) with appropriate adjustment of rotameters to accommodate higher throughputs (45 ℓ/min). The essential function of the system – to feed a homogeneous slurry to the test hydrocyclone and monitor its operation – remained unaffected by these changes.

A.2 Operating Procedure

Before running, a low mass concentration of nylon powder (typically 700 mg/ℓ) is set up in the mixing tank with water, which already has dissolved in it 30 mg/ℓ surfactant (dodecylbenzenesulphonic acid) to promote particle wetting and discourage flocculation without excessive foaming. When the pump is switched on, the suspension circulates through the hydrocyclone under test and back to the tank (via Rotameters) where the two submerged discharge flows generate a mixing action. This is supplemented by a hydrocyclone bypass flow when low hydrocyclone throughputs are involved – the minimum total discharge flow required to maintain adequate mixing* (1/2" diameter pipe orifices) for suspension volumes of 20 → 30ℓ was considered to be ~20 ℓ/min. Other ancillary mixing devices were also tried, including a rotary stirrer and an independent circulatory pump, but generally considered an unnecessary addition to the rig.

---

* The quality of the mixing can be checked either qualitatively, by observation of any tendency for sedimentation to occur at the bottom of the tank, or quantitatively, by sizing analysis of the inlet sample.

Sampling, to obtain particle separation data, is usually by whole stream diversion for the hydrocyclone outlet flows and by isokinetic sampler (10% diversion) for the inlet flow, into sample bottles. Whilst whole stream diversion will provide a totally representative sample of the flow at a given moment, to keep sample volumes within acceptable limits sample times must be short (a few seconds) and hence sampling to determine the typical make up of a stream becomes susceptible to small time scale fluctuations in the flow. Strictly, samples should be representative of a particular hydrocyclone operational state and so both the outlet samples are taken simultaneously or as close together as possible. The isokinetic sampler uses an axial, upstream facing, thin-walled sample tube with an external control valve. The valve is opened until the static pressure at the wall of the sample tube falls to that at the wall of the main pipe. Assuming flow is turbulent, this condition indicates that sample stream and pipe flow velocities are the same (isokinetic). Hence, streamlines will be undistorted and (given a homogeneous distribution of the dispersion across the pipe) the sample representative of the flow. Sampling times of tens of seconds are typical.

Sizing of the dispersions in the samples is achieved by taking a few mℓ of an agitated sample for analysis in a Coulter Counter TAII, so that migration probabilities for individual particles can be derived. The Coulter Counter operates by drawing the dispersion (diluted in an electrolyte, Isoton, to an appropriate concentration) from a stirred beaker into a glass tube through a small orifice across which an electrical potential has been applied. When a particle passes through the orifice it increases the resistance of the electrical circuit by an amount which is a function of its size. This change is monitored and with calibration the equivalent spherical volume diameter of the particle is obtained. In practice a 'count' would be registered in one of the 16 possible size bands covering the range of diameters associated with the particular orifice size used. After a few tens of seconds operation a complete size distribution of the sample can be built up.

Particle concentrations are obtained by weighing the sample bottles before and after sampling to get the mass of the sample, then filtering the suspension (through Millipore pre-filters) and after drying, the filtrate weight is evaluated to give the mass concentration of nylon in the sample. It is the filtering process

that limits the inlet solid concentrations which can be practically tested – as a filter cake becomes thicker, the rate of flow through it decreases.

System integrity in a recirculation rig is subject to disruption by the sampling process. Sample volumes extracted from the system to monitor a typical run amounted to 1.5ℓ in total and although, in general, outlet sample sizes were related to discharge stream flowrates (which tended to be inversely linked to their particle concentrations) a lowering of the tank particle concentration, by ~4% per run, could usually be found. As separation efficiencies are monitored in terms of concentration ratios, this aspect of change would be unimportant to subsequent runs except that a net loss of larger particles is also evident. This effect was considered insignificant up to a maximum of four consecutive runs ($\delta\bar{d} < 3\% \bar{d}$). After four runs the suspension was discarded and a new mix set up.

APPENDIX B

WATER–OIL EXPERIMENTATION

B.1 Rig Design and Operation

The principal test rig (L3) was designed to assess the dewatering capabilities of hydrocyclones ($D \simeq 35mm$) for a range of oils (any ρ, $\mu \lesssim 40cP$) at ambient temperatures with K_i up to phase inversion and wide variation in other operating parameters (see Table 7.1). The layout of the rig is shown in Fig. 7.3 and Plate II and its capabilities summarised in Table 7.1. The system functions as follows.

The oil and water are sourced, pressurised and metered separately before being tee–ed together and mixed. The oil is supplied using a multi–stage centrifugal pump (valve controlled flow) to a Fisher 2100 series (viscosity independent up to $\mu = 40cP$) variable area flowmeter or Rotameter. The water is fed from compressed air pressurised cylinders, via control valves set in parallel to give both fine and coarse adjustment, through one of three Rotameters (conventional 2000 series), allowing good flow control and measurement over a wide range. The combined streams then pass through a variable speed turbine pump (N up to 2100 rpm) which provides adjustable mixing of the flow before it enters the test hydrocyclone. Hence, a conditioned feed is set up in which Q_i, K_i and d_i can be independently varied (within certain limits).

Beyond the hydrocyclone, valves are set to control split ratio and apply back–pressure so that any gas core (typically air coming out of solution from the oil) is small or absent. Flow measurement to obtain the split is concentrated on the upstream discharge as it usually comprises a single component flow (>99% oil) facilitating the use of a 2100 series Rotameter. Extreme split ratios ($1-F < 10\%$ or $>85\%$ at maximum Q_i), however, would be evaluated using a measuring cylinder and stop–watch on the smaller discharge stream. The separation effect is also monitored from the upstream because the typically low values of K_u would be lost within the measurement error if downstream water/oil levels were used to evaluate K_u by volume balance (equation 4.3). K_u has

been determined by both flow sampling based methods and on-line using a capacitance meter (Aquasyst). These techniques have been discussed in Section 7.3.1.

The two streams from the hydrocyclone ultimately discharge freely, (at atmospheric pressure) into the dump tank - the starting point for the oil recycle leg of the rig. Some oil and water segregation occurs very rapidly under gravity in the tank and this is taken advantage of by using a floating take-off pipe for the recyle flow. This oil-rich stream is drawn out of the dump tank using a low shear Monopump and fed through a high efficiency Fram coalescer-separator (1μ cartridge) to remove the water (back to the dump tank). The speed of the Monopump is set to give the same flow as the oil feed pump, such that the level of oil in the feed tank remains roughly constant. Hence, oil can be circulated around the rig on a continuous basis, whilst water builds up in the dump tank. When full, testing must be suspended and a period allowed for the water to settle out from the oil before being pumped down the drain. The water cylinders also need refilling from the mains.

Two aspects of the recycled oil need particular consideration - its water content and its temperature:-

The 'dryness' of the oil is monitored qualitatively by ensuring the liquor is clear passing through the oil feed Rotameter (this has been shown to represent around 50 ppm by volume total, presumably dissolved*, water from Karl-Fischer analysis, described in Section 7.3.1). Such a condition is easily achieved for kerosine over the full operational range of the rig. However, for more viscous distillates, some limits on flowrate and mixing are required for the coalescer-separator to work effectively, although low levels of carryover may be acceptable in some tests.

Oil temperatures will usually rise on passage through the test rig (by an amount which will be a function of the operating conditions and ambient temperatures), so a cooling loop circulating cold tap water is installed in the oil

---

* Handbook data suggests a 55 ppm limit for solubility of water in kerosine at 20°C [143].

feed tank to limit this change. Temperatures are recorded throughout the rig using thermocouples and whilst an overall range of inlet temperatures between 17–26°C has been measured, the bulk of testing has been kept within 19–23°C.

Rig pipework is typically 3/4", in either rigid uPVC or, adjacent to the hydrocyclone, reinforced flexible hose. Static pressure tappings, which can be selectively linked to a precision Bourdon gauge, are positioned 1m beyond the hydrocyclone in the outlet streams, where any swirl has largely decayed away, and 0.8m ahead of the inlet manifold. Hence, the pressure drops derived from these readings will incorporate any losses connected with pipework $\leftrightarrow$ hydrocyclone transitions (see Appendix D) as well as across the hydrocyclone itself.

Hydrocyclone orientation for the tests varied between horizontal and vertical (upstream outlet uppermost). However, the maintenance of steady performance through a staged 360° revolution of geometry 15NSP(T) indicates this factor is unimportant.

Test details and monitored operating conditions are manually fed into a computer terminal adjacent to the rig which is connected to the Departmental Cromenco running a "Hydrocyclone Test" program written in BASIC by the author (Section B.5.1). One function of the program is to correct the raw input data where required. Over–reading of the upstream Rotameter due to the presence of water is allowed for based on empirical data (from Fig. B.1). The effect of operating temperature on μ is generated from measured values at two temperatures in the operating range – being closely estimated using the de Guzman–Andrade equation, $\mu = Ae^{B/T}$ (A,B constants and T is °K) [136]. The very small changes in density with temperature are considered to be too small to warrant correction. (See Section 7.2.1 for typical variation in μ and ρ). In addition, the program provides immediate feedback of K_i, $1-F$ and Q_i based on input Q_w, Q_o and Q_u Rotameter readings (corrected as appropriate), facilitating rapid and accurate setting of test conditions. When rig adjustments are complete and all data entered, the program calculates the resulting performance parameters and prints out a complete record of the test.

B.2 Water/Oil Interfacial Characteristics

B.2.1. Interfacial tension measurement

Periodic readings of γ were made using a commercial ring tensiometer and results are summarised in Table B.1. It is evident that for the water/kerosine systems, where 'ex rig' and 'ex feed' samples indicate at least a week of test rig operation behind them, the more representative (and typically more contaminated) samples exhibit a lower value for γ but a less reproducible measurement. For these 'dirtier' samples it was generally more difficult to obtain any kind of reading and they also showed greater variation with interface age. In the context of Table 7.2, a practical standardised form for γ was needed and this has been based on oil (ex rig)/distilled water sample data for a contact time of 5 min, which facilitates the measurement process whilst still appearing to reflect the changes in the interfacial tension if both liquids had been ex rig, albeit at a higher level (typically up by 5–10%, but see later this section). As might be anticipated, the maximum values for γ in the ranges shown are associated with test periods following rig cleaning or inventory renewals.

OIL PHASE	WATER PHASE	γ (N/m $\times 10^{-3}$)	TEMP (°C)	TEST DATE
kerosine (ex barrel)	distilled	39.2 ± 0.2	20	17/2/86
kerosine (ex rig)	distilled	27.8-30.0 ± 0.5	20 - 23	6/80-5/86
kerosine	ex feed cylinders	25.5-28.5 +0 -2	20-23.5	6/80-5/85
HGO(07) (ex rig)	distilled	23.0 +0.5 -1.0	23	7/3/86
	1000ppm Panabath in distilled	12.7 ± 1.0	23	7/3/86
	ex feed cyl. (post flushing)	16.5 + 1.0 -1.5	22	22/4/86

Sampling of oil/water phases contemporaneous with testing; 2 → 7 minute interface age.

Table B.1 INTERFACIAL TENSION MEASUREMENTS USING A RING TENSIOMETER

OIL PHASE	WATER PHASE	γ(N/m $\times 10^{-3}$) AT 25°C, TIME = 0	TIME TRENDS
Kerosine (ex rig 6/86)	distilled	34.4 ± 0.3 (36.1 ± 0.4 at 20°C)	no data
	ex feed cylinders	29.3 ± 0.8	28.4 5min 28.4 15min
kero(63) (ex rig 29/7/86)	distilled	26.5 ± 0.2	no data
	100ppm Phylatol in distilled	23.7 ± 0.1	22.2 5min 21.2 15min
HGO(07) (ex rig 4/86)	distilled	22.5 ± 0.5	no data
	1000ppm Panabath in distilled	13.8 ± 0.2	12.8 5min 12.0 8min 11.3 13min

Tests carried out 4.8.86; pendant water droplet in oil

Table B.2 INTERFACIAL TENSION MEASUREMENTS USING VIDEO IMAGE PROFILE DIGITIZING OF PENDANT DROPS

A second technique for measuring interfacial tension was also tried, on a limited number of samples, in which γ is calculated by video image analysis of the shape of a pendant drop [135]. This is a non-invasive method developed at Southampton University which enables time trends down to a fraction of a second to be studied in a thermostatically controlled environment. It also allowed data to be collected for the first time on the water/kero(63) system, as difficulties in penetrating the oil/water interface with the tensiometer ring had been encountered (similar problems encountered with HGO(07) systems as well). Results are shown in Table B.2.

It is noteworthy that the 5% fall in γ for distilled water/kerosine over a temperature change from 20 to 25°C is of a similar order to the variation in γ shown in Table B.1 over extended time periods. Measurements with pendant drops also confirm that some of the reading uncertainties shown with the ring tensiometer reflect actual changes in sample γ. Short time scale fluctuations (0.01s) of up to ± 5% affected all samples tested, whilst longer term (minutes) downward trends were found on analysis of the less pure systems (including those containing biocide – see following section). This is interpreted as a gradual net migration of surfactant material to the interface (emulsion ageing), superimposed on a rapidly fluctuating movement of material back and forth across the oil/water boundary. It should be emphasized that the 'time = 0' measurement follows a finite period (up to a few tens of seconds) when the drop is generated and equipment aligned, during which some degree of diffusion of material to the interface may have occurred. However, for the ring tensiometer this time interval (between first contact of liquids and completion of measurement) may be several minutes. This may help to account for the higher values of γ obtained by the image analysis technique for kerosine samples, where diffusion rates appear to be appreciably faster than for the more viscous HGO(07) samples, for which there is much closer agreement between the two methods. With regard to the separation process, where interfaces are only a matter of seconds old, the 'time = 0' measurement is probably most representative.

Hence, the standardised ring tensiometer measurement may be quite realistic, the effect of an extended contact time between the liquids being balanced by the use of distilled rather than rig water.

B.2.2 Microbial contamination

Infection of hydrocarbon systems by micro–organisms is an increasingly common problem with paraffinic systems being particularly susceptible [137]. Generally the 'bugs' live in the water phase and feed off the oil and although growth is not possible in dry oil, microbial spores will survive there indefinitely growing when a water phase is present.

The effects of infection are 3-fold:-

(1) physical presence of microbes - can act as surfactants (especially bacteria) or build up as slimes or mats which can block filters, affect the accuracy of flowmeters, obscure transparent sections of rig and interfaces in settled samples

(2) degradation of oil - in aerobic conditions largely by oxidation of the H-C structure and to a lesser extent consumption of essential nutrients (especially S, N and K).

(3) by-products of microbial growth - in particular long chain organic acids which can be corrosive and highly surfactant

Analysis of the rig feed water supply using dip slides showed the presence of microbes in the system, principally aerobic bacteria (up to 10^5 colonies/mℓ, probably Pseudomonas) with some fungal growth as well (probably Cladosporium). Protozoa and nematodes were also identified in a professional analysis by BDH, Poole. On combination with the kerosine, considerable multiplication of microbes occurred, most particularly in the dump tank, where large interfacial areas were present as the dispersion settled out after rig operation.

Whilst the progressive build up in microbes (and their by-products) could be monitored by a slight fall in γ with time, the effect on the experimentation was most evident at high K_i. This is illustrated in Fig.7.4, where periods of hydrocyclone testing using water-kerosine are shown plotted against a water content parameter K_{imax} that represents the limit of K_i above which values of K_u/K_i increase beyond 0.05, for supra-critical split ratios. K_{imax} appeared to be comparatively independent of geometry for a given test period. Hence, although a number of geometries were tested over the periods shown, it was considered that the changes in K_{imax} in the longer term might reflect differences in the onset of phase inversion in the feed. This view was reinforced by observations of changes in the viscous and reflective/refractive qualities of the feed flow roughly coincident with K_{imax}, and by use of simple miscibility checks. This involved jetting a flow sample into a beaker of either clean kerosine or water and seeing whether dilution occurs (continuous phase sample miscible with phase in beaker) or globules develop (continuous phase sample not miscible with phase in beaker).

Whilst the contamination was tolerated for kerosine, with occasional flushing of tanks and pipework and replacement of the oil, the introduction of more viscous blends resulted in a 'bug' population explosion which physically halted effective operation of the rig. Biocide was considered as the best means of controlling the contamination problem, being cheap, specific and continuously acting. The chronology of its application is as follows.

The biocide tried to remedy the heavy contamination built up in the viscous HGO(07) system (3/86) was Panabath M at a dosage of 1000 ppm in the water phase (recommended by Barbara Crouch, BP Sunbury). This broadly acting biocide seemed reasonably effective at killing microbes but had a very substantial effect on the water/oil interface – roughly halving interfacial tension (see Table B.1) and changing the system to such an extent that hydrocyclonic separation became virtually impossible (see Fig.9.19).

On removal of the biocide and introduction of kerosine to the rig again (5/86) a degree of recontamination occurred very rapidly and with the setting up of kero(63) (6/86) a second biocide was tried, Phylatol (recommended by Dr. Robert Sloss, BDH, Poole). This contained no added dispersants and a lower concentration of 100 ppm was used with anticipated action more as a biostat than a biocide i.e. discouraging growth rather than actually killing. However, a discernible lowering of interfacial tension still resulted (see Table B.2) and although hydrocyclone separation efficiency could be adequately analysed, by the end of the test programme microbial contamination seemed to have advanced rather than receded.

For tests with kero(SG) (12/86), 200 ppm Panabath M was added to the water primarily to provide a controlled reduction in γ. This is shown in Table B.3, which illustrates that, whilst a perhaps predictable drop in γ for oil against distilled and against Panabath + distilled aqueous phases occurs over the test period, against rig water γ actually appears to have increased. This suggests most of the biocide has been degraded and, hence, that emulsion stability may not have been maintained very closely. This conclusion is reinforced by some inconsistent drop size data (see Section 7.3.2) and the seemingly unhindered microbial build up in the rig. This casts further doubt on the usefulness of biocides for micro–organism control in this test system.

KERO(SG) +... (ex rig)	pre-tests 26/11/86	post-tests 5/1/87
distilled water	37.5	30
200ppm Panabath in distilled	23	19
rig water (200ppm Panabath)	} 23*	25

Measurements taken before and after the experimental test period using a ring tensiometer, adjusted to 20°C and quoted to nearest 0.5 N/m $\times 10^{-3}$
*Estimated by analogy with Table B.1.

Table B.3 CHANGES IN INTERFACIAL TENSION FOR KERO(SG) SYSTEM

Emphasis is now being placed on microbial control by changes to the rig and its operating procedure to ensure that the chances of water and oil coming into prolonged contact are minimised. This includes replacing the existing water feed cylinders with stainless steel casks, exchanging blind-ended pressure tapping lines with flush-fitting transducers and increasing the number of drainage points in the rig. Regarding operating procedure, the present practice of cycling oil through the main test section after tests to flush the system whilst also cleaning up the oil in the dump tank, to be supplemented by pumping the water bottom from this tank, via a suitable coalescer/separator, to waste at the same time. Hence, the water/oil interface would be eliminated from the dump tank between tests. It is hoped this 'good housekeeping' programme, together with regular changes of oil inventory, will keep the growth of microbes down to an insignificant level in future.

B.3 Water-in-Oil Analysis

B.3.1 Water concentration measurement using the Aquasyst

General aspects of the application of this capacitance based technique to crude oil flows can be found in references [144, 145]. Initial testing in the lab with kerosine was with the prototype MkI Aquasyst (WMC5170Z analyser; EC500Z

cell insert electronics) and standard, low pressure, single probe cell (DC502) manufactured by Endress and Hauser. Changes to the cell geometry (see main text 7.3.1) could only be accommodated with the later available MkII multi–processor system (WMC5250Z analyser, EC501Z cell insert electronics) which together with revision 4.0 software provided the following features:–

1. The ability to self–calibrate the system and allow for changes in cell active and stray capacitance

2. A water content measurement range to 45% with adjustable "look–up" tables for calibration (showing expected changes in dielectric constant over a range of user fixed reference water concentrations and temperatures).

3. Panel adjustable filtering of the signal from the cell.

4. Option of dual cell operation, allowing the possibility of making simultaneous hydrocyclone feed and discharge measurements to give a direct indication of separation efficiency.

5. Self–diagnosis of faults.

Calibration – the cell modifications undertaken altered the active capacitance (C_a) and stray or standing capacitance (C_s) of the unit, effectively the gain and offset. This required the system to be recalibrated and this was achieved by comparing the measured capacitance (C) between two liquids of known 'high' and 'low' dielectric constant (D_k).

$$C = D_k C_a + C_s \qquad (B.1)$$

The liquids used were $CC\ell_4$ (D_k = 2.238 at 20°C) and CS_2 (D_k = 2.641 at 20°C) and for the Southampton cell (coated) C_a = 82.6 pF and C_s = 28.0 pF.

Inputting the calibration curve (as a look–up table) for the effect on D_k (≡ C) of changing water contents was achieved by setting up known concentrations using the feed Rotameters in the rig and bypassing the test section (Fig.7.3). The accuracy of this approach is discussed in Appendix B.4.

The curve for kerosine (Fig. B.2 and Table B.4) indicates a % lower sensitivity to water level changes than predicted by the Endress and Hauser general calibration curve for crudes, which they originally hoped would be independent of oil type. The experimental curve did not appear to have a dependency on the mixing pump speed at the calibration flowrate of 40 ℓ/min (v_{cell} = 3.4 m/s), indicating independence of the drop size distribution reaching the cell.

% H_2O	$\delta D_k \equiv$ 'E' value			
	Endress & Hauser Generalised	kerosine	HGO(07)	HGO(07) + biocide, γ=0.013N/m
1	0.072	0.069	0.071	0.070
2	0.146	0.136	0.146	0.146
3	0.223	0.206	0.223	0.223
4	0.302	0.278	0.302	0.308
5	0.384	0.353	0.384	0.410
7.5	0.600	0.546	0.592*	0.636*
10	0.835	0.752	0.850*	0.907*
15	1.365	1.28	1.47*	1.61*
20	1.988	1.89	2.29*	2.42
25	2.78			
30	3.58			
35	4.68			
40	5.77			
45	7.16			

* these values can be considered as means around which substantial variation has been observed.

Table B.4 AQUASYST LOOK-UP TABLE FOR WATER CONTENT

	<23°C	>23°C
kerosine	0.019	0.011
HGO(07)	0.040	0.025

Coefficients are as % water per °C.

Table B.5 TEMPERATURE COEFFICIENTS FOR AQUASYST

For HGO(07) (Fig.B.3 and Table B.4) a higher sensitivity than expected is observed, although up to 5% water the curve is identical to the general calibration. Reproducing points on the curve from day to day, however, was problematical, especially above 5%. The rapid microbial growth associated with this system may have a bearing on this lack of consistency. Certainly the addition of biocide (1000 ppm Panabath), reducing interfacial tension (Table 7.2) and drop size (Fig.7.10), produces a slightly different curve. A similar direction of change was also found for increased mixing with the straight water– HGO(07) dispersion.

Temperature Effects – the capacitance technique is particularly sensitive to temperature changes and even over the relatively small range resulting from test rig operation, significant Aquasyst reading changes could result if uncorrected. Fig.B.4 shows this effect by recirculating oil through the test rig to generate a temperature rise with the Aquasyst temperature compensation switched off. Both kerosine and HGO(07) show a linear relationship between temperature and reading but with a change of gradient at 23°C (coefficient details given in Table B.5). Whether this is a real capacitance effect or an artifice of the electronics is difficult to judge, but so long as it can be allowed for, the water content reading should be unaffected.

One further characteristic which comes out from Fig.B.4 is the ineffective way temperature is monitored in the Aquasyst for anything but the slowest transients. A resistance thermometer is set in the end wall of the cell and an accurate temperature measurement relies on this block of metal being in thermal equilibrium with the oil. The plot for temperature vs. reading change for HGO(07) has been made using both the Aquasyst sensor and an independent thermocouple which projects into the pipe immediately ahead of the cell and, hence, is considered to reflect flow temperature more accurately. Air temperature was 18.5°C and the rate of temperature increase averaged 0.12°C/min over the test as a whole. Although the two temperature measurements agree fairly closely for small temperature differences between oil and outside, by the end of the run the internal sensor is noticeably under– reading (by ~10% of the oil/air temperature difference). Although this situation is probably worse in the narrower Southampton cell than the standard unit, generally it seems that the operation of the temperature compensation is partly dependent on the air temperature and also the system will not be responsive to short term temperature transients.

Zero Drift – as a matter of course, the Aquasyst would be zeroed on dry recirculating oil before each run, even though any water build up could normally be removed (reading → 0.00%) in the post–run flushing process (clean oil at 60–70ℓ/min for at least 3 mins). However, a progressive shift upwards in dielectric constant for the zero condition is evident on a longer term basis (Fig.B.5). The periods covered in this plot are for when the Aquasyst was in regular use, typically a few hours each day. Dismantling the cell at the end of these test intervals showed water droplets adhering to the central electrode. This implies that there is some stabilising mechanism associated with this long term build up effect, possibly microbial filaments. It is intriguing, however, that the HGO(07) system is affected in a similar way to kerosine, even though the short term build up phenomenon (i.e. during running) was not evident for the former oil.

B.3.2 Drop sizing

The Photographic Process – the initial drop sizing equipment, developed at the time of test rig L2, comprised a camera mounted on a microscope which was focussed into an optical flow cell, back–lit by a fast flash unit [70]. A rectangular flow cell had been used with a very high aspect ratio (27.5:1) to allow a gradual, area retaining transition from 1/2" pipe (taken as a 50% flow 'Y' split off the 3/4" feed pipe) to the 4mm thick optical section. However, only a limited operational range could be covered with this system (see Table 7.1) and, in parallel with the construction of test rig L3, the sizing technique was also modified. The most critical change was the construction of a more robust and compact (3.5 × 10mm working section) optical cell (Fig.B.6) with isokinetic sampling of flow from the 3/4" feed pipework through a 1/4" hose (14% take–off area) of a length (0.6m) so that the cell's position relative to the mixing pump would be equivalent to that of the hydrocyclone inlet (as also with the earlier technique). The 0.3μs Pulse argon spark flash was retained but as a more powerful 2 × 2.5J unit (twin sparks), whilst a more light efficient, wide aperture macro lens system was introduced to magnify the image, instead of the original binocular microscope. The agreement of sizing results from these two methods (see Figs.7.10a and 7.11, pre– and post–1984) confirms the viability of using isokinetic sampling and the self–consistency of the techniques in general.

The complete set up for the revamped system is shown in Plate VI (with some positional details given in Fig.B.6). Working from L → R and background → foreground, the argon metering/control unit (typically 40 mℓ/min at 2 bar) feeds the cylindrical flash unit, fronted by an adjustable condenser lens, which directs the flash onto the flow cell. (Ar shielding gives better spark reproducibility). Beyond this is an Olympus OM2 series 35mm F2 macro lens and autobellows (mag. range × 4.5 → 13) with which the flash is synchronised. The components of the system are mounted on an optical bench to facilitate alignment.

Alignment was achieved by connecting a Mastersix light meter to the camera eyepiece via a fibre optic link so that peak light intensities could be easily recognised with just oil in the cell. The anticipated use of this technique for assessing light levels associated with particular dispersion conditions was not possible, however, as with a water–oil mixture in the cell the flash was absorbed/scattered to a degree that the light meter was not sensitive enough to register.

After some experimentation, Ilford HP5 400ASA emerged as the preferred choice of film to be used, offering a reasonable compromise between speed and definition with straight forward processing. Prints were made on a Kodak, lightweight, high contrast paper (Tristar TP5) using the recommended processing chemicals (Unifix and Dektol). Enlarger magnifications tended to be kept constant at × 6 to give overall droplet magnifications (dependent on the bellows setting on the camera) between × 58 and × 76. An indication of the limits on how much the negative can be blown up before the grain becomes conspicuous can be seen in Plate VII.D, where an original × 58 picture has been brought up to × 76 (to match the other photographs in the plate) by increasing the enlarger magnification to × 7.9.

The most critical aspect of the technique was the focussing of the macro camera system. At the fairly wide operating apertures (f4/f8), the depth of field was only 0.2–0.3mm, so to avoid out–of–focus drops obscuring the in–focus ones the system would first be focussed on the inner wall of the cell window, then the whole camera unit moved in by 0.1mm using the vernier scale on the optical bench. However, play in the adjustment system was of a similar

magnitude to this movement, making it difficult to get the precise positioning required. The siting scratch on the cell window can still be seen in some instances (e.g. Plate VII.A).

During proving tests it was found that a single flash gave a slightly clearer photograph than the synchronised double flash. Investigations using a fast response photodiode linked to a CRO showed that this was because no better than a 0.5μs peak to peak gap could be achieved between the two 0.3μs pulses (even by the manufacturer), effectively giving at best a 0.8μs exposure time. Hence, greater time was available for drop movement during double flash operation (with $\bar{v}_{cell}$ = 3m/s at typical cell flowrates, Q_i = 40–45 ℓmin, a drop travelling at this velocity would move 2.5μ).

Other signs of droplet motion were also evident. In kerosine, for example, picture quality could usually be improved by suddenly stopping the flow (using a valve downstream of cell) and immediately taking a 'static' picture of the dispersion. Fig.7.11 shows that this tends to oversize the dispersion compared with the dynamic case, but trends are useful and the differences get smaller for more stable systems. The 'fuzziness' associated with the dynamic samples may well be related to turbulence, as at $\bar{v}_{cell}$ = 3 m/s Re $\simeq$ 5300 for kerosine, whilst the other oils, which do not appear to be affected to the same extent, have Re $\simeq$ 2800 (critical) for kero(63) and Re $\simeq$ 750 (laminar) for HGO(07). The dispersion for HGO(07) does show an elongation of the larger droplets in the direction of flow, however (Plate VII.B), and this probably reflects the interaction of high wall shear stresses with a low μ_p/μ ratio [96] and relatively high interfacial elasticity (sizing data only taken for HGO(07) systems incorporating biocide).

The Analytical Process – having got a photograph of the dispersion, the next stage is interpretation and analysis. Plate VII shows the range of picture quality obtained, which has been catagorised from 'A' down to 'D'. Generally, the higher the water content or mixing level the poorer the photograph and the dependency is roughly summarised in Fig.B.7.

Automated image analysis seemed an attractive drop size measurement option because of the potential to bypass the photographic element by direct use of video pictures and also the rapidity with which images can be processed. However, to work effectively the dispersed elements have to offer good contrast against their background, not overlap and be evenly illuminated over the whole picture, and difficulties were encountered even with 'A' standard photographs and sophisticated analysers (trials at Winfrith A.E.E. using an IBAS2 system).

A sizing technique is required where the operator chooses what are to be regarded as countable drops, followed by rapid measurement and logging. The system adopted was based round a Zeiss TGZ3 sizer/counter modified to operate with a BBC microcomputer (Plate VIII).

The TGZ3 operates by projecting a disc of intense light onto a screen, over which the photomacrograph is placed. The droplet to be measured is centred over the light disc whose diameter can then be adjusted to exactly match that of the drop. This diameter is registered by depression of a foot pedal which also activates a spiked arm that punches a hole through the drop to show that it has been counted. Before modification, the Zeiss would catagorise the diameter into one of 48 channels, but the addition of a potentionmeter to the diameter adjustment spindle linked through the analogue input port to the BBC allowed drop sizes to be recorded directly on the computer (having first input the magnification factor) with a much greater degree of sensitivity. A file containing individual drop sizes could then be built up and stored on floppy disc for later analysis (see Section B.5.2).

A typical count of 300 (the minimum used with all A and B quality photographs) takes around 30 minutes and measurement accuracies are ± 2.5% for the lower two thirds of the size range and ± 5% above this e.g. for × 76 these ranges are 7* – 240μ and 240 – 365μ respectively. How representative the distribution recorded is of the dispersion in the cell will clearly depend on the extent to which information can be reliably extracted from the photomacrograph. This is a function of picture quality and operator consistency and with reference to Plate VII interpretation was guided as follows:–

---

* 7μ was about the smallest drop diameter which could be effectively measured with this technique.

'A' No significant overlap – all in–focus drops counted. Full size range recorded.

'B' Overlap present – all discernible complete drops counted. Probably losing smaller drops.

'C' Overlap becomes significant – all discernible drops counted including those where only part of outline ($\rangle$ 2/3) evident. Bottom of size range under–represented.

'D' Probably only larger drops evident and then only from ~1/2 their outline – where drop size can be inferred count made.

General exclusions – non–spherical and otherwise distorted drops e.g. those behind larger drops.

As we are concerned with a separation process based on volume efficiency, size distributions have been analysed based on drop volume (α d^3). Hence, the errors introduced by not picking up the smallest drops are generally less than those due to not getting a representative balance for the largest drops. Nevertheless, the poorer picture quality, the greater the tendency to overvalue the mean/median and the more difficult becomes the assessment of distribution shape and spread.

The BASIC program used to analyse the drop size files (Section B.5.3) classifies the drops into 5μ size bands up to 100μ and 10μ bands above this, according to their percentage by volume. The median and geometric standard deviation are then calculated from cumulative volume oversize data, being respectively $\bar{d}$ [= $d_{(50)}$] and σ_g [= $\frac{1}{2}((d_{(84)}/d_{(50)}) + (d_{(50)}/d_{(16)}))$]. This form of dispersion characterisation reflects the tendency for drop sizes to be log normally distributed (see Section 7.3.2), when the median and geometric mean are the same.

B.4 Errors

Under consideration here is the accuracy and repeatability with which the operating parameters for the water–oil tests were measured (refer to Chapter 7 and earlier sections of this Appendix).

Q_i, K_i, $1-F$ (Rotameter based) – 2100 series Rotameters (Q_o, Q_u) were gravimetrically flow calibrated to give a maximum reading error within 2%, and for 2000 series (Q_w) to within 2.5%. For flows registering in the upper 2/3rd of the scale, combining these measurements on a probabilistic basis [138] over typical operating ranges (Table 7.1), the following parameter percentage errors can be obtained:–

Q_i (Q_w+Q_o)	1.5 – 2.0%
K_i (Q_w/Q_i)	3.0 – 4.5% (see also under K_u)
$1-F$ $(1-(Q_u/Q_i))$	25 – 3%

This substantial range in accuracy for split reflects $1-F$ changing between 10 and 85%. To put some perspective on this, the 25% error in accuracy for $1-F$ = 10% reduces to ~5% for repeatability by considering flow stability and scale resolution. (Repeatability for Q_i and K_i would be expected to be within ~1.0–1.5%).

ΔP – the precision Bourdon gauge (0–10 barg) used to record pressures from static pessure tappings around the hydrocyclone was accurate to ± 0.07 bar (manufacturer's calibration). Comparing these readings against dead weight calibrated transducers showed the gauge to be underreading by 0–2% over the pressure range 1 → 5 barg (main operating conditions). Allowing also for the small reduction in reading due to dynamic head effects (a maximum of 0.04 bar), static pressure drops will have maximum errors as illustrated by the following:–

P_i (barg)	$P_{u/d}$(barg)	ΔP (bar)
5	1	4 $^{+\ 0.11}_{-\ 0.02}$
5	4	1 $^{+\ 0.11}_{-\ 0.07}$
2	1	1 $^{+\ 0.08}_{-\ 0.02}$

$\underline{K_u}$ (see Section 7.3.1) – the primary technique used for this measurement was the full stream sampling/settling/measuring cylinder method (FSS/MC). Using measuring cylinders to BS604, scale errors varied between 0.6 and 2% of the rated cylinder volume. Making allowances for decanting and reading errors, for a typical 4ℓ sample, water concentrations up to 0.25% should be accurate (maximum probable error) to ± 0.01%, for 0.25–1.0% to ±0.02%, whilst for K_u > 1% a percentage probable error of ~2% can be expected. Repeatability to within half these values is normal. These results apply to any water–oil system where a clear interface has developed and the oil phase is transparent (i.e. contains no free water). As this was difficult to achieve conveniently with HGO(07), the accuracy achieved by other techniques became of interest.

The isokinetic sampling/Karl–Fischer technique (IS/KF) comprised sampling from the pipeline isokinetically (take–off area 5% that of pipe cross–section) and then to analyse the sample (~0.5ℓ) following the BP interpretation of the Karl Fischer method [Ref.146]. In outline, the procedure starts with the homogenisation of the sample using a high speed mixer (Ultra Turax TP18/10) from which a sub–sample is drawn (~1mℓ) which is then put into the Karl Fischer apparatus (model 602) to be titrated against a pre–calibrated reagent to give a total water mass figure.

Fig.B.8 shows how these two methods compare against Rotameter set water concentrations, the means by which the Aquasyst was calibrated, for HGO(7).

The FSS/MC method required almost 10 days for a reasonable interface to develop at room temperature, but as biocide had not yet been added to the rig this also allowed time for microbial growth to develop and the consistent underreading reflects the resulting 'spoiling' effect. Nevertheless, agreement is good, the difference falling from 3 → 1% as K increases and the water flow is read closer to full scale on the Rotameter.

The IS/KF method shows suprisingly close agreement with the Rotameter data ($\lesssim$ 2% error) for K $\lesssim$ 2%, considering the multiple sampling involved (1 in 500 from 1 in 20). The progressive fall off in reading with increasing K seems to be a product of water drop–out in the primary sample between switching off the

mixer and taking the sub–sample for titration. This method could be improved by the addition of an emulsion stabilising chemical into the primary sample, which would then have to be discarded afterwards.

(Note – tests with kerosine revealed more substantial negative discrepancies, even at low K ($\simeq$ 0.1%). Again these are believed to be a result of being unable to adequately homogenise the primary sample i.e. water is starting to settle out immediately the mixer is switched off and before the sub–sample can be taken).

For the Aquasyst, using the Southampton cell with kerosine over a range of Q_u = 15–60 ℓ/min and K_u = 0.08–0.18% (as determined by FSS/MC), readings taken within 10s of completion of the setting of the hydrocyclone feed conditions (2000 rpm mixing, K_i = 5%) overvalued K_u by between 0.02–0.08%. So, practically, accuracies of up to ± 0.03% are possible allowing for this overshoot and ignoring the error in the reference values of K_u. At higher water concentrations (1–15%) and for stable operation, absolute accuracy is probably limited by that of the Rotameters used in the calibration and is therefore comparable with the accuracy of K_i (repeatability is similar as well). Data are fewer with HGO(07) and although readings are stable with time, up to 5% water, accuracies are estimated to be only ±0.1–0.25%, whilst in the 5–30% range errors can only be kept below 10% by check calibrating at the water contents and mixing levels anticipated for the test, immediately prior to running.

$\underline{d_i}$ – because of the complexity of factors involved in obtaining drop size distributions (Appendix B.3.2) and their dependency on a range of operating parameters, evaluating the accuracy of measurement is very difficult. Generally, $\bar{d}_i$ can probably be repeated to within ±10%, with a tendency to be oversized for the smaller sized distributions (significant numbers of drops $< 7\mu$) and poorer quality photographs (smaller drops more easily 'lost' against the background).

$\underline{\rho,\ \mu,\ \gamma}$ – from density bottle tests, using distilled water as a reference liquid, ρ_o is believed to be accurate to within 0.1% and μ_o, calculated from kinematic viscosity measurements in a u–tube viscometer (BS188/RF) again calibrated with distilled water ($\mu = \nu\rho$), to ~1%; assessment of γ is involved and reference should be made to Section B.2.1 of this Appendix.

Temperature effects, where significant, are discussed in other sections (notably 7.2.1, B.1, B.2.1 and B.3.1).

In conclusion, it should be stated that error estimation for previous work in this area (Chapter 2) has been omitted or at best given only cursory attention.

B.5 Computer Programs

B.5.1 Hydrocyclone water–oil separation test

```
 0 SET 10,3
10 REM Program for recording hcy performance in water-oil separation tests
20 REM No corrections to density for changes in temp.
22 REM Rotameters set as at 27/11/86 (theoretically corrected from KERO set)
25 REM 4.12.86 : version 2
30 DIM G$@80,V$@80,M$@80
34 PRINT : PRINT
35 PRINT"H/C WATER-OIL SEPARATION TESTS: KERO(SG) ONLY (TEMPS 15-25 degC)"
36 PRINT"-------------------------------------------------------------" : PRINT
40 INPUT"FILENAME?  F$
50 OPEN#1,F$
60 REM Pre start up data
70 INPUT"DATE? "D$
80 INPUT"GEOMETRY?  G$
90 INPUT"OPERATING VARIABLES? "V$          !(return) if all const.
110 DEN=792                                !density at 20 deg C
120 VIS=1.58                               !dyn. viscosity at 20 deg C
130 INPUT"WATER TEMP. (deg.C)? "TW
160 INPUT"WASHING PUMP SPEED (rev/min)? "M
170 INPUT"EXPECTED MEAN INLET DROP SIZE (micron)? "DI
180 REM Post start up data
190 PRINT
195 INPUT"UPSTREAM WATER CONC. (%)? "XU
200 INPUT"WATER FEED (l/min)? "QW
210 INPUT"OIL FEED (l/min)? "QO
220 INPUT"OIL TANK TEMP. (deg.c)? "TR
230 TDIF=TR-TW
240 PRINT'"OIL)WATER TEMP. DIFF. (deg.C) =";
250 PRINT USING"##.#",TDIF
260 PRINT
265 INPUT"INLET TEMP. (deg.C)? "TC
275 INPUT"UPSTREAM FLOWRATE (l/min)? "QU
300 JUMP=0
310 REM Correctins & calculations
320 VISC=4.32E-03*EXP(1729/(273+TC))       !viscosity correction for temp
340 DENDF=998-DEN                          !using den. water at 20 deg C
350 QUC=QU*((100-(0.106*XU))/100)          !emp correction to QU for XU
380 QI=QO+QW
390 XI=100*QW/QI
400 F=(1-QUC/QI)*100                       !split to downstream (labelled in text as 1-F)
```

```
410 PRINT"  QI(l/min)     KI(%)      F(%)"
420 !    ##.#          ==.#        ##.#
430 PRINT USING 420,QI,KI,F
440 PRINT
450 REM  Variables correction subroutine
460 ON ESC GOTO 1250                          !disable escape key
470 PRINT : PRINT"IF ANY VALUE INCORRECT PRESS (ESCAPE), ;
480 INPUT"IF ALL CORRECT PRESS (RETURN)";C$
490 IF JUMP=1 THEN 300
500 PRINT : ESC                               !enable escape key
510 INPUT"INLET,DOWNSTREAM,UPSTREAM,PRESSURE (barg)? "P,PD,PU
520 INPUT"MASHING PUMP SUCTION PRESSURE (barg)? "PM
530 INPUT"OTHER MEASUREMENTS/COMMENTS? "M$
540 PID=P-PD
550 PIU=P-PU
560 PDU=PD-PU
570 PIM=P-PM
580 REM Efficiency calcs.
590 EU1=KU/KI                                 !upstream conc. ratio
600 EU2=1-(KU/KI)                             !oil stream quality
610 EU3=(100-F)*(100-KU)/(100-KI)/100         !oil recovery
620 KD=KI*100/F-((100-F)/F*KU)
630 ED1=KD/KI                                 !downstream conc. ratio
640 ED2=1-(100-KD)/(100-KI)                   !water stream quality
650 ED3=F/100*KD/KI                           !water recovery
660 N=(100-F)*(KI-KU)/(KI*(100-KI))           !overall efficiency
670 REM Evaluation of dimensionless constants
680 IF LEFT$(G$,2)="36"THEN(D=0.0356 : DIN=0.0129)
682 IF LEFT$(G$,5)="26NS4"THEN(D=0.0258 : DIN=9.3E-03)
684 IF LEFT$(G$,5)="26NS5"THEN(D=0.0258 : DIN=9.3E-03)
686 IF LEFT$(G$,5)="26NS6"THEN(D=0.0258 : DIN=9.3E-03)
688 IF LEFT$(G$,5)="35NS7"THEN(D=0.035 : DIN=0.0128)
690 IF LEFT$(G$,4)="30D0"THEN(D=0.03 : DIN=0.0141)
700 VI=QI/DIN^2*2.11E-05
710 DENAV=KI*10+(1-KI/100)*DEN
720 RE=VI*D*DEN*1000/VISC                     !Reynolds No. (using DEN  )
725 HY=QI*DENDF*DI^2/D^3/VISC*1.666E-14       !Hydrocyclone number (using mean d)
730 CPIU=200000*PIU/DENAV/VI^2                !inlet to u/s pressure coeff. (using DENAV)
740 CPID=200000*PID/DENAV/VI^2                !inlet to d/s pressure coeff. (using DENAV)
750 REM Print to file
760 PRINT#1,F$,,D$
770 PRINT#1,'G$,,"KEROSINE S.G. + 200ppm PANABATH (IFT=0.023N/m)"
780 PRINT#1,'V$
790 PRINT#1
800 !DENSITY DIFF.= ### Kg/m^3  OIL VISCOSITY = ##.## cP[##.##]      OP.TEMP. = ##.# deg.C
810 PRINT#1,USING 800;DENDF,VISC,VIS,TC
820 PRINT#1
830 !QI = ##.# l/min      KI = ##.# %       F = ##.# %
840 ![QW=##.## QO=##.#]                     [QU=##.##]
850 PRINT#1,USING 830;QI,KI,F
860 PRINT#1,USING 840;QW,QO,QU
870 !MEAN DI = ###.= micron      MASHING PUMP SPEED = ==== rpm
880 PRINT#1
890 PRINT#1,USING 870;DI,M
895 PRINT#1
900 PRINT#1,"PRESSURE DROPS (PXY=PX-PY),bar"
910 PRINT#1,"       PIU            PID            PDU"
920 !       #.##           #.##          ##.##
930 PRINT#1,USING 920;PIU,PID,PDU : PRINT#1
940 !UPSTREAM CONC. RATIO = #.####     OVERALL EFFICIENCY = #.###
950 PRINT#1,USING 940;EU1,N : PRINT#1
960 PRINT#1,"COMMENTS: "M$
970 PRINT#1
980 PRINT#1,'"PERFORMANCE: "
```

```
 990 !         KU = ##.### %    KD = ##.## %  ( KD/KI = ##.## )
1000 PRINT#1,USING 990,KU,KD,ED1
1010 !   OIL STREAM QUALITY #.###         WATER STREAM QUALITY #.###
1020 !      OIL RECOVERY #.###               WATER RECOVERY #.###
1030 PRINT#1,USING 1010,EU2,ED2
1040 PRINT#1,USING 1020,EU3,ED3
1050 PRINT#1,"TEMPERATURES:"
1060 !   INLET TEMP.= ##.# deg.C
1070 !   WATER CYL. = ##.# deg.C       OIL TANK = ##.# deg.C        T.DIFF = ##.# deg.C
1080 PRINT#1,USING 1060,TC
1090 PRINT#1,USING 1070,TW,TR,TDIF
1100 PRINT#1,"PRESSURES:"
1110 !   PI = #.## barg     PRESSURE RISE THRU MIXING PUMP = ##.## bar
1120 !   [PD=#.## PU=#.##]  [PSUC=#.##]
1130 PRINT#1,USING 1110,P,PIM
1140 PRINT#1,USING 1120,PD,PU,PM
1150 PRINT#1,"DIM. CONSTANTS:"
1160 !   RE = #######        HY = #.#######
1165 !   [VI = #.## m/s]
1170 !   CPIU = ##.#        CPID = ##.#
1180 PRINT#1,USING 1160,RE,HY
1185 PRINT#1,USING 1165,VI
1190 PRINT#1,USING 1170,CPIU,CPID
1200 CLOSE#1
1210 OPEN#0,"LP:"
1220 TYPE F$
1230 CLOSE#0
1240 END
1250 REM Variables correction subroutine
1260 JUMP=1
1270 PRINT'"ENTER CORRECTED VALUES OR PRESS (RETURN) IF NO CHANGE"
1280 INPUT"WATER FEED (l/min)? "QW
1290 INPUT"OIL FEED (l/min)? "QO
1300 INPUT"UPSTREAM FLOWRATE (l/min)? "QU
1310 GOTO 490
```

B.5.2 Drop size logging from Zeiss TGZ3

```
    1 CLOSE£0
    5 CNT=0
    7 CLS
   10PRINT:PRINT"DATA LOGGING PROGRAM FOR ZEISS TGZ3        (28/7/86,I.C. SMYTH,U
NIV SO'TON)"
   15PRINT"_____.":PRINT
   20PRINT"(for settings lin/E; calibration based on ch.1/2 to ch.47/48 ADVAL3/1
6 values 4054 to 15.....stop to stop values 4095 to 3)"
   25 PRINT:PRINT"Hit SPACE BAR to record onto disc":PRINT:PRINT"750 drops max":
PRINT:PRINT"DO NOT USE CH.48 & AVOID CH.32-47 TO MINIMISE ERROR"
   30PRINT:PRINT:PRINT
   40 DIM AVE(750),A(750)
   50 INPUT"PHOTO NUMBER/FILENAME?"P$
   60 INPUT"MAGNIFICATION x"MAG
   62 PRINT"Are you resuming an OLD file OR starting a NEW file?"
   66 INPUT"(1=NEW 2=OLD)  "X
   68 ON X GOTO 5000,6000
   70 DEF PROCSAMPLE
   75 CLOSE£0
   77 PRINT:PRINT"Ready to count (to exit press ESCAPE)"
   80 FOR K=1 TO 750-CNT
   90 AV=0
  100 REPEAT
```

```
  110 IF INKEY(-99) THEN 500
  120 UNTIL ADVAL(1)DIV16>2000:REM DEPRESSION OF FOOTPEDAL
  125 REM 10 SAMPLES (1 EVERY 10 SAMPLING INTERVALS) TO AV. OUT ELECTRICAL FLUCT
UATIONS
  130 FOR I=1 TO 10
  150 AV=AV+ADVAL(3)DIV16
  160 FOR L=1 TO 10
  170 NEXT L
  180 NEXT I
  190 REM DROP SIZE IN MICRONS
  195 AV=AV-150:REM "MIN" OFFSET
  200 IF ADVAL(2)>20000 THEN AVE=9.05-AV*.0002095 ELSE AVE=27.16-AV*.0006289:REM
 TEST FOR RED OR STD RANGE &CONVERSION TO MM
  210 AVE(K)=INT(AVE*1000/MAG+.5)
  220 PRINT "SIZE(MICRONS)="AVE(K)
  230 PRINT
  260 VDU7
  265 FOR J=1 TO 30
  266 NEXT J
  270 IF ADVAL(1)DIV16>2000 THEN 260:REM LOOP TO ENSURE ONE MEASUREMENT PER DEPR
ESSION OF FOOTPEDAL
  280 NEXT K
  290 ENDPROC
  500 IF X=1 THEN 5020 ELSE 6030
 1000 CLOSE£0
 5000 REM NEW DATA
 5010 PROCSAMPLE
 5020 PROCDUMFL
 5030 PROCREADFL
 5040 PROCFILLARR
 5050 PROCARRTFL
 5060 PROCDRONFL
 5070 PROCSAMPLE
 6000 REM OLD FILE
 6010 PROCDRONFL
 6020 PROCSAMPLE
 6030 PROCREADFL
 6040 PROCFILLARR
 6050 PROCARRTFL
 6060 PROCDRONFL
 6070 PROCSAMPLE
10000 CLOSE£0
10010 DEF PROCDUMFL
10020 X=OPENOUT P$
10030 FOR I=1 TO 750
10040 A=-1
10050 PRINT£X,A
10060 NEXT I
10070 CLOSE£X
10080 ENDPROC
10090 DEF PROCREADFL
10100 X=OPENIN P$
10110 FOR J=1 TO 750
10120 INPUT£X,B
10130 A(J)=B
10140 NEXTJ
10150 CLOSE£X
10160 ENDPROC
10170 REM
10180 DEF PROCFILLARR
10190 I=0:J=0:P=0
10200 REPEAT
10210 I=I+1
10220 IF A(I)=-1 GOTO 10230 ELSE 10260
10230 FOR J=1 TO (K-1)
10240 A(I+(J-1))=AVE(J)
10250 NEXT J
10260 REM
10270 UNTIL J=K
10280 ENDPROC
10290 DEF PROCARRTFL
10300 X=OPENOUT P$
```

```
10310 FOR I=1 TO 750
10320 PRINT£X,A(I)
10330 NEXTI
10340 CLOSE£X
10350 ENDPROC
10360 DEF PROCDRONFL
10370 X=OPENIN P$
10380 CNT=0
10390 REPEAT
10400 CNT=CNT+1
10410 INPUT£X,Y
10415 IF Y=-1 GOTO 10430
10420 PRINT Y
10430 UNTIL Y=-1
10440 CLOSE£X
10450 CNT = CNT-1
10460 PRINT"DROP COUNT ON FILE= " CNT
10470 PRINT "FILENAME:"P$
10490 ENDPROC
```

B.5.3 Drop size analysis

```
 10 CLOSE£0
 20 REM Program to classify and analyse drop size data
 30 PRINT"**** DROP SIZE CLASSIFICATION AND ANALYSIS PROGRAM NO.2 ****":PRINT"
    (25.11.86 ICS)":PRINT
 40 PRINT"(48 classes; DMAX=380 microns)":PRINT
 50 DIM X(50),A(50),W(50),Y(50),C(50),D(50),G(50),F(50),H(50)
 60 LET B=0 : P=0 : Q=0 : S=0 : T=0 : QH=0 : QL=0
 70 INPUT"PHOTO NUMBER?"P$
 80 INPUT"DATE?"Z$
 90 INPUT"SYSTEM TYPE?"K$
100 INPUT"TEMPERATURE (deg.C)?"T$
110 INPUT"H/C INLET FLOWRATE (l/min)?"Q$
120 INPUT"WATER CONC. (%)?"C$
130 INPUT"MASHING PUMP SPEED (r.p.m.)?"M$
140 INPUT"MAGNIFICATION?x"MG$
150 INPUT"PHOTO QUALITY?"PQ$
160 INPUT"FLOW?"CL$
170 REM Classify data from drop size file
180 DMIN=1000:DMAX=0
190 Y=OPENIN P$
200 REPEAT
210 INPUT£Y,X
220 IF X=-1 THEN 340
230 PRINTX
240 IF X<DMIN THEN DMIN=X
250 IF X>DMAX THEN DMAX=X
260 IF X/5<=20 THEN 270 ELSE 300
270 XA=X/5
280 XB=XA+.9
290 GOTO 320
300 XA=X/10
310 XB=XA+10.95
320 XC=INT(XB)
330 Y(XC)=Y(XC)+1
340 UNTIL X=-1
350 CLOSE£Y
360 REM Input boundary conditions
370 FOR I=1 TO 49 : READ W(I) : NEXT I
380 FOR I=1 TO 48 : S=S+Y(I) : NEXT I :REMtotal number drops counted
390 FOR I=1 TO 48 : D(I)=(W(I)+W(I+1))/2 : NEXT I :REM mid-points in microns
400 FOR I=1 TO 48 : C(I)=D(I)^3 : NEXT I :REMmid-points cubed
410 FOR I=1 TO 48 : F(I)=C(I)*Y(I) : NEXT I :REM frequency by volume
```

```
  420 FOR I=1 TO 48 : T=T+F(I) : NEXT I :REM total volume of drops
  430 FOR I=1 TO 48 : G(I)=F(I)/T : NEXT I :REM volume fraction
  440 FOR I=1 TO 48 : H(I)=G(I)+H(I-1) : NEXT I :REM cummulative vol fraction
  450 REM Calculation of volumetric median (geometric mean)
  460 FOR I=1 TO 48
  470  IF H(I)=0.5 THEN 500
  480  IF H(I)<0.5 AND H(I+1)>0.5 THEN 510
  490 NEXT I
  500 Q=W(I+1) : GOTO 520
  510 Q=((0.5-H(I))/(H(I+1)-H(I))*(W(I+2)-W(I+1)))+W(I+1)
  520 REM Geometric standard deviation
  530 FOR I=1 TO 48
  540 IF H(I)=0.8413 THEN 570
  550 IF H(I)<0.8413 AND H(I+1)>0.8413 THEN 580
  560 NEXT I
  570 QH=W(I+1):GOTO 590
  580 QH=((0.8413-H(I))/(H(I+1)-H(I))*(W(I+2)-W(I+1)))+W(I+1)
  590 FOR I=1 TO 48
  600 IF H(I)=0.1587 THEN 630
  610 IF H(I)<0.1587 AND H(I+1)>0.1587 THEN 640
  620 NEXT I
  630 QL=W(I+1):GOTO 650
  640 QL=((0.1587-H(I))/(H(I+1)-H(I))*(W(I+2)-W(I+1)))+W(I+1)
  650 R=((QH/Q)+(Q/QL))/2
  660 REM Calculation of volume moment mean & variance
  670 FOR I=1 TO 48 : B=B+F(I)*D(I)/T : NEXT I
  680 FOR I=1 TO 48 : P=P+F(I)*((D(I)-B)^2)/T : NEXT I
  690 REM Creation of vol % undersize file readable by SCIGRAF plotting program
  700 INPUT"DO YOU WANT TO CREATE A SCIGRAF FILE?(Y/N)"SC$
  710 IF SC$="N" GOTO 820
  720 I=48
  730 SG$="S"
  740 PSG$=P$+SG$
  750 X=OPENOUT PSG$
  760 PRINT£X,I
  770 FOR J=1 TO 48
  780 PRINT£X,H(J),W(J+1)
  790 NEXT J
  800 CLOSE£X
  810 PRINT:PRINT"SCIGRAF FILE CREATED  "PSG$:PRINT
  820 REM Print to VDU/local printer
  830 INPUT"DO YOU WANT PRINTER ON (Y/N)?"D$
  840 IF D$="N" GOTO 860
  850 VDU2
  860 PRINT"PHOTO NUMBER "P$,"      DATE "Z$;SPC(7);K$:PRINT
  870 PRINT"WATER CONC (%) "C$;SPC(23);
  880 @%=&304
  890 PRINT"DROP COUNT"S
  900 PRINT"WASHING PUMP SPEED (rpm) "M$"       SIZE PARAMETERS (microns):"
  910 PRINT"H/C INLET FLOW (l/min) "Q$;SPC(17);"DMAX "DMAX;"    DMIN "DMIN
  920 @%=&20107
  930 PRINT"TEMPERATURE (degC) "T$;SPC(16);"MEDIAN "Q;
  940 @%=&20204:PRINT"  GEO SD "R;" ("QH/Q;"/"Q/QL")":@%=&20107
  950 PRINT"MAG x "MG$;SPC(4);"PHOTO QUALITY "PQ$;SPC(10);"MEAN "B"    STD DEV "
SQR(P)
  960 PRINT"3.5X10 CELL/FLOW  "CL$
  970 PRINT : PRINT
  980 PRINT"CHANNEL NO";SPC(3);"MID-PT DIA";SPC(3);"   COUNT  ";SPC(3);"% DIFF V
OL";SPC(3);" DIAMETER ";SPC(3);" % CUM VOL"
  990 PRINT;SPC(13);"(microns)";SPC(31);"(microns)"
 1000 PRINT
 1010 FOR I=1 TO 48
 1020 @%=&205
 1030 PRINT I;SPC(8);
 1040 @%=&20107
 1050 PRINT D(I);SPC(6);
 1060  @%=&306
 1070 PRINT Y(I);SPC(7);
 1080 @%=&20208
 1090 PRINT G(I)*100;SPC(5);
```

```
1100 @%=&306
1110 PRINT W(I+1);SPC(7);
1120 @%=&20208
1130 PRINT H(I)*100
1140 @%=10
1150  IF H(I)>0.99999 GOTO 1210
1160 NEXT I
1170 REM Class boundaries (1)
1180 DATA 0,5,10,15,20,25,30,35,40,45,50,55,60,65,70,75,80,85,90,95,100
1190 DATA 110,120,130,140,150,160,170,180,190,200,210,220,230,240,250
1200 DATA 260,270,280,290,300,310,320,330,340,350,360,370,380
1210 VDU3
1220 END
```

APPENDIX C

INTERNAL FLOW MEASUREMENT – THE LDA SYSTEM

C.1 Test Rig

This comprises a tap water recirculating system (total capacity including reservoir ~250ℓ) pumping a constant 23(±1) ℓ/min through the test hydrocyclone (36NS4P(T)). Valves, positioned well away from the hydrocyclone outlets so as not to interact with any residual swirl in the discharge flows, were used to control split and eliminate any air core by raising back pressures, with flowrates being metered in the inlet and downstream outlet pipes. The hydrocyclone is mounted along a movable bench so that it can be longitudinally positioned with respect to the LDA system, which is mounted at right angles to the hydrocyclone axis on a milling machine bed, allowing the measuring volume to be accurately traversed across the hydrocyclone.

C.2 LDA System

The optical arrangement adopted for the flow measurements in the hydrocyclone is a forward scatter, reference beam format shown in Fig C.1 making use of a medium powered laser. The principle of operation is outlined in the main text (Section 6.1), but more specifically, when light from the laser (frequency f_o) is scattered by a moving particle in the water the frequency of light scattered at an angle α to the main beam is given by

$$f' = f_o + \frac{2\, n_{aw}\, v\, \sin(\alpha/2)}{\lambda} \qquad (C.1)$$

where

n_{aw} – refractive index of air to water (1.332)

λ – wavelength of incident beam
(He–Ne laser = 0.6328μ)

v — velocity component of the particle which bisects the angle between the incident and scattered light beams and is in their plane; taken to be representative of the fluid velocity (see later)

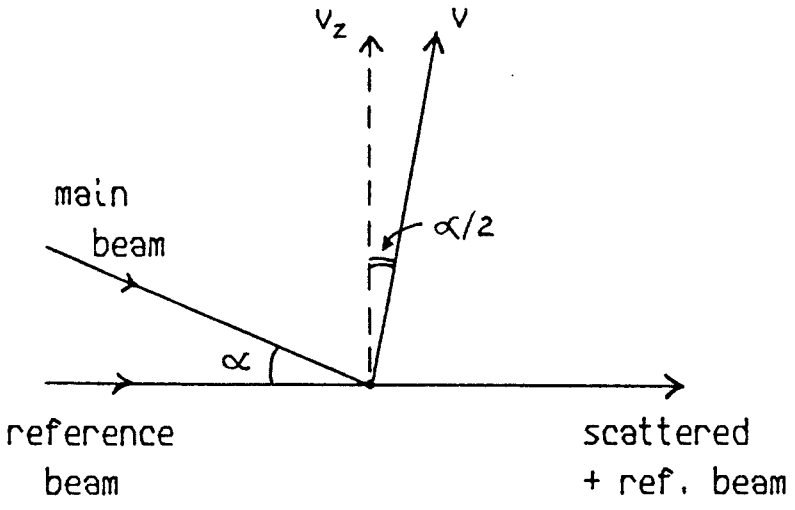

As the LDA is being used in this instance, the reference beam is positioned perpendicular to the hydrocyclone axis to facilitate alignment. This means that

$$v = v_z \cos(\alpha/2) + v_r \sin(\alpha/2) \qquad (C.2)$$

and as $\alpha/2$ is small (typically 6–6.5°) and v_r tends to be much small than v_z in hydrocyclones, the radial component can be assumed to be near zero and the axial velocity calculated accordingly.

The frequency of the scattered light is too high ($\sim 10^{15}$ Hz) to be detected directly by conventional means and so it is combined with a reference beam, usually split off from the main beam, to define a measuring volume and generate a beat frequency (f_b) which can be picked up by the photomultiplier (typically kHz/MHz range). If the reference beam frequency is the same as that of the main beam, then f_o is eliminated in the heterodyning process such that

$$f_b = \frac{2n_{aw}\, v_z \sin(\alpha/2) \cos(\alpha/2)}{\lambda} \qquad (C.3)$$

However, this gives no indication of whether velocities are positive or negative and as the hydrocyclone is known to have axial flow reversals, the reference beam needs to be frequency shifted to allow the direction of the flow to be determined and facilitate the measurement of low velocities (which generate signals that would otherwise be liable to be masked by noise). This was achieved by focussing the main beam onto a rotating Perspex disc whose surface had been rolled with plasticene to produce a scattering effect. Some of this light can then be used as a reference beam which will have a frequency shift f_1, defined by the scattering angle (β) and the velocity component of the spinning disc parallel to the flow direction. The beat frequency of the light collected by the photomultiplier now becomes

$$f_b = \left| f_1 \pm \frac{2n_{aw}\, v_z\, \sin(\alpha/2)\, \cos(\alpha/2)}{\lambda} \right| \qquad (C.4)$$

This signal is processed using a frequency tracking filter which presents a voltage output (proportional to the beat frequency) to a digital voltmeter from which time averaged (10s period) components of the voltage can be determined. Knowing the frequency/voltage calibration for the system and using equation C.4, these can be converted to axial velocities with the aid of a computer program.

C.3 Scattering Particles

These are naturally present in the process water as particles of calcium carbonate with diameters mostly in the range 0.5 – 1.0μ [88]. However, improved signal to noise ratio was achieved by supplementary seeding of the flow with talc at ~10 ppm (vol.) , as recommended by Loader [86]. Calculations show that the particles follow the movements of the water flow very closely.

C.4 Evaluating 'α' and Measuring Volume Position

Both the beam intersection angle, α , (required in the calculation of v_z) and the position of the measuring volume are affected by refraction at the hydrocyclone wall. When traversing the LDA optics across the hydrocyclone, the

strong signal produced by the inner wall surface is distinctive and from there unit movement of the optical bench (AB) can be converted to an effective movement of the measuring volume within the hydrocyclone (XY) by trignometric considerations, in which α is also evaluated. This is illustrated in Fig. C.2 and detailed below for the two wall geometries encountered:–

Cylindrical section.

$$\tan \alpha = \frac{XZ}{XY} \quad \text{and} \quad \tan \beta = \frac{AC}{AB}$$

now

$$AC = XZ$$

$$\therefore \quad \frac{XY}{AB} = \frac{\tan\beta}{\tan\alpha}$$

but

$$\frac{\sin\beta}{\sin\alpha} = n_{aw} \qquad \text{i.e.} \quad \alpha = \sin^{-1}\left[\frac{\sin\beta}{n_{aw}}\right]$$

$$\therefore \quad \frac{XY}{AB} = \frac{(n_{aw}^2 - \sin^2\beta)^{\frac{1}{2}}}{\cos\beta} \qquad (C.5)$$

Conical Section (cylindrical outside wall).

$$\frac{XT}{\sin\gamma} = \frac{ST}{\sin\delta} \quad \text{and} \quad \frac{XW}{\sin\epsilon} = \frac{XT}{\sin\Omega}$$

$$\therefore \quad XW = \frac{\sin\epsilon \sin\gamma}{\sin\Omega \sin\delta} . ST$$

now $$ST = AB \tan\beta$$

$$\therefore \quad \frac{XW}{AB} = \frac{\sin\epsilon \sin\gamma}{\sin\Omega \sin\delta} . \tan\beta$$

as $$\frac{XW}{\sin\alpha} = \frac{XZ}{\sin(180-\Omega)} \quad \text{and} \quad \frac{XY}{XZ} = \cos(\Omega-\alpha)$$

$$XY = \frac{\cos(\Omega-\alpha) \sin\Omega}{\sin\alpha} . XW$$

$$\therefore \quad \frac{XY}{AB} = \frac{\cos(\Omega-\alpha)\sin\epsilon\ \sin\gamma}{\sin\alpha\ \sin\delta} \cdot \tan\beta \qquad (C.6)$$

where

$$\varphi = \sin^{-1}\left[\frac{\sin\beta}{n_{aw}}\right]$$

$$\gamma = \varphi + 90$$

$$\delta = 180 - \theta - \gamma$$

$$\epsilon = \cos^{-1}\left[\frac{n_{aw}}{n_{ap}} \cdot \sin(\varphi+\theta)\right]$$

$$\Omega = 90 - \epsilon - \theta$$

$$\alpha = \Omega - \left[\sin^{-1}\left[\frac{n_{ap}}{n_{aw}} \cdot \sin\theta\right]\right]$$

and θ, β, n_{aw} and n_{ap} (air/Perspex refractive index) are known in these tests, XY is very closely approximated by XZ (to within 0.3%) i.e. the traverse across the cone can be considered to be effectively horizontal, although small off-axis adjustments to the receiving optics were required.

In future work, use of a refractive index matching 'bath' is envisaged to eliminate refraction problems [139, 140].

C.5 Errors

The assessment of the overall accuracy of the v_z measurements, ~10% too low by comparison with discharge flowrates in Section 6.2, should be viewed in the context of poor combined stability and flow metering errors of ±6% for Q_u

and between ±6% → 20% for Q_d, generating probable errors of 8 → 19% in the split ratio $(1-F = 50 \rightarrow 10\%)$..

Regarding the LDA set up itself – the assumption that $v_z >> v_r$ has already been alluded to in Section C.2. The alignment of the optical system was problematical with the refraction effects encountered and as a result the signal to noise ratio was low making effective tracking (and hence averaging) of the turbulence broadened signal difficult in some instances. One element of bias introduced into the measurement results is from the steep velocity gradients encountered across the measuring volume. Assuming the scattering particle distribution is homogeneous, more particles will pass through an area of high velocity within the measuring volume per unit time than a slower moving area, increasing the signal strength relating to this component, causing the average produced by the voltmeter to be weighted on the high side. Similarly, if particle concentrations occur in a slower moving portion of the measuring volume, e.g. the wall boundary layer, the bias could be reversed. Measurement of α is believed to be accurate to within 30'.

A more general discussion of the workings and applications of LDA systems can be found in Durst et al. [141] or Drain [142], whilst fuller consideration of this particular system is given by Blackmore [88].

APPENDIX D

HYDROCYCLONE GEOMETRY

All designs tested were constructed essentially of Perspex modules, although the end wall was brass in some instances, with hydrodynamically smooth internal surfaces. Vortex finders were in brass and of adjustable length for most units with wall thicknesses between 0.033 – 0.06D. Feed pipework always reduced in area to that of the inlet through smooth contractions (included angle $< 30°$) with the inlet dimensions maintained for at least a length D prior to entry. Similarly outlet fittings extend beyond the defined length of the hydrocyclone (L) by D at each end prior to abrupt expansion into the discharge hoses (the significance of this is commented on in Section 6.2.1). Plate IX illustrates some of these points.

The hydrocyclone coding used, e.g. 35NS7(V), can be subdivided into three parts. The first two digits indicate the size of the unit (in terms of D to the nearest mm), the middle section denotes the geometry type (i.e. NS7), whilst the bracketed letter indicates the inlet format (in this case a volute type; S and T represent single and twin tangential inlets respectively).

The test geometries used are shown and defined in Figs.D.1 – D.15 and the terms of definition are illustrated on the following page. With the exception of the more complex early designs, dewatering geometries can generally be specified in terms of parameters D, D_i (and b if necessary, plus inlet type and number), D_u, ℓ, L1, D1, θ, α, D_d and L, with length/diameter values commonly non–dimensionalised by reference to D.

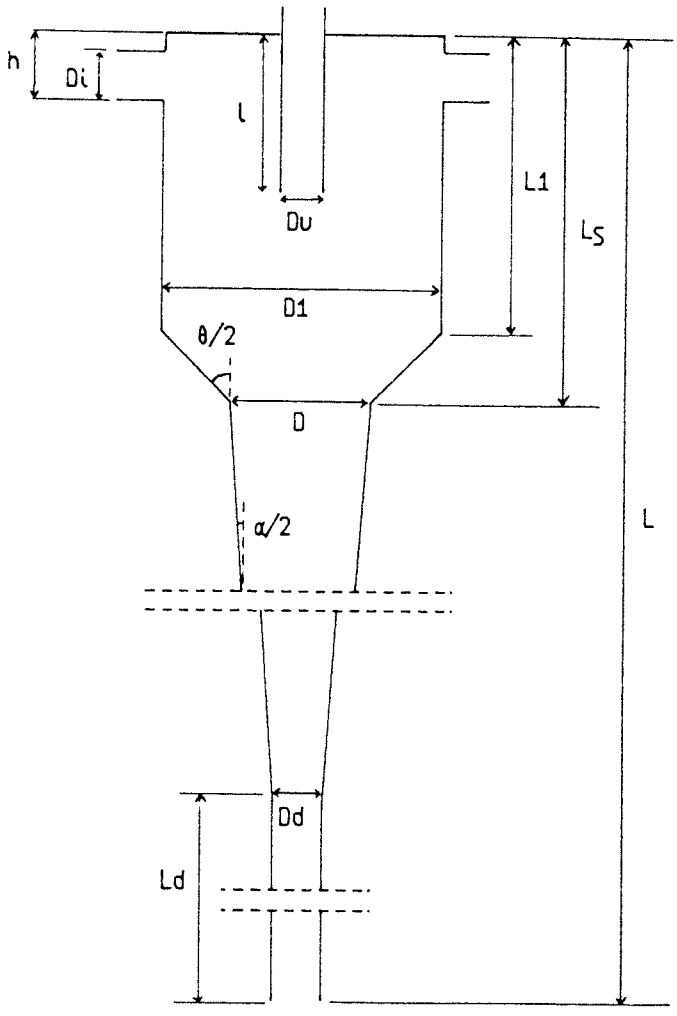

INLET TYPE:

tang = tangential entry

volute = inward spiral of entry channel a distance 'b' over 360°

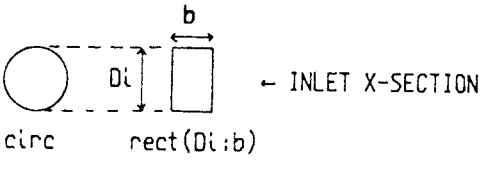

SWIRL NUMBER:

$$S = \frac{\pi D Xi}{2Ai}$$

Xi = distance of the tangential component of the inlet centre line from the h/c axis

Ai = inlet area

REFERENCES

1. BRADLEY, D. "The Hydrocyclone". Pergamon Press, 1965.

2. SVAROVSKY, L. "Hydrocyclones". Holt, Rinehart and Winston, 1984.

3. DEBENHAM, P.S. "The Hydrocyclonic Separation of Water Droplets from a Light Oil". BSc. Project Report, Dept. of Mech. Engg., Univ. of Southampton, 1979.

4. BOHNET, M. "Separation of Two Liquids in the Hydrocyclone". Chemi-Ing-Techn., 41, No.5 and 6, 381-387, 1969, (in German). English translation available through ASLIB (U.K.).

5. BURRILL, K.A. and WOODS, D.R. "Separation of Two Immiscible Liquids in a Hydrocyclone". Ind. Engg. Chem. Process Des. Develop., 9, No.4, 544-552, 1970.

6. COLMAN, D.A., THEW, M.T. and CORNEY, D.R. "Hydrocyclones for Oil-Water Separation". Paper 11, Proc. Int. Conf. on Hydrocyclones, Cambridge, Oct. 1980. Pub. BHRA, Cranfield, 1980.

7. COLMAN, D.A. and THEW, M.T. "The Concept of Hydrocyclones for the Separation of Light Dispersions". Paper F2, 2nd Int. Conf. on Hydrocyclones, Bath, Sept 1984. Pub. BHRA, Cranfield, 1984.

8. COLMAN, D.A. and THEW, M.T. "Correlation of Separation Results From Light Dispersion Hydrocyclones". Chem. Eng. Res. Des., 61, 233-240, July 1983.

9. HITCHON, J.W. "Cyclones as Liquid-Liquid Contactor Separators" Report No.CE/R-277, U.K. A.E.R.E., 1959.

10. BRADLEY, D. "The Hydraulic Cyclone as a Liquid-Liquid Contactor and Separator". Report No. CE/M177, U.K. A.E.R.E., 1956.

11. JOHNSON, R.A., GIBSON, W.E. and LIBBY, D.R. "Performance of Liquid–Liquid Hydrocyclones". Ind. Eng. Chem. Fundam., 15, No.2, 110–115, 1976.

12. BRADLEY, D. and PULLING, D.J. "Flow Patterns in the Hydraulic Cyclone and their Interpretation in Terms of Performance". Trans. Inst. Chem. Engrs., 37, 35–45, 1959.

13. LISTEWNIK, J. "Some Factors Influencing the Performance of Deoiling Hydrocyclones for Marine Applications". Paper E3, 2nd Int. Conf. on Hydrocyclones, Bath, Sept. 1984. Pub. BHRA, Cranfield, 1984.

14. BEDNARSKI, S. and LISTEWNIK, J. "Hydrocyclones for Simultaneous Removal of Oil and Solid Particles from Ships' Oily Waters". Paper G2, 3rd Int. Conf. on Hydrocyclones, Oxford, Sept. 1987. Pub. Elsevier, 1987.

15. LYNN, N.F. "The Removal of Sea Water and Solid Contamination from Distillate Fuels: A Preliminary Evaluation of Hydrocyclones". Naval Ship Research and Development Centre, Bethesda (U.S.), Report 28–616, Sept. 1973.

16. OKLAHOMA STATE UNIVERSITY. "Hydrocyclones for Separating an Immiscible Heavy Phase From a Light Phase Liquid". U.S. Patent 3784009, 8.1.74.

17. OKLAHOMA STATE UNIVERSITY. "Hydrocyclone for Simultaneously Separating Immiscible Heavy Liquids and Solids from a Lighter Liquid". U.S. Patent 3776385, 4.12.73.

18. REGEHR, H.U., "The Use of the Hydrocyclone for Separation", Forsch. Ing.–Wes., 28, 11–27, 1962 (in German). English translation, Dpt. Mech. Engg., Univ. Southampton, 1968.

19. SHENG, H.P., WELKER, J.R. and SLIEPCEVICH, C.M. "Liquid–Liquid Separations in a Conventional Hydrocyclone". Can. J. Chem. Engg., 52, 487–491, August 1974.

20. TEPE, J.B. and WOODS, W.K. "Design of an Ether–Water Contacting System". Report No. AECD–2864, U.S. Atomic Energy Commission, Jan. 1943.

21. SIMKIN, D.J. and OLNEY, R.B. "Phase Separation and Mass Transfer in a Liquid–Liquid Cyclone". A.I. Ch.E.J., 2 (4), 545–551, 1956.

22. TERNOVSKII, I.G. and KUTEPOV, A.M. "The Possibility of Separating Water–Petroleum Emulsions in Hydrocyclones". Izv. Vyssh. Uchelon. Zaved, Neft Gaz, 1979, 22 (3), 25–30, (in Russian). English translation; Report No. ME/80/23, Dept. of Mech. Engg., Univ. of Southampton, Dec. 1980.

23. ADELSHIN, A.B. and IVANOV, N.V. "Dehydration of Crude Oil by Use of Hydrocyclones". Neft Khoz, No.8, 45–47, Aug. 1976 (in Russian).

24. VAN ROSSUM, J.J. "Separation of Emulsions in a Cyclone". Chpt. 9 in "Cyclones in Industry", Ed. Rietema, K., Elsevier, 1961.

25. McGARRY, P. and FLAVELL, R.E. "New Solutions for Offshore Problems". Special Issue of Effluent and Water Treatment J. (U.K.), "Insight", 17–22, Sept. 1978.

26. STOCKWELL, A., GRAHAM, D.E., and CAIRNS, R.J.R. "Crude Oil Emulsion Dehydration Studies". Int. Conf. of Oceanology, Brighton, March 1980.

27. BP PET. DEV. Production Data (Forties), Dyce, 1981.

28. BANSAL, V.K. and SHAH, D.O. "Microemulsion and Tertiary Oil Recovery". Ch.7, 149–173, in "Microemulsions – Theory and Practice". Price, L.M. (Ed.), Academic Press, 1977.

29. JACKSON, G.F. et al. "Oil Content in Produced Brine On Ten Louisiana Production Platforms", Reports EPA–600/2–81–209, U.S. Environmental Protection Agency, Cincinnati, Sept., 1981.

30. MONSON, L.T. "Chemical Resolution of Petroleum Emulsions". Ch.4 in "Surface Operations in Petroleum Production", Chilingar G.V. and Beeson, C.M. (Eds.), Elsevier, New York, 1969.

31. HADFIELD, D. "Hydrocyclones in Offshore Oil–Water Separation Systems", B.Sc. Project Report, Dpt. of Mech. Engg., Univ. of Southampton, May 1985.

32. HADFIELD, D. Private Communication, BWN Vortoil, Gloucester, 1988.

33. GEIGER, K. Private Communication, Shell Expro, London, 1988.

34. WATERMAN, L.C. and PETTEFER, R.L. "Oil Field Emulsions and Their Electrical Resolution". Ch.3 in "Surface Operations in Petroleum Production", Chilingar, G.V. and Beeson, C.M. (Eds.), Elsevier, New York, 1969.

35. BROWN, C.E. et al. "The Influence of Interfacial Properties on Immiscible Displacement Behaviour". "European Symposium on Enhanced Oil Recovery", Brown, J. (Ed.), 19–37. Pub. Inst. Offshore Engg., Heriot–Watt. Univ., Edinburgh, 1979.

36. BRITISH PETROLEUM CO. LTD. "Our Industry Petroleum", 5th Ed., BP Co. Ltd., 1977.

37. BP TRADING LTD. "Forties Export Crude", Brief Technical Appraisal, March 1976.

38. BROWN, C.E. et al., "Crude Oil/Water Interfacial Properties – Emulsion Stability and Immiscible Displacement". BP Internal Symp. "Enhanced Oil Recovery by Displacement with Saline Solutions", Brittanic Ho., London, 1977.

39. CARNE, M. Private Communication. Shell Expro. London, 1988.

40. NEBRENSKY, J.R., MORGAN, G.E. and OSWALD, B.J. "Cyclone for Gas/Oil Separation". Paper 12, Int. Conf. on Hydrocyclones, Cambridge, Oct. 1980. Pub. BHRA, Cranfield, 1980.

41. DAVIES, E.E. and WATSON, P. "Miniaturised Separators for Offshore Platforms". Ch.8 (and Discussion) from Proc. W. Scotland Inst. of Petr. and Norwegian Petr. Inst. Conf., "North Sea Development – Experience and Challenge", Glasgow, Feb. 1979. Pub. Heyden, 1979.

42. CAVILL, H. "The Outlook for Crude Oil and Energy Prices". Chem. Engr., 14, Jan. 1987.

43. VERGHESE, J. "Platform Topsides Design Routes to Weight and Cost Reduction". I. Chem. E. Meeting of SONG Group. "Offshore Facilities: Opportunities for the Future", Aberdeen, Dec. 1987.

44. HEAD, J. and RUMLEY, J. "Design of Production Facilities for Floating Offshore Platforms". Chem. Engr., 17–21, Jan. 1987.

45. VEKRIS, E., CUNNINGHAM, J. and HODGKIESS, T. "Topsides Weight/Space Savings on Offshore Platforms Optimisation of Process Equipment and Supply Systems". Report ME–86–03, Glasgow Marine Technology Centre, 1986.

46. VAN DER VELDEN, J. Private Communication, Shell Expro, London, 1988.

47. BRADFIELD, D. "Fibre Coalescers for Deoiling Water". I. Chem. E. 2nd SONG Research Forum, "Process Intensification", Nottingham Univ., April 1987.

48. DAVIES, E.E. "Compact Separators for Offshore Production". Proc. Symp. "New Technologies for the Exploration and Exploitation of Oil and Gas Resources", Luxembourg, Dec. 1984, 1, 621–629. Pub. Graham and Trotman, London, 1985.

49. THEW, M.T. "Hydrocyclone Redesign for Liquid–Liquid Separation". Chem. Engr., 17–23, July/Aug. 1986.

50. HARRISON, D. and WATKINS, R. "Evaluation of Forties Main Oil Line Pump Seals". Paper A1, Proc. 10th Int. Conf. on Fluid Sealing, Innsbruck, April 1984. Pub. BHRA, Cranfield, 1984.

51. WALLACE, H. "Crude Oil Dehydration: A Look at Methods and Costs". World Oil, 73–75, Nov. 1979.

52. GREATOREX, R. "Some Aspects of Impurities in Fuel Oils". Ch.21 from "Mechanisms of Corrosion by Fuel Impurities", Int. Conf., Marchwood Engg. Labs. (UK), May 1963, Johnson, J.R. and Littler D.J. (Eds.).

53. ZEMEL, B. "Separator Hydraulics – I. Tracer Response Studies Can Pinpoint Separator Problems". Oil and Gas J., 75, No.52, 53–56, Dec. 19, 1977.

54. VENTRIGLIO, D.R. et al. "Water and Particulate Contamination From Distillate Fuels: Preliminary Evaluation of Hydrocyclones". U.S. Naval Ship R. & D. Centre Report 28–508, June 1973.

55. LYNN, N.F. "Removal of Sea Water from Distillate Fuels by Centrifugation – Part II". U.S. Naval Ship R. & D. Centre Report 28–516, April 1973.

56. ABDUL'MANOV, KH. A. and VAGABOV, I.I. "Hydrocyclone for Separating Oil and Liquid Ammonia". Kholod. Tekh., Tr. Resp. Nauchn. Konf. Sekts. Kholod. Ustanovok, 72, 61–64 (In Russian). Len. Tekh. Ins. Kholod. Prom–st., Leningrad, 1971.

57. LEWIS, J. Private Communication, Unilever Research, Dec. 1983.

58. NAPIER–MUNN, T. Private Communication, De Beers Research, South Africa, Sept. 1984.

59. TENGBERGEN, H.J. and RIETEMA, K. "Efficiency of Phase Separations". Ch.2 from "Cyclones in Industry", Rietema, K. and Verver, C.G. (Eds.), Elsevier, 1961.

60. ISHII, M. and ZUBER, N. "Drag Coefficient and Relative Velocity in Bubbly, Droplet or Particulate Flows". AIChE J., 25, No.5, 843–855, Sept. 1979.

61. BARNEA, E. and MIZRAHI, J. "Separation Mechanisms of Liquid–Liquid Dispersions in a Deep Layer Gravity Settler: Part III". Trans. IChE, 53, 75–82, 1975.

62. GRAIFER, V.I., LAZAREV, G.A. and LEONT'EV, M.I. "Effect of Various Factors on the Viscosity of Crude Oil and Water Emulsions". Int. Chem. Engg., 15, No.2, 274–277, April 1975.

63. DEALY, J.M. "Viscometers for Online Measurement and Control". Chem. Eng., 91, Part 20, 62–70.

64. THOMPSON, D.G., TAYLOR, A.S. and GRAHAM, D.E. "Emulsification and Demulsification Related to Crude Oil Production". Symp. "The Formation of Liquid–Liquid Dispersions – Chemical and Engineering Aspects", 56–65, I.Chem.E. (London and S.E.), London, Feb. 1984. Chameleon Press.

65. BEDEAUX, D. "The Effective Viscosity for a Suspension of Spheres". J. Colloid & Interface Science, 118, No.1, 80–86, July 1987.

66. ABRAHAMSON, J. and ALLEN, R.W.K. "The Efficiency of Conventional Return Flow Cyclones at High Temperatures". Proc. Symp. "Gas Cleaning at High Temperatures". Univ. Surrey, Guildford, Sept. 1986. I.Chem. E. Series No.99, 31–43, 1986.

67. COLMAN, D.A. "The Hydrocyclone for Separating Light Dispersions". Ph.D. Thesis, Dept. of Mech. Engg., Univ. of Southampton, Feb. 1981.

68. SMYTH, I.C. et al. "Small Scale Experiments on Hydrocyclones for Dewatering Light Oils". Paper 14, Proc. Int. Conf. on Hydrocyclones, Cambridge, Oct. 1980. Pub. BHRA, Cranfield, 1980.

69. HEYWOOD, H. "Uniform and Non–Uniform Motion of Particles in Fluids". Al–8, 3rd Congr. Europ. Fed. Chem. Engg., London, 1962.

70. SMYTH, I.C., "The Development and Performance Analysis of Hydrocyclones for Removing Water Dispersed in Oil". Report ME/82/17, Dpt. Mech. Engg., University of Southampton, Jan. 1983.

71. SHILOH, K., SIDEMAN, S. and RESNICK, W. "Coalescence and Break Up in Dilute Poly–Dispersions". Can. J. Chem. Engg., 51, 542–549, Oct. 1973.

72. DAVIES, J.T. "Turbulence Phenomena". Academic Press, 1972.

73. CHEREMISINOFF, N.P. "Instrumentation for Complex Fluid Flows". Technomic Pub. Co., Lancaster, Penn., 1986.

74. SMITH, J.L. "An Analysis of the Vortex Flow in the Cyclone Separator". J. Basic Engg., Trans. ASME, Paper No.61–WA–188, 1–8, 1962.

75. YEH, Y. and CUMMINS, H. "Localized Fluid Flow Measurements with a He–Ne Laser Spectrometer". Applied Physics Letters, 4, 176–178, 1964.

76. KELSALL, D.F. "A Study of the Motion of Solid Particles in a Hydraulic Cyclone". Trans. Inst. Chem. Eng., 30, 87–104, 1952.

77. KNOWLES, S.R., WOODS, D.R. and FENERSTEIN, I.A. "The Velocity Distribution in a Hydrocyclone Operating Without an Air Core". Can. J. Chem. Engg., 51, 263–271, 1973.

78. TURNER, J. and STANBURY, J. (eds) "Laser Anemometry Advances and Applications". Proc. Int. Conf., Univ. Manchester, Dec. 1985. Pub. BHRA, Cranfield, 1985.

79. DURST, F. "Review – Combined Measurements of Particle Velocities, Size Distributions and Concentrations". Trans. ASME, 104, 284–296, Sept. 1982.

80. PARFITT, J.W.E. "The Determination and Analysis of Residence Time Distributions for Hydrocyclones for the Removal of Water Dispersed in Oil". B.Sc. Project Report, Dpt. of Mech. Engg., Univ. Southampton, 1985.

81. DABIR, B. and PETTY, C.A. "Measurements of Mean Velocity Profiles in a Hydrocyclone Using LDA". Chem. Eng. Commun., 48, 377–388, 1986.

82. DABIR, B. and PETTY, C.A. "A Comparative Study Using LDA of Mean Velocity Profiles in Hydrocyclones Having Different Vortex Finder Geometries". Pacific Region Meeting of the Fine Particle Soc., Honolulu, Hawaii, Aug. 1983.

83. BHATTACHARYYA, P.K. "The Flow Field Inside a Conventional Hydrocyclone". Paper H2, Proc. 2nd Int. Conf. on Hydrocyclones, Bath, Sept. 1984. Pub. BHRA, Cranfield, 1984.

84. EXALL, D.I. "Flow Patterns in a Cylindrical Hydrocyclone Measured with a LDV Probe". Council for Scientific and Industrial Res. Report CENG062, Pretoria, S. Africa, Dec. 1974.

85. BHATTACHARYYA, P.K. "Experiment and Theory of the Flowfield Inside the Southampton University Light Phase Hydrocyclone". Report ME/84/4, Dpt. of Mech. Engg., Univ. Southampton, March 1984.

86. LOADER, A.J. "Instability and Turbulence in Confined Swirling Flow Investigated by L.D.A." Ph.D. Thesis, Dpt. of Mech. Engg., Univ. of Southampton, Sept. 1981.

87. BEDI, P.S. and THEW, M.T. "Localized Velocity and Turbulence Measurement in Turbulent Swirling Flows Using Laser Doppler Anemometry". Opto-Electronics, 5, 9-25, 1973.

88. BLACKMORE, C.S. "An Investigation of Confined Swirling Flow Using a LDV". Ph.D. Thesis, Dpt. Mech. Engg., Univ. Southampton, March 1975.

89. SHINNAR, R. "On the Behaviour of Liquid Dispersions in Mixing Vessels". J. Fluid. Mech., 10, 259-275, 1961.

90. HAMMER, E.A. and THORN, R. "Capacitance Transducers for Non-Intrusive Measurement of Water in Crude Oil". Int. Conf. on the Metering of Petroleum and its Products, London, 5th March 1985, Oyez Scientific.

91. SMYTH, I.C. "Commissioning of Endress and Hauser Aquasyst WMC 5170Z as Part of Water-Oil Separation Rig Upgrading at Univ. Southampton". Report ME/85/4, Dpt. Mech. Engg., Univ. Southampton, April 1985.

92. HOLLAND, F.A. "Fluid Flow for Chemical Engineers". Edward Arnold, 1973.

93. SCHLICHTING, H. "Boundary Layer Theory". McGraw–Hill, 1960 (4th Ed.).

94. ELEY, D.D. et al., "Electron Micrography of Emulsions of Water in Crude Petroleum". J. of Colloid and Interface Sc., 54, No.3, March 1976.

95. NEZHATI, K. and THEW, M.T. "De–Oiling Hydrocyclones: Optimisation of 2 Stage Geometry". Report ME/86/19, Dpt. Mech. Engg., Univ. Southampton, Oct. 1986.

96. KARAM, H.J. and BELLINGER, J.C. "Deformation and Break–Up of Liquid Drops in a Simple Shear Field". I. & E.C. Fund, 7, No.4, 576–581, Nov. 1968.

97. SMYTH, I.C, and THEW, M.T. "Dewatering Hydrocyclones: Effect of Various Distillate Blends and Characterisation of Water–Oil Dispersions". Report ME/86/18, Dpt. Mech. Engg., Univ. Southampton, May 1987.

98. HAYASHI, S. "Simultaneous and Instantaneous Measurements of Concentration and Droplet Size Distribution in 2–phase Flows". "Fluid Control and Measurement", Harada, M. (Ed.), Vol.2, 825–830, Pergamon, 1986.

99. MALVERN INSTRUMENTS, "Concentration Limits for 2200/3300 Particle Sizers". Tech. Bull. No.4.

100. FELTON, P.G., HAMIDI, A.A. and AIGAL, A.K. "Measurement of Drop Size Distribution in Dense Sprays by Laser Diffraction". Paper IVA/4, Int. Conf. "Liquid Atomising and Spraying Systems", Imp. Coll., Univ. London, 1985.

101. DAVIES, J.T. "Drop Sizes of Emulsions Related to Turbulent Energy Dissipation Rates". Ch. Eng. Sc., 40, No.5, 839–842, 1985.

102. KOLMOGOROV, A.N. "On the Disintegration of Drops in a Turbulent Flow". Doklady Akad. Nauk., SSSR, 66, No.5, 825–828, 1949.

103. HINZE, J.O. "Fundamentals of the Hydrodynamic Mechanism of Splitting in Dispersion Processes". AIChE J., 1, No.3, 289–295, 1955.

104. LEVICH, V.G. "Physiochemical Hydrodynamics". Prentice Hall, 1962.

105. HESKETH, R.P., FRASER RUSSELL, T.W. and ETCHELLS, A.W. "Bubble Size in Horizontal Pipelines". AIChE J., 33, No.4, 663–667, 1987.

106. FIDDLER, S. Private Comm., Oil Stocks, BP Int., Research Centre, Sunbury (U.K.), May 1987.

107. PHIPPS, L.W. "The Fragmentation of Oil Droplets in Emulsions by a High Pressure Homogenizer". J. Phys. D: Appl. Phys., 8, 448, 1975.

108. VAN DER LINDEN, J.P., KRUITEN, E. and LE LORRAIN, H.R. "(De)mixing of Viscous Dispersions". I.Ch.E. Symposium Series No.94, "Developments in Process Engineering", 225–233, London, 1985.

109. LEE, J.C. "Fundamentals of Drop Breakage in the Formation of Liquid–Liquid Dispersions". I.Ch.E. (London and S.E.) Symposium. "The Formation of Liquid–Liquid Dispersions – Chemical and Engineering Aspects", 43–55, London, Feb. 1984, Chameleon Press.

110. OGAWA, A. "Separation of Particles From Air and Gases". Vol.III, C.R.C. Press, Boca Raton, Florida, U.S.A, 1984.

111. COLLINS, S.B. and KNUDSEN, J.G. "Drop Size Distributions Produced by Turbulent Pipe Flow of Immiscible Liquids". AICHE J., 1072–1080, Nov. 1970.

112. NEESE, Th., DALLMAN, W. and ESPIG, D. "Effect of Turbulence on the Efficiency of Separation in Hydrocyclones at High Feed Solids Concentrations". Paper B3, Proc. 2nd Int. Conf. on Hydrocyclones, Bath, Sept. 1984. Pub. BHRA, Cranfield, 1984.

113. SMITH, D.V. and DAVIES, G.A. "Coalescence in Droplet Dispersions". Can. J. Ch. Engg., 48, 628–637, 1970.

114. WARD, J.P. "Turbulent Flow of Liquid–Liquid Dispersions: Drop Size, Friction Losses, and Velocity Distributions". Ph.D. Thesis, 64–13379, Oregon State Univ., 1964.

115. WILLIAMS, T. Private Comm., Dpt. Electrical Engg., Univ. Southampton, 1982.

116. SELKER, A.H. and SLEICHER, C.A. "Factors Affecting Which Phase Will Disperse When Immiscible Liquids are Stirred Together". Can. J. Ch. Engg., 43, 298–301, 1965.

117. GUILINGER, T.R., GRISLINGAS, A.K. and ERGA, O. "Phase Inversion Behaviour of Water–Kerosine Dispersions". Ind. Eng. Chem. Res., 27, 978–982, 1988.

118. SEYMOUR, L.R., VERHOFF, F.H. and CURL, R.L. "Droplet Breakage and Coalescence Processes in an Agitated Dispersion. 2. Measurement and Interpretation of Mixing Experiments". Ind. Engg. Chem. Fund., 17, No.2, 101–108, 1978.

119. SMITH, G.W. "Simulation Modelling of Hydrodynamic Effects in Dispersed Phase Systems". Ph.D. Thesis, Illinois Institute of Tech., Chicago, U.S.A., Aug. 1985.

120. BAPAT, P.M., TAVLARIDES, L.L. and SMITH, G.W. "Monte Carlo Simulation of Mass Transfer in Liquid–Liquid Dispersions". Ch. Engg. Sc., 38, No.12, 2003–2013, 1983.

121. MEDRONHO, R. de A. "Scale Up of Hydrocyclones at low Feed Concentrations". Ph.D. Thesis, Univ. Bradford, 1984.

122. SMYTH, I.C. "Preliminary Investigations of Mozley 1" Cyclone as a Bulk Water/Oil Separator". Report ME/80/11, Dpt. Mech. Engg., Univ. Southampton, May 1980.

123. SMYTH, I.C. and THEW, M.T. "The Effect of Upstream Outlet (Vortex Finder) Diameter on the Dewatering Capability of an Adapted Deoiling Hydrocyclone Geometry". Report ME/86/11, Dpt. Mech. Engg., Univ. Southampton, May 1986.

124. VAN KOOY, J.G. (RIETEMA, K. discussion), "The Influence of Reynolds Number on the Operation of a Hydrocyclone". Cyclones in Industry, Ch.5, 64–67, Rietema , K. (Ed.), Elsevier, 1961.

125. THEW, M.T., WRIGHT, C.R. and COLMAN, D.A. "RTD Characteristics of Hydrocyclones for the Separation of Light Dispersions". Paper E1, Proc. 2nd Int. Conf. on Hydrocyclones, Bath, Sept. 1984. Pub. BHRA, Cranfield, 1984.

126. BEDNARSKI, S. "Graphical and Analytical Interpretation of Investigation Results of the Flow in Hydrocyclones with Variable Process and Design Parameters". Paper H1, Proc. 2nd Int. Conf. on Hydrocyclones, Bath, Sept. 1984, Pub. BHRA, Cranfield, 1984.

127. NEZHATI, K. and THEW, M.T. "Further Development of De–Oiling Hydrocyclones". Report ME/85/11, Dpt. Mech. Engg, Univ. Southampton, 1985.

128. JARDIN, G.T. "The Effect of Surfactants on the Separation of Free Air From Water Using a Hydrocyclone". B.Sc. Project Report, Dpt. Mech. Engg., Univ. Southampton, April 1988.

129. SMYTH, I.C. and THEW, M.T. "Comparative Tests on the Solids Removal Performance of Three Hydrocyclones for the M.O.L. Pump Seals". Report ME/82/6, Dpt. Mech. Engg., Univ. Southampton, April 1982.

130. WATKINS, R. Unpublished Results of Trial with Southampton Hydrocyclone Design on Seals Rig with Simulated Forties, B P Research Centre, Sunbury, Dec. 1984. (Permission to use data obtained from B P Pet. Dev.).

131. HAYES, J.J. et al., "Hydrocyclones for Treating Oily Water: Development and Field Testing in the Bass Strait". OTC5079, Proc. 17th Offshore Technology Conf., Houston, 1985.

132. MELDRUM, N. "Hydrocyclones: A Solution to Produced Water Treatment". OTC5594, Proc. 19th Offshore Technology Conf., Houston, 1987.

133. MARSDEN, P.G., COLMAN, D.A. and THEW, M.T. "Microcomputer Control of a System of Hydrocyclones". Paper C1, Int. Conf. on the Use of Micros in Fluid Engg., London, 1983. Pub. BHRA, Cranfield, 1983.

134. HARGREAVES, J.H. "Use and Minor Development of the Boysan–Colman (De–Oiling) Hydrocyclone Program". Report ME/88/4, Dpt. Mech. Engg., Univ. Southampton, 1988.

135. GIRAULT, H.H.J., SCHIFFRIN, D.J. and SMITH, B.D.V. "The Measurement of Interfacial Tension of Pendant Drops Using a Video Image Profile Digitizer". J. Colloid and Interface Science, 101, No.1, 257–266, Sept. 1984.

136. PERRY, R.H. and CHILTON, C.H. (Eds.), "Chemical Engineer's Handbook", 5th Ed., McGraw–Hill, 1982.

137. HILL, E.C. and HILL, G.C. "Micro-Organisms in Marine Fuel: Fouling and Corrosion". Marine Engg. Research, 14-16, Dec. 1985.

138. BARRY, B.A. "Errors in Practical Measurements in Science, Engineering and Technology". Wiley, 1978.

139. EDWARDS, R.V. and DYBBS, A. "RI Matching for Velocity Measurements in Complex Geometries". TSI Quarterly, X, Issue 4, 3-11, Oct-Dec. 1984.

140. FOGWELL, T.W. "Window Materials for Use with Flow Visualisation Techniques". AERE-R12313, Harwell, U.K., July 1986.

141. DURST, F., MELLING, A. and WHITELAW, J.H. "Principles and Practice of Laser Doppler Anemometry". Academic Press, 1976.

142. DRAIN, L.E. "The Laser Doppler Technique", Wiley, 1980.

143. KATZ, D.L. et al., "Handbook of Natural Gas Engineering". Ch.5, McGraw-Hill, 1958.

144. GIMSON, C. "Evaluation and Performance of an On-line Water Content Analyser". Paper from Conf. on Determination of Water Content in the Custody Transfer Metering of Crude Oil, London, 24th Feb. 1986, IBC Technical Services.

145. SHIRRAN, G. "Offshore Experience with the Endress and Hauser Water in Hydrocarbons Monitor Report". NMJ053, North Sea Flow Metering Workshop 1986, N.E.L., East Kilbride, 7-9 Oct. 1986.

146. "Total Water Content of Crude Oil by Karl Fischer Titration". BP423/79/T, BP Internal Publication.

FIG.3.1 3-PHASE HORIZONTAL FREE WATER KNOCKOUT DRUM

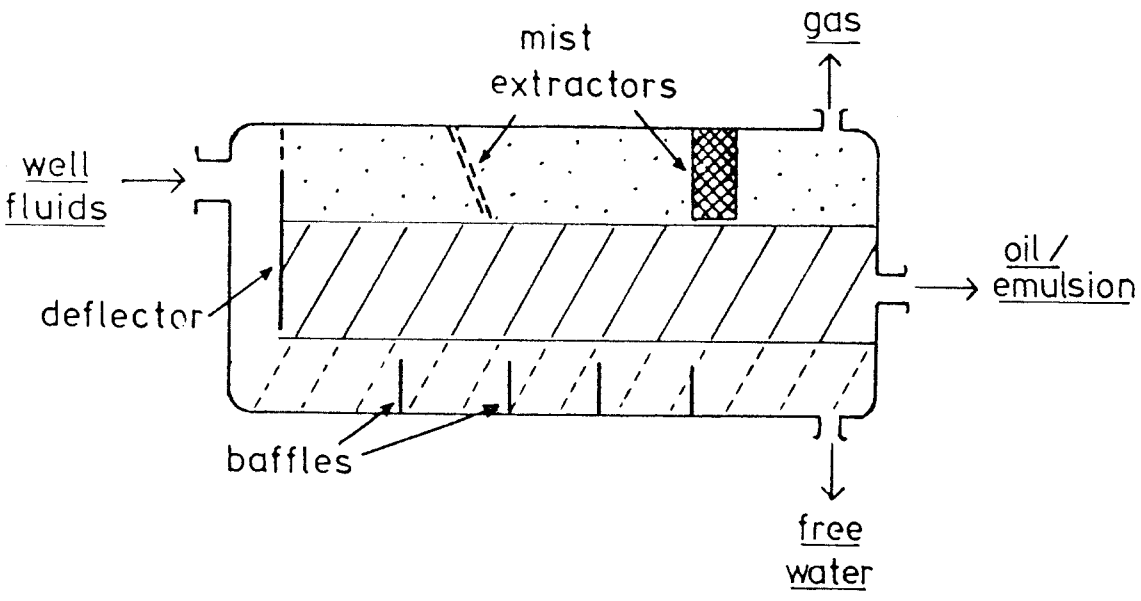

FIG.3.2 ELECTRIC DEHYDRATOR

- 120 Hz supply
- electrodes electrified with opposing polarity (usually one of electrodes is earthed)

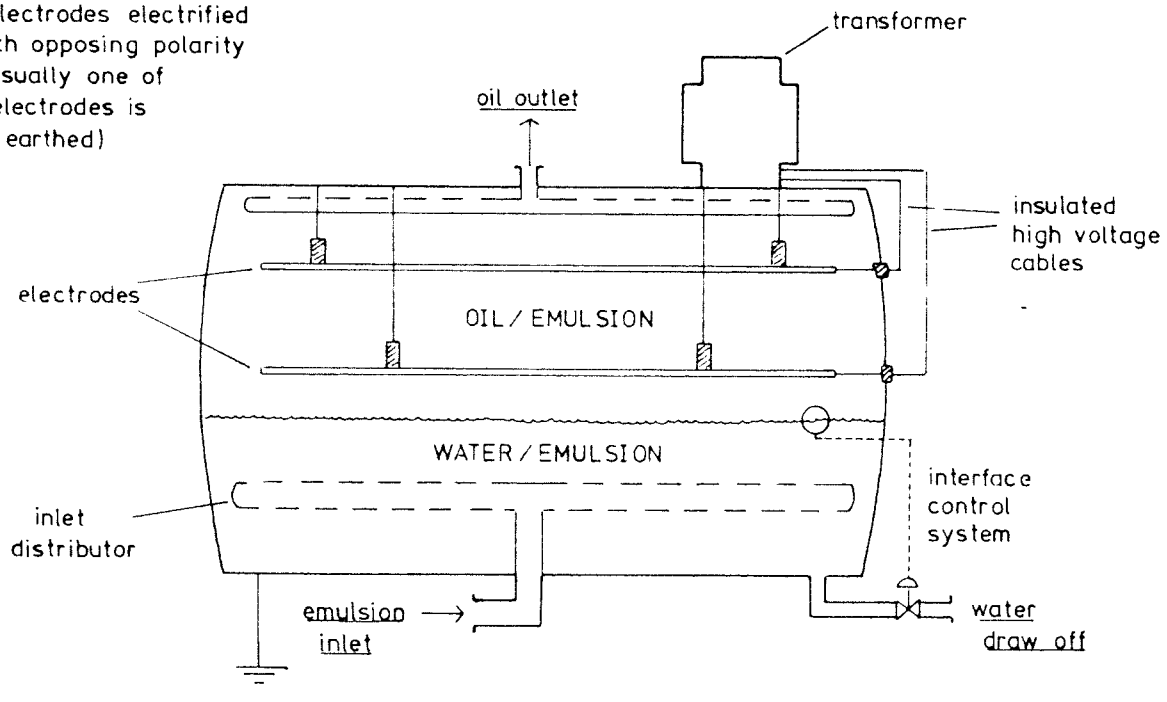

FIG.3.3 COALESCER SEPARATOR INCORPORATING CRUDE AND OILY WATER TREATMENT

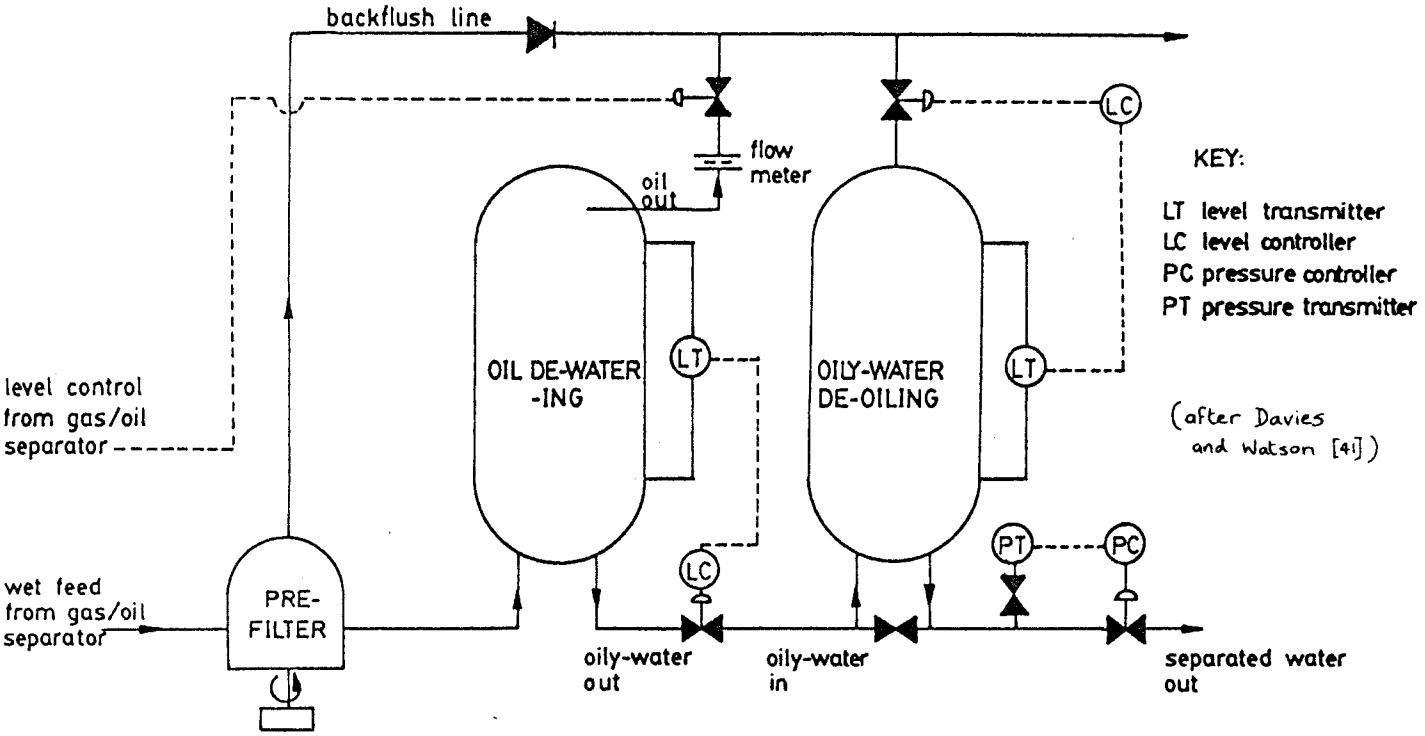

FIG.3.4 OFFSHORE DEWATERING PROCESS FLOW DIAGRAM - FORTIES ALPHA

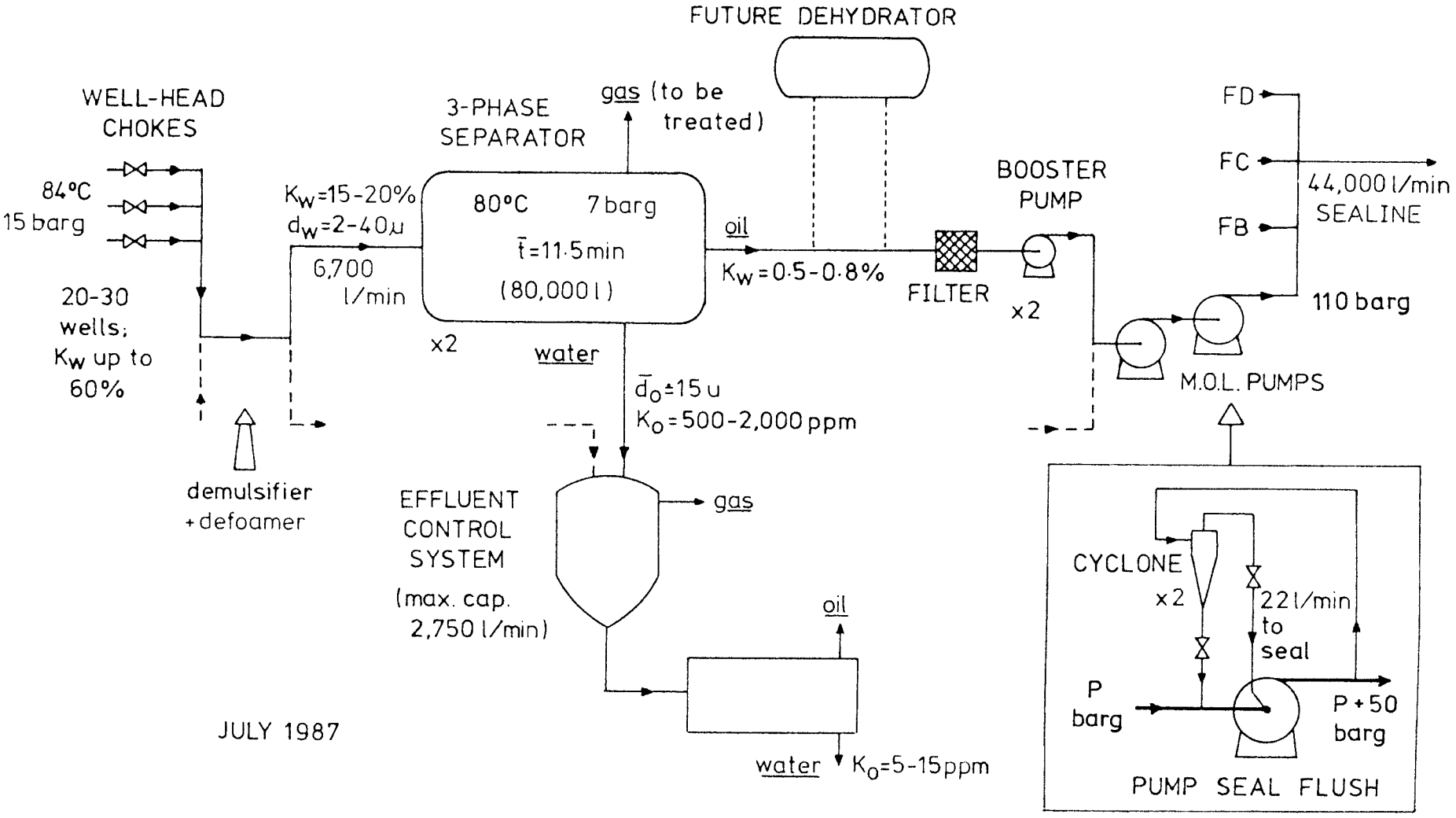

FIG.3.5 ONSHORE DEWATERING PROCESS FLOW DIAGRAM - KINNEIL

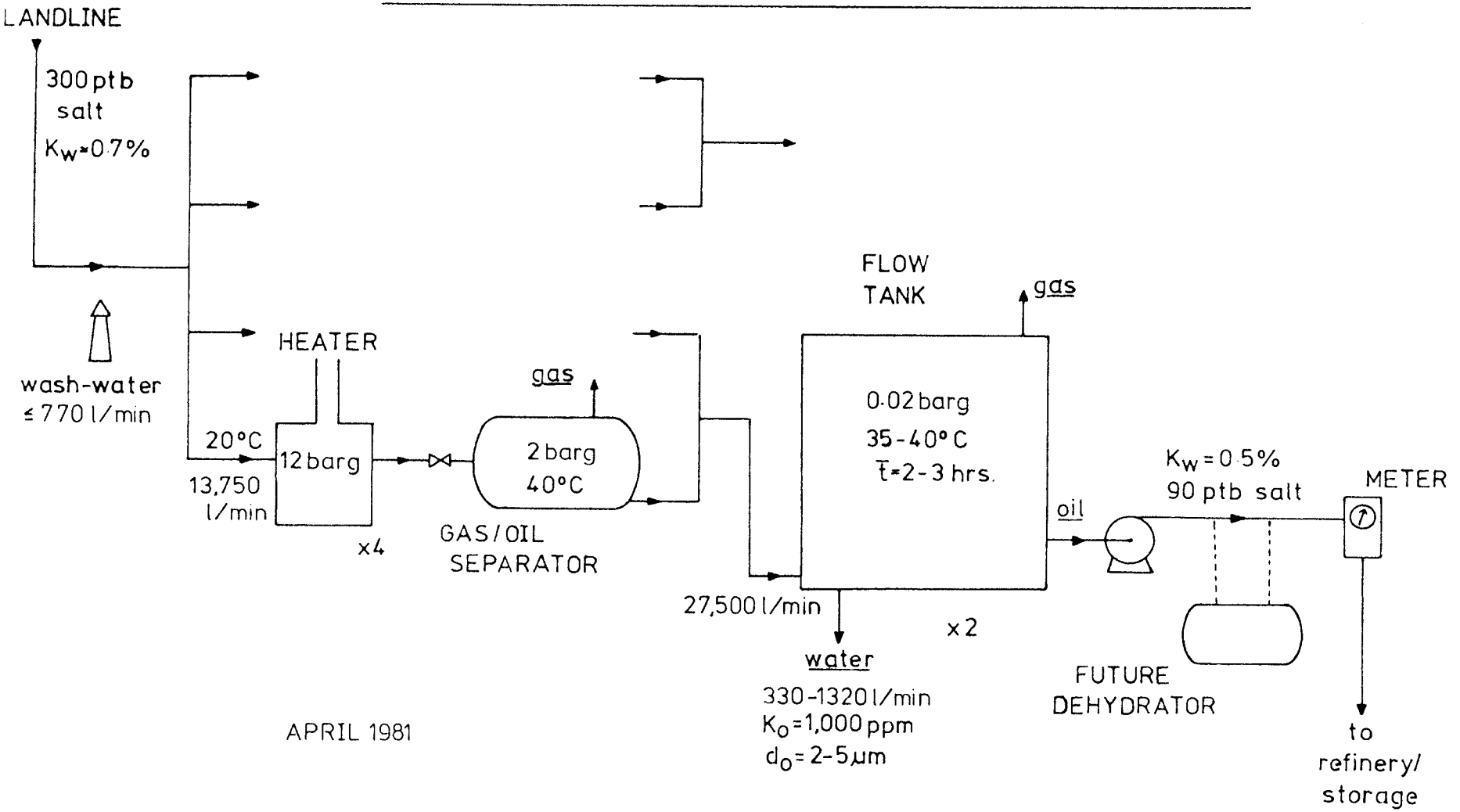

FIG.4.1 EFFECT OF SPLIT ON EFFICIENCY PARAMETERS FOR OPTIMAL SEPARATION

EQUATIONS FOR CURVES:

	$\leq (1-F)_{crit}$	$> (1-F)_{crit}$
$\frac{K_u}{K_i}$	$\frac{1-[(1-F)K_d/K_i]}{F}$	$K_u = 0\%$
$\frac{K_d}{K_i}$	$K_d = 100\%$	$\frac{1}{1-F} - \left[\frac{K_u F}{K_i(1-F)}\right]$
E	$\frac{F-1+[(1-F)/K_i]}{(1-K_i)}$	$\frac{F}{(1-K_i)}$
E_{or}	1	$\frac{F}{(1-K_i)}$

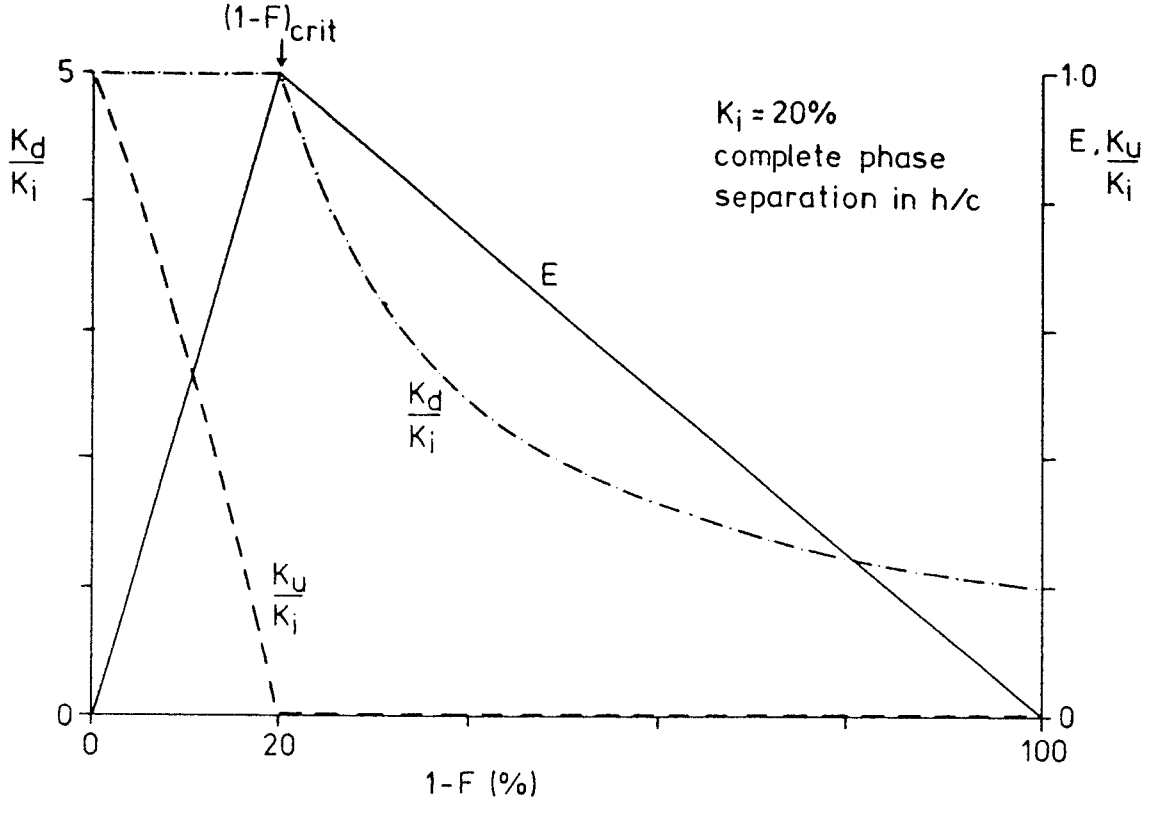

FIG.4.2 EFFECT OF Ki ON UPSTREAM PRESSURE COEFFICIENT

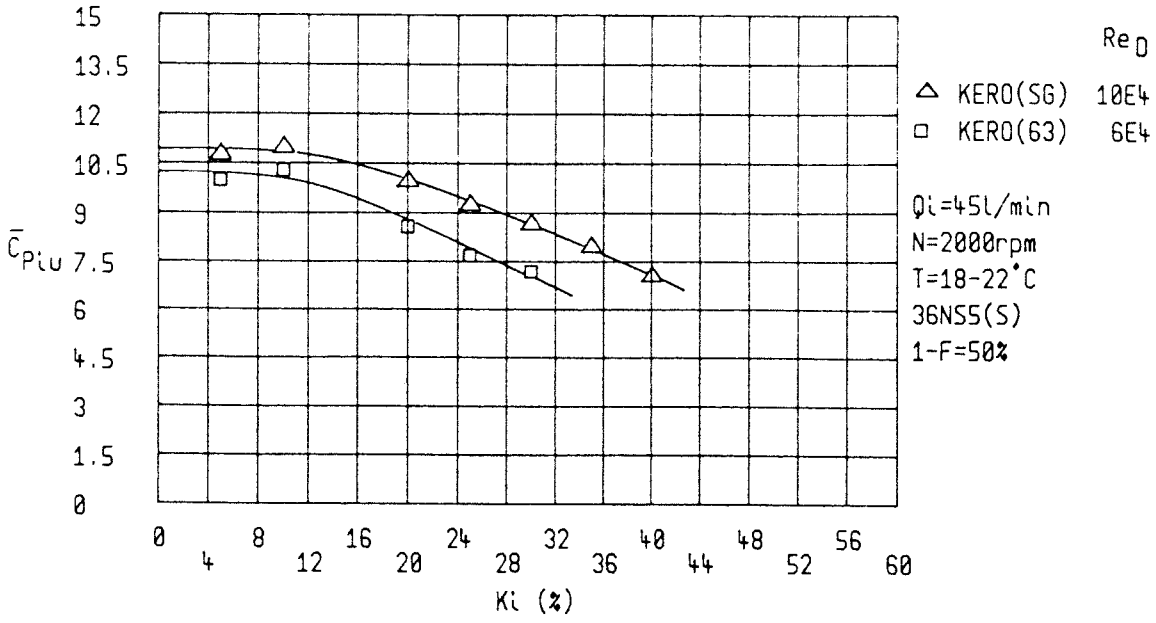

FIG.4.3 EFFECT OF Ki ON DOWNSTREAM PRESSURE COEFFICIENT

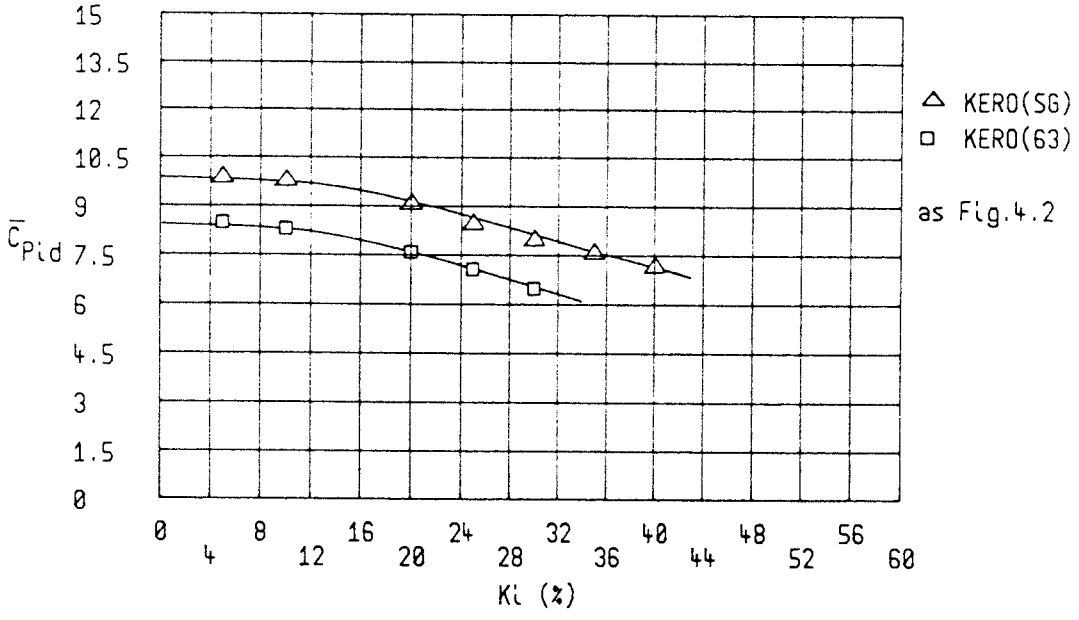

FIG.5.1 GEOMETRY DEVELOPMENT USING NYLON-WATER : EFFECT OF FLOWRATE ON SEPARATION

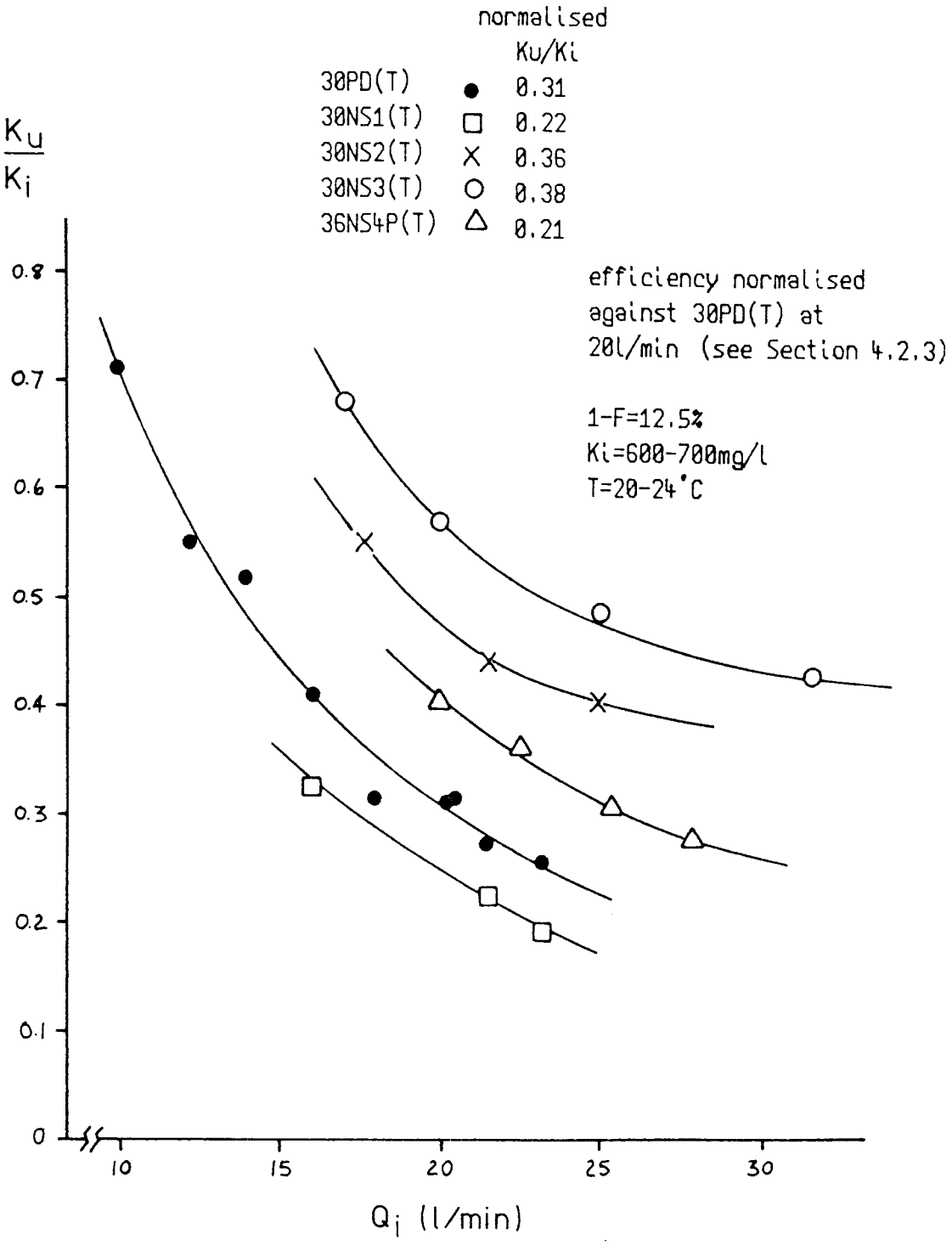

FIG.5.2 GEOMETRY DEVELOPMENT USING NYLON-WATER : EFFECT OF FLOWRATE ON PRESSURE DROP

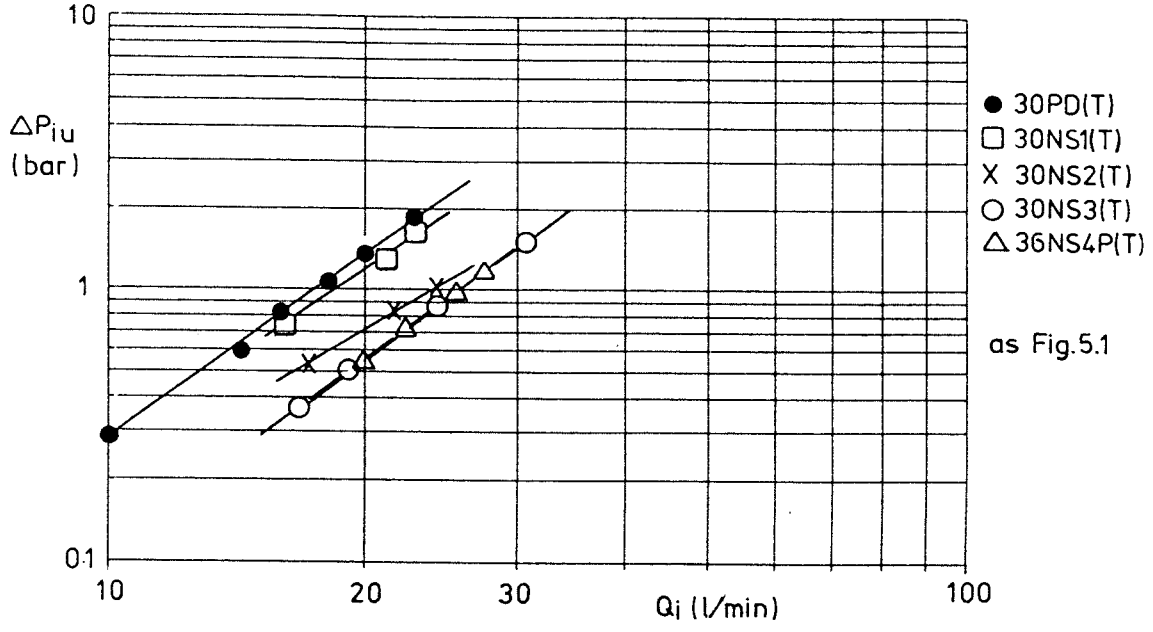

FIG.5.3 PERCENT CUMULATIVE VOLUME UNDERSIZE PARTICLE SIZE DISTRIBUTIONS FOR NYLON AND WATER-KEROSINE

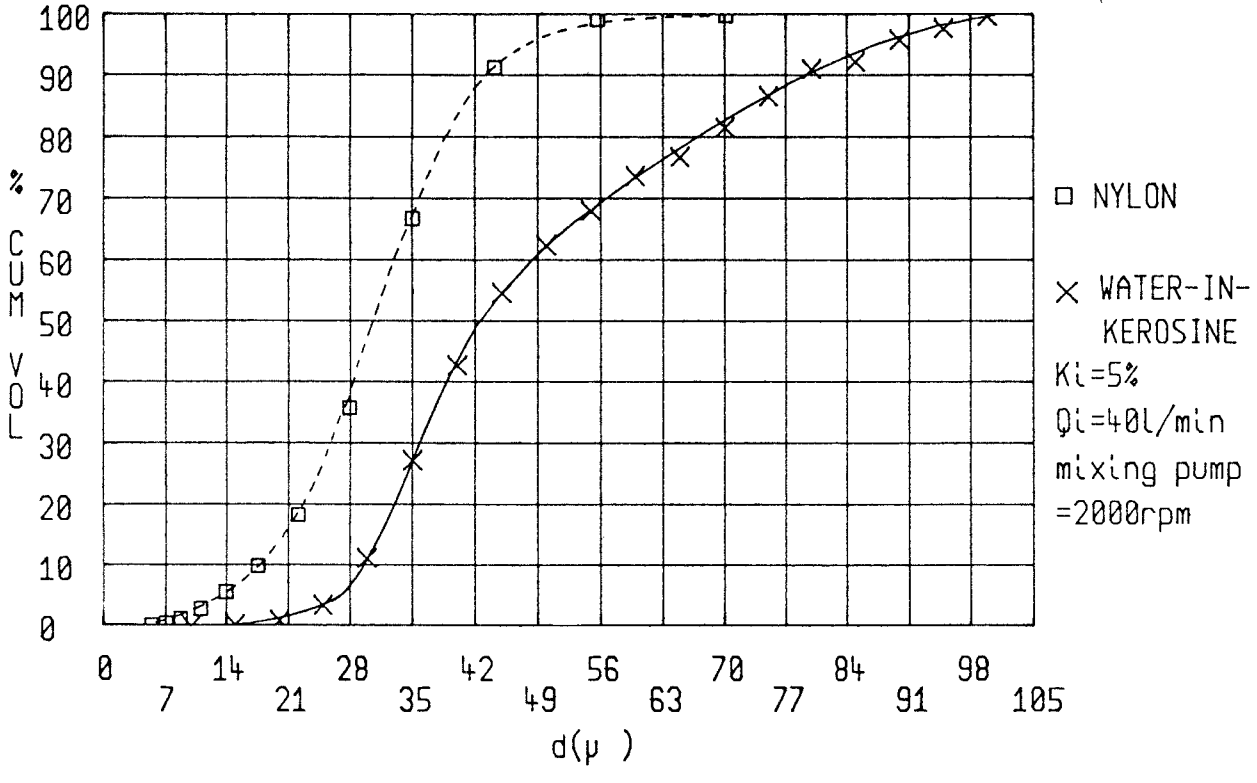

FIG.5.4 REDUCED MIGRATION PROBABILITY AGAINST HYDROCYCLONE NUMBER FOR NYLON-WATER IN 36NS4P(T)

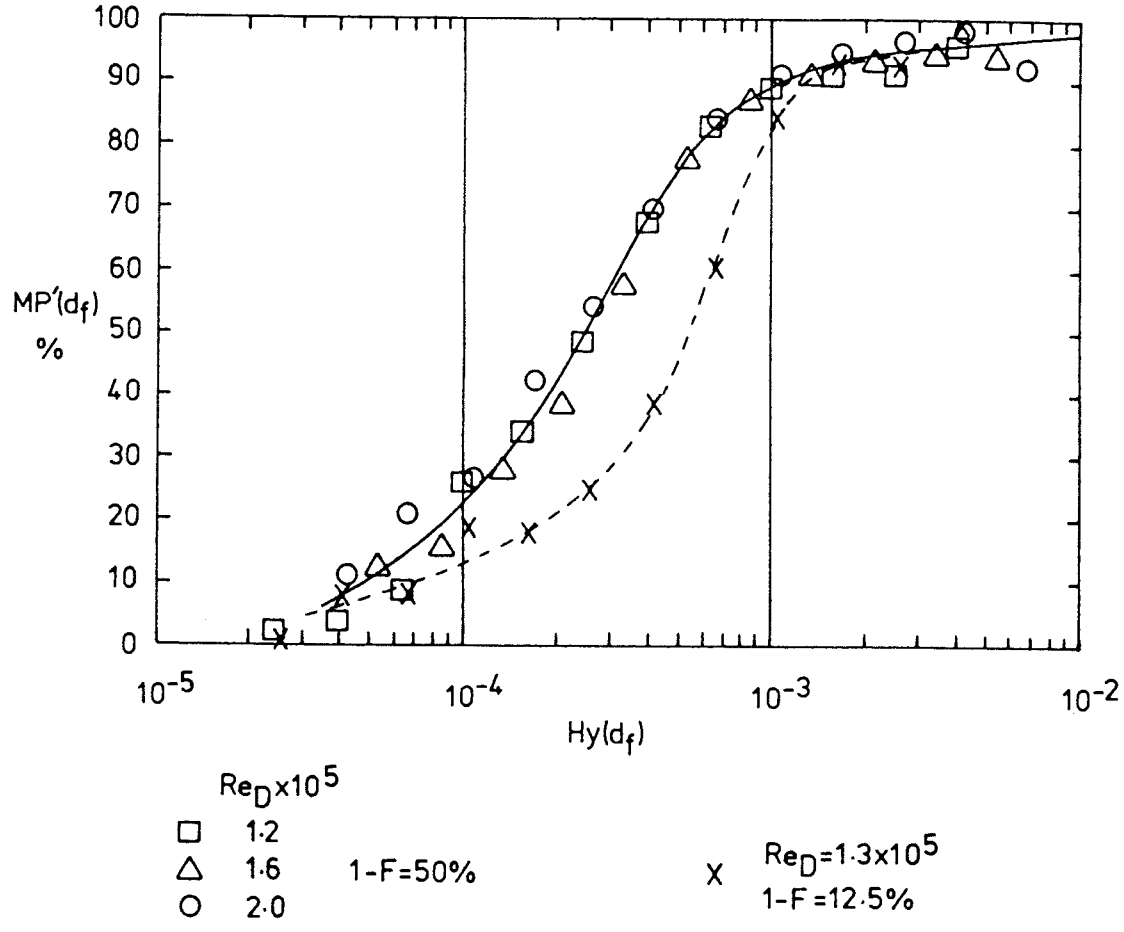

FIG.5.5 REDUCED MIGRATION PROBABILITY AGAINST HYDROCYCLONE NUMBER FOR NYLON-WATER IN 32MANF.A

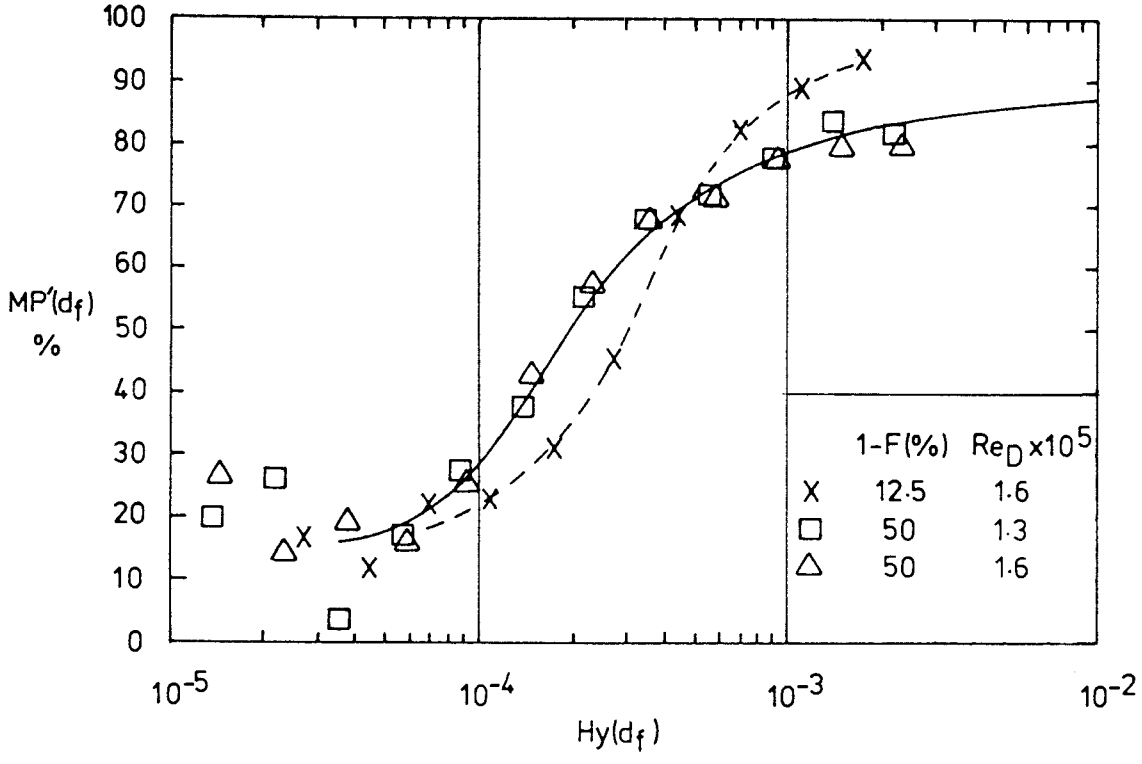

FIG.5.6 COMPARISON OF EXPERIMENTAL WATER-KEROSINE SEPARATION WITH PREDICTIONS DERIVED FROM NYLON-WATER SEPARATION

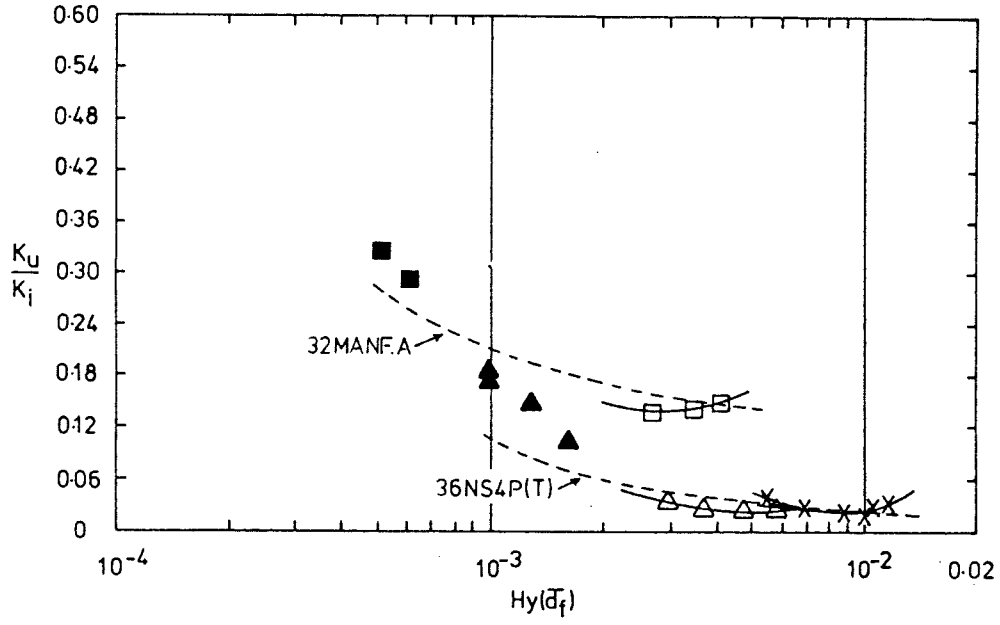

	NYLON-WATER	WATER-KEROSINE
32MANF.A	■	□
36NS4P(T)	▲	△
26NS4P(T)		X

1-F=50%

----- PERFORMANCE PREDICTED USING $\bar{d}_f$ AND FIGS. 5.4 and 5.5

(SEE ALSO SECTION 5.2.4)

FIG.5.7 ASSESSMENT OF PRELIMINARY GEOMETRY DEVELOPMENTS WITH WATER-KEROSINE - SEPARATION PERFORMANCE

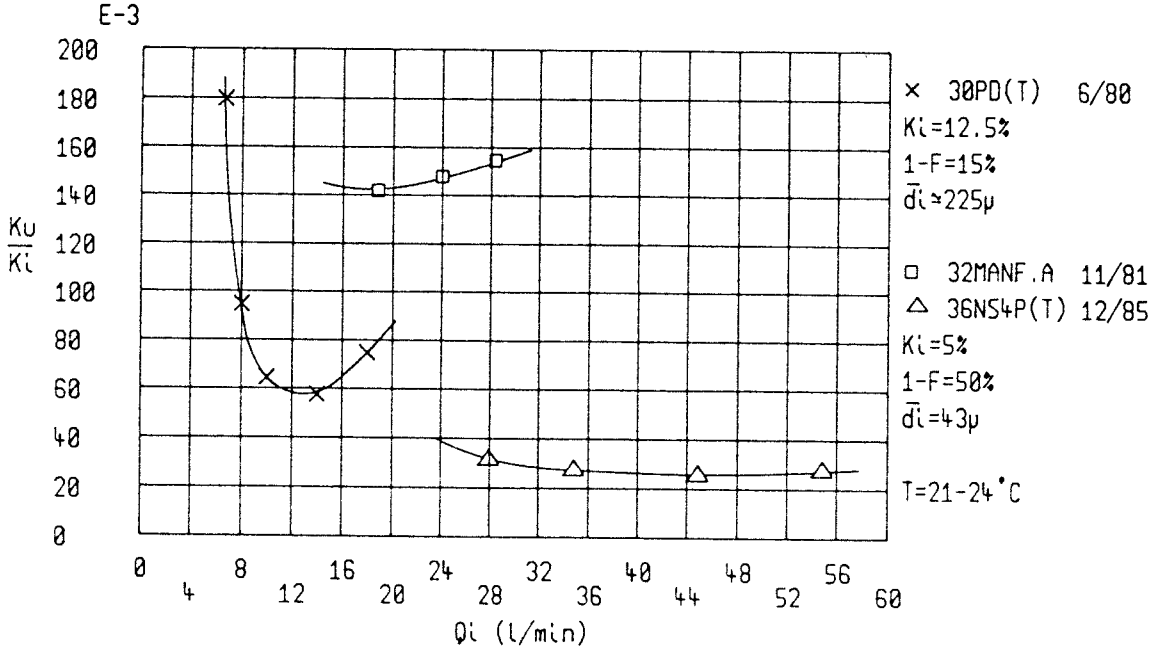

FIG.5.8 ASSESSMENT OF PRELIMINARY GEOMETRY DEVELOPMENT WITH WATER-KEROSINE - PRESSURE REQUIREMENTS

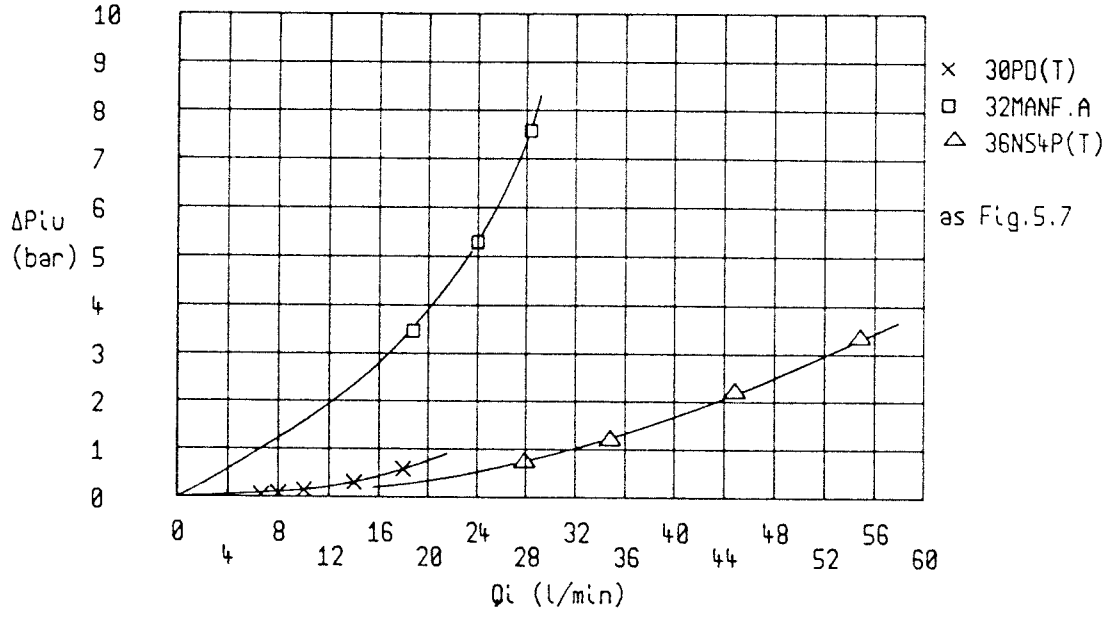

FIG.6.1 AXIAL VELOCITY PROFILES AT VARIOUS SPLITS IN 36NS4P(T)

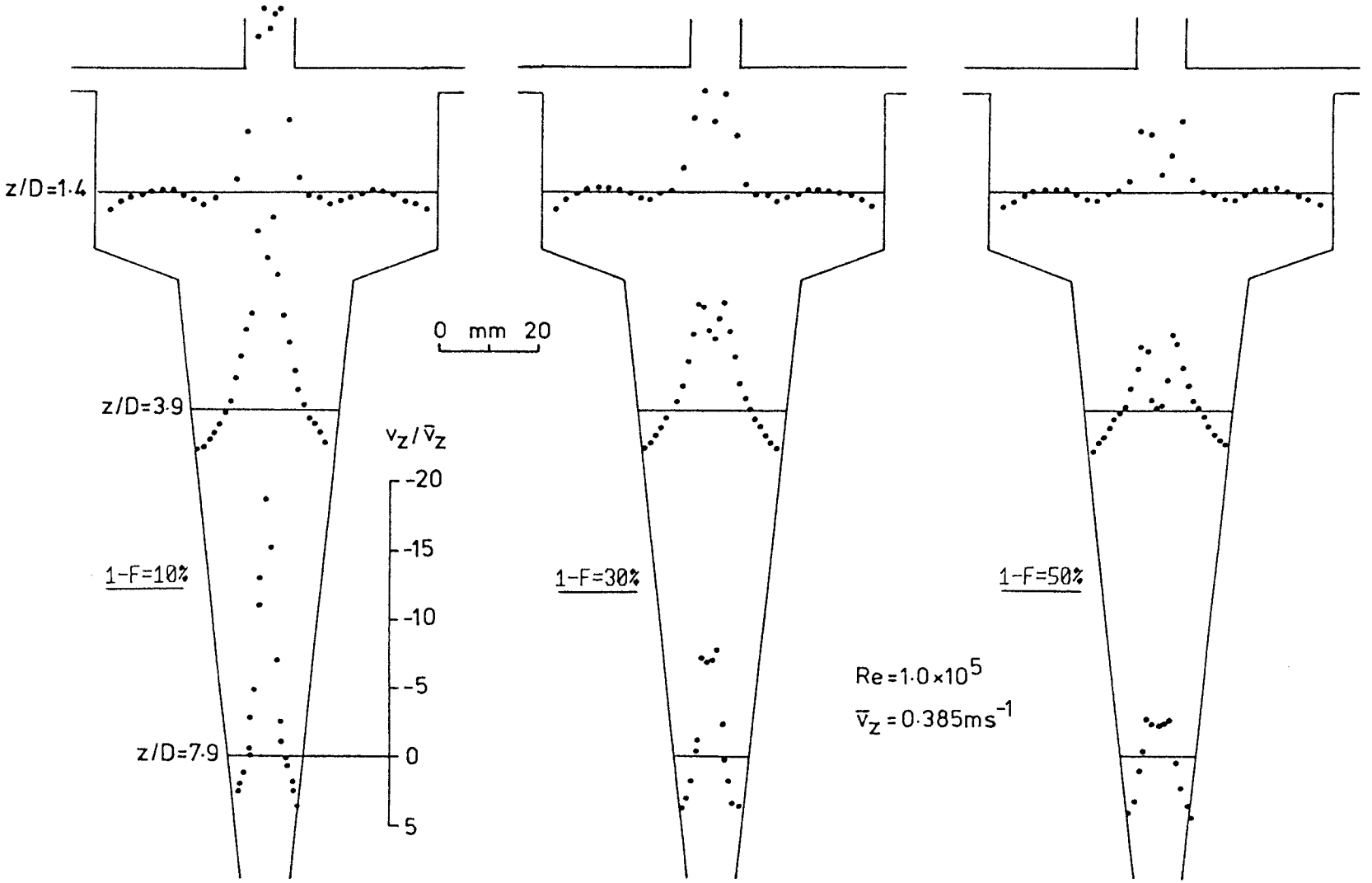

FIG.6.2 ANTICIPATED FLOW PATTERNS IN THE SWIRL CHAMBER AND UPPER CONE IN 36NS4P(T)

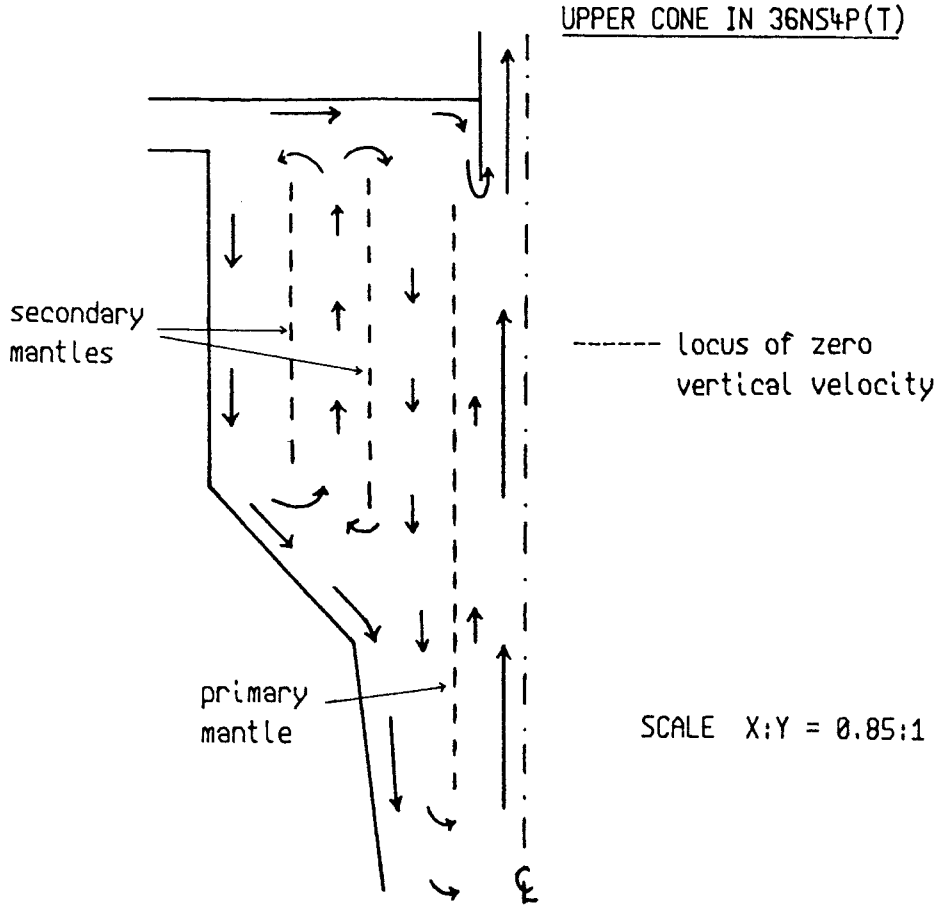

FIG.6.3 TIME AVERAGED RADIAL VELOCITY GRADIENTS IN 36NS4P(T)

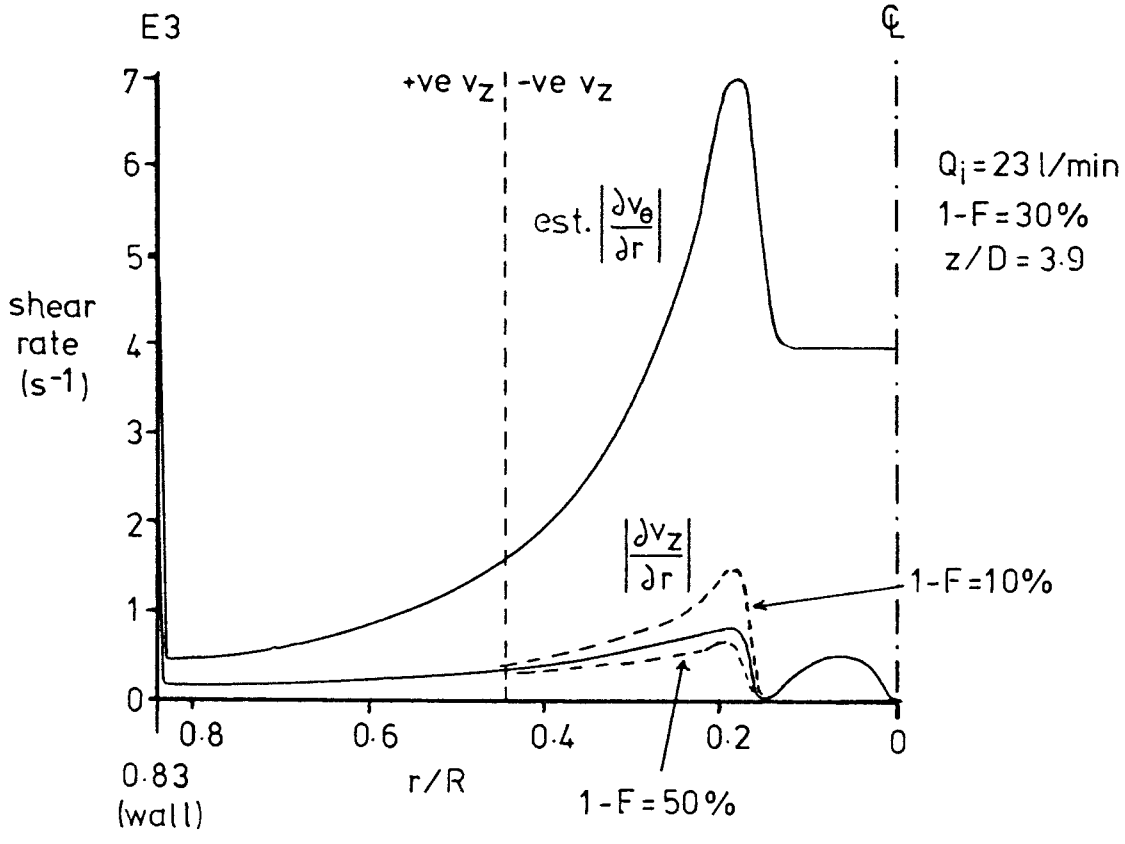

FIG.7.1 WATER-OIL SEPARATION TEST RIG (L1)

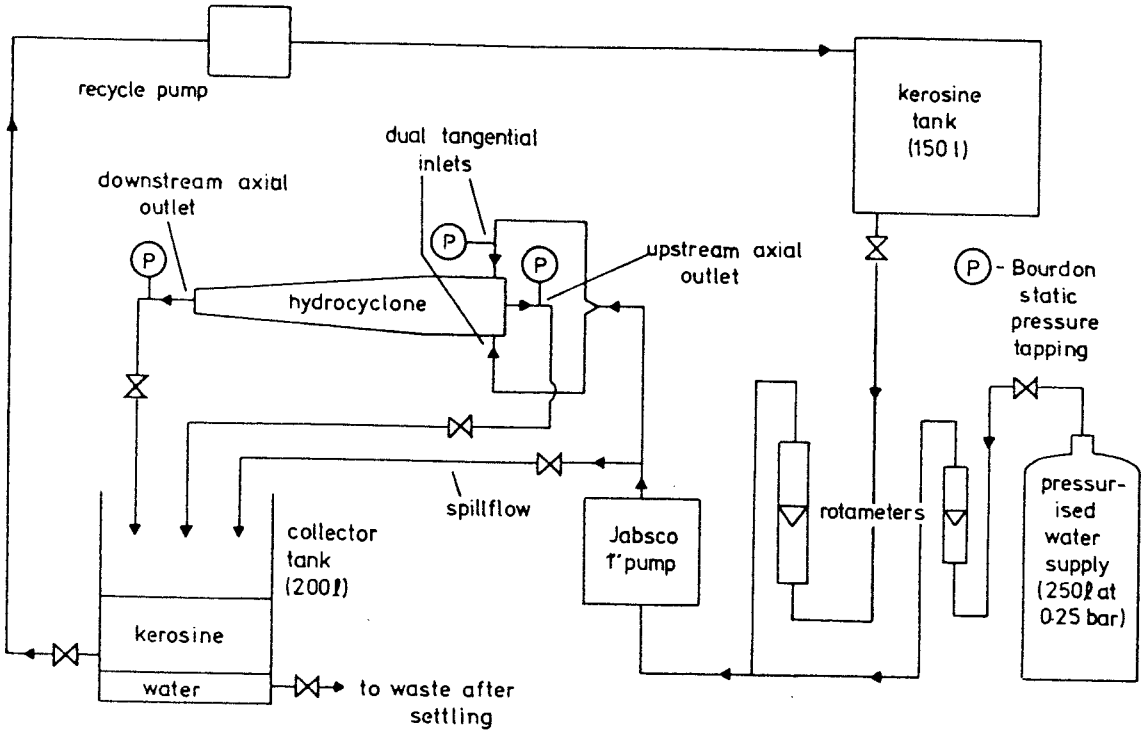

FIG.7.2 WATER-OIL SEPARATION TEST RIG (L2)

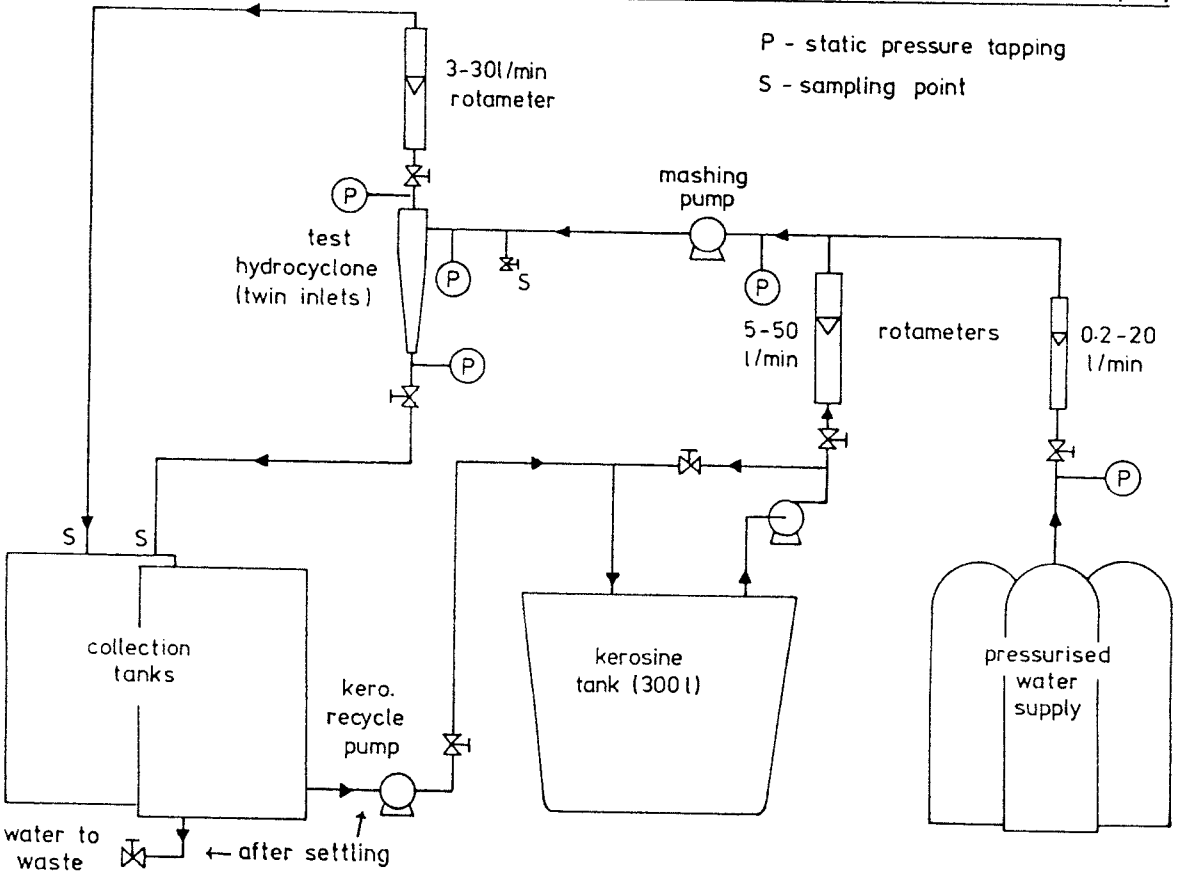

FIG.7.3 WATER-OIL SEPARATION TEST RIG (L3)

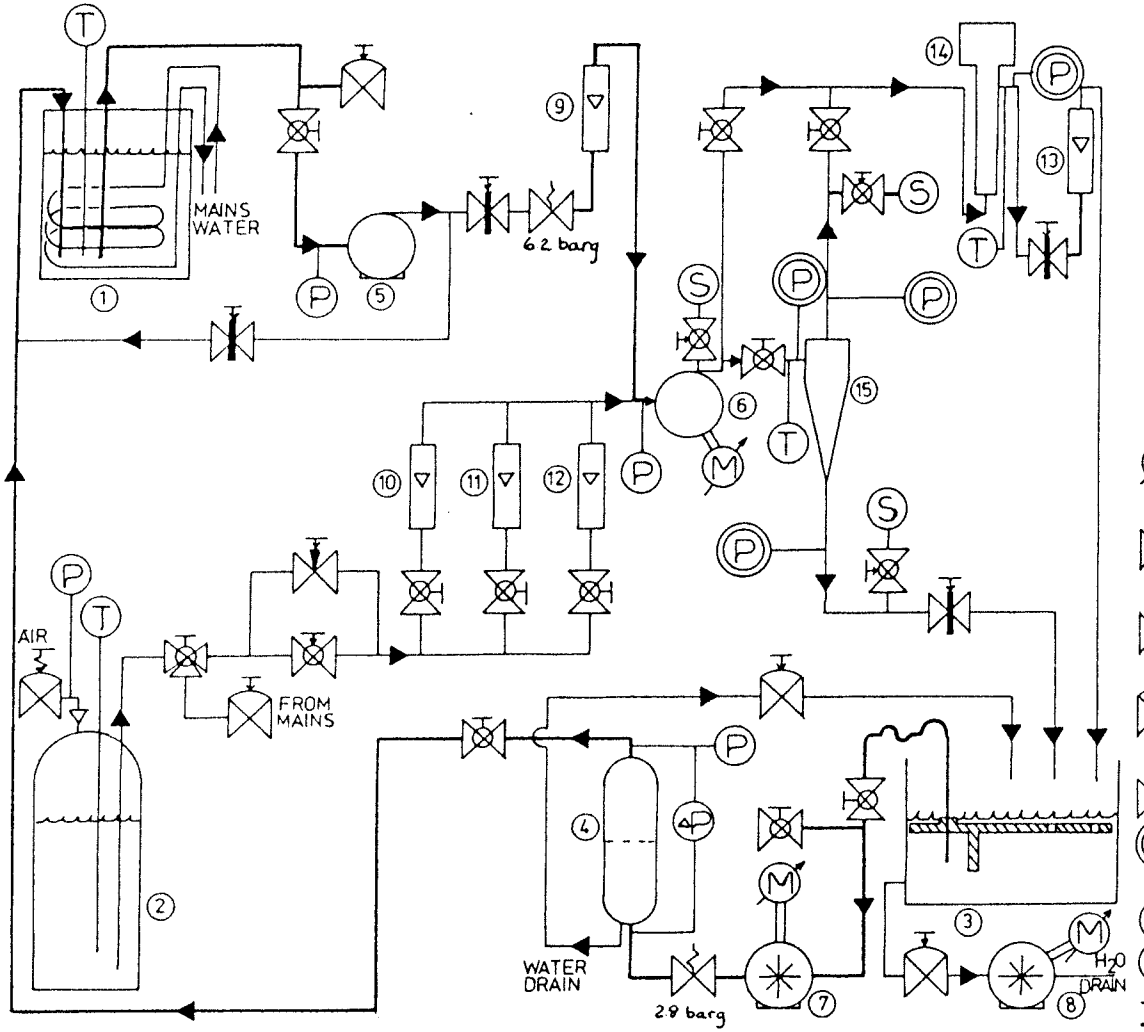

1 OIL/KEROSINE FEED (280L)
2 PRESSURISED WATER FEED (180 L)
3 DUMP TANK (500 L)
4 FRAM FILTER COALESCER
5 GRUNDFOS CENTRIFUGAL PUMP (CP3-100K)
6 WORTHINGTON SIMPSON TURBINE MASHING PUMP (1 1/4" T22)
7 SINGLE STAGE MONO PUMP (CAB12G 1K3/A110J)
8 JABSCO PUMP (1")
9 ROTAMETER (15-75 L/MIN , VISC. INDPT.)
10 ROTAMETER (0.2-2 L/MIN)
11 ROTAMETER (1-10 L/MIN)
12 ROTAMETER (3-30 L/MIN)
13 ROTAMETER (10-60 L/MIN, VISC. INDPT.)
14 AQUASYST WATER-IN-OIL CONC^N METER (WMC 5170 Z)
15 TEST HYDROCYCLONE

M VARIABLE SPEED MOTOR

ON/OFF AND CONTROL BALL VALVE

CONROL GATE VALVE

SAUNDERS CONTROL VALVE

PRESSURE RELIEF VALVE

P PRESSURE MEASUREMENT BOURDON PRECISION AND STANDARD GAUGES RESPECTIVELY

T TEMPERATURE MEASUREMENT

S ISOKINETIC SAMPLING POINT

— ≤ 3/4" PIPE
— ≥ 1" PIPE

APRIL 1985 , UNIVERSITY OF SOTON

FIG.7.4 Ki LIMITS FOR WATER-KEROSINE SEPARATION

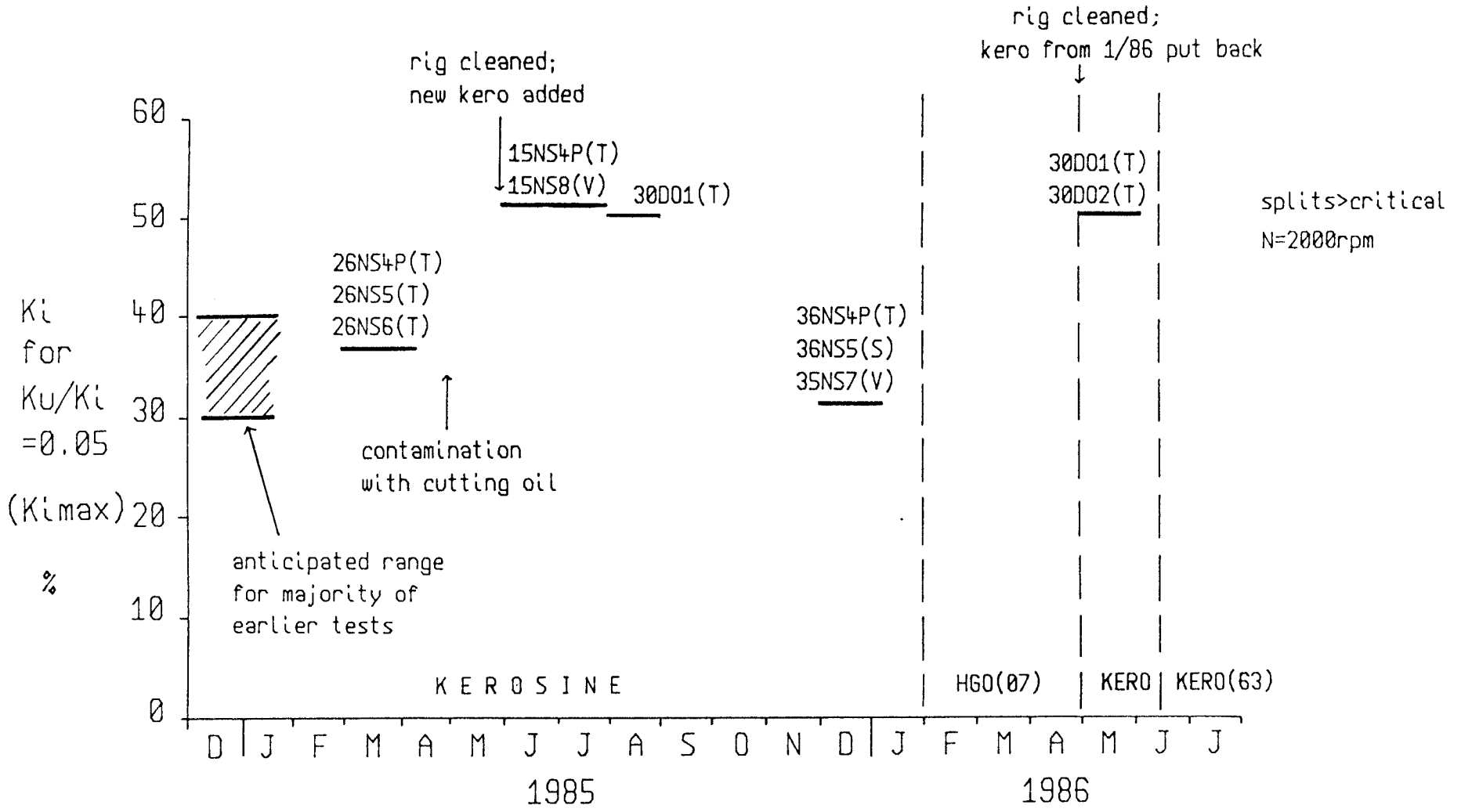

FIG.7.5 INTERNAL GEOMETRY CHANGES IN AQUASYST CELL

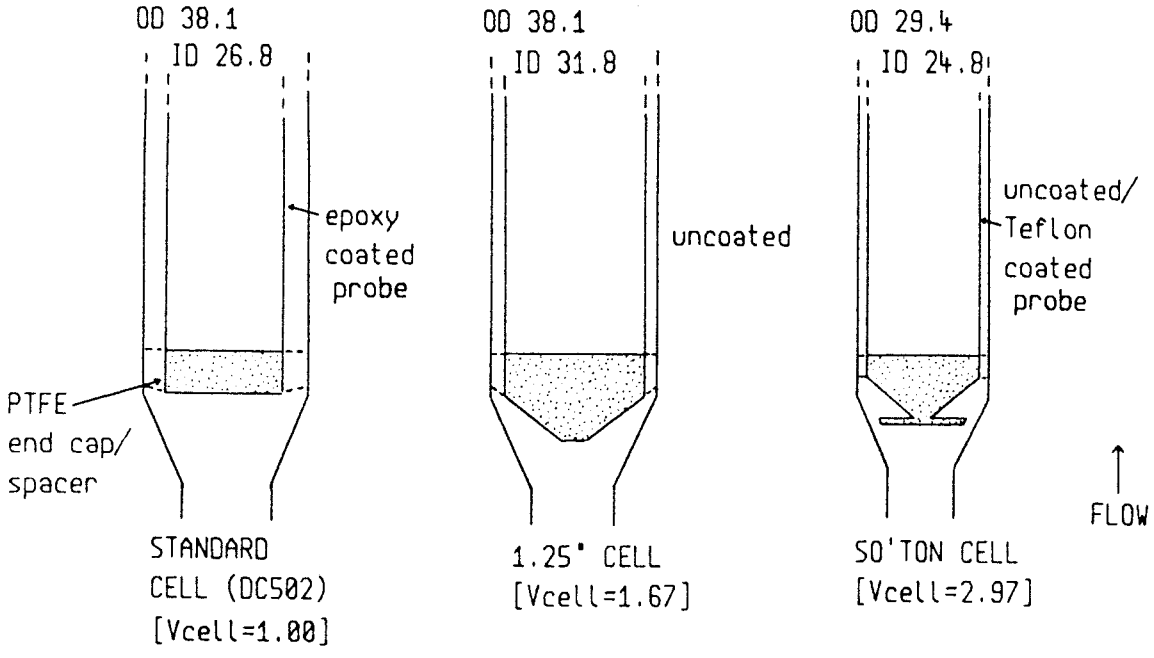

FIG.7.6 RATE OF INCREASE OF AQUASYST READINGS WITH CELL FLUID VELOCITY

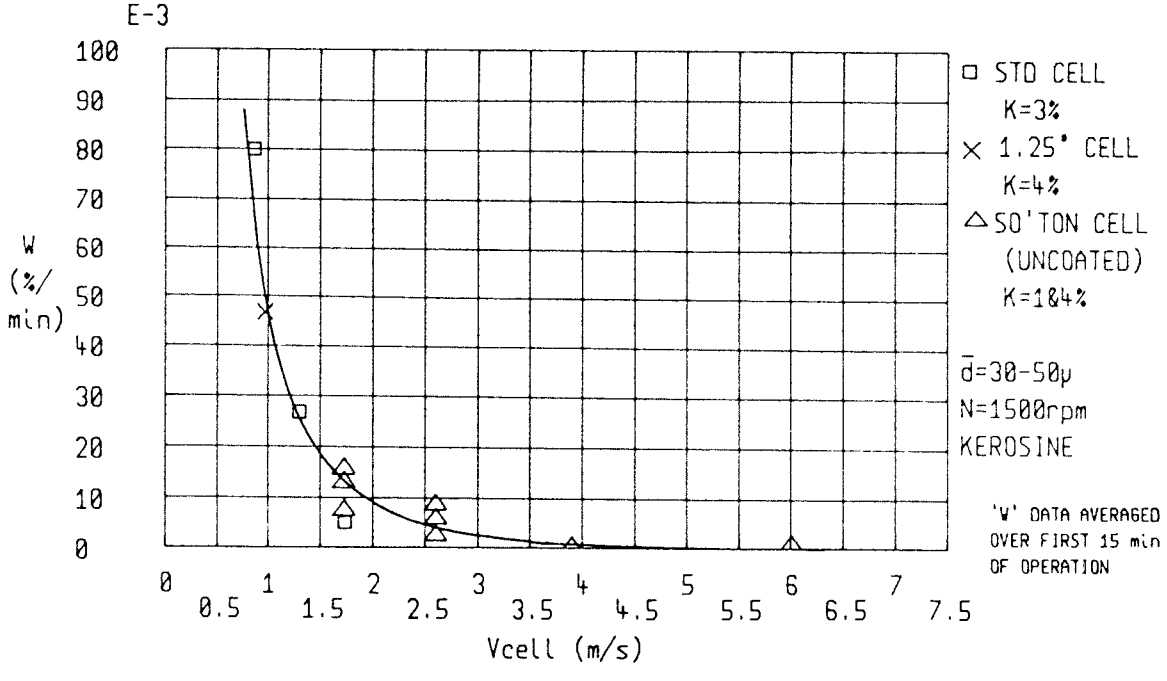

FIG.7.7 COMPARISON OF 3 AQUASYST CELLS MEASURING WATER CONTENT IN UPSTREAM DISCHARGE FROM A HYDROCYCLONE

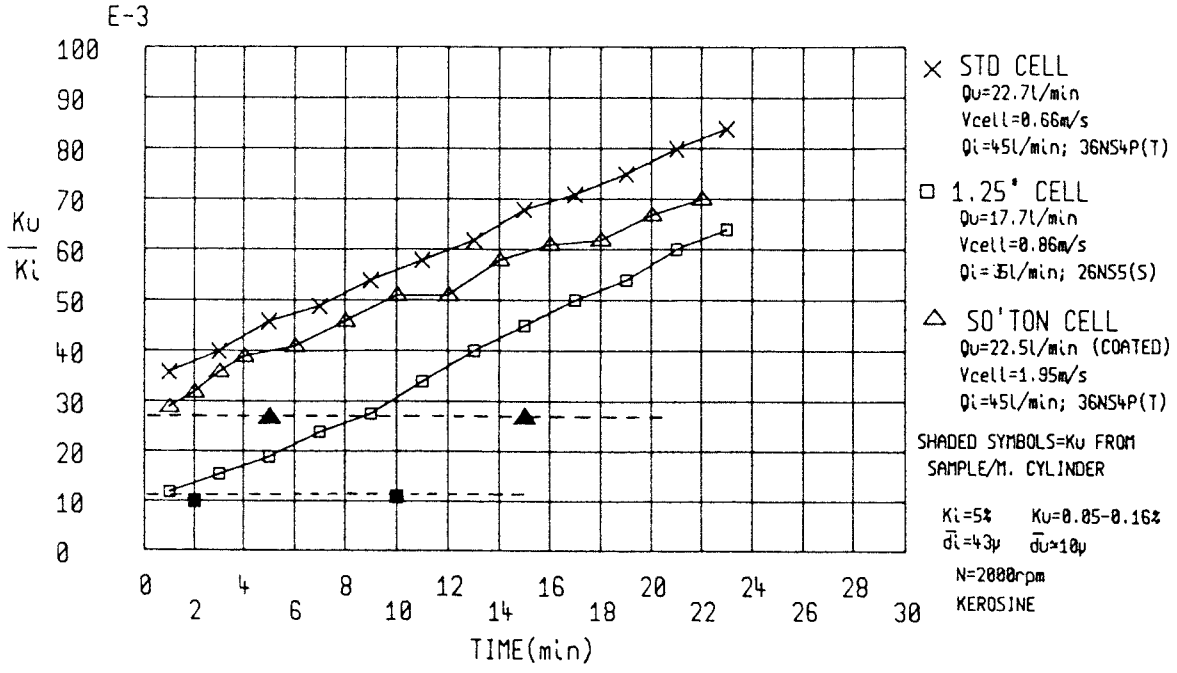

FIG.7.8 EFFECT OF SYSTEM CONTAMINATION ON AQUASYST OPERATION - ΔK (AQUASYST-ROTAMETER) VS. TIME

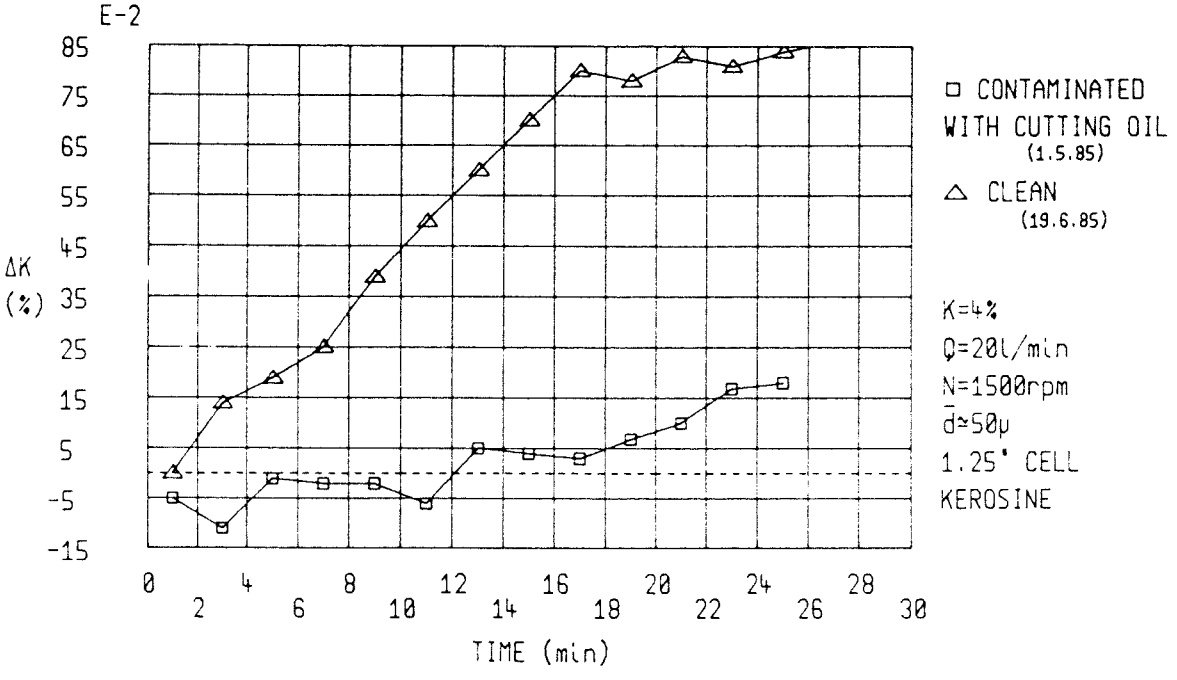

FIG.7.9 DROP SIZE DISTRIBUTIONS FOR VARIOUS OILS

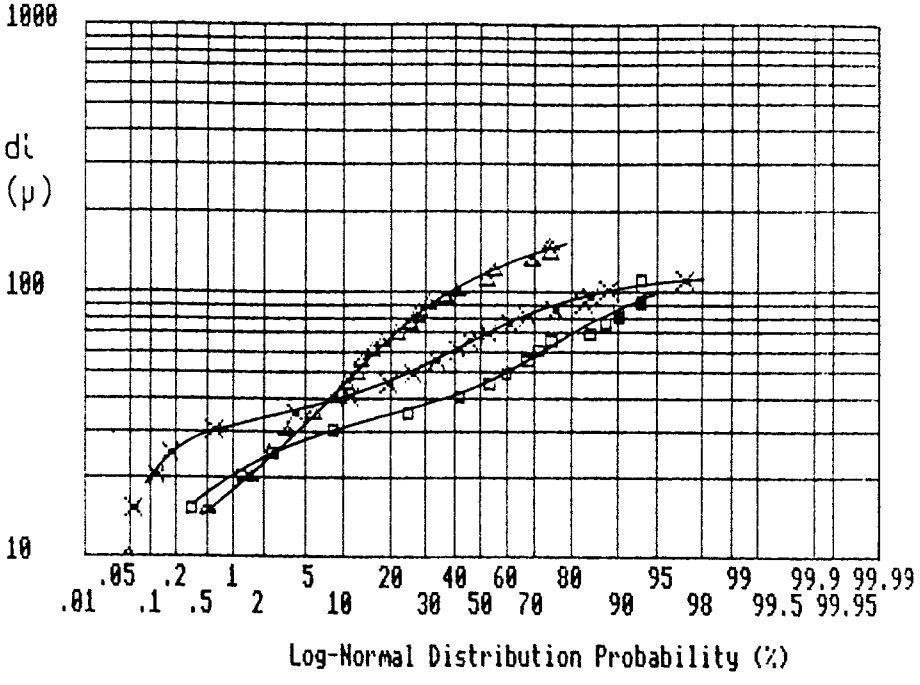

△ HGO(07);
y=0.013N/m
Ki=5%
N=750rpm
Qi=40l/min
σg=1.6
× KERO(63)
Ki=30%
N=1500rpm
Qi=45l/min
σg=1.5
□ KEROSINE
Ki=5%
N=2000rpm
Qi=40l/min
σg=1.5

FIG.7.10 EFFECT OF MIXNG PUMP SPEED ON DROP SIZE (Ki=5%)

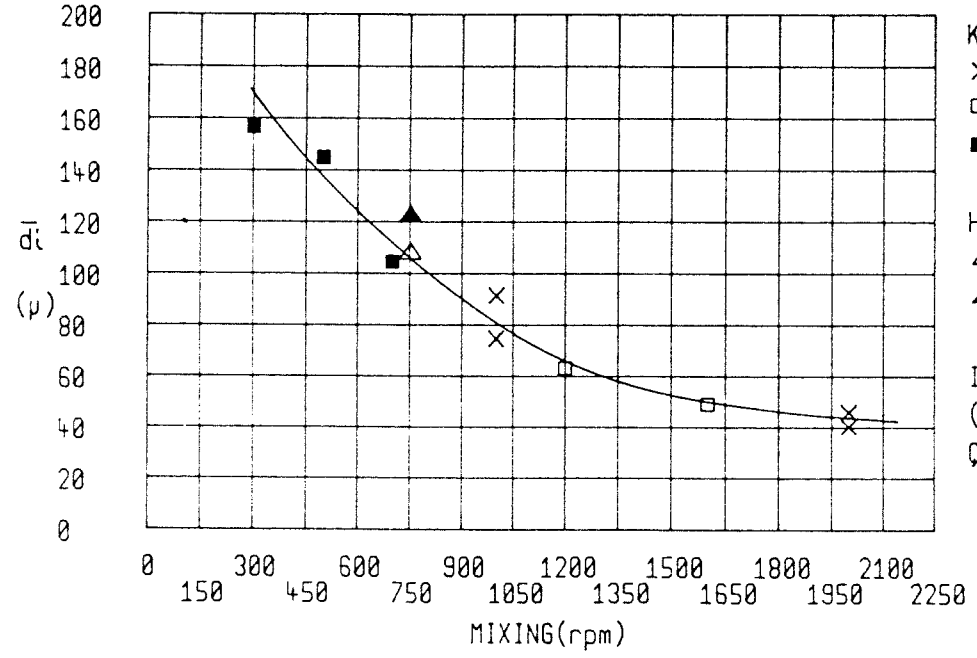

KEROSINE
× 11/85;6/86
□ 3/83
■ 7/82

HGO(07) 3/86
△ y=0.013N/m
▲ y=0.017N/m

ISOKINETIC
(*STATIC)
Qi=40-45l/min

T=20-25°C
σg=1.3-1.7

FIG.7.11 EFFECT OF MIXING PUMP SPEED ON DROP SIZE (Ki=10%)

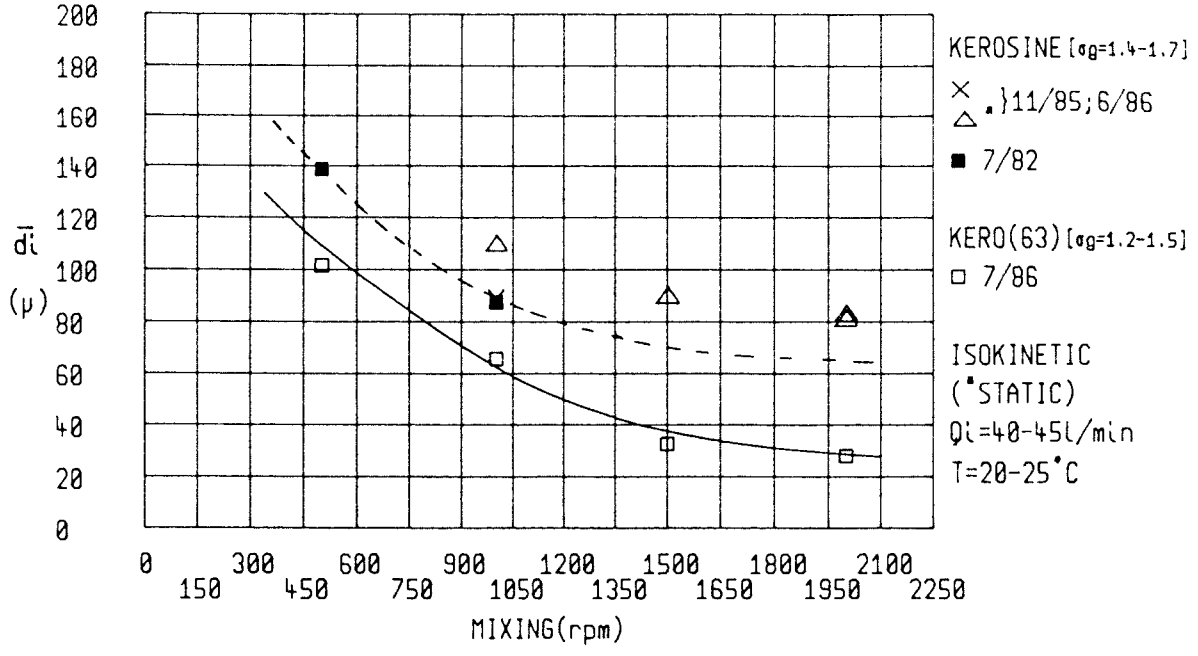

FIG.7.12 EFFECT OF WATER CONTENT ON DROP SIZE AT VARIOUS MIXING PUMP SPEEDS

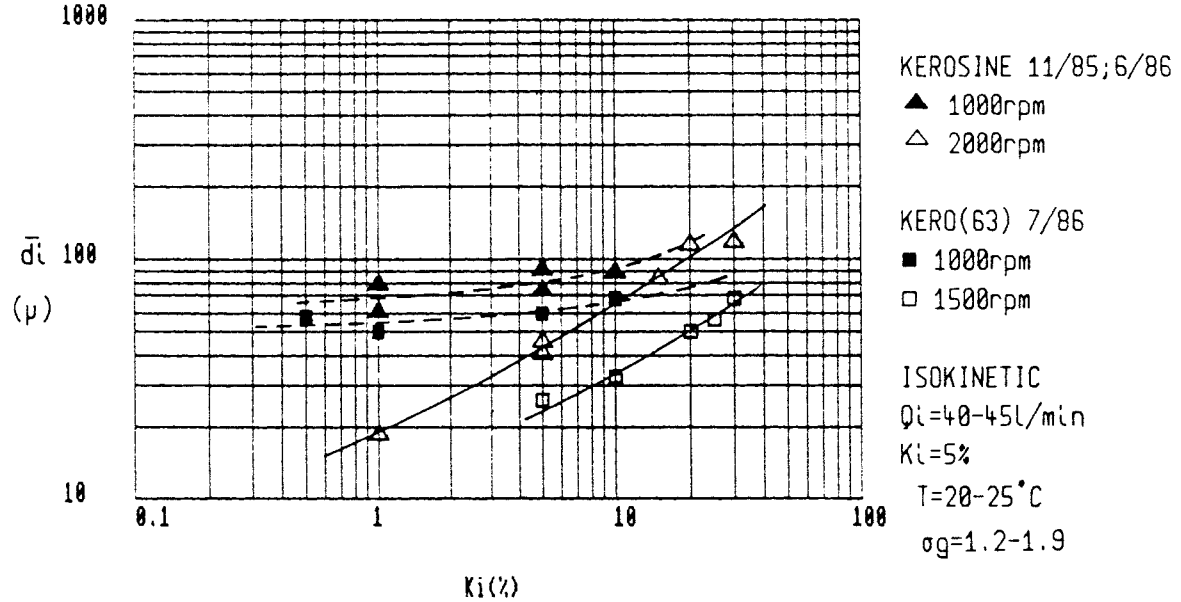

FIG.7.13 EFFECT OF FLOWRATE ON DROP SIZE AT VARIOUS MIXING PUMP SPEEDS

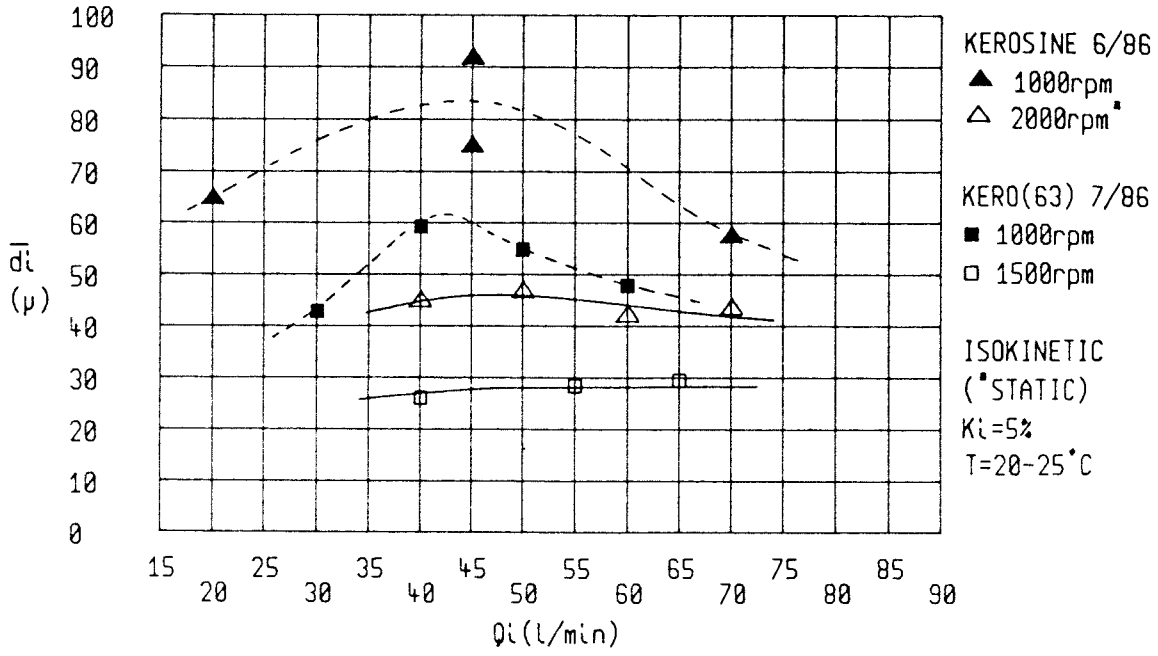

FIG.7.14 PRESSURE RISE THROUGH MIXING PUMP VS. FLOWRATE

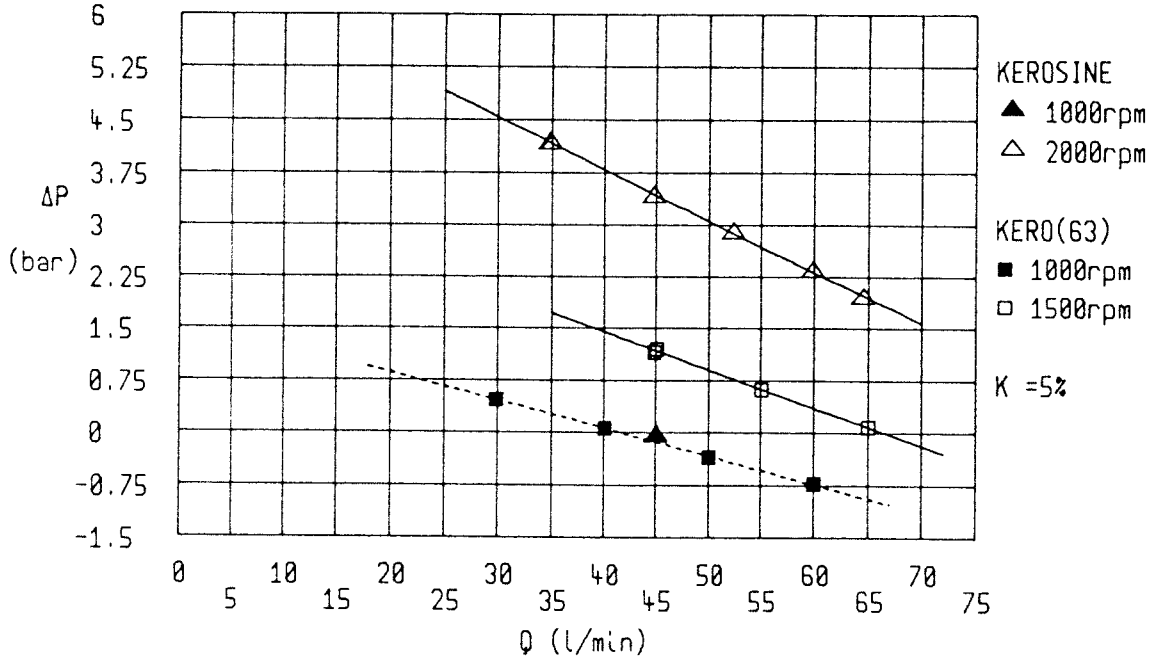

FIG.8.1 MICROPHOTOGRAPHIC TECHNIQUE FOR ANALYSIS OF NEAR WALL DISPERSIONS IN THE HYDROCYCLONE

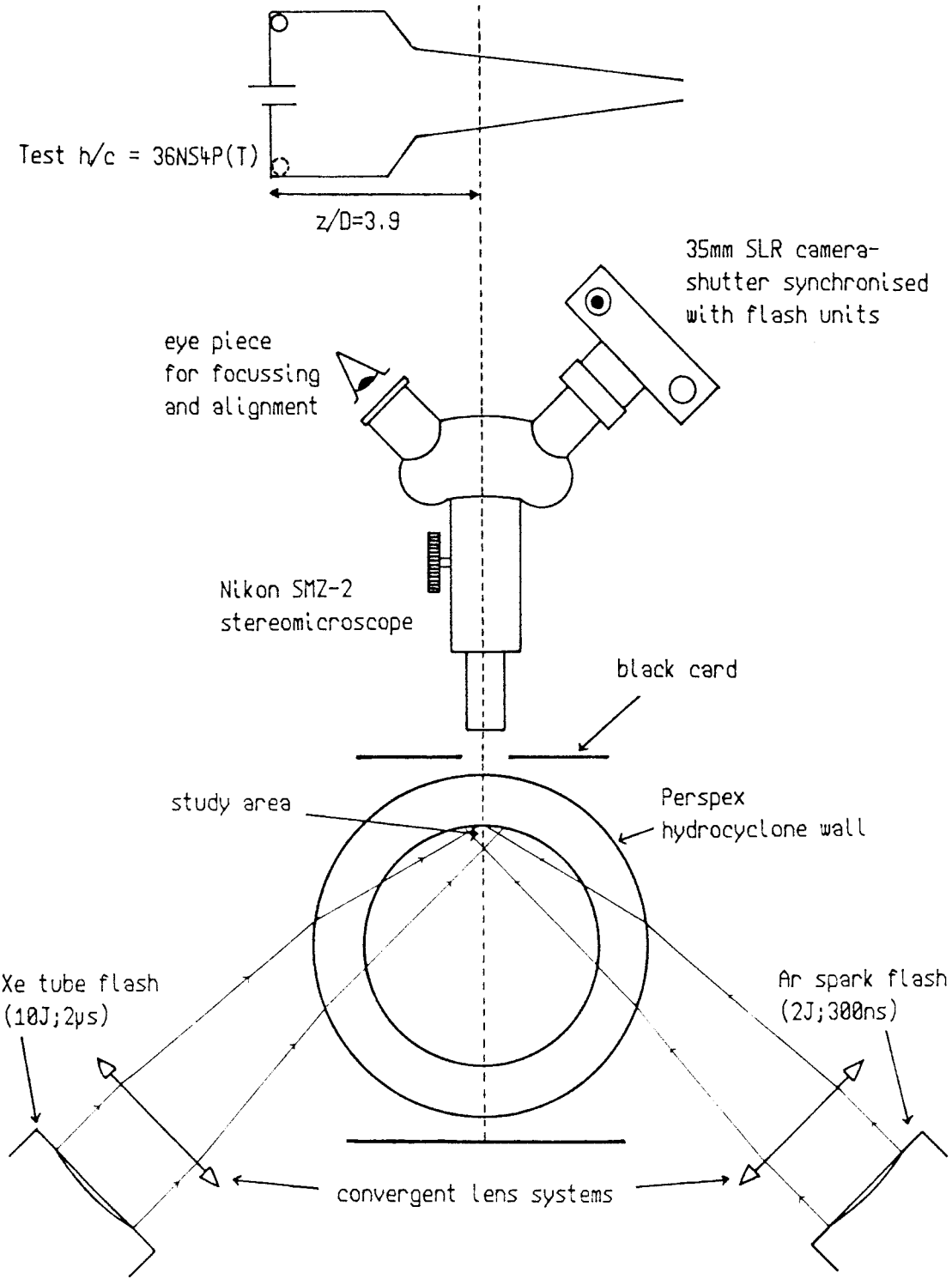

FIG.8.2 SCHEMATIC REPRESENTATION OF REGIONS OF DROP BREAKAGE AND COALESCENCE IN TURBULENT FLOW

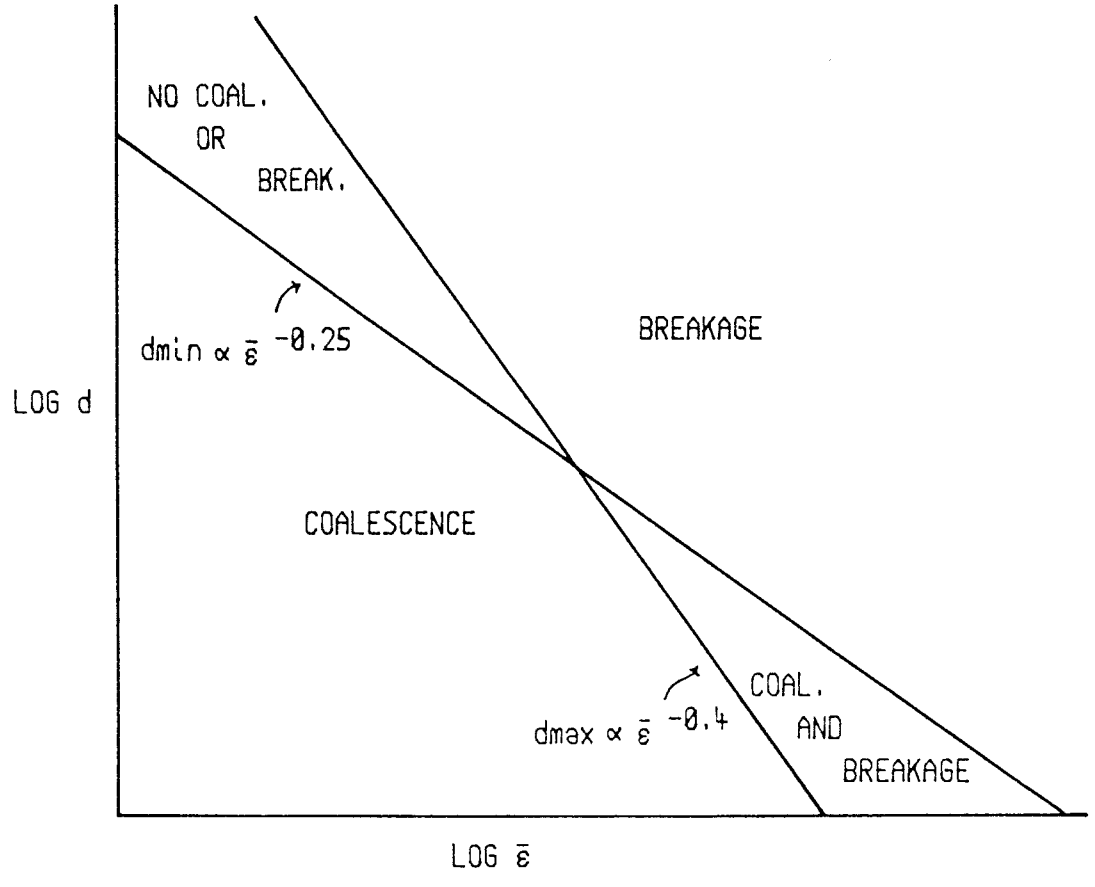

after Shinnar, 1961 [89]

FIG.9.1 EFFECT OF FLOWRATE ON PERFORMANCE - KEROSINE SYSTEMS

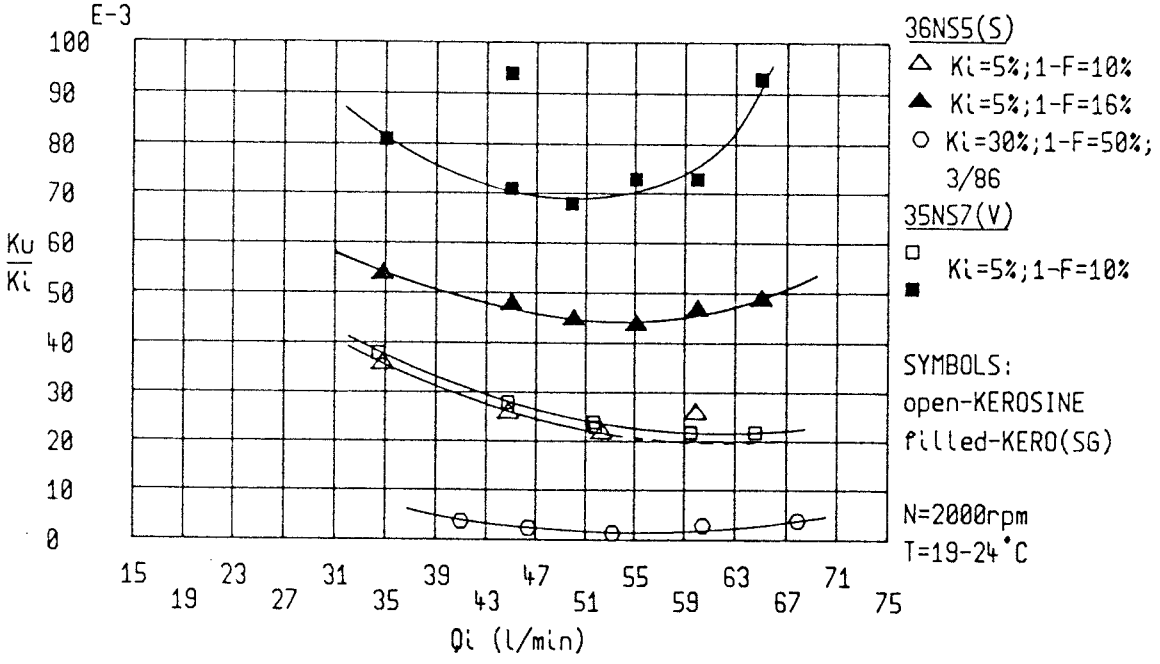

FIG.9.2 EFFECT OF FLOWRATE ON PERFORMANCE - KERO(63)

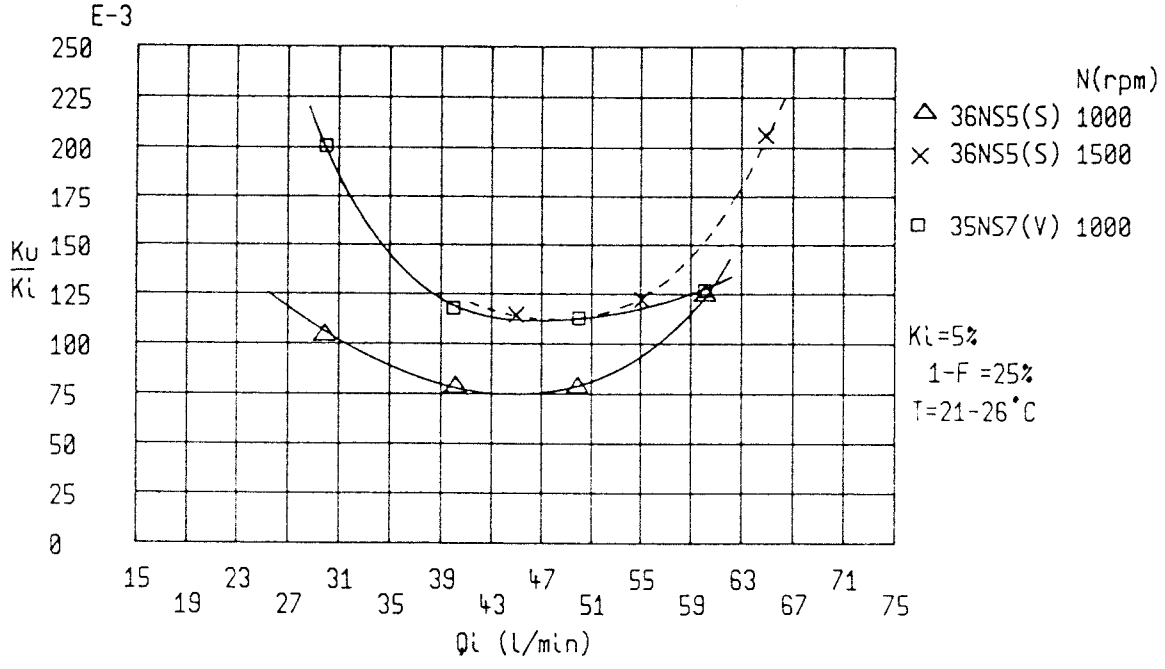

FIG.9.3 COMPARISON OF TEST GEOMETRIES - SEPARATION PERFORMANCE WITH KEROSINE

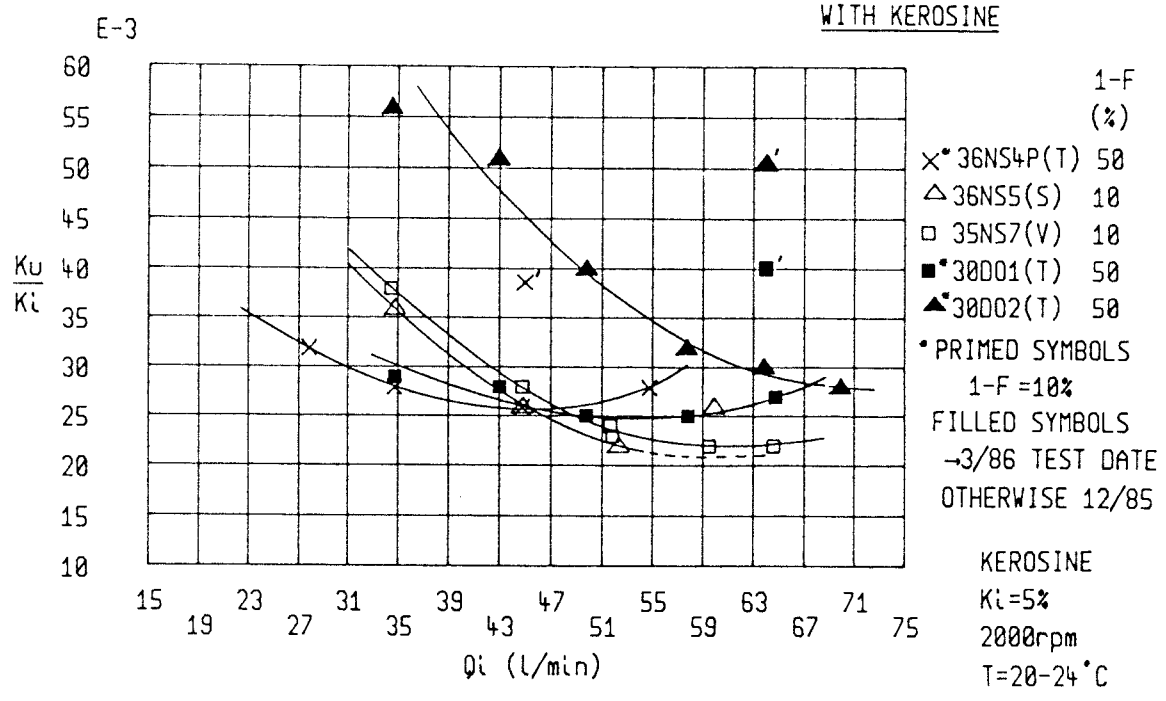

FIG.9.4 COMPARISON OF TEST GEOMETRIES - PRESSURE DROP WITH KEROSINE

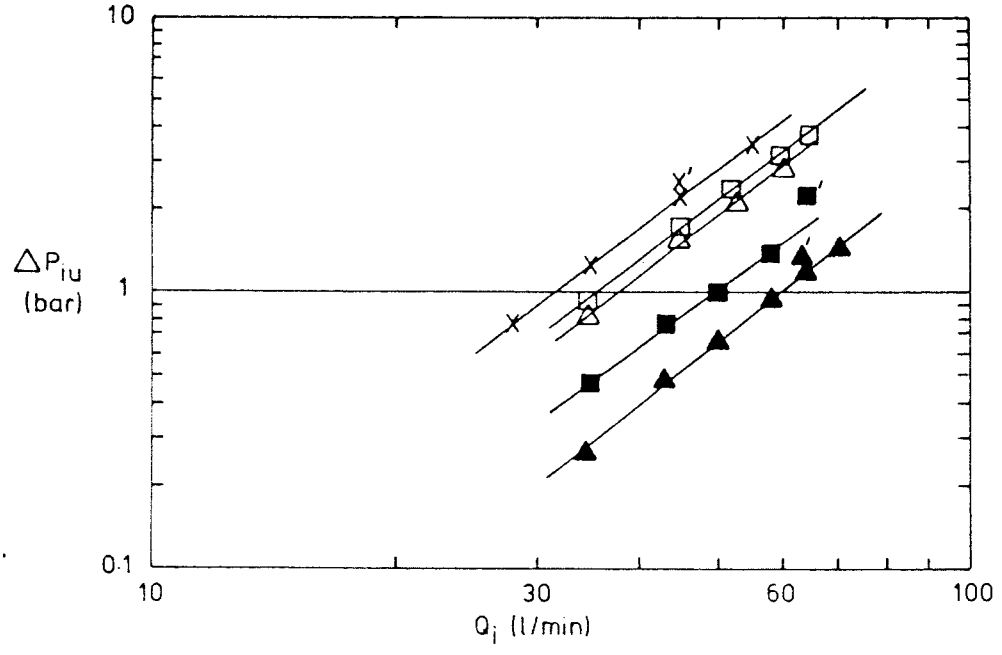

as Fig.9.3

FIG.9.5 CHARACTERISATION OF SEPARATION USING INLET VELOCITY FOR DIFFERENT SIZES OF NS4P(T)

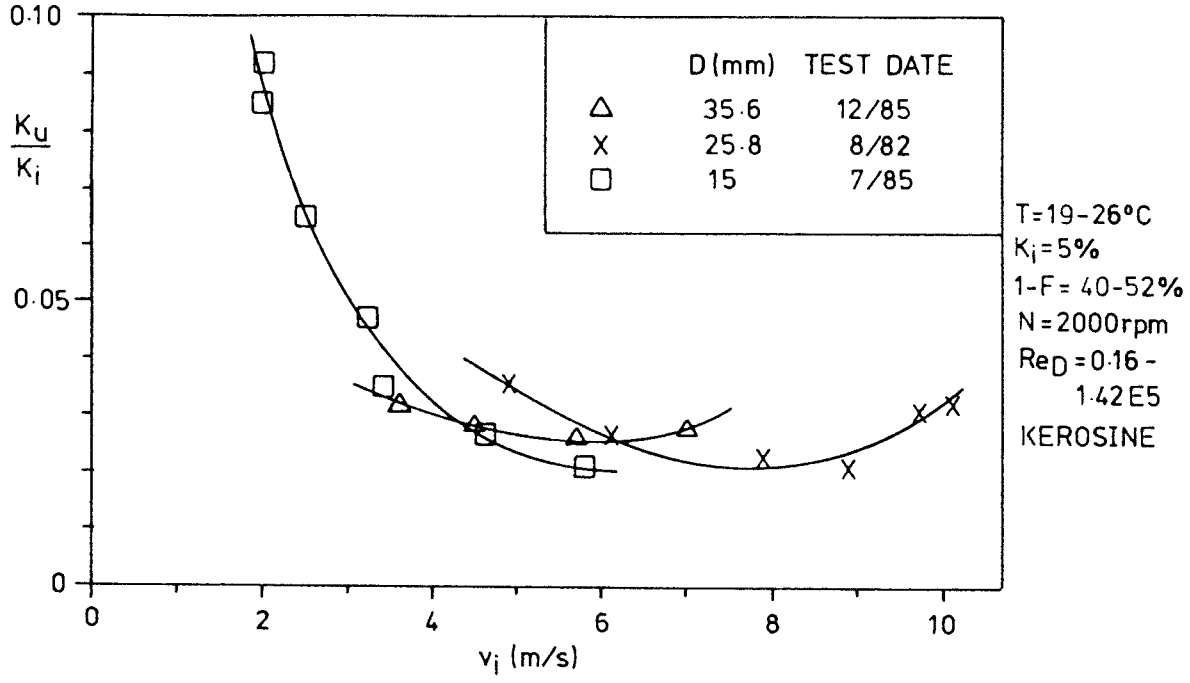

FIG.9.6 EFFECT OF OIL TYPE ON PRESSURE/SPLIT RELATIONSHIP

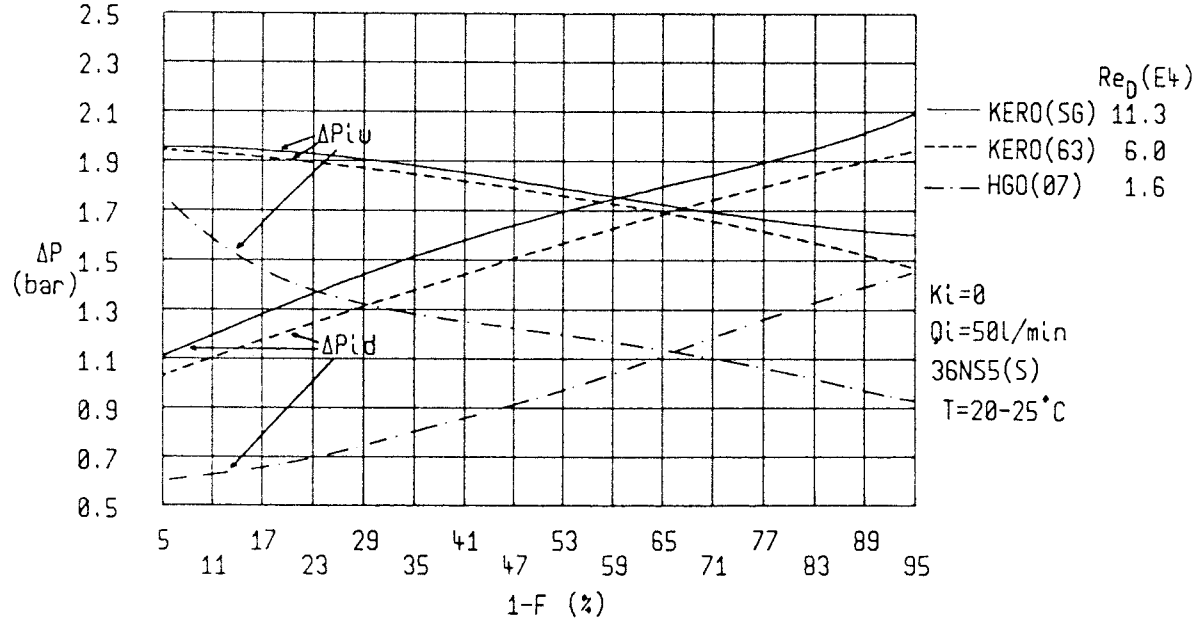

FIG.9.7 EFFECT OF SPLIT ON EFFICIENCY PARAMETERS FOR PRACTICAL SEPARATION TESTS

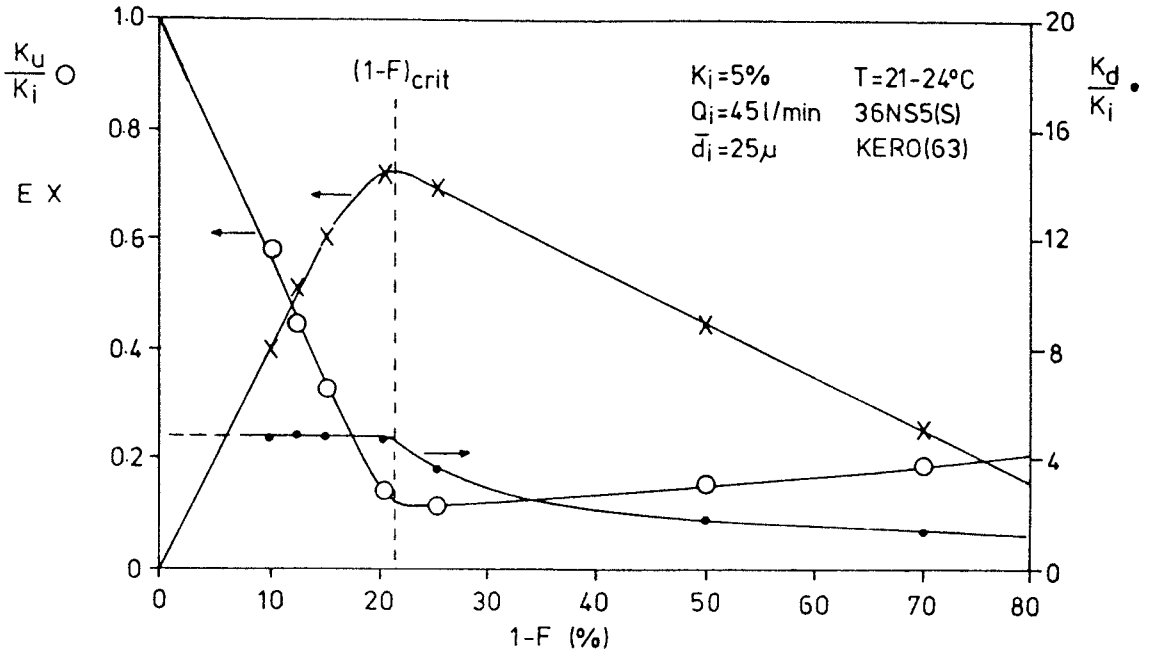

FIG.9.8 EFFECT OF SPLIT ON PERFORMANCE - KEROSINE, K_i=5-25%

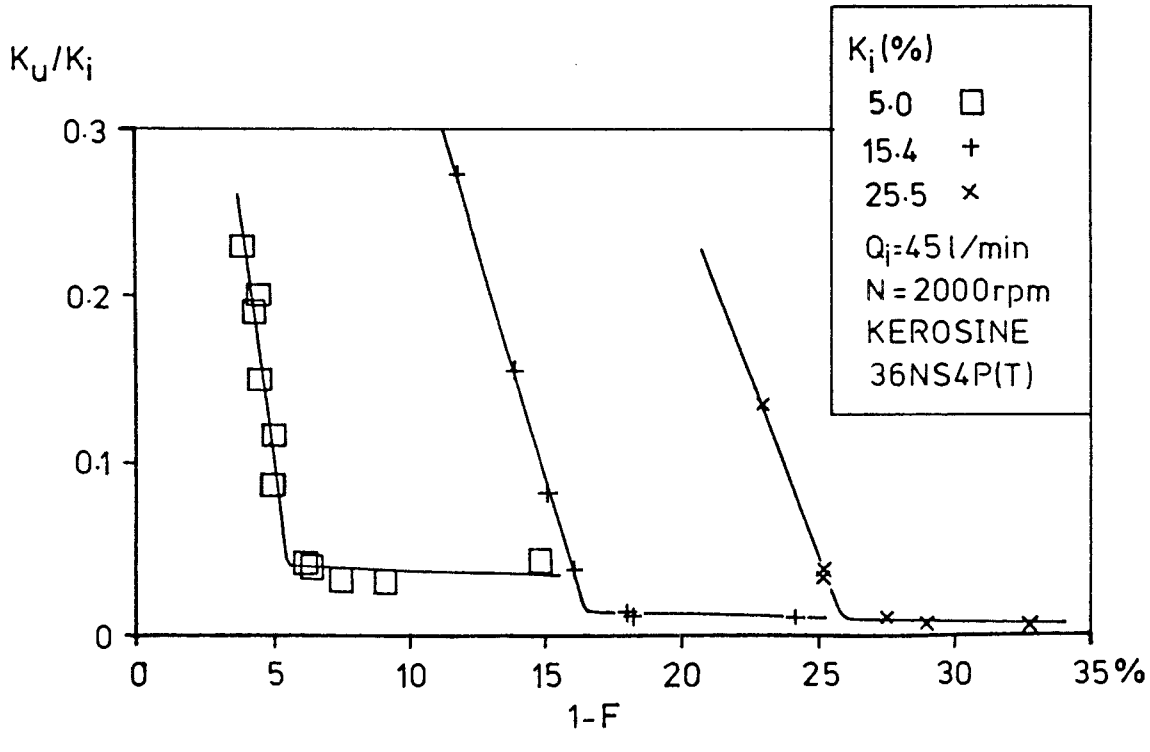

FIG.9.9 EFFECT OF SPLIT ON PERFORMANCE - KEROSINE, Ki=20-45%, VARIOUS GEOMETRIES

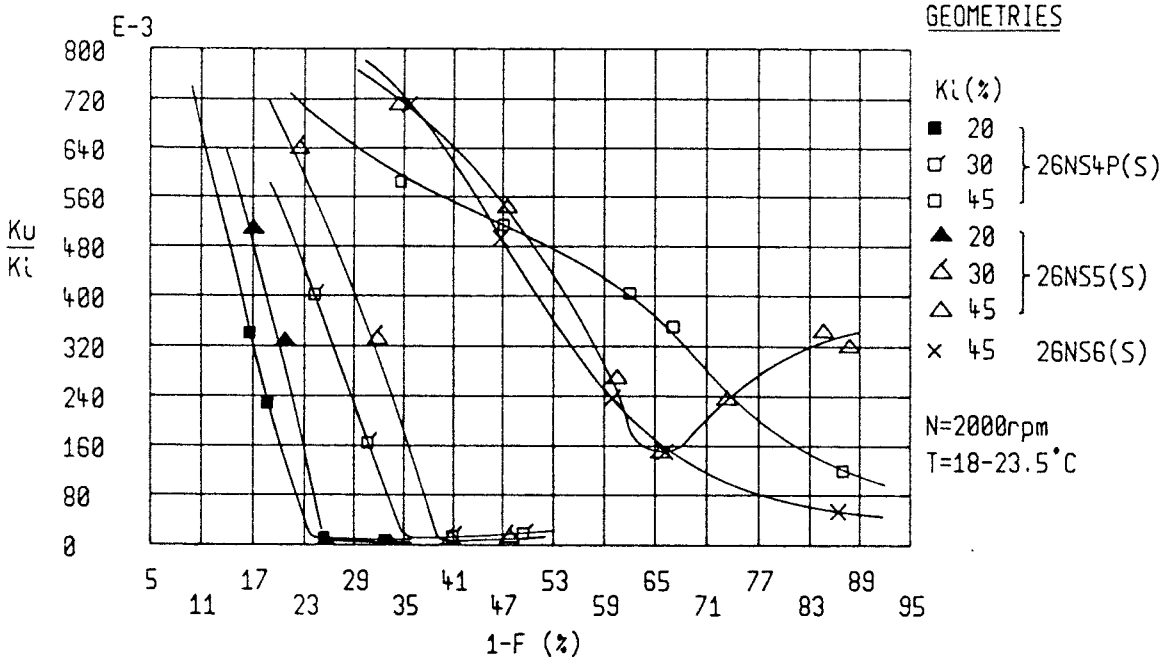

FIG.9.10 EFFECT OF SPLIT ON PERFORMANCE - Ki=5%, VARIOUS OILS

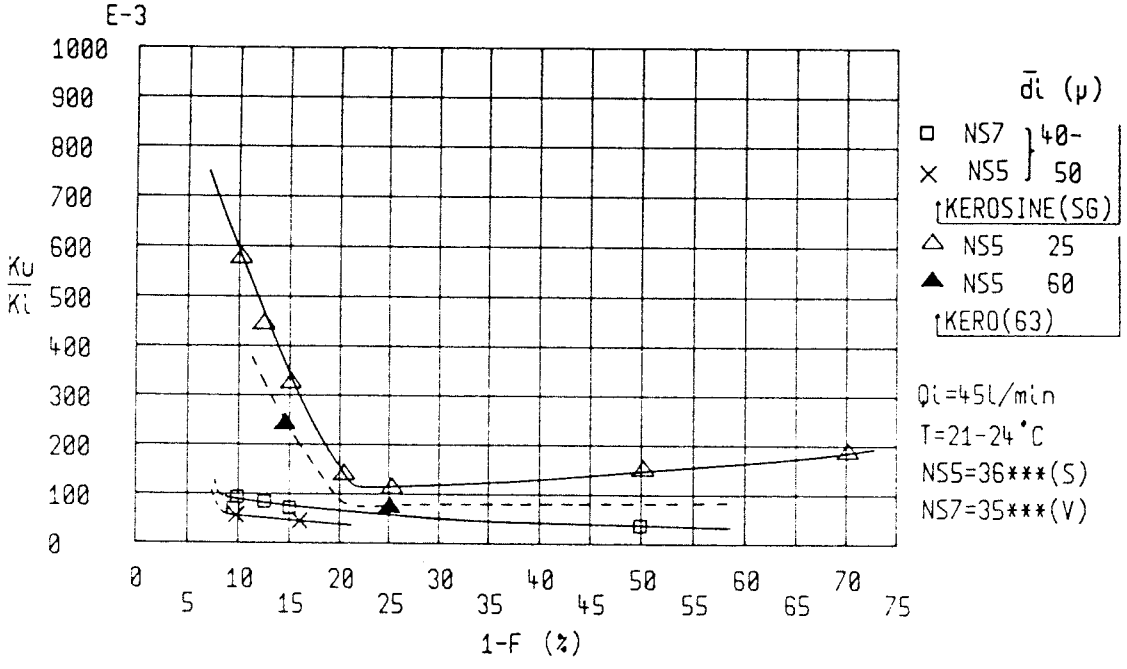

FIG.9.11 EFFECT OF SPLIT ON PERFORMANCE - HIGH Ki, VARIOUS OILS

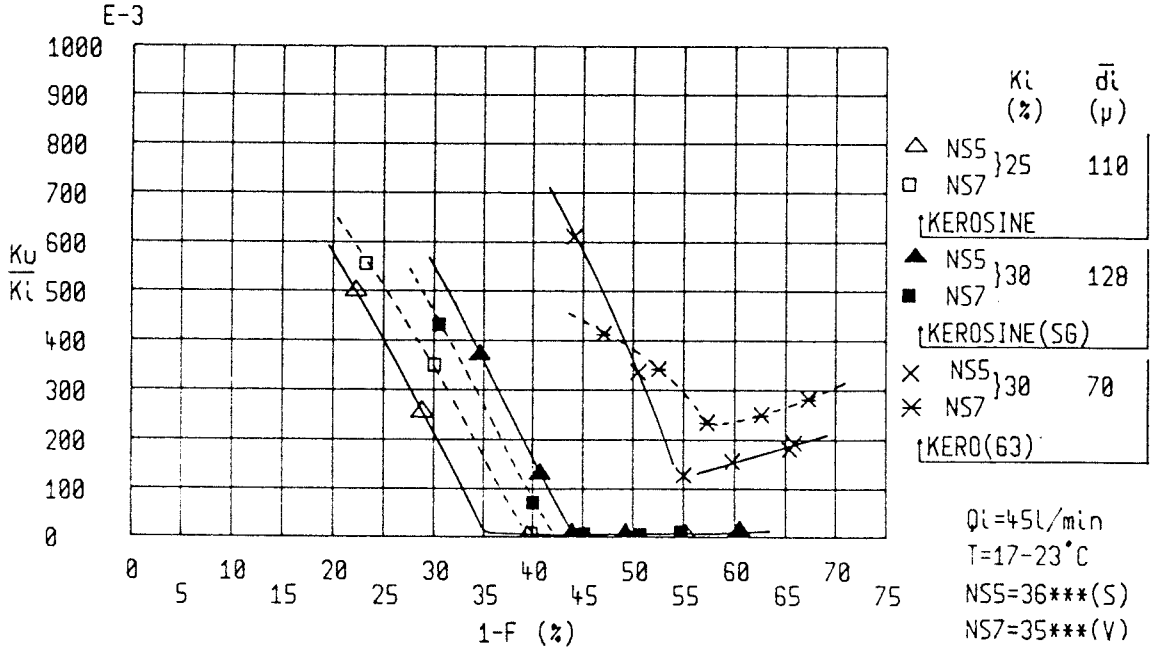

FIG.9.12 DEPENDENCY OF CRITICAL SPLIT RATIO ON Ki AND OIL TYPE

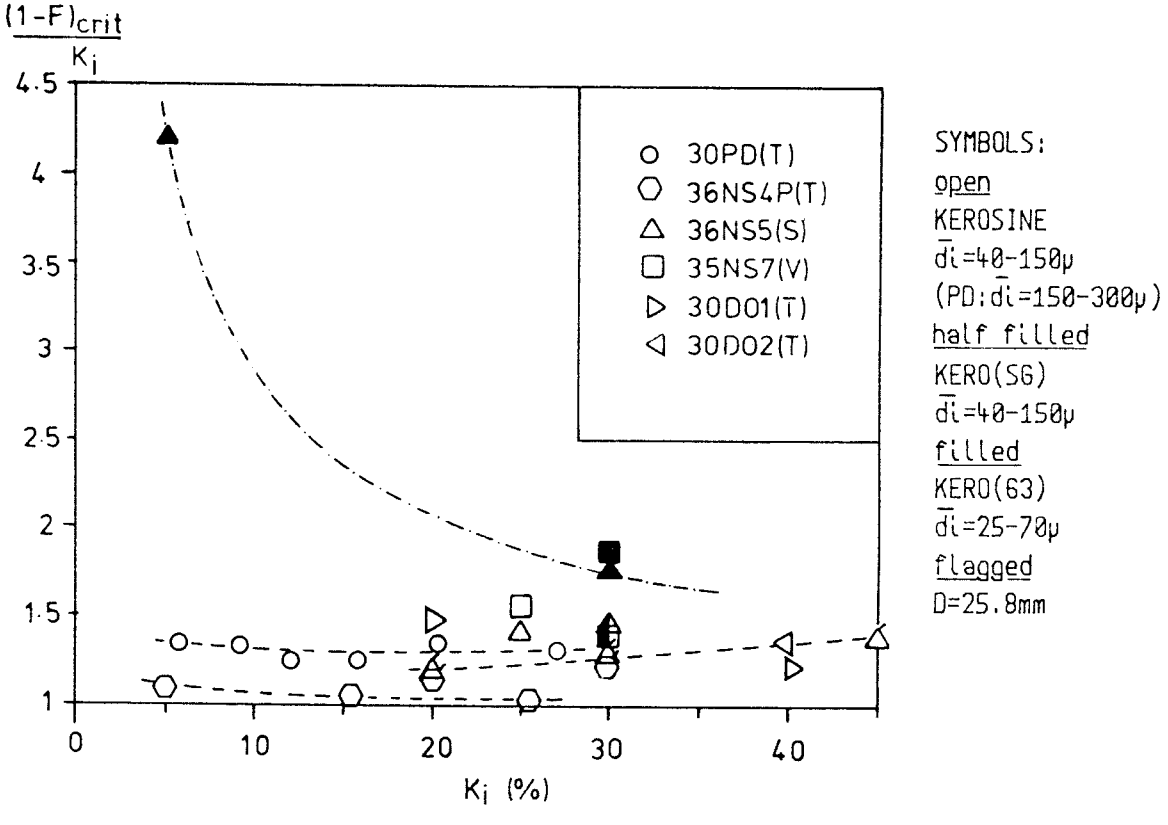

FIG.9.13 EFFECT OF WATER CONTENT ON PERFORMANCE

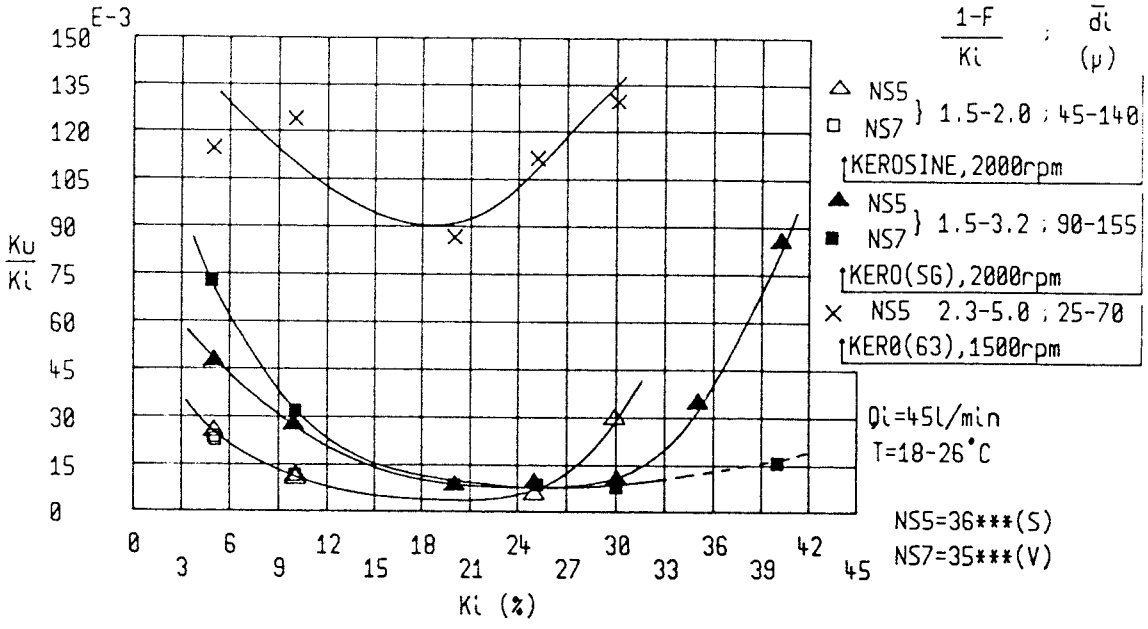

FIG.9.14 EXPECTED Ku FOR VARIABLE Ki (GENERALISED RELATIONSHIP)

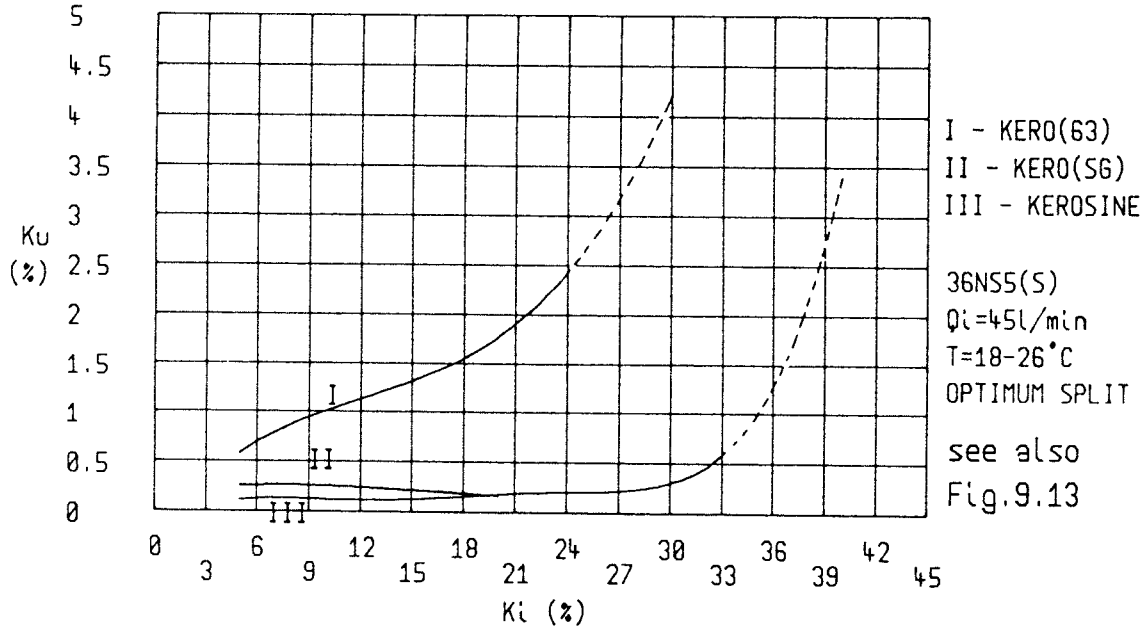

FIG.9.15 EFFECT OF WATER CONTENT (UP TO 55%) ON PERFORMANCE OF D=15mm GEOMETRIES

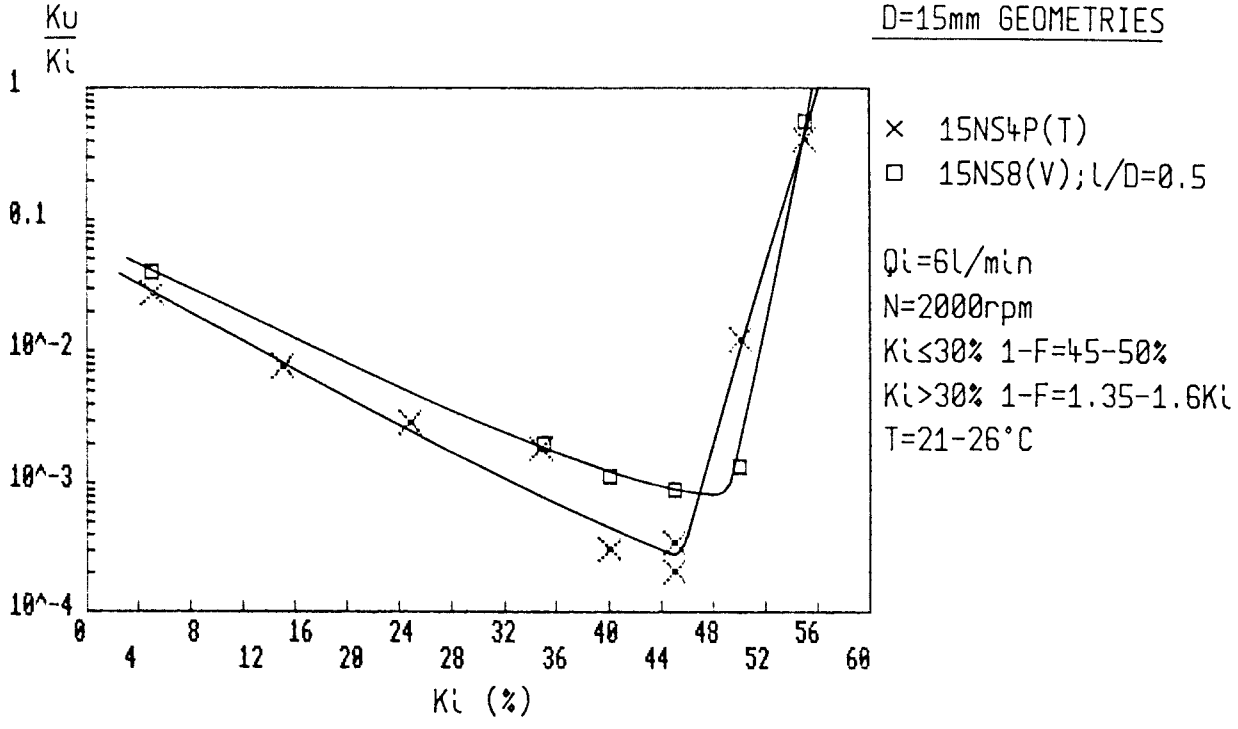

FIG.9.16 PRESSURE/SPLIT RELATIONSHIP AT HIGH Ki

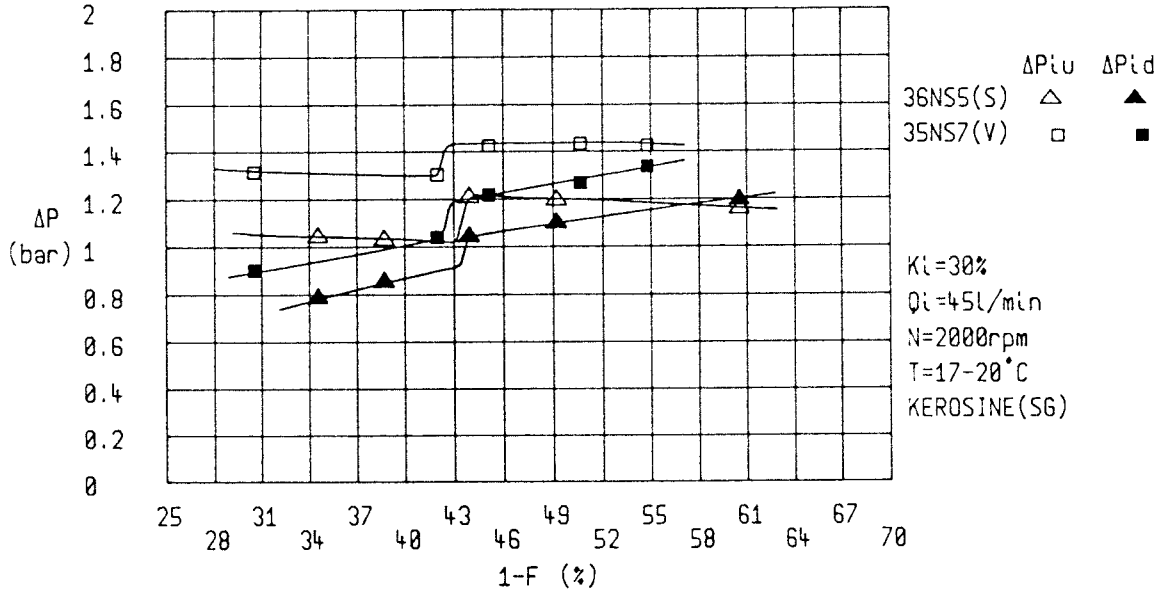

FIG.9.17 EFFECT OF MIXING ON PERFORMANCE - KEROSINE

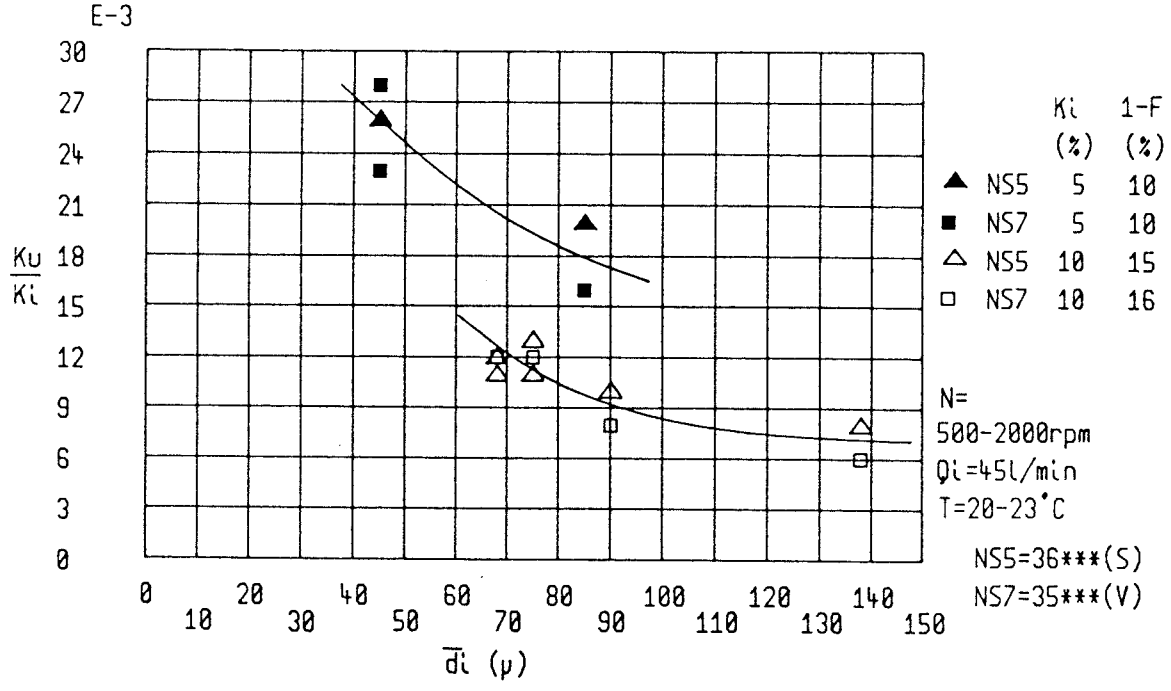

FIG.9.18 EFFECT OF MIXING ON PERFORMANCE - KERO(63)

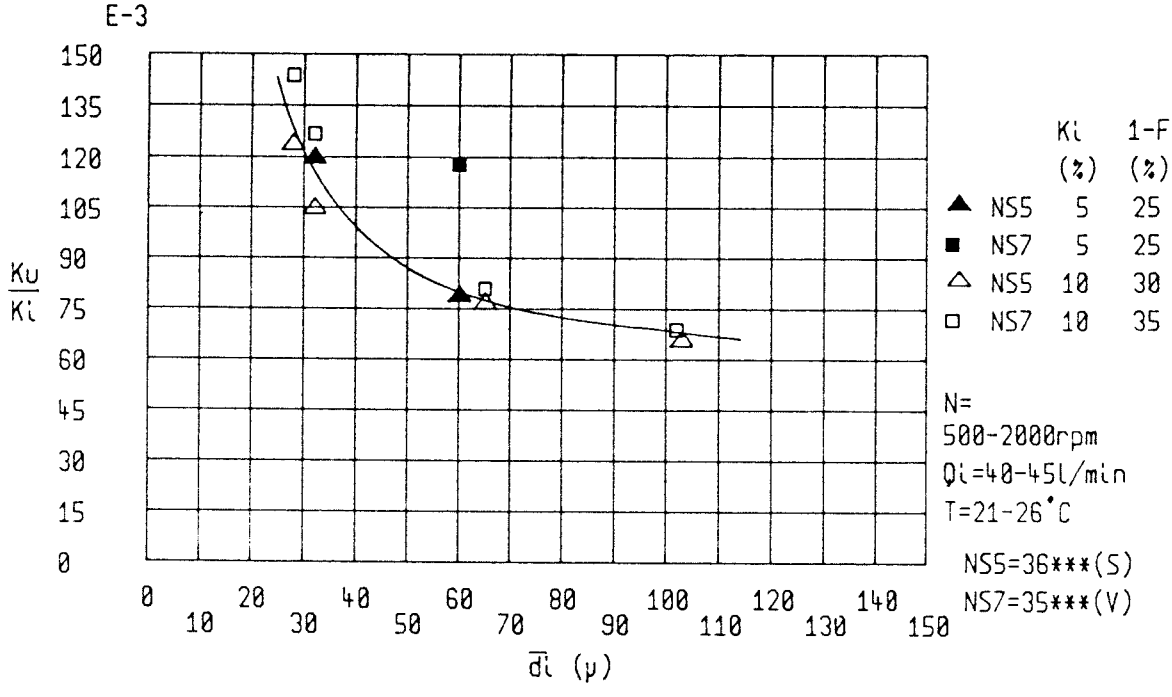

FIG.9.19 EFFECT OF FLOWRATE ON PERFORMANCE - HGO(07)

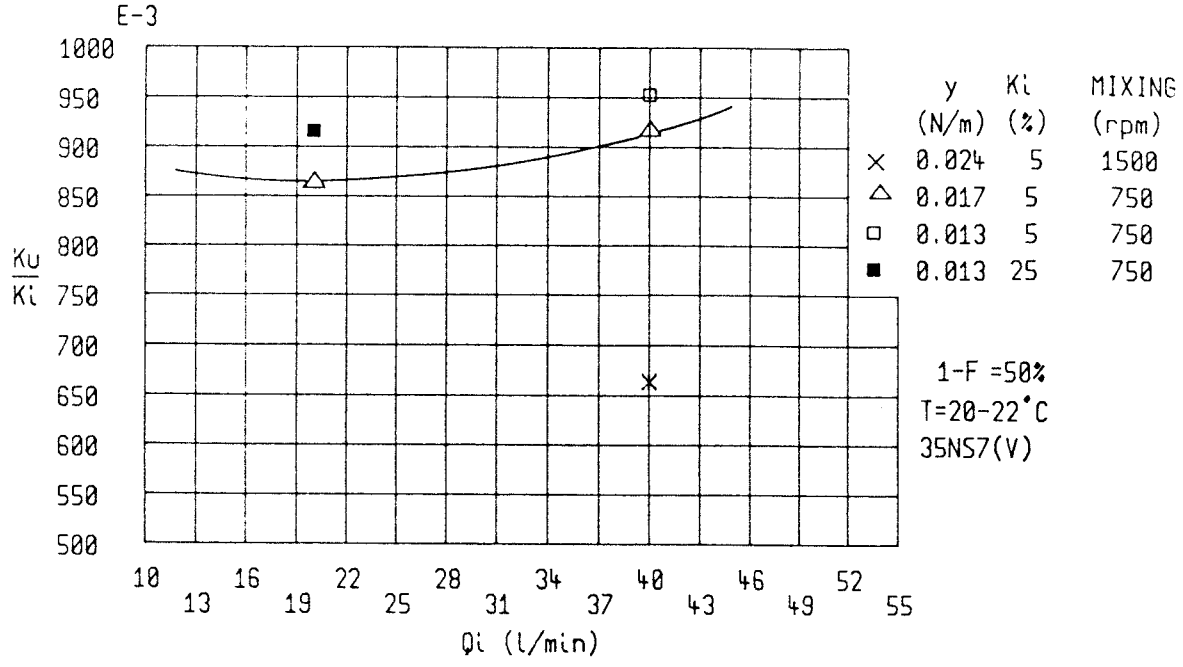

FIG.9.20 EFFECT OF OIL VISCOSITY ON PERFORMANCE (GENERALISED RELATIONSHIP)

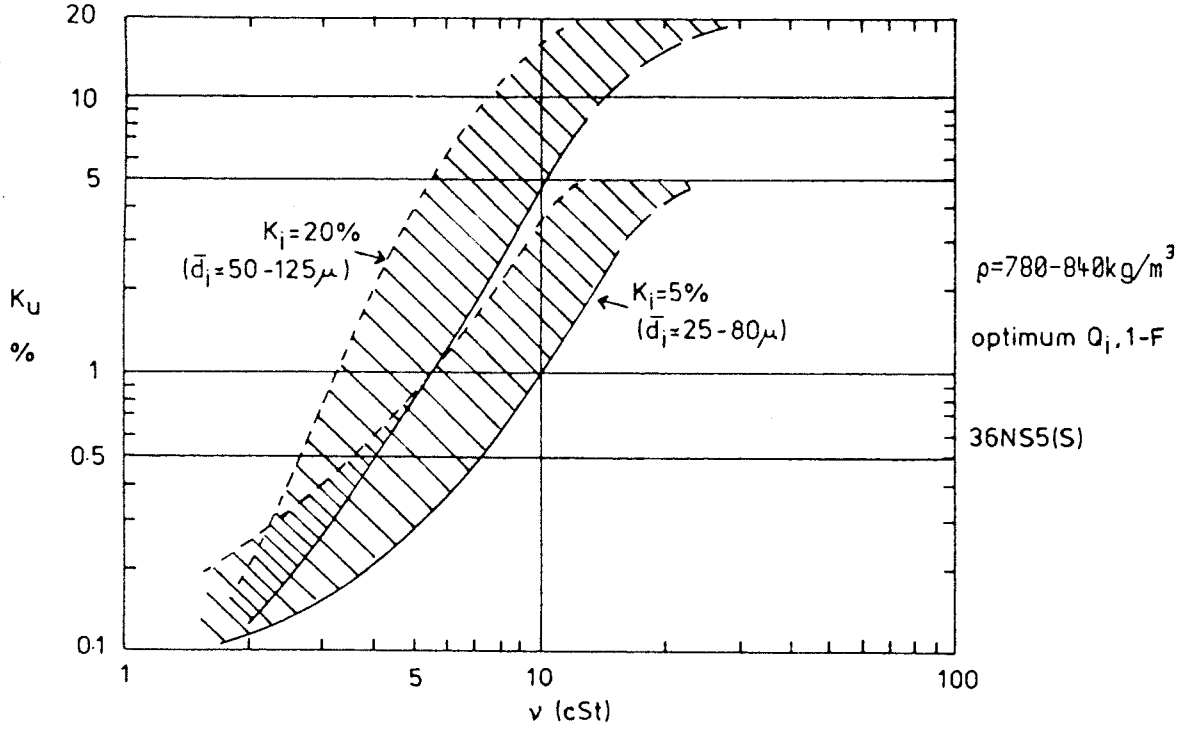

FIG.9.21 PERFORMANCE CHARACTERISATION USING Ku/Ki AND Hy($\bar{d}$)

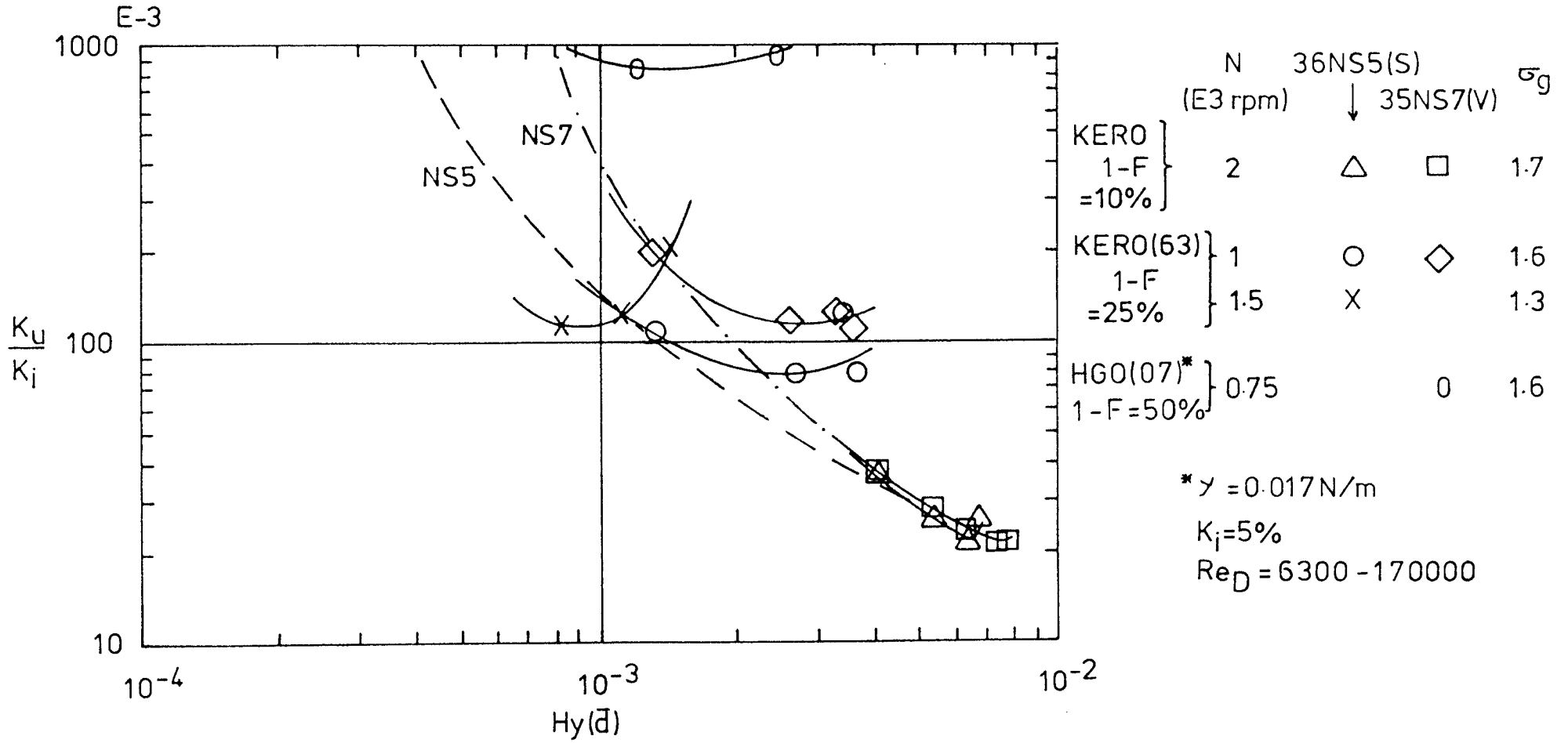

FIG.9.22 PRESSURE DROP COEFFICIENT/REYNOLDS NUMBER RELATIONSHIP

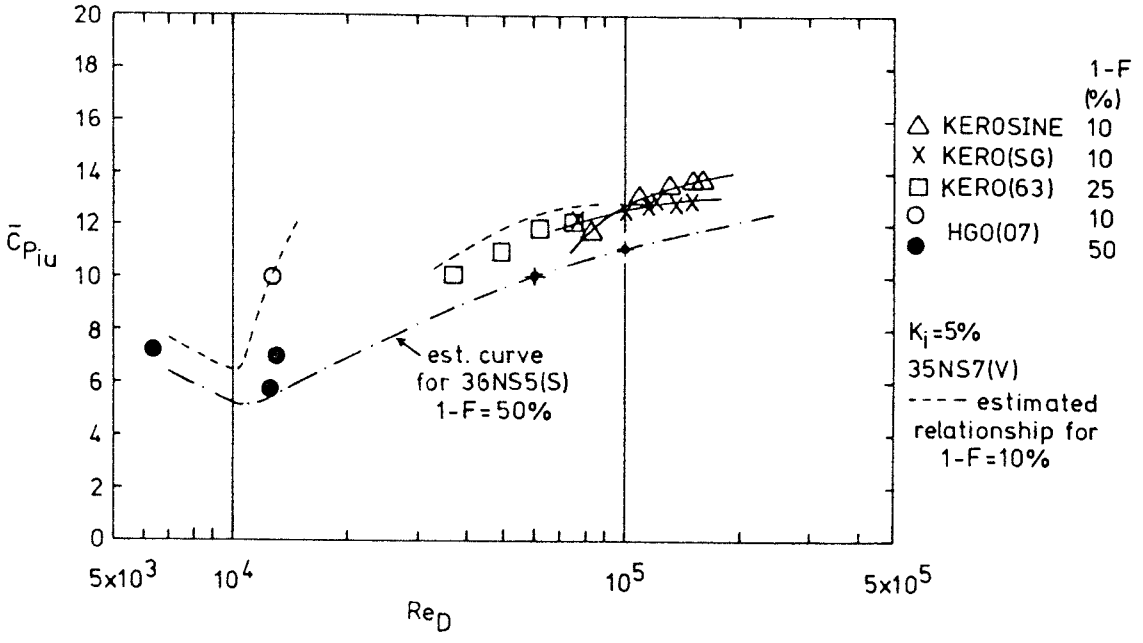

FIG.9.23 CHARACTERISATION OF SEPARATION USING $Hy(\bar{d})$ FOR DIFFERENT SIZES OF NS4P(T)

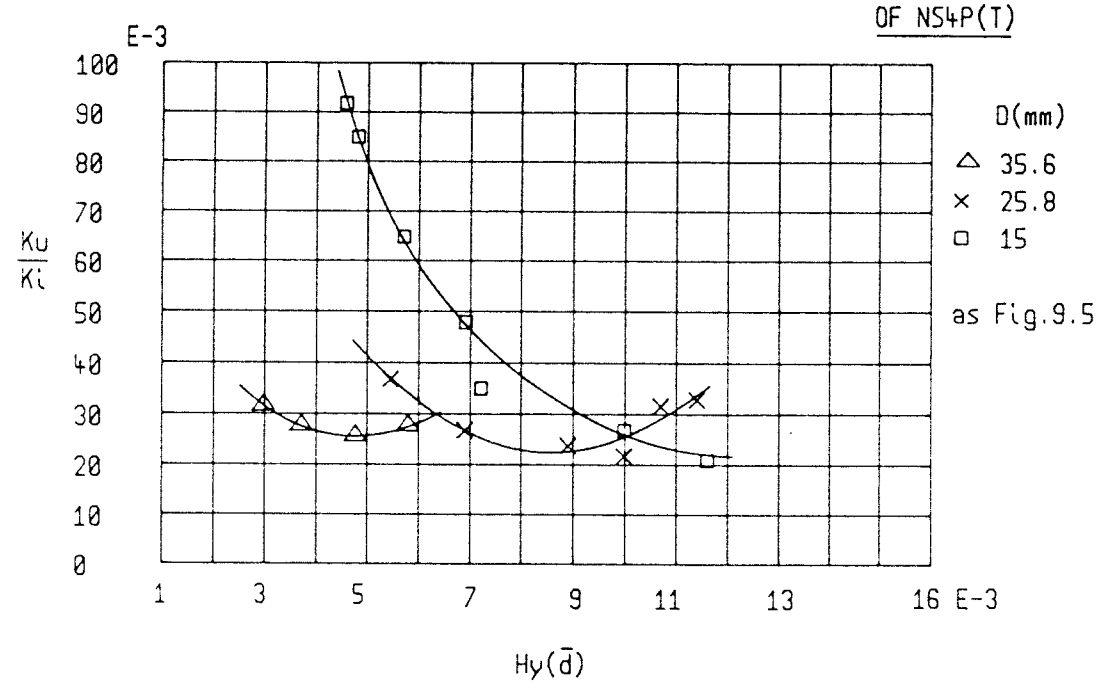

FIG.9.24 PRESSURE DROP COEFFICIENT (UPSTREAM)/REYNOLDS NUMBER RELATIONSHIP INCORPORATING SPLIT AND Ki EFFECTS - 35NS7(V)

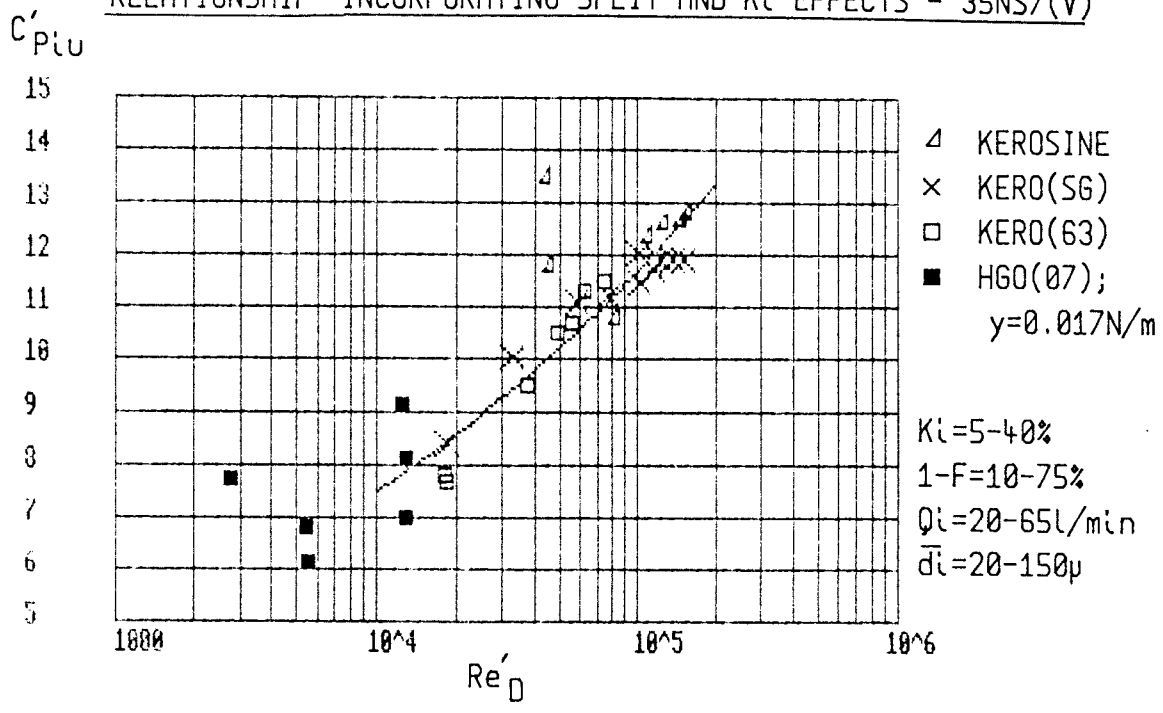

FIG.9.25 PRESSURE DROP COEFFICIENT (DOWNSTREAM)/REYNOLDS NUMBER RELATIONSHIP INCORPORATING SPLIT AND Ki EFFECTS - 35NS7(V)

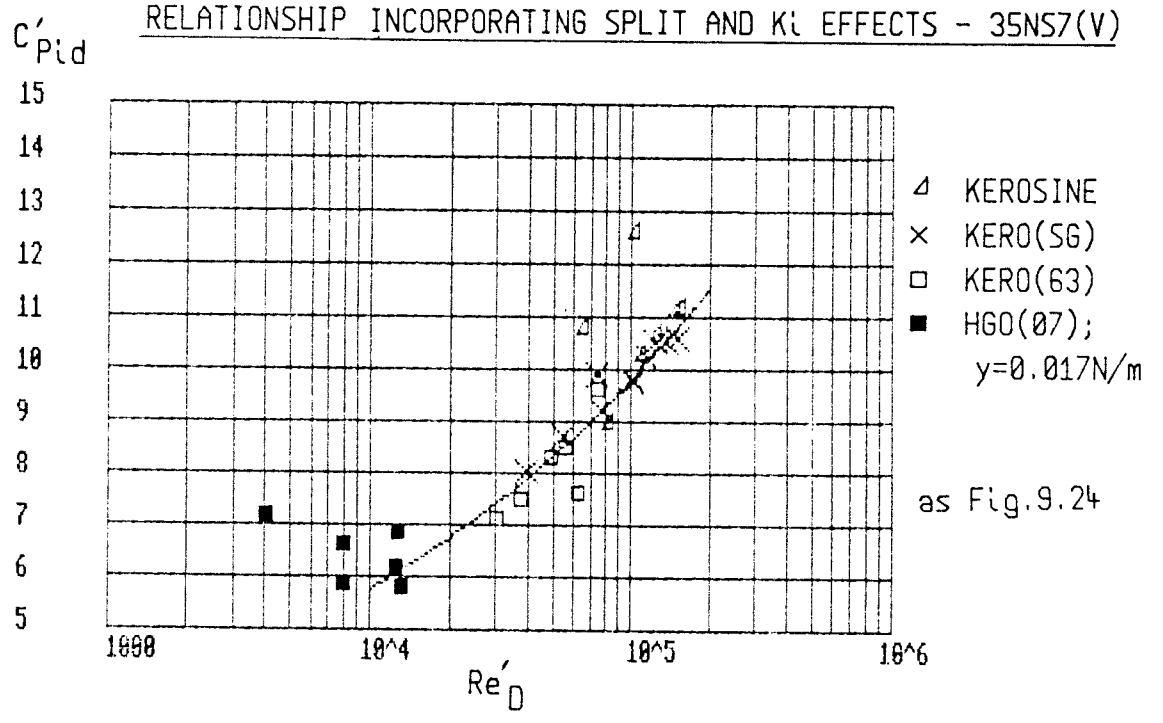

FIG.9.26 ACCOMMODATION OF HYDROCYCLONE SIZE CHANGES ON PRESSURE DROP/ REYNOLDS NUMBER PLOT

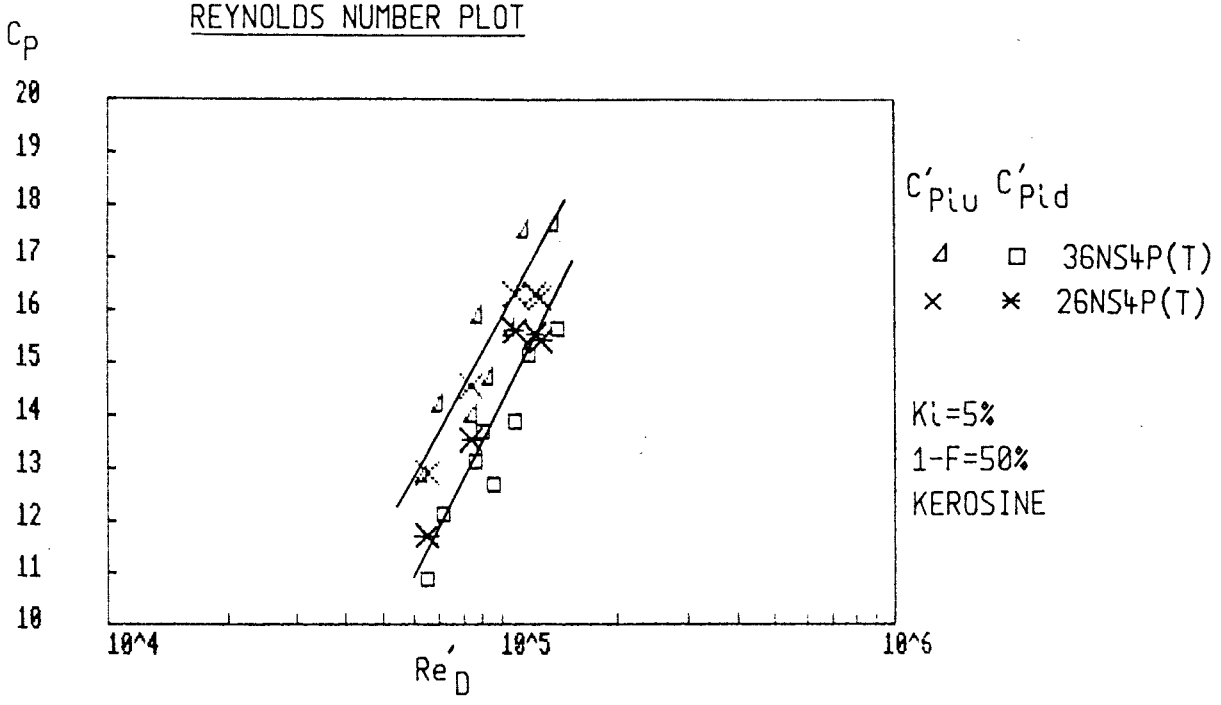

FIG.9.27 EFFECT OF FEED FLOWRATE AND VORTEX FINDER LENGTH ON PERFORMANCE - D=15mm GEOMETRIES

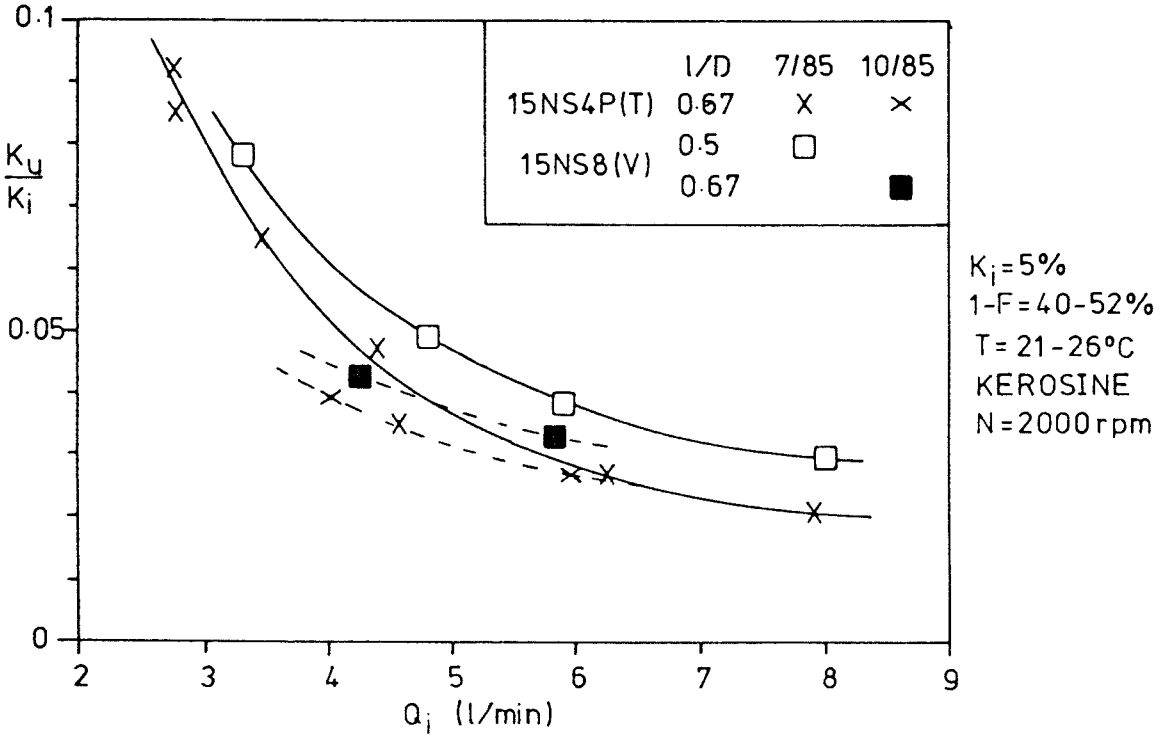

FIG.9.28 COMPARISON OF PERFORMANCE BETWEEN SINGLE AND TWIN INLET GEOMETRIES

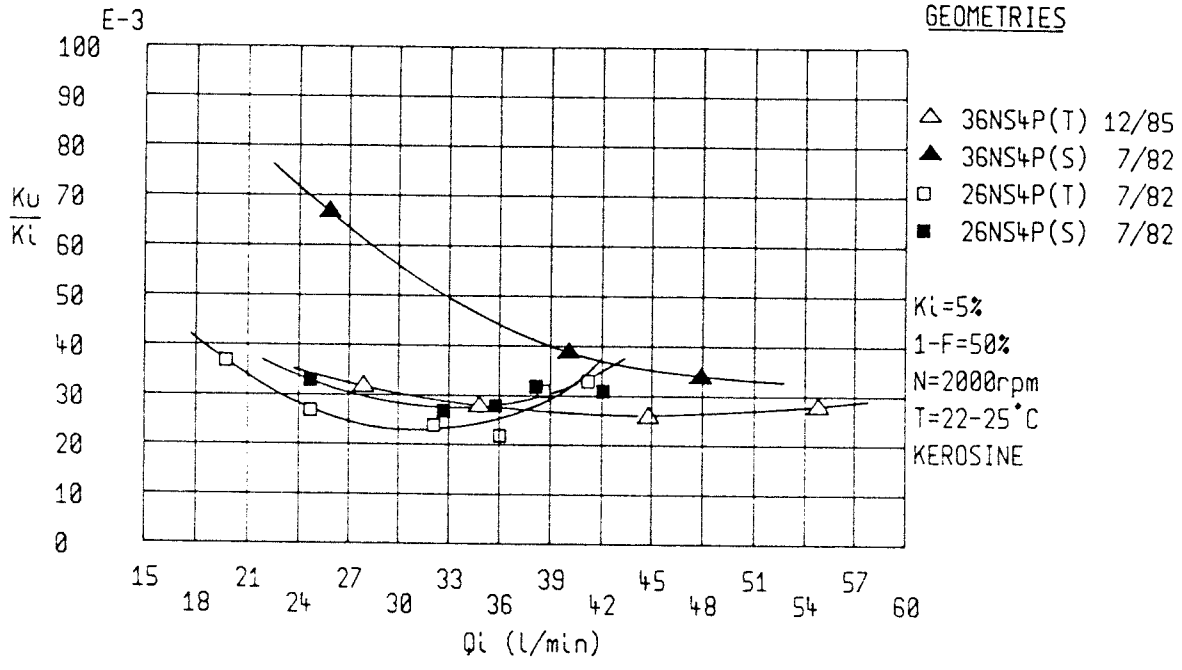

FIG.9.29 EFFECT OF WATER CONTENT ON PERFORMANCE - MODIFIED DEOILER GEOMETRIES

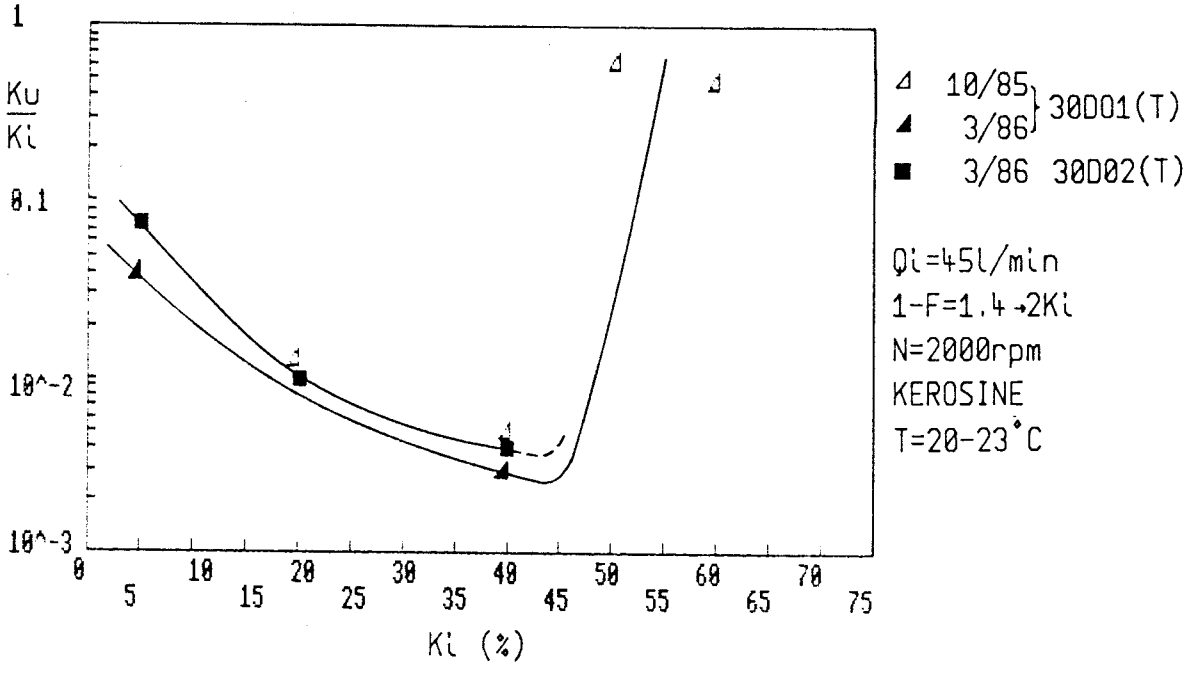

FIG.9.30 EFFECT OF VORTEX FINDER LENGTH ON PERFORMANCE - MODIFIED DEOILER GEOMETRIES

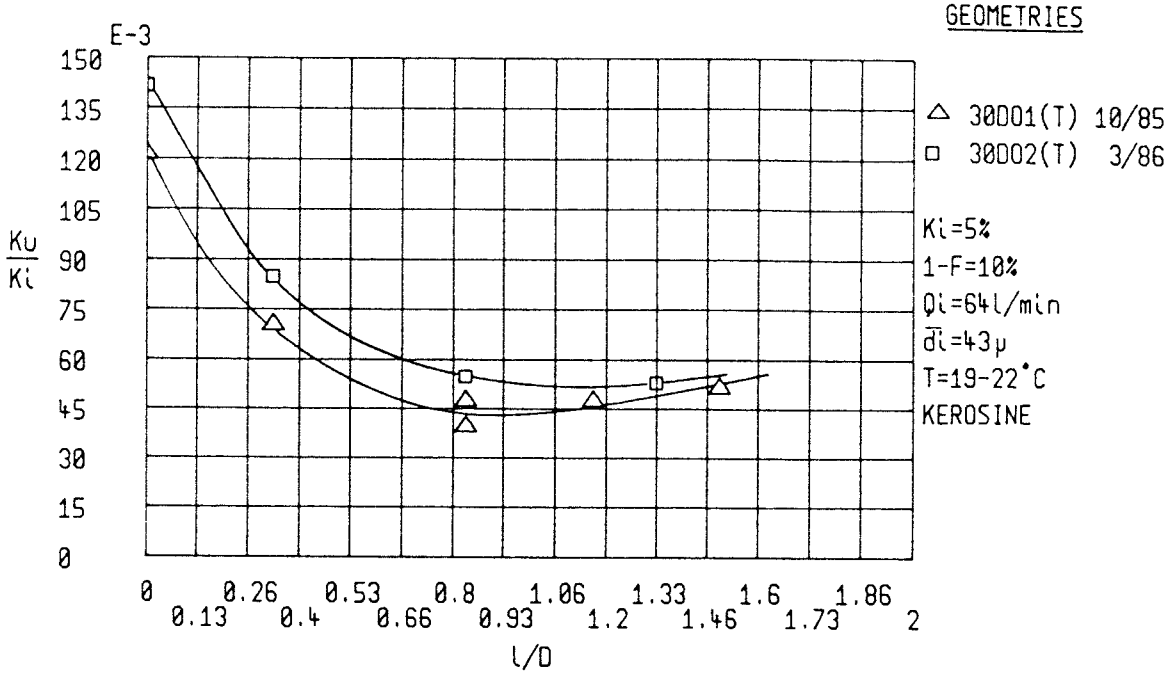

FIG.9.31 EFFECT OF CHANGES TO THE DOWNSTREAM OUTLET ON SEPARATION - VARIABLE Ki,KEROSINE

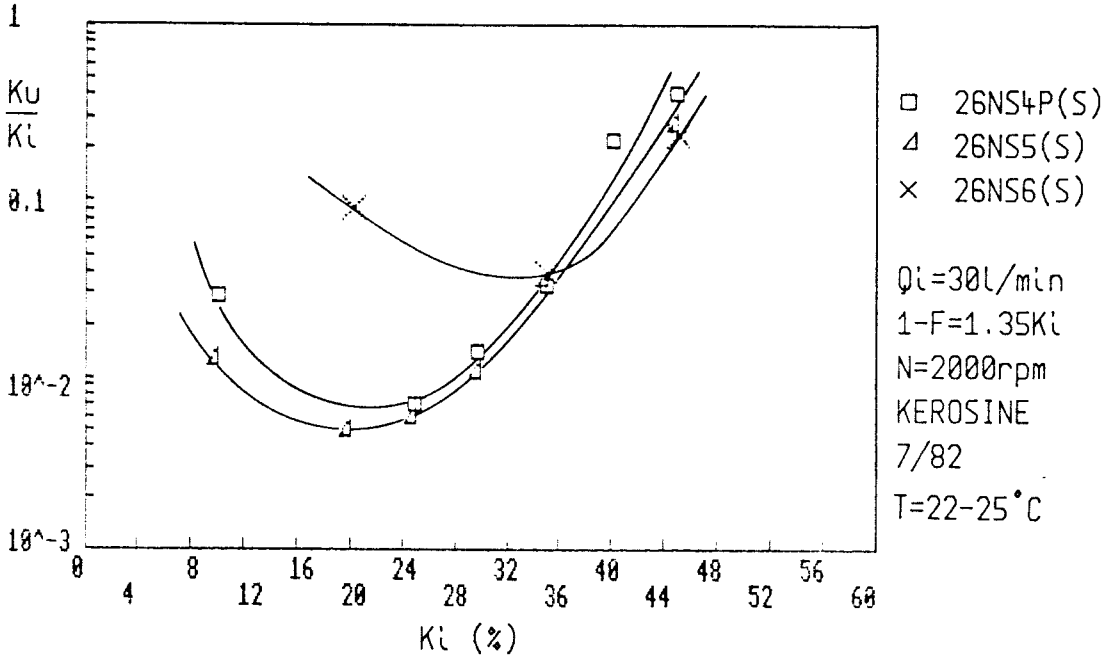

FIG.9.32 EFFECT OF CHANGES TO THE DOWNSTREAM OUTLET ON PRESSURE DROP - VARIABLE Qi, KEROSINE

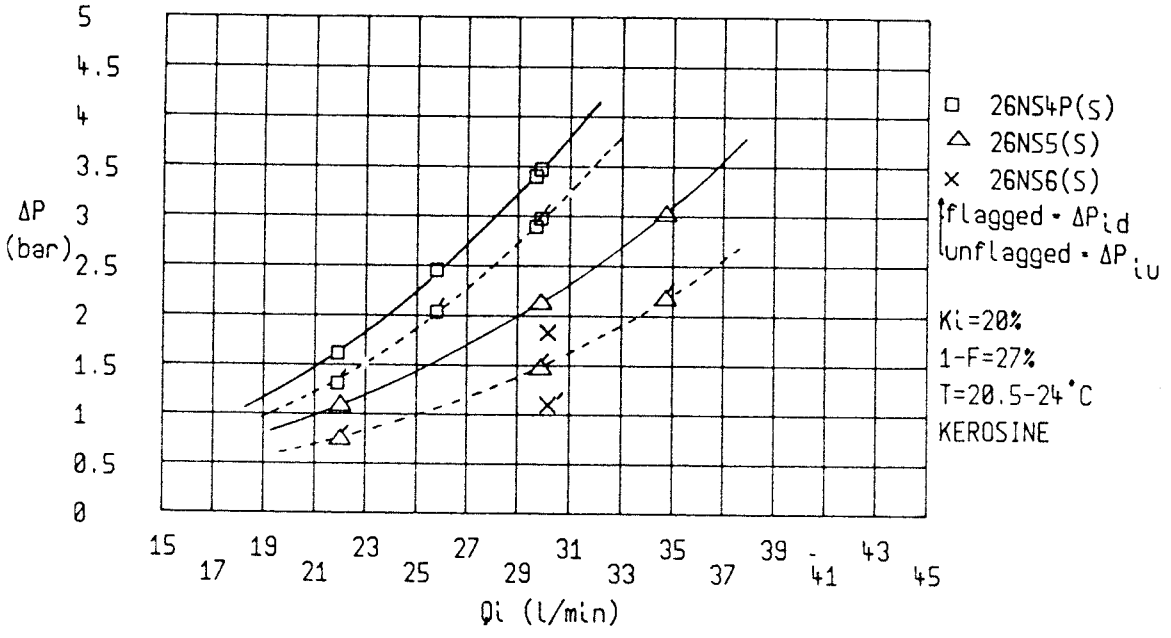

FIG.10.1 M.O.L. PUMP SEAL TEST RIG AT SUNBURY

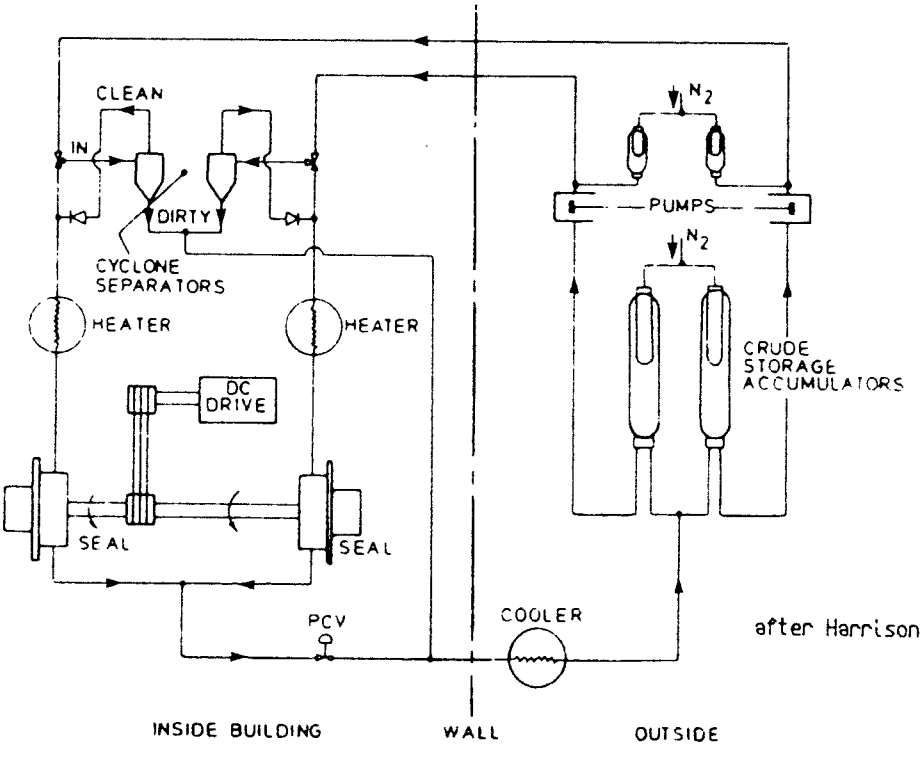

after Harrison et al.[50]

FIG.10.2 COMPARISON OF HYDROCYCLONE TEST RESULTS BETWEEN WATER-KEROSINE SYSTEM AT THE UNIVERSITY AND FORTIES SIMULATION AT SUNBURY

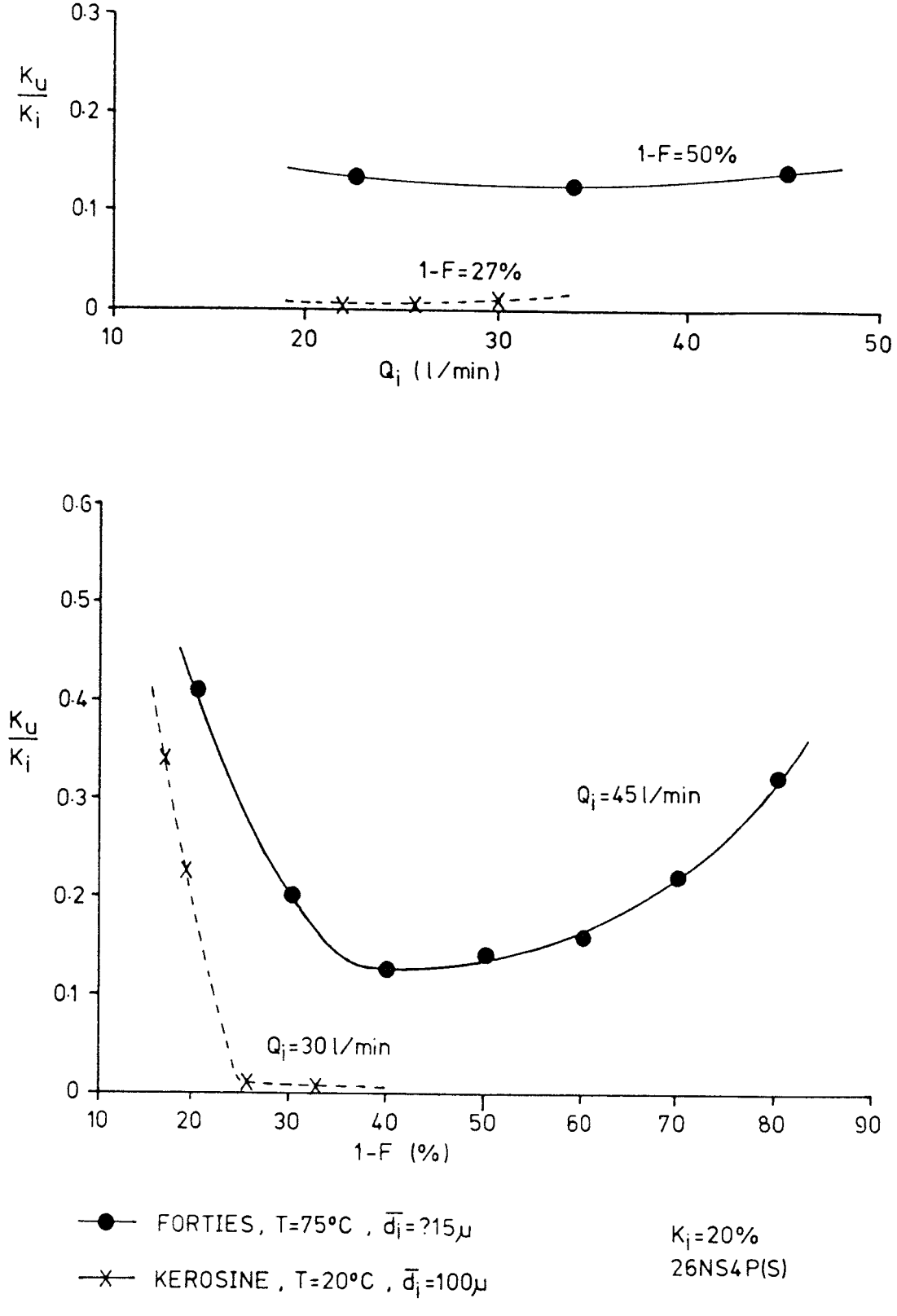

FIG. 10.3 PRODUCTION SEPARATOR TRAIN INCORPORATING DEWATERING AND DEOILING HYDROCYCLONES

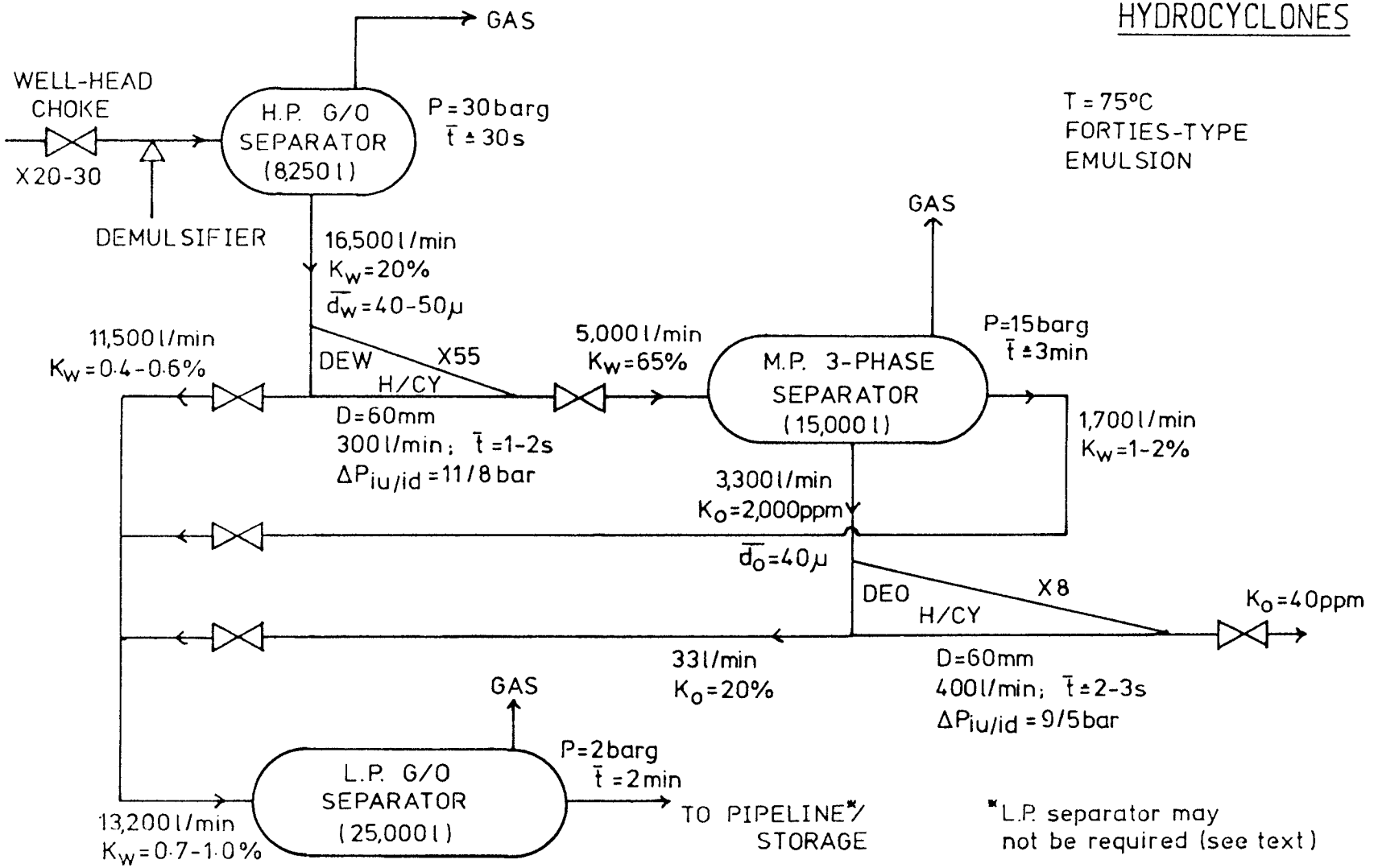

FIG.A.1 NYLON-WATER SEPARATION TEST RIG

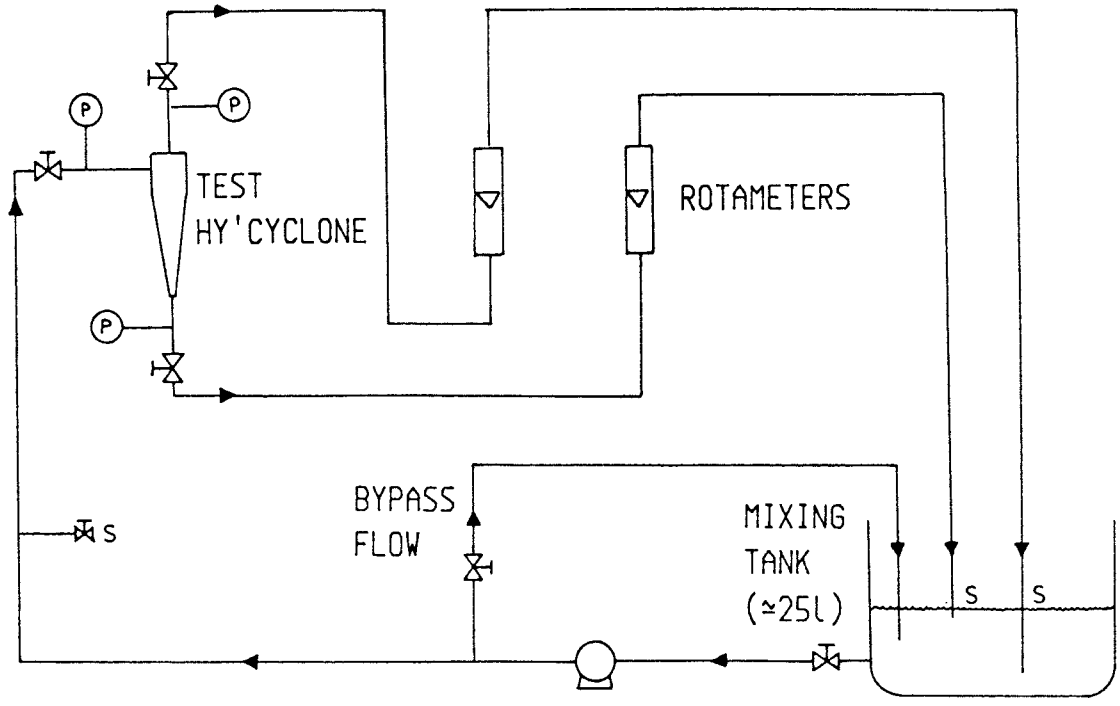

'S' SAMPLE POINT
'P' PRESSURE MEASUREMENT

FIG.B.1 EFFECT OF Ku ON THE OPERATION OF THE UPSTREAM ROTAMETER

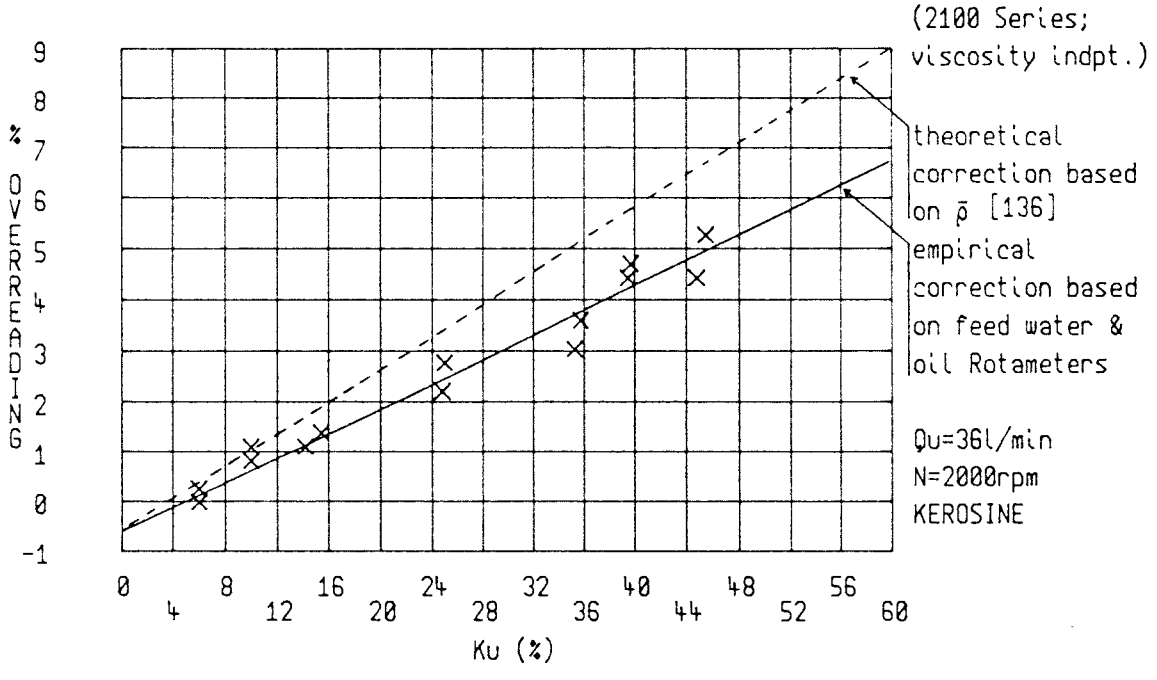

FIG.B.2 AQUASYST CALIBRATION CURVE FOR KEROSINE

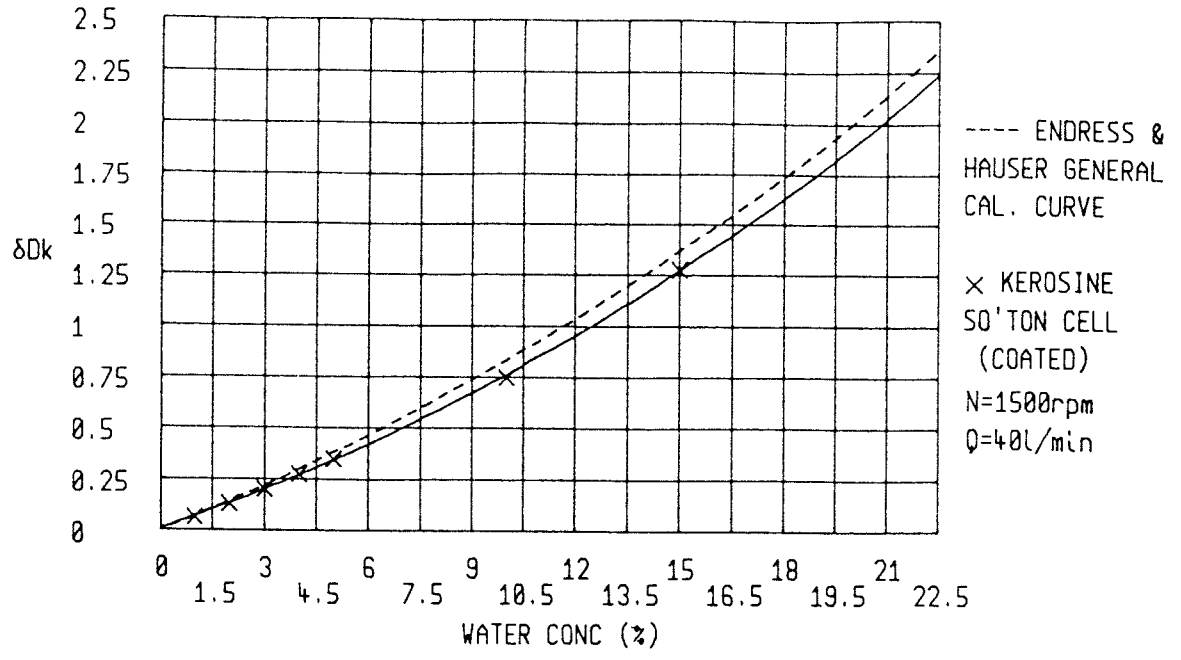

FIG.B.3 AQUASYST CALIBRATION CURVE FOR HGO(07)

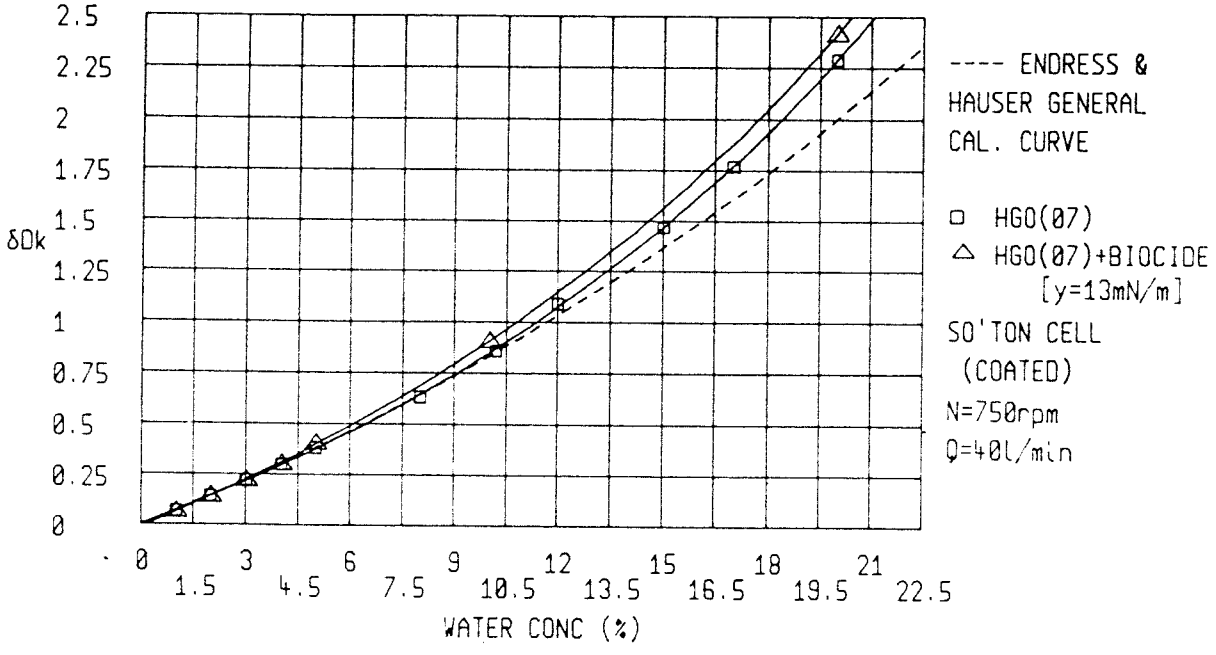

FIG.B.4 EFFECT OF TEMPERATURE ON AQUASYST READING (OIL ONLY)

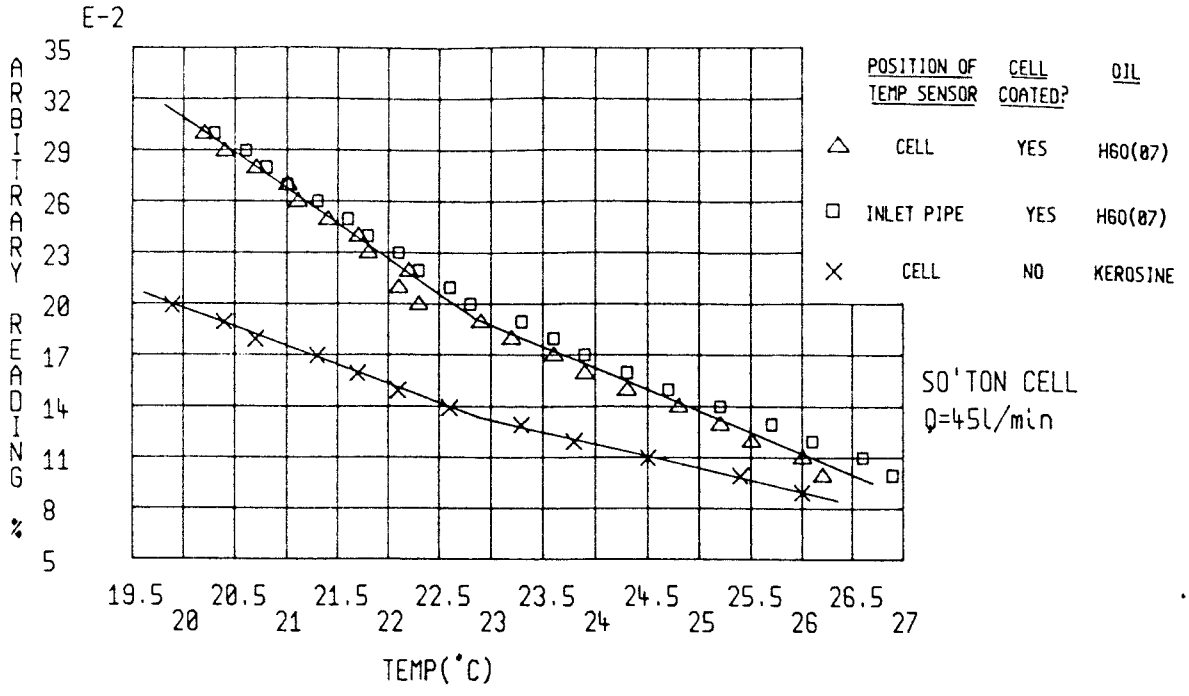

FIG.B.5

AQUASYST ZERO DRIFT AS SHOWN BY CHANGE IN DIELECTRIC CONSTANT [Dk(DAYn)-Dk(DAY0)] FOR DRY OIL

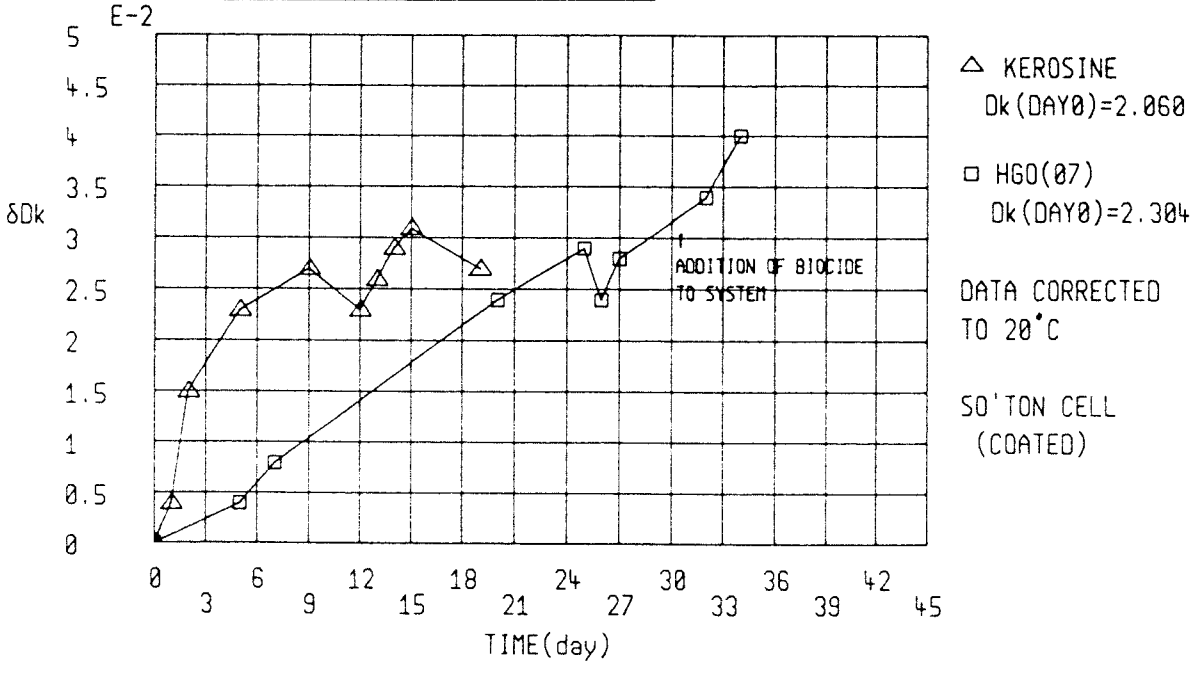

FIG.B.6 USE OF 3.5x10mm CELL TO PHOTOGRAPH DROPS

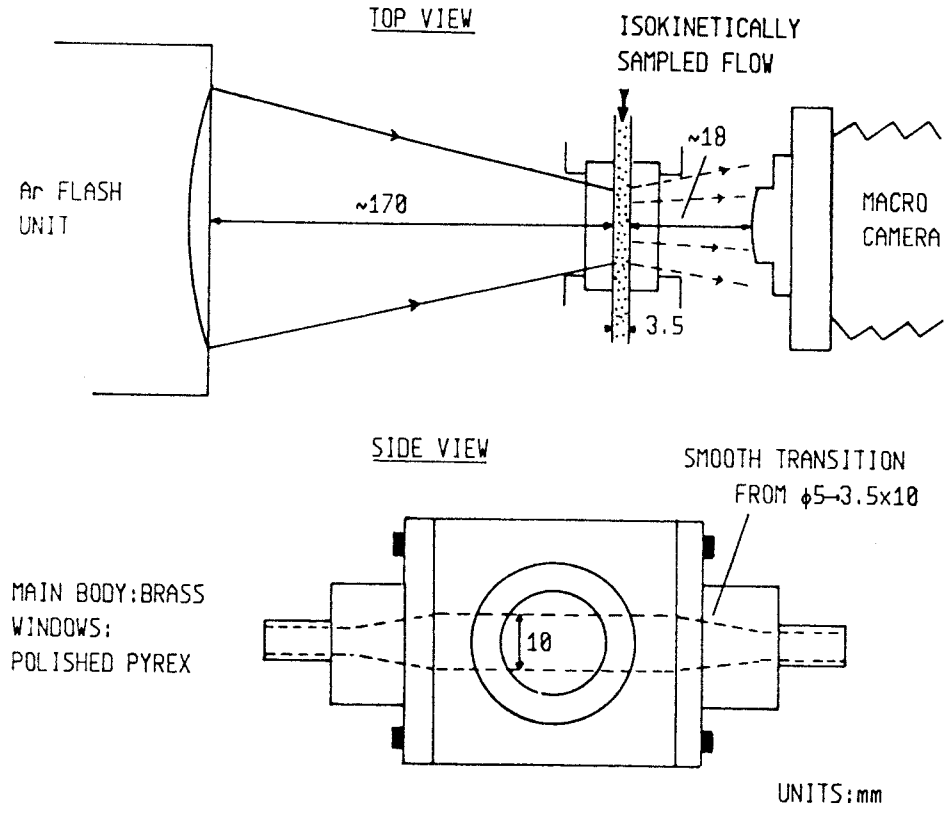

FIG.B.7 QUALITY OF PHOTOMACROGRAPHS

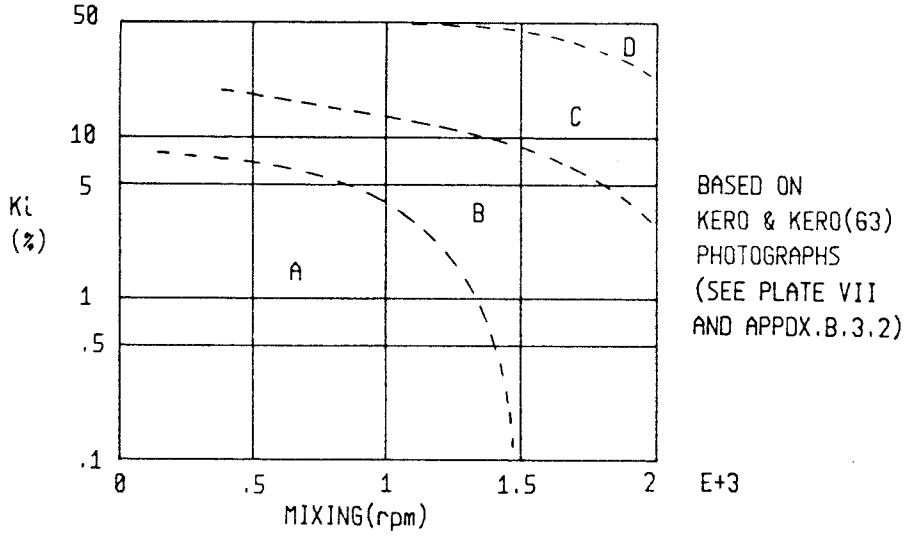

FIG.B.8 COMPARISON OF TECHNIQUES FOR MEASURING WATER CONTENT AGAINST ROTAMETER SET VALUE

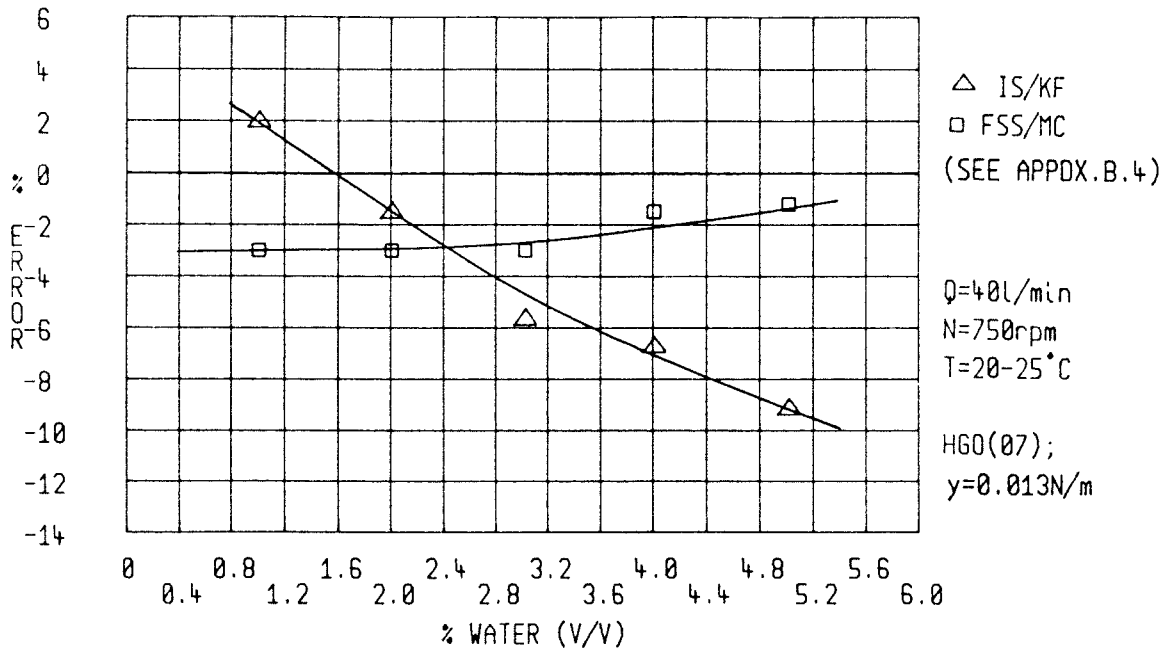

FIG.C.1 OPTICAL ARRANGEMENT FOR LDA

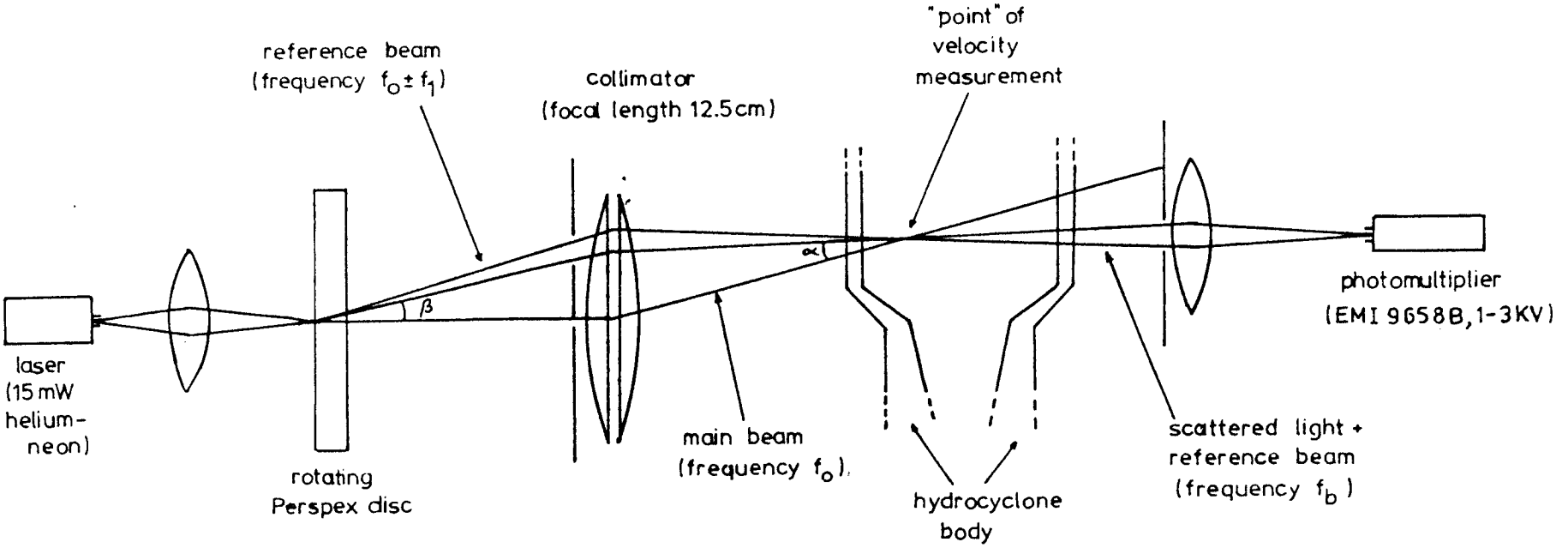

FIG.C.2 BEAM REFRACTION THROUGH HYDROCYCLONE WALL

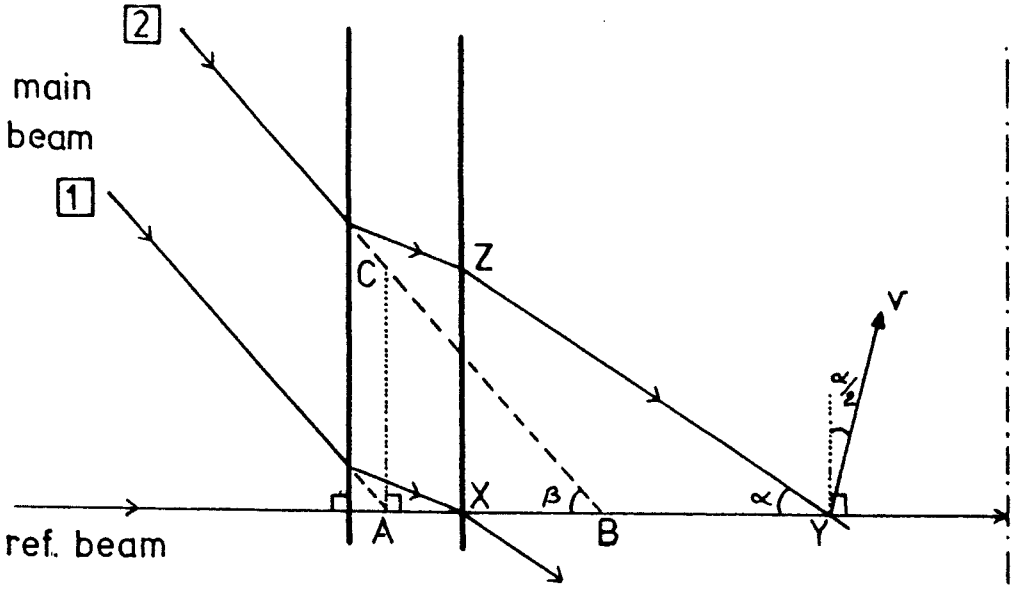

CYLINDRICAL
SECTION

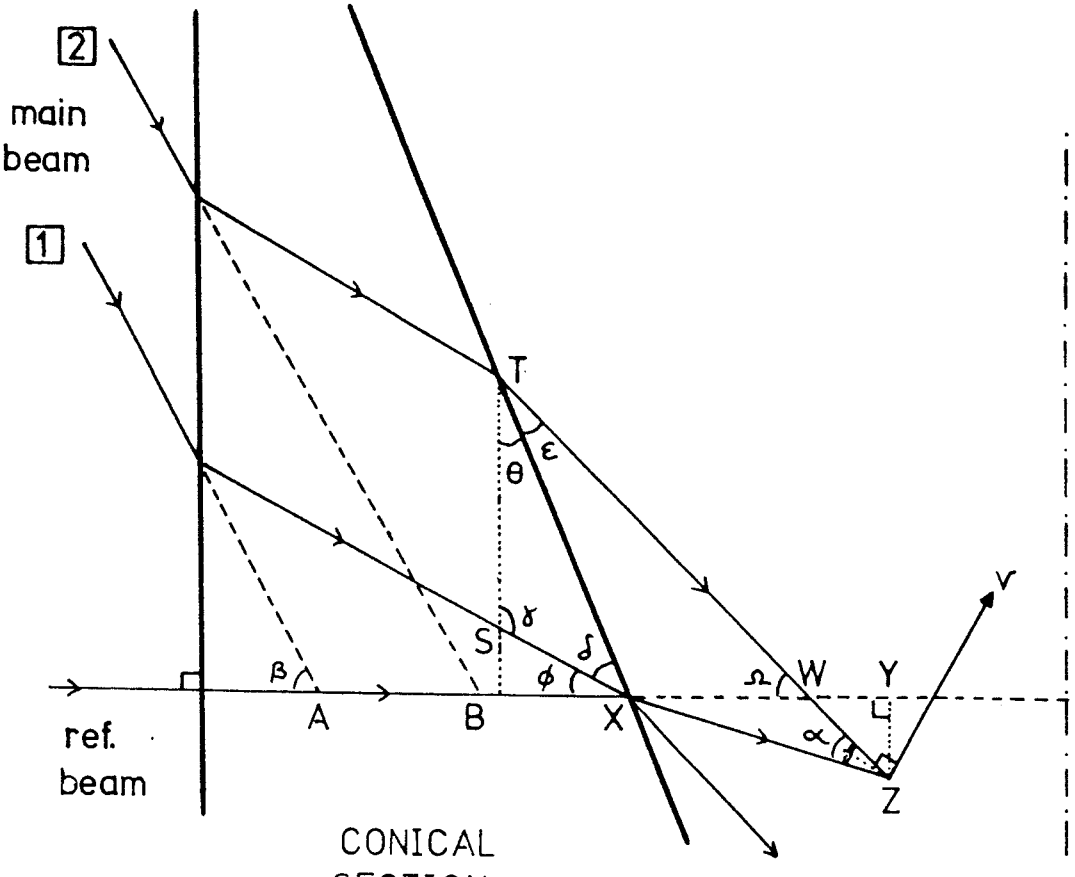

CONICAL
SECTION

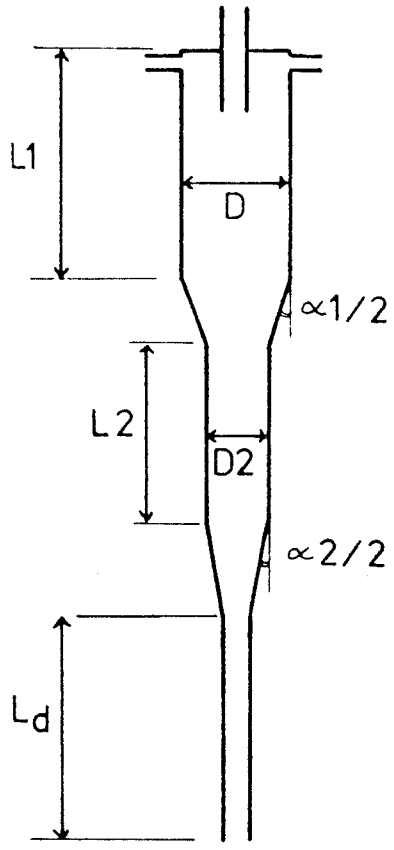

FIG.D.1 FIG.D.2 FIG.D.3

	30PD(T)	30NS1(T)	30NS2(T)
Di/D	0.177	0.177	0.250
(Ai/A)	(0.0625)	(0.0625)	(0.125)
Du/D	0.300	0.300	0.300
Dd/D	0.267	0.267	0.267
D2/D	0.533	0.533	0.533
l/D	1.10	1.00	1.00
h/D	0.24	0.24	0.24
L1/D	4.33	1.87	1.87
L2/D	3.17	0.47	0.47
Ld/D	5.80	5.80	5.80
L/D	16.3	16.5	16.5
α1(°)	20	4	4
α2(°)	10	10	10
S	13.2	13.2	6.0

D=30mm ; tang.circ. inlets (all geometries)

FIG.D.4

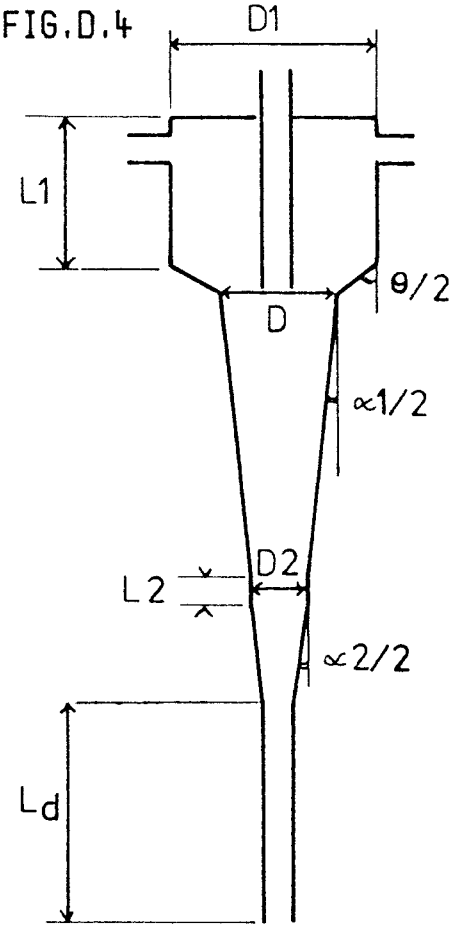

30NS3(T)

Di/D	0.420
(Ai/A)	(0.250)
Du/D	0.300
Dd/D	0.267
D1/D	1.87
D2/D	0.533
l/D	2.67
h/D	0.89
L1/D	2.23
L2/D	0.47
Ld/D	5.80
L/D	17.3
θ(°)	90
α1(°)	4
α2(°)	10
S	6.4

D=30mm;
tang.
rect.(1.5:1)
inlets

FIG.D.5

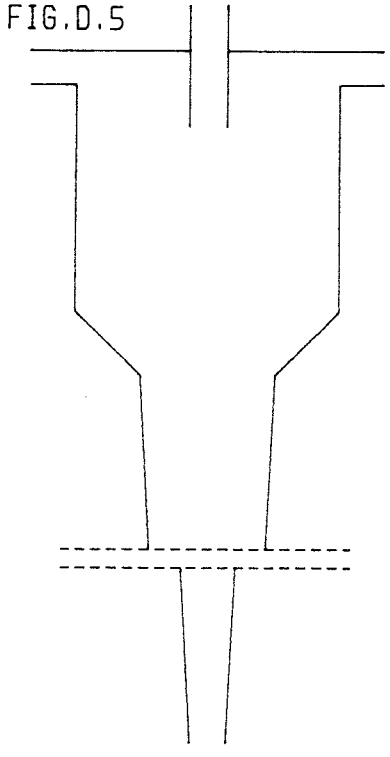

36NS4P(S)

Di/D	0.362
S	12.0

36NS4P(T)

D= 35.6 mm

Di/D	0.256
(Ai/A	0.131)
Du/D	0.281
Dd/D	0.270
D1/D	1.94
l/D	0.56
L1/D	1.92
Ld/D	0.00
L/D	9.35
THETA	90.00 deg
ALPHA	6.00 deg

H/C VOL 0.404 litre
SWIRL NO 12.8

INLET TYPE:
tang,circ

SCALE: X:Y=1:1

FIG.D.6

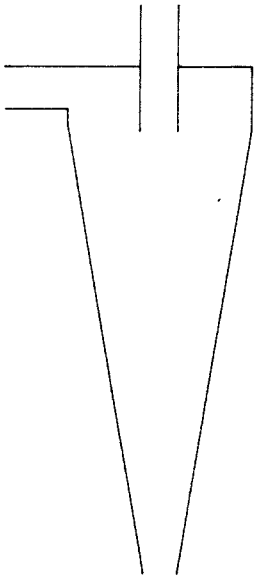

32MANF.A

D= 32.0 mm

Di/D	0.225
(Ai/A	0.051)
Du/D	0.206
Dd/D	0.188
D1/D	1.00
l/D	0.34
L1/D	0.31
Ld/D	0.00
L/D	2.74
THETA	180.00 deg
ALPHA	19.00 deg

H/C VOL 0.033 litre
SWIRL NO 15.3

INLET TYPE:
tang,circ

SCALE: X:Y=1:1

FIG.D.7

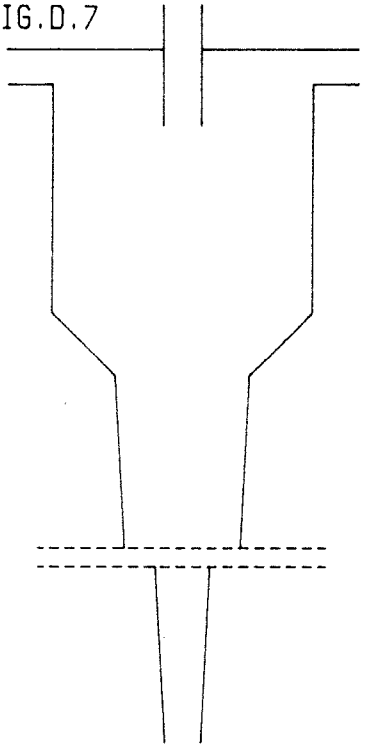

26NS4P(T)

D= 25.8 mm

Di/D	0.256
(Ai/A	0.131)
Du/D	0.283
Dd/D	0.271
D1/D	1.94
l/D	0.56
L1/D	1.94
Ld/D	0.00
L/D	9.37
THETA	90.00 deg
ALPHA	6.00 deg

H/C VOL 0.155 litre
SWIRL NO 12.8

INLET TYPE:
tang,circ

SCALE: X:Y=1:1

26NS4P(S)

Di/D	0.360
S	12.2

FIG.D.8

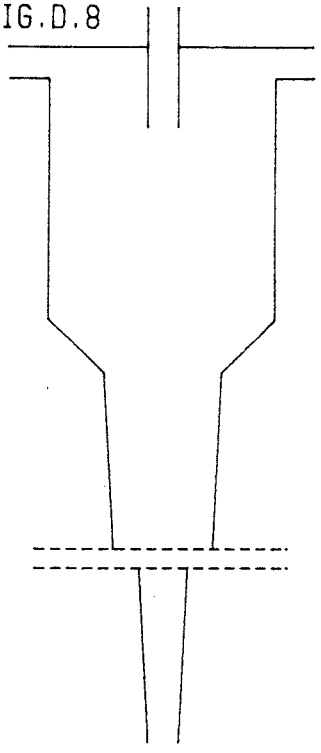

15NS4P(T)

D= 15.0 mm

Di/D	0.253
(Ai/A	0.128)
Du/D	0.267
Dd/D	0.267
D1/D	1.93
l/D	0.67
L1/D	2.30
Ld/D	0.00
L/D	9.76
THETA	90.00 deg
ALPHA	6.00 deg

H/C VOL 0.034 litre
SWIRL NO 13.1

INLET TYPE:
tang,circ

SCALE: X:Y=1:1

FIG.D.9

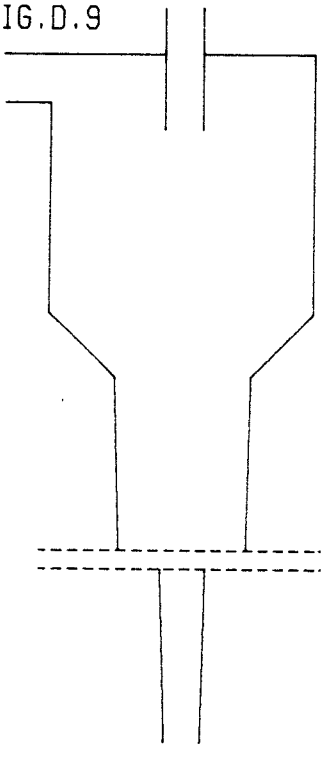

SEE ALSO
PLATE IX

36NS5(S)

D= 35.6 mm

Di/D	0.362
(Ai/A	0.131)
Du/D	0.281
Dd/D	0.264
D1/D	1.94
l/D	0.56
L1/D	1.92
Ld/D	0.00
L/D	16.44
THETA	90.00 deg
ALPHA	3.00 deg

H/C VOL 0.515 litre
SWIRL NO 12.0

INLET TYPE:
tang,circ

SCALE: X:Y=1:1

FIG.D.10

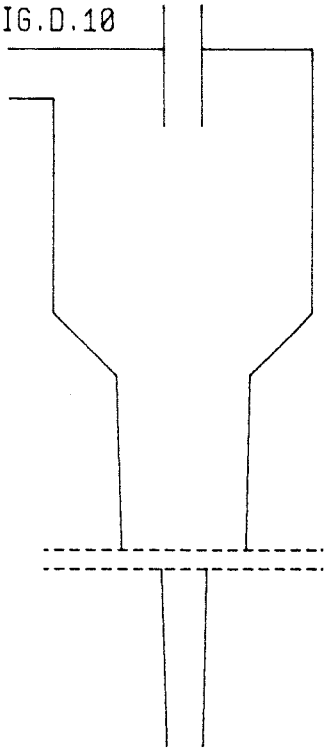

26NS5(S)

D= 25.8 mm

Di/D	0.360
(Ai/A	0.130)
Du/D	0.283
Dd/D	0.271
D1/D	1.94
l/D	0.56
L1/D	1.94
Ld/D	0.00
L/D	16.33
THETA	90.00 deg
ALPHA	3.00 deg

H/C VOL 0.197 litre
SWIRL NO 12.2

INLET TYPE:
tang,circ

SCALE: X:Y=1:1

FIG.D.11

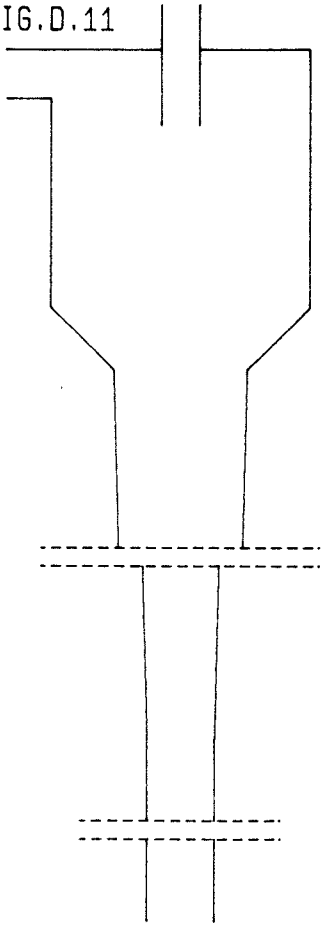

26NS6(S)

D= 25.8 mm

Di/D	0.360
(Ai/A	0.130)
Du/D	0.283
Dd/D	0.500
D1/D	1.94
l/D	0.56
L1/D	1.94
Ld/D	4.40
L/D	16.36
THETA	90.00 deg
ALPHA	3.00 deg

H/C VOL 0.203 litre
SWIRL NO 12.2

INLET TYPE:
tang,circ

SCALE: X:Y=1:1

FIG.D.12

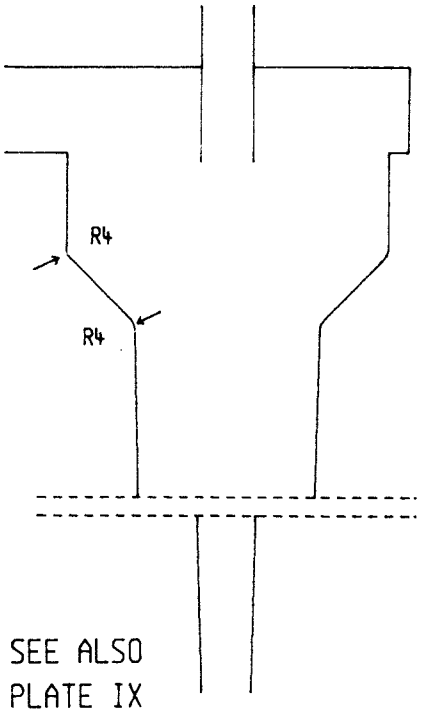

SEE ALSO
PLATE IX

35NS7(V)

D= 35.0 mm

Di/D	0.457
(Ai/A	0.133)
Du/D	0.280
Dd/D	0.268
D1/D	1.74
l/D	0.51
L1/D	1.00
Ld/D	0.00
L/D	15.35
THETA	90.00 deg
ALPHA	3.00 deg

H/C VOL 0.336 litre
SWIRL NO 15.0

INLET TYPE:
volute,rect(2:1)

SCALE: X:Y=1:1

FIG.D.13

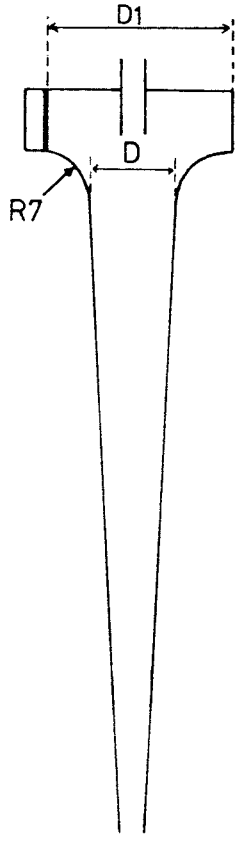

15NS8(V)

D= 15.0 mm

Di/D	0.667
(Ai/A	0.172)
Du/D	0.267
Dd/D	0.267
D1/D	1.93
l/D	0.67
L1/D	0.67
Ld/D	0.00
L/D	8.13
THETA	≡90.00 deg
ALPHA	6.00 deg

H/C VOL 0.018 litre
SWIRL NO 12.8

INLET TYPE:
volute,rect(3.3:1)

SCALE: X:Y=1:1

FIG.D.15

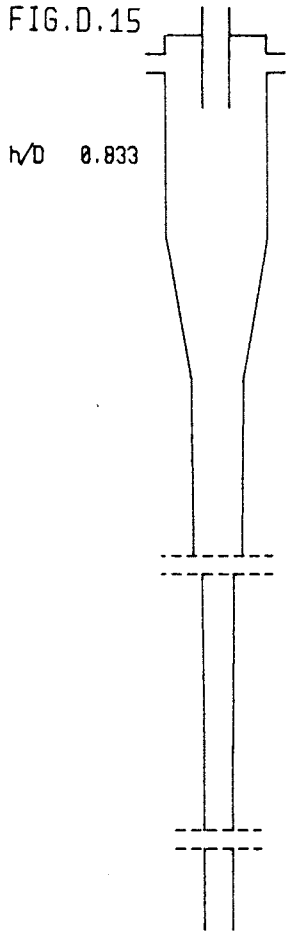

30D02(T)

D= 30.0 mm

Di/D	0.333
(Ai/A	0.222)
Du/D	0.500
Dd/D	0.530
D1/D	1.93
l/D	1.00
L1/D	3.40
Ld/D	22.00
L/D	48.28
THETA	20.00 deg
ALPHA	1.33 deg

H/C VOL 0.783 litre
SWIRL NO 7.2

INLET TYPE:
tang,circ

SCALE: X:Y=1:1

FIG.D.14

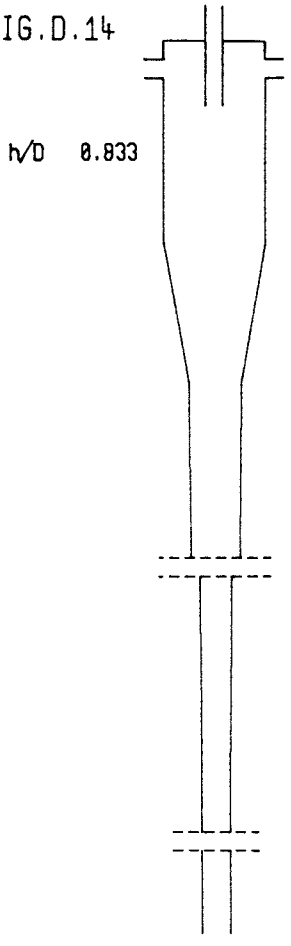

30D01(T)

D= 30.0 mm

Di/D	0.333
(Ai/A	0.222)
Du/D	0.333
Dd/D	0.530
D1/D	1.93
l/D	0.83
L1/D	3.40
Ld/D	22.00
L/D	48.28
THETA	20.00 deg
ALPHA	1.33 deg

H/C VOL 0.783 litre
SWIRL NO 7.2

INLET TYPE:
tang,circ

SCALE: X:Y=1:1

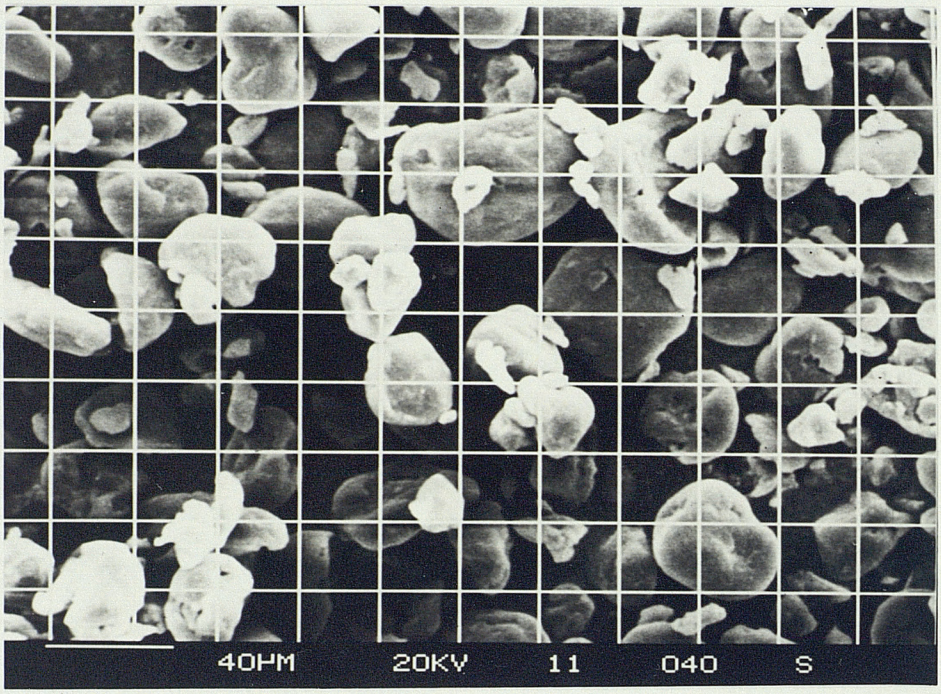

PLATE I ELECTRONMICROGRAPH OF NYLON POWDER

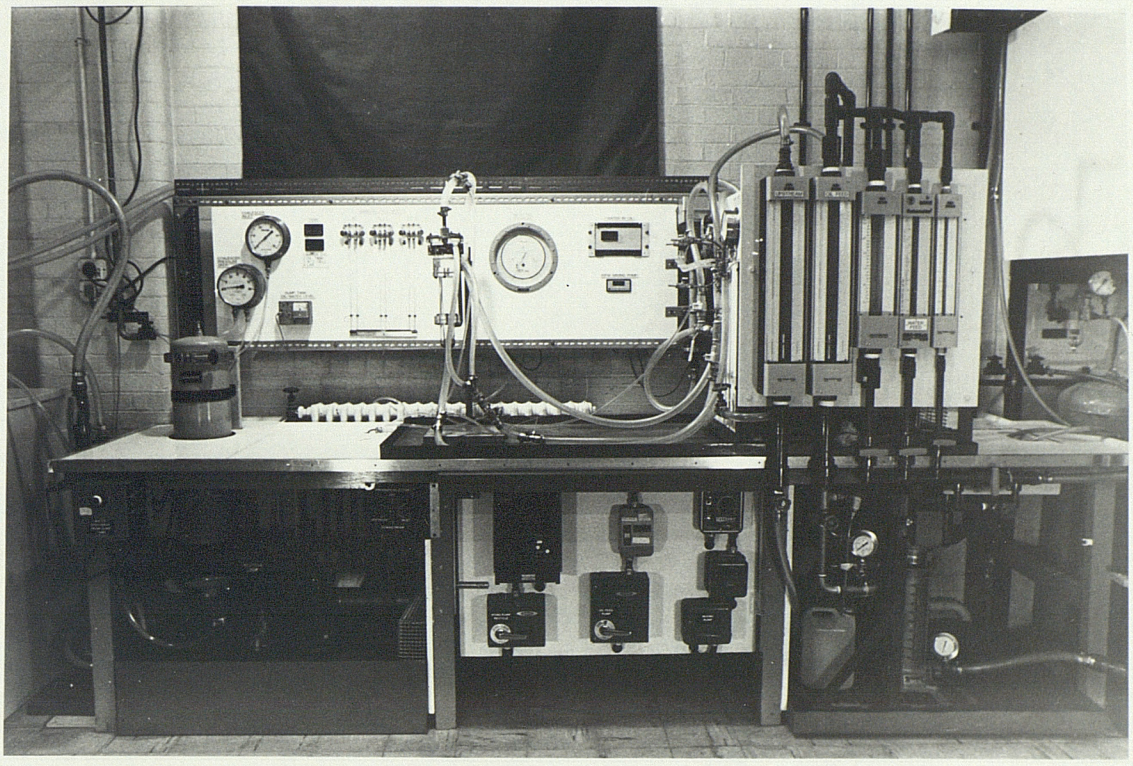

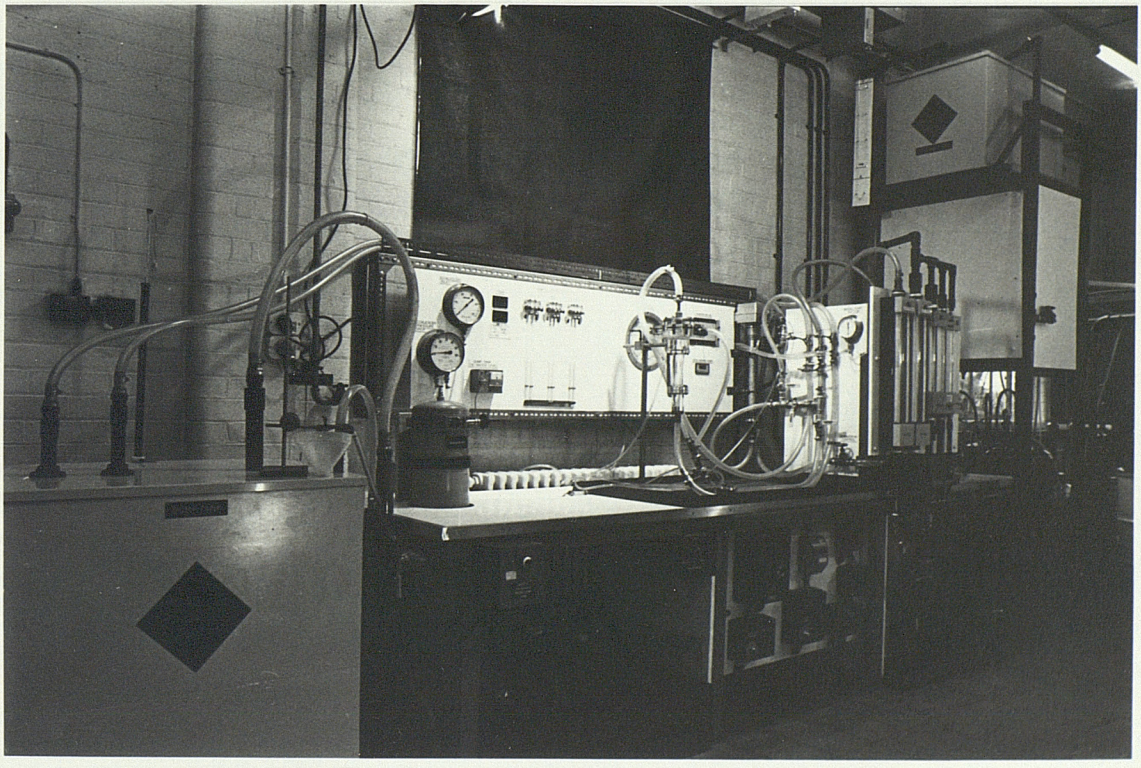

PLATE II WATER-OIL SEPARATION TEST RIG (L3)

a

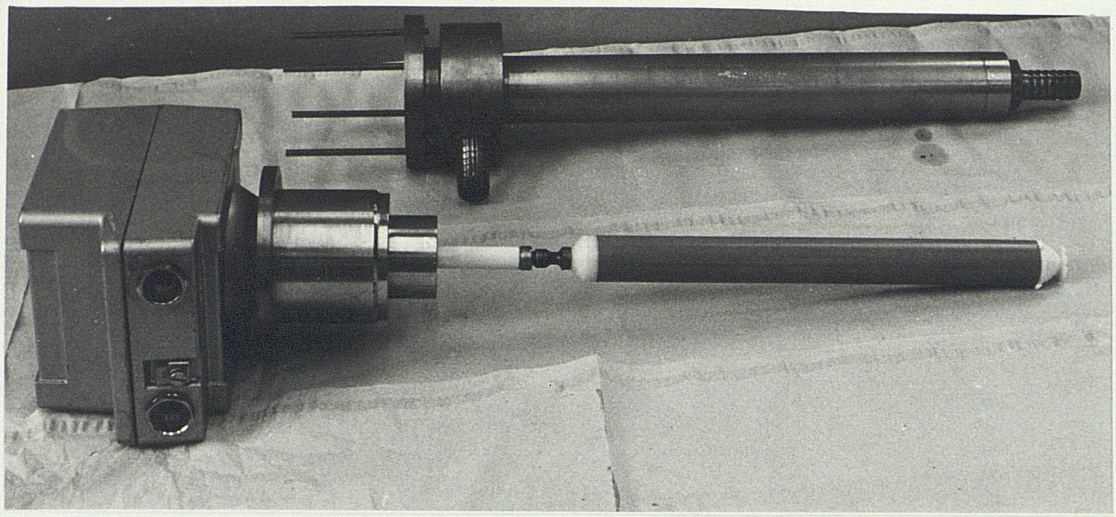

b

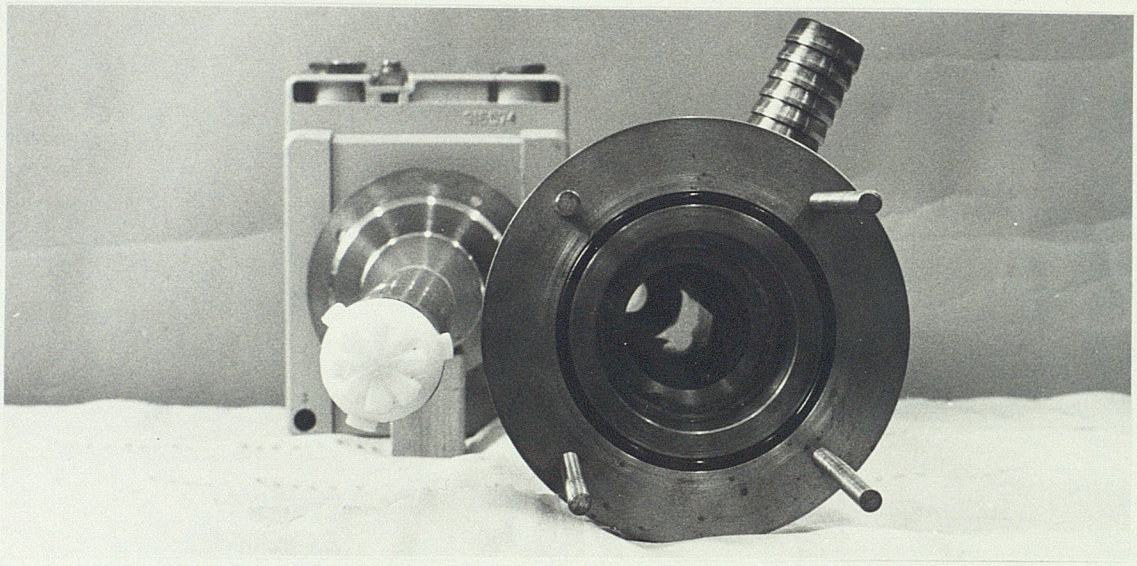

c

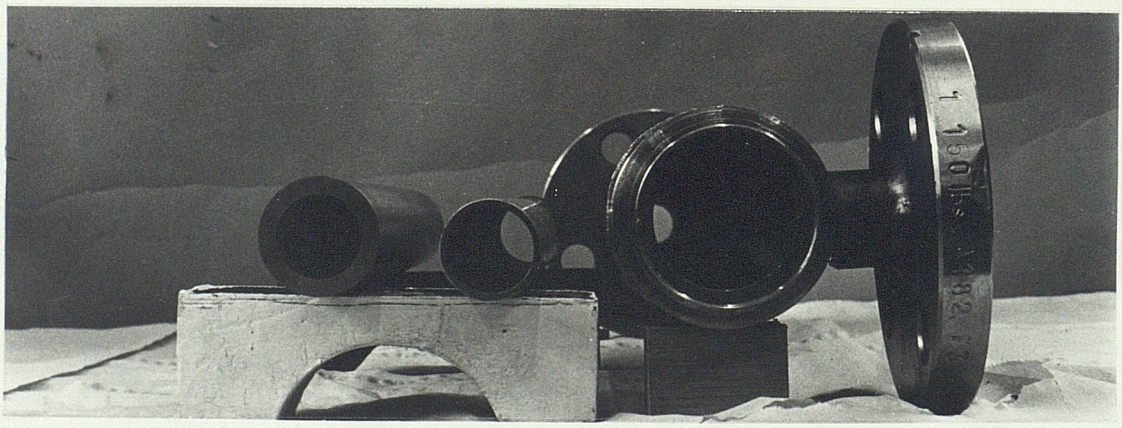

PLATE III AQUASYST WATER-IN OIL ANALYSER

a&b SOUTHAMPTON CELL

c (L→ R) INNER ELECTRODES:- 1.25" & STANDARD CELL ; COMMON OUTER ELECTRODE/CASING

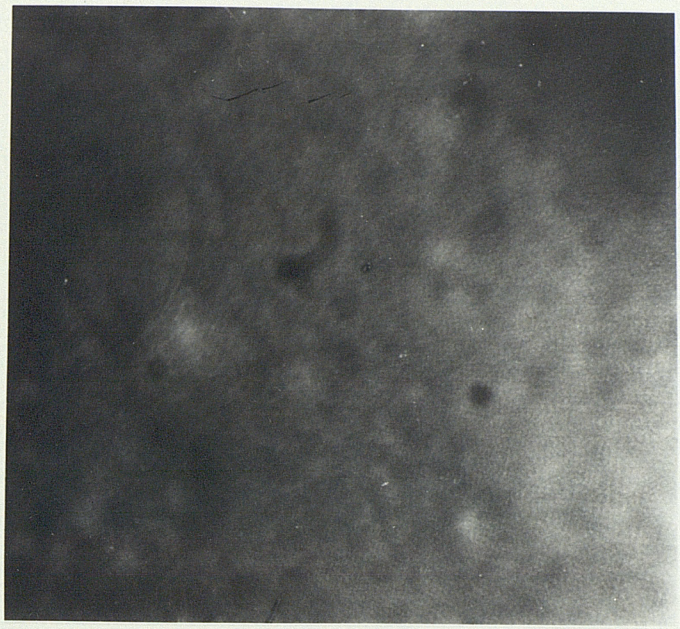

Ki=5%

Ki=10%

200μ

PLATE IV NEAR WALL DROPS WITHIN THE HYDROCYCLONE
(SEE ALSO TABLE 8.1 & FIG.8.1)

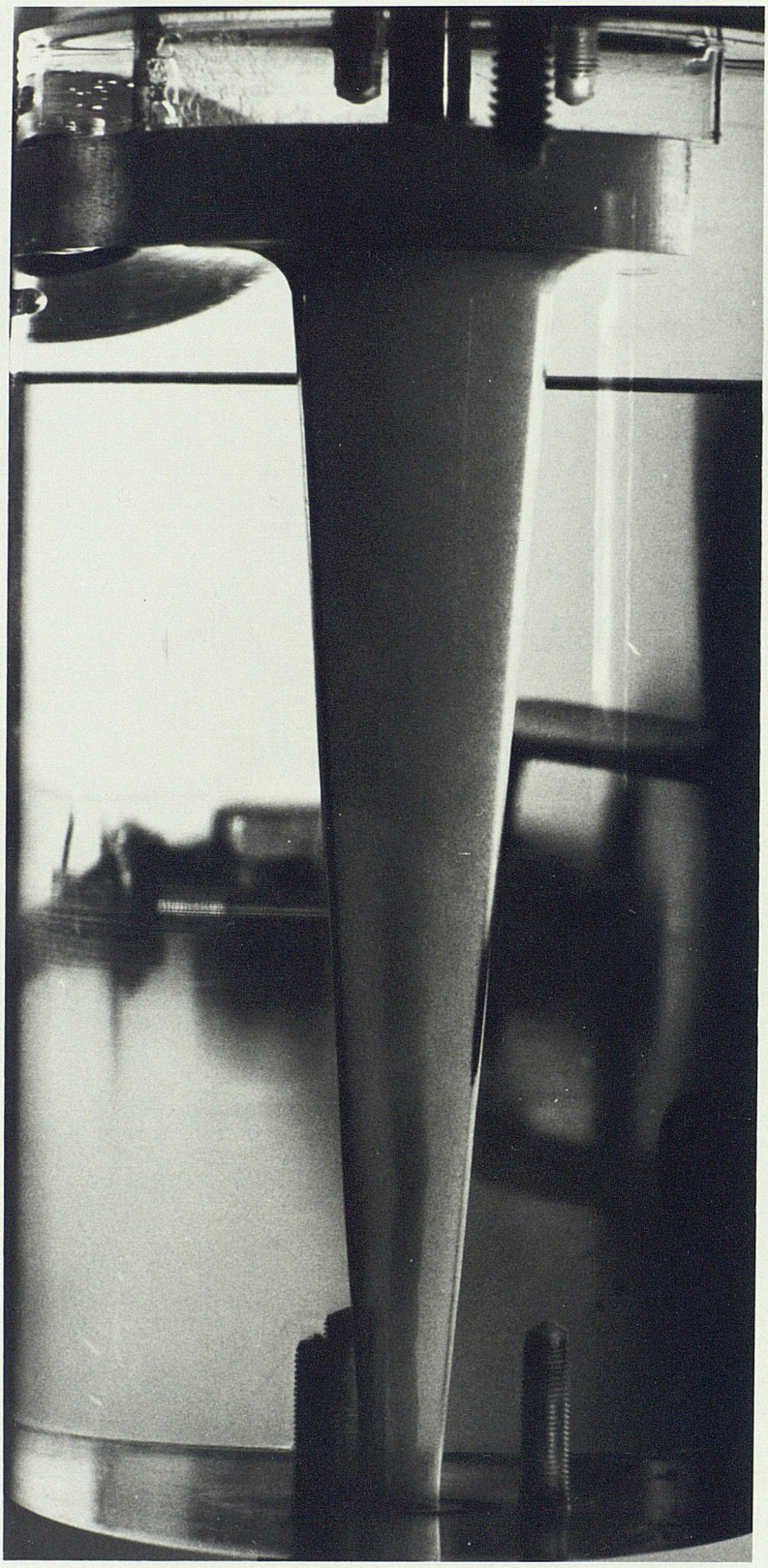

PLATE V PHASE INVERSION IN THE LOWER CONE OF HYDROCYCLONE 15NS8(V) FOR A WATER-KEROSINE FEED (K_i=50%)

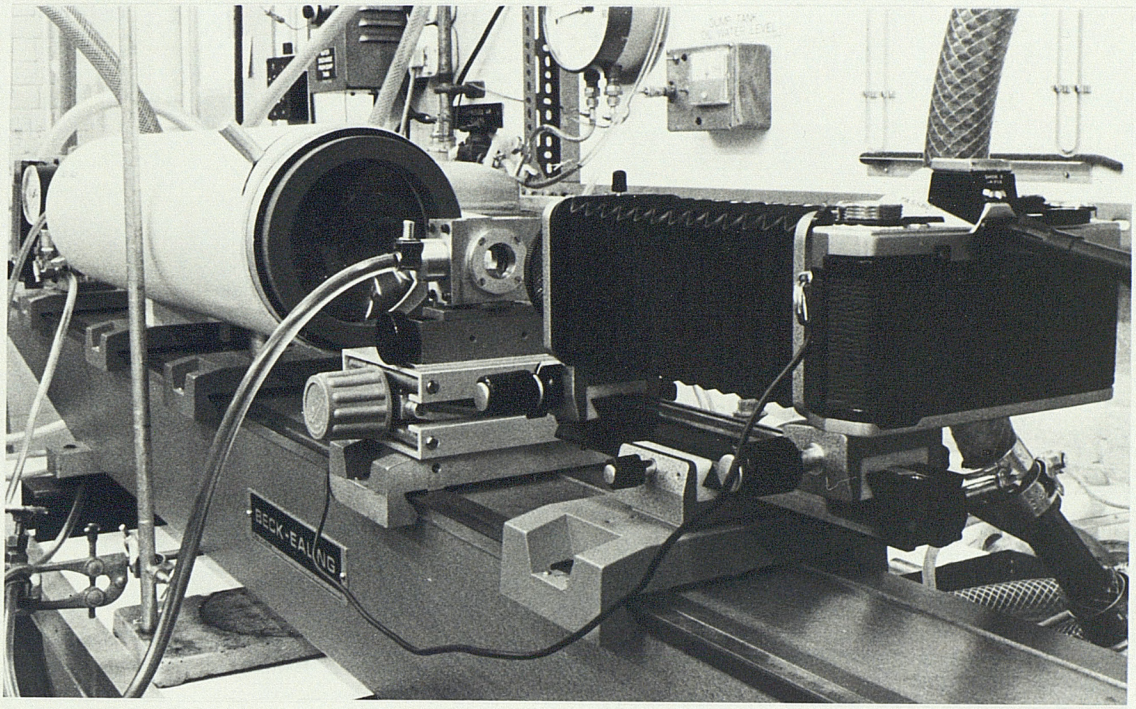

PLATE VI MACROPHOTOGRAPHIC DROP SIZING EQUIPMENT
(SEE ALSO FIG.B.6)

A

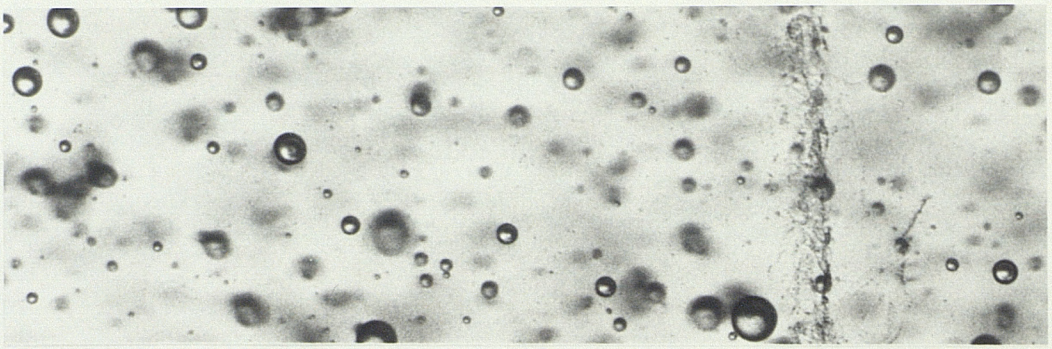

B

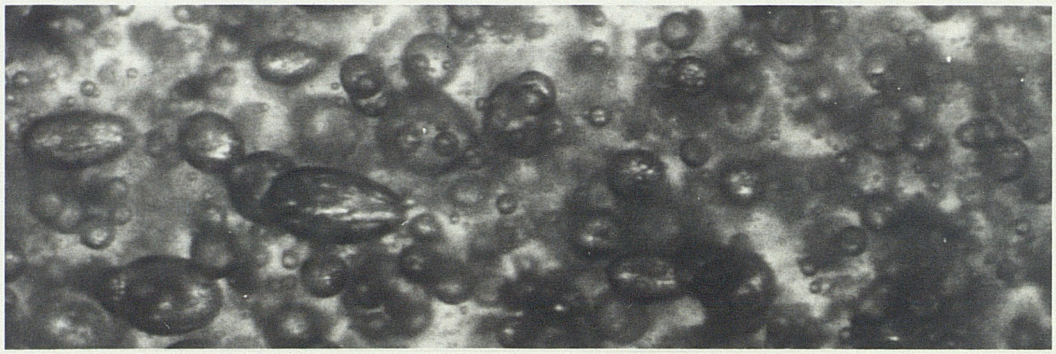

C

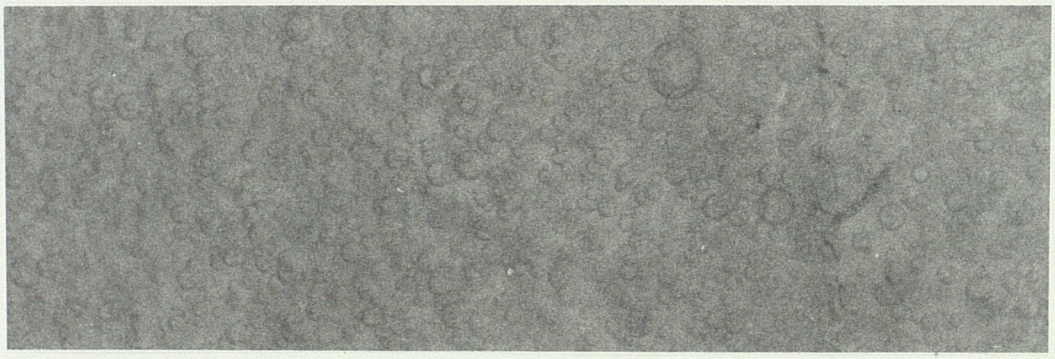

D

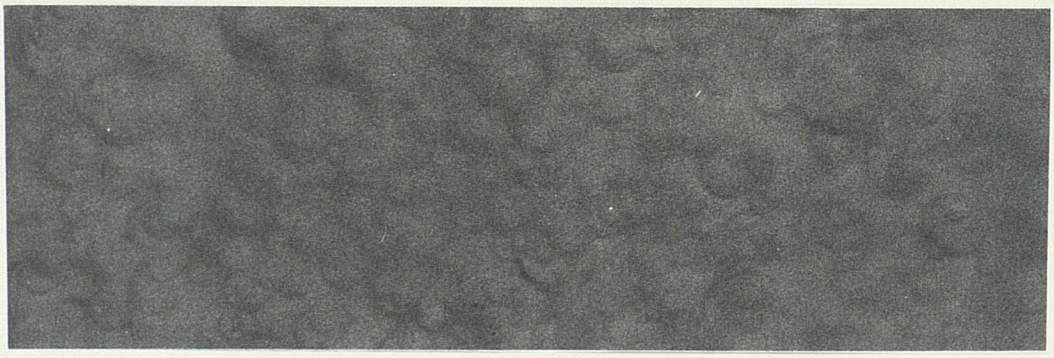

100μ ← FLOW ISOKINETIC Qi=45l/min

PLATE VII DROP PHOTOMACROGRAPHS (QUALITY RANGE)

'A' KERO(63) 7/86; Ki=0.5% N=1000rpm

'B' HGO(07) 3/86 y=0.011N/m; Ki=5% N=750rpm

'C' KERO(63) 7/86; Ki=10% N=1500rpm

'D' KEROSINE 6/86; Ki=30% N=2000rpm

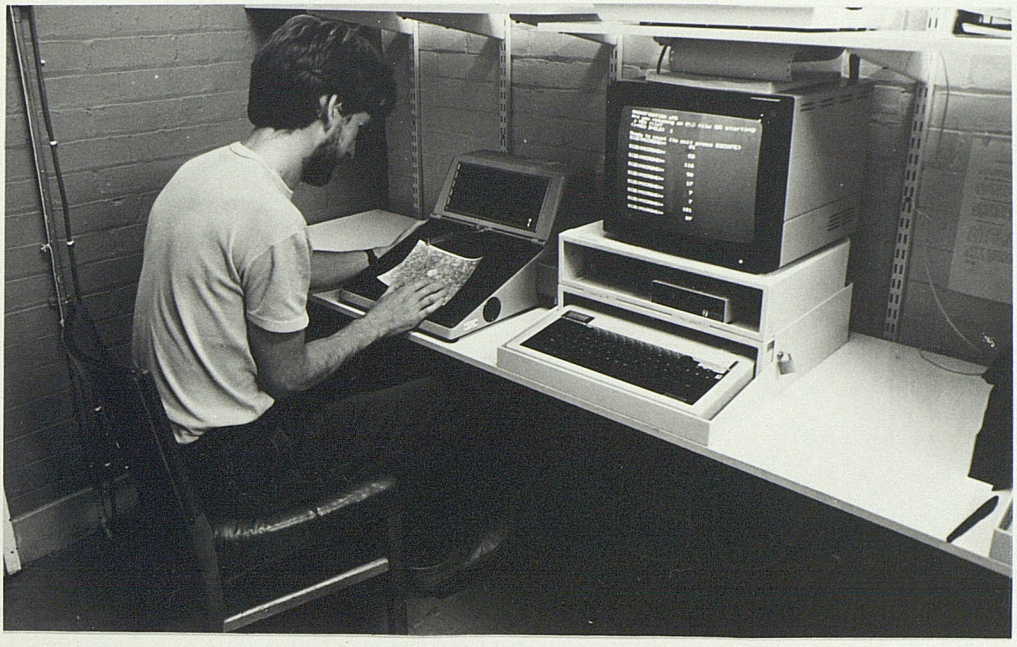

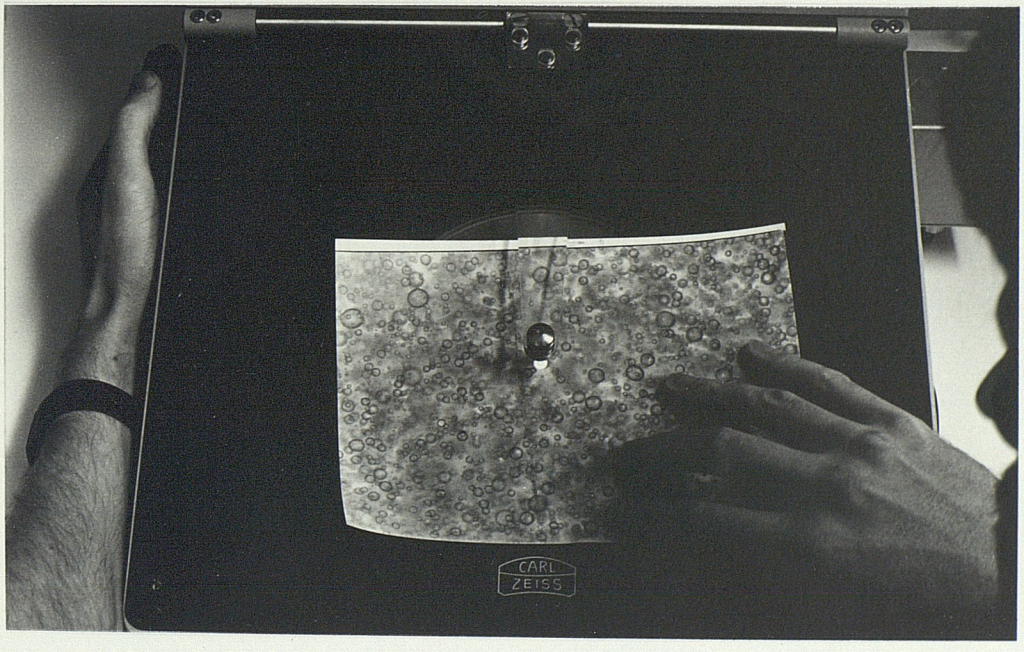

PLATE VIII ANALYSIS OF DROPLET PHOTOMACROGRAPHS USING A ZEISS TGZ3 SIZER AND BBC MICROCOMPUTER

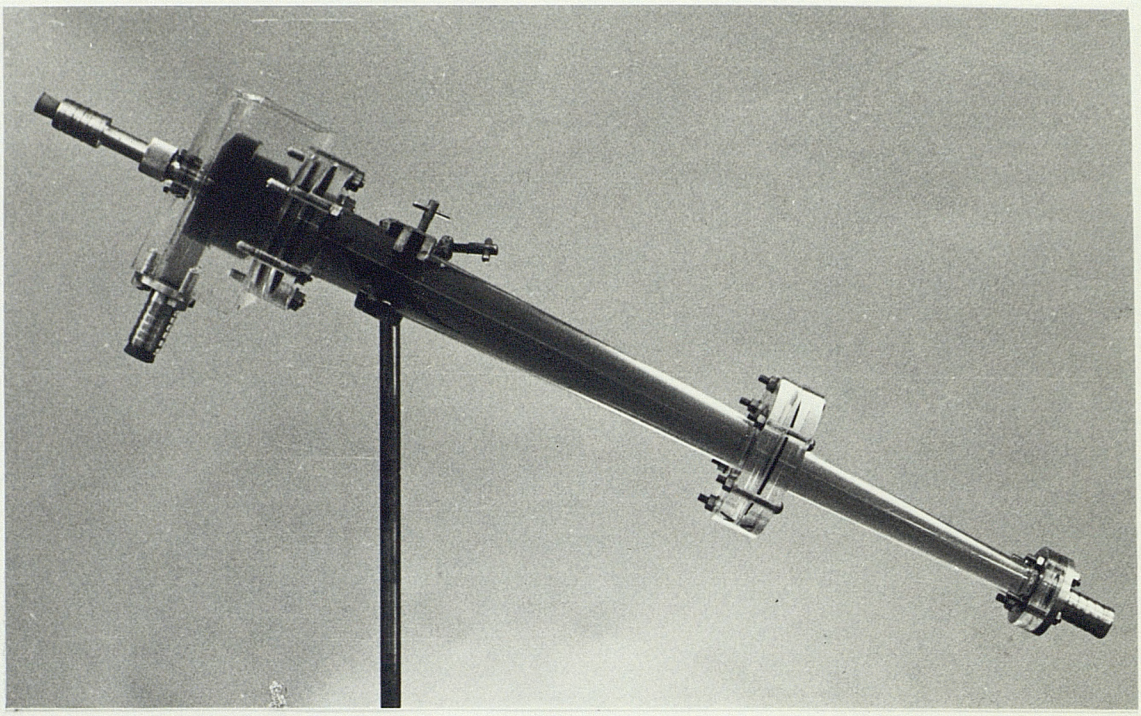

a

b

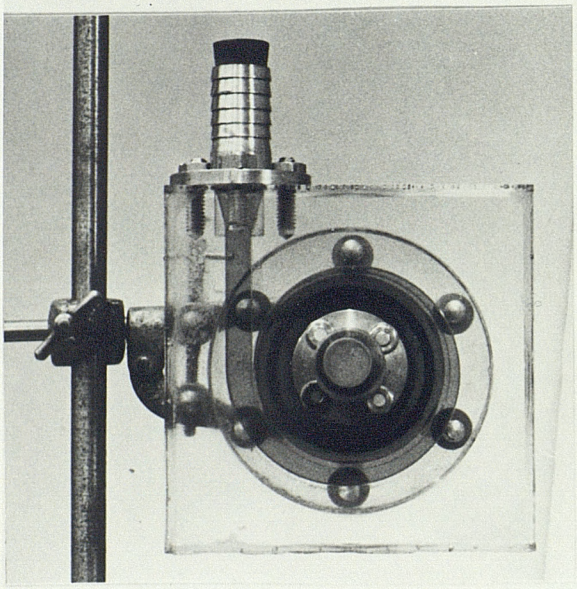

c

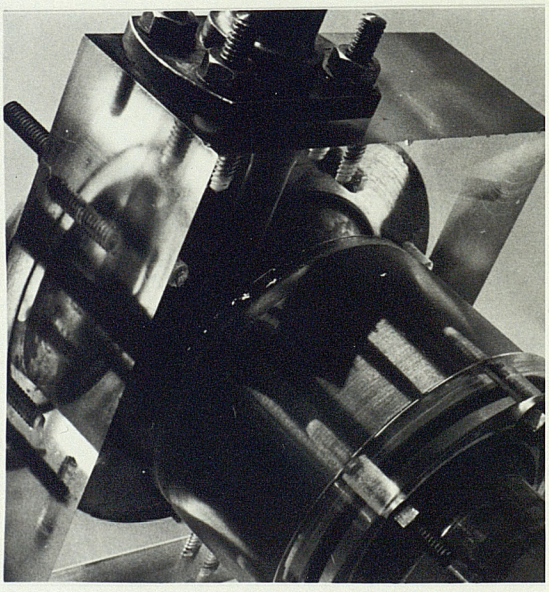

PLATE IX DEWATERING GEOMETRIES

a&b 35NS7(V)

c 36NS5(S)